SCUOLA
NORMALE
SUPERIORE

Classe di Scienze

Corso di perfezionamento in Fisica

XXXIV ciclo

New Physics Ideas from Strongly Coupled Theories

Settore Scientifico Disciplinare **FIS/02**

Candidata

Sonali Verma

Relatori

Prof. Roberto Contino

Prof. Enrico Trincherini

Anno accademico 2018–2023

Per Somu

Acknowledgements

I would like to begin by thanking my advisor, Roberto Contino, for giving me the opportunity to doctorate as his student. I am grateful for his patience and the time that he invested in discussions and projects that I greatly enjoyed. Over these years, I have learned many things from him, from his way of thinking about physics, his tremendous optimism, and his deep humility. I am indebted to him for motivating me throughout all my Ph.D. projects and associated decisions.
I cannot thank Enrico Trincherini, my surrogate internal supervisor enough, for taking care of the bureaucracy and for looking out for me. I am doubtful I'd have made it through without his therapy sessions.
Gui Pimentel's arrival to the hep Scuola Normale group has been like spring. I am grateful to him for his shock therapy/advice sessions and for his encouragement and openness to discuss physics and all else.
I would like to thank Rashmish Mishra for his collaboration in physics projects, his friendship, his advice, and the countless Indian dinners.
The absence of two of my colleagues in Normale: Marco Costa and Salvatore Bottaro, would've made the Ph.D. excruciatingly painful. Thank you, Marco, for sharing discussions and eagerness from Electroweak precision to CFT. I doubt I'd have gotten anything done had it not been for your hourly disturbing office chants. Thank you Salvatore for your patience and collaboration over all these years, model classification would've been more dreary without your company.

I would also like to thank other present and past members of the Unipi/Normale hep group, particularly Paolo Panci, Dario Buttazzo and Alessandro Vichi for discussions and advice; Alessandro Podo for his friendship, discussions and wisdom; Ludovico Vittorio for discussions about the lattice and for his liveliness.
I am also indebted to Scuola Normale Superiore for giving me the opportunity and an invaluable environment. During my Ph.D. I had the privilege to spend extended periods of time in other groups, these periods proved to be interesting scientifically and personally. I would like to thank the Sapienza high energy group in Rome for the lovely summer of 2022; in particular, Victor Miralles, Pere Arnan, Luca Silvestrini, and Marco Nardecchia for discussions, and their openness and for introducing me to schiacciata con friarelli.

I would like to especially thank the DESY theory/cosmology group in Hamburg for the 9 months' visit. I am grateful to Christophe Grojean and Geraldine Servant for their kindness, discussions, and advice and for their support. Thanks to Andrea Mitridate for teaching me about pulsars and for telling me how to organize my directories - hopefully one day I'll manage the latter better. Thanks in particular to Matthias Koschnitzke for his kindness, Hyungjin Kim for discussions and advice during the DESY visit.

All of this would've been very hard without the support of my family, friends, and extended family in Pisa and Ferrara: I thank Marxa - for all, Lauri - for being a friend and insidiously turning into a sister, Paolino for his comradeship, T for his carefully picked content, Vassuccia, and Vale for always cheering me.
Lastly and most importantly, I thank my parents and brother in India for putting up with me and for their constant lifelong support.

Contents

Chapter 1

Introduction or: How to Look for New Physics

Many pressing problems in the Standard Model (SM) require solutions and approaches that are complementary - much like the two parts presented in this thesis. Let us begin with a close look at a historical example - the *hierarchy problem* which can solved using such a complementary strategy.

The hierarchy problem (See Ref. [1] for a review of the problem and possible solutions) arises in the SM since the SM Higgs mass is not protected against large quantum corrections by any symmetry. This implies that the Higgs mass would be quadratically sensitive to high scales (and thus any heavy new particle that arises at thresholds). The largest one-loop correction to the SM Higgs mass comes from SM top quark loops. This is given by:

$$\delta m_H^2 \sim -\frac{6\ y_t^2}{16\pi^2}\ \Lambda^2 \tag{1.1}$$

where Λ is the cut-off scale of the SM when seen as an effective field theory (EFT), while y_t is the SM top Yukawa coupling. A large cut-off value for the Λ scale $\sim$ Planck Mass $M_{Pl} \sim 10^{19}$ GeV[1] would imply $\delta m_H^2 \gg m_H^2$ with m_H^2 being the bare mass term, giving rise to the so-called hierarchy problem. To explain the observed physical Higgs mass $m_H^{physical}$of 125 GeV, a large tuning would be required between the Higgs bare mass and couplings entering the one-loop correction. Whereas, if the one-loop correction in Eq. 1.1 is set to be of the order of the physical Higgs mass 125 GeV, to avoid an *unnatural* cancellation between the bare Higgs mass and the one-loop correction, we would get:

$$\Lambda \sim 4\pi m_H^{physical} \sim \mathcal{O}(\text{TeV}) \tag{1.2}$$

where we have ignored $\mathcal{O}(1)$ couplings. Clearly, a new physics theory *with new SM-charged degrees of freedom arising at the TeV scale* would be a natural way out of this problem.

Infact, this problem was commonly solved by introducing *Supersymmetry* (SUSY) (See Ref. [2] for a recent review and references within). Under SUSY, particles come as degenerate pairs of a boson and a fermion, thus each SM particle gets a "superpartner" which only differs from it by its spin. Loop corrections from QCD-charged SUSY top partners called *stops* cancel one-loop corrections to the SM Higgs mass from SM tops. Since these new SUSY particles carry SM color, it was expected that they would be copiously produced in collisions at the Large Hadron Collider (LHC). So far searches at LHC have turned null results on such heavy new particles (See for example

[1] At $m \gtrsim M_{Pl}$, particle-antiparticle creation by the gravitation field become important, thus, quantum gravitational effects cannot be ignored. This sets the upper bound on the $\Lambda \sim M_{Pl}$ above which SM cannot be the fundamental theory to describe interactions.

results in [3]).

Let's turn to alternatives to such SM-charged particles which can also resolve the hierarchy problem: these are given by *Neutral Naturalness* [4, 5]. Such theories introduce a $\mathcal{Z}_2$ symmetry such that the SM gauge group and particles have a *mirror or twin counterpart carrying no SM quantum numbers.* The one-loop top correction to the Higgs mass can now be canceled by the twin top partner charged under a *hidden* QCD. Due to the absence of the SM QCD coupling, these top partners would not be produced in large numbers at LHC. The production of these *hidden top partners* is through the "Higgs Portal", a mixing between the SM Higgs and twin/mirror Higgs sector. Indeed such hidden sectors barely interact with visible matter and can go completely unobserved in high-energy detectors (missing energy) or else show up as macroscopic displaced decays (displaced vertices). More traditional high-energy colliders are not equipped to observe *long-lived particle* signatures typical of such hidden valley sectors. However, in the last decade or so, a heavy program for dedicated experiments for searching for such physics has been underway (See Ref. [6] for a review). Note that other (non-top) hidden sector particles can be much lighter than the EW scale. Such hidden sectors can be probed at high-intensity experiments running at a much lower centre of mass energy than high-energy colliders. We will explore probing such a light SM-neutral dark sector in the first part of the thesis (see Chapter 2 and Chapter 3).

Hierarchical Structure of Fundamental Physics

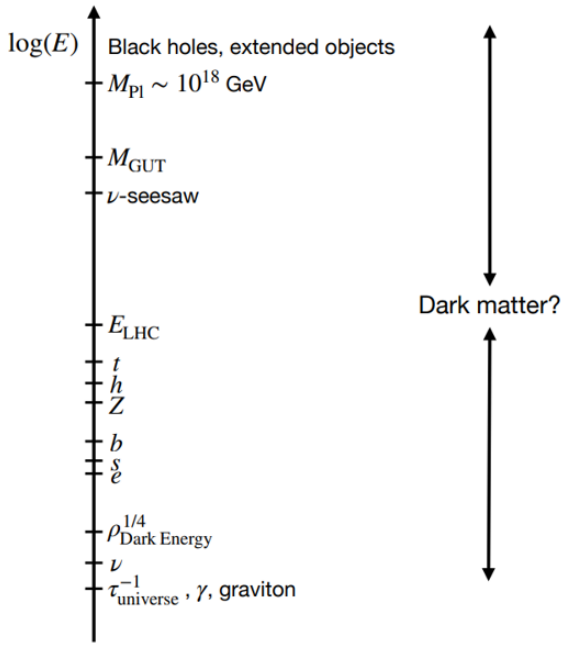

Figure 1.1: Cartoon showing various scales relevant in fundamental physics, taken from [2].

Fig. 1.1 shows a mix of energy/mass scales based on experimental measurements as well as untested theoretical predictions. It is evident that describing both visible matter as well as new or invisible matter requires understanding and/or creating a hierarchy of scales. Moreover, answers to the various open problems in fundamental physics can also span many orders of mass scales. Let us concentrate on the *dark matter (DM) problem*: a possible DM candidate compatible with all astrophysical and cosmological evidence could well be anywhere between $\mathcal{O}(10^{-21})$ eV to all the

way up to $\mathcal{O}(M_\odot)$ (See Ref. [7] for examples of such DM models).

Why should we care about the Dark Matter problem?

Much evidence for dark matter in the form of observational measurements has been collected across many length scales [2]. The earliest hints of dark matter arose from its gravitational effect on galaxies, to explain the flatness of galaxy rotation curves [12–14]. The flatness (contrary to Keplerian prediction) of rotation curves suggests that an extended "dark halo" reaches beyond stellar distributions. Gravitational lensing has also been used to detect dark matter surrounding galaxy clusters [15]. Due to the strong lensing effect, distant galaxies appear as tangential arcs. These distortions have been widely studied to deduce the distribution of dark matter around galaxy clusters (See [16] for example).
A very important probe for establishing the cold dark matter (CDM) paradigm is the observation of the CMB fluctuations [17]. Energy injection between recombination and reionization will affect the thermal history of the universe during the dark ages. The measurements of the Cosmic Microwave Background (CMB) probe the dark ages and thus, indirectly can constrain any new physics that would lead to such energy injection. DM annihilation into SM around red-shift of last scattering ($z \sim 1000$) will inject energetic particles into the photon-baryon fluid. While cooling, these particles will heat and ionize neutral hydrogen, increasing the ionization level after recombination thus, modifying the CMB anisotropy spectrum. (See Ref. [18])
Further, the large-scale structure of the Universe is very well described by the standard cosmological model of ΛCDM, where the presence of CDM provides a crucial contribution via its overall energy density and through the primordial density perturbations (See for example Ref. [19] for more details). Moreover, the gravitational influence of dark matter [17] is also key in the formation of structure.

Instead of being an isolated dark particle, dark matter can come alongside its own zoo of dark particles or *dark sector* which is dark or hidden. Such a dark sector could either be composed of SM-charged fields or SM-neutral fields. If the dark sector is SM-neutral, it can couple to SM either through gravity or via weakly coupled portal interactions. Despite being feebly coupled to the SM, such dark sectors can still give interesting phenomenological signals at experiments (see chapters 2 and 3).

This thesis attempts to solve this dark matter/dark sector problem in the two historical ways described earlier, either via:

- a heavy SM-charged new physics sector (Chapter 5 and Chapter 6), or
- a light SM-neutral new physics sector (Chapter 2 and Chapter 3).

Let us return to the issue of creating a large separation of scales in a theory.

Can strongly coupled theories create hierarchies?

Let us remind ourselves of Dimensional Transmutation in QCD - the most concrete example we know of how non-perturbative physics can successfully explain *hierarchies*. We will eventually

[2] An alternative to the dark matter explanation is provided by theories of Modified Newtonian Dynamics (MOND) [8]. However, popular candidates of MOND theories give a notably worse fit to CMB and large scale structure data compared to the ΛCDM fit [9, 10]. In addition, a recent analysis [11] of Milky Way observable data is also in tension with MOND.

see how this same underlying mechanism can be used (and is used in this thesis too) to construct theoretical models trying to explain the biggest BSM puzzles of our times.

Let us look at the case of massless QCD with only two flavours of quarks "up" and "down" quarks with mass $m = 0$. This massless QCD can be parameterized by its running coupling constant $\alpha_{QCD}(\mu)$ where μ is the renormalization group (RG) scale. We can begin with the RG equation:

$$\frac{d\,\alpha(\mu)}{d\,ln\,\mu} = \beta(\alpha) \tag{1.3}$$

The proton mass m_p is the physical scale at which the QCD coupling becomes "strong". For this example of QCD with $n_f = 2$, the 1-loop beta function coefficient is $\beta_0 = 29/3$ giving

$$\beta(\alpha_{QCD}) = -\frac{29}{6\pi}\alpha^2_{QCD}(\mu) \tag{1.4}$$

We can now write the mass of the proton m_p choosing μ to be the Planck Scale M_{Pl} as:

$$m_p = M_{Pl}\, e^{-1/C\,\alpha_{QCD}(M_{Pl})} \tag{1.5}$$

where $C = 29/6\pi$. To get the required hierarchy of $m_p/M_{Pl} \sim 10^{-18}$, we require $\alpha_{QCD}(M_{Pl}) \sim 10^{-2}$. This is very powerful. *A hierarchy of* $\mathcal{O}(10^{-2})$ *in the UV-coupling gets exponentially stretched to explain the IR mass parameters we anticipated.* This can be the guiding principle for uncovering BSM mechanisms that can help us address questions like *the stability of dark matter.*

I) Hierarchy for dark matter stability

While dark matter (DM) has to be stable over cosmological timescales, some rare decaying DM may give rise to observable signals in the spectrum of high-energy cosmic rays. These decays would be induced by operators involving both DM and the SM. These *indirect detection bounds* can constrain the DM lifetime. Current strongest bounds on $m_{DM} \sim \mathcal{O}(100\text{ TeV})$ come from IceCube and γ-ray measurements implying the lower bound on lifetime [20–22]:

$$\tau_{DM} \geq 10^{28}\text{ sec} \tag{1.6}$$

If the DM decay occurs by some operator of dimension D characterised by a coupling κ, the bound in Eq. 1.6 can be translated to a hierarchy of scales between the physical DM mass m_{DM} and the UV scale suppressing the operator. The DM width decaying to SM can be estimated as:

$$\Gamma \sim \frac{\kappa}{8\pi}\frac{m_{DM}^{2D-7}}{\Lambda_{\text{UV}}^{2D-8}} \tag{1.7}$$

Fixing $\kappa = 1$, and Λ_{UV} to the Planck Scale, we can get:

$$\text{For}\quad D = 5,\quad m_{DM} \sim 10^{-5}\text{ GeV} \Rightarrow \frac{m_{DM}}{\Lambda_{\text{UV}}} \sim 10^{-22} \tag{1.8}$$

$$\text{For}\quad D = 6,\quad m_{DM} \sim 10 - 100\text{ TeV} \Rightarrow \frac{m_{DM}}{\Lambda_{\text{UV}}} \sim 10^{-14} - 10^{-15} \tag{1.9}$$

For an SM-charged dark sector, collider signatures of SM-charged states put strong constraints on a $\mathcal{O}(\text{GeV})$ scale DM candidate. However, a DM candidate having mass $\sim 10 - 100$ TeV is sufficiently heavy to be out of reach of colliders. Let us focus on such a heavy DM candidate. The creation of such a hierarchy as given in Eq. 1.9 naturally leads us to a QCD-like theory where

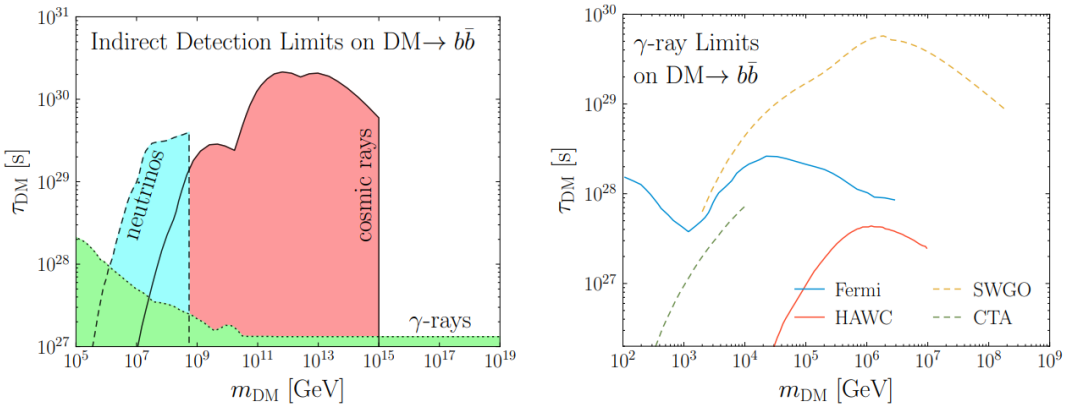

Figure 1.2: *Left:* A subset of current indirect detection constraints on the DM lifetime for decays to $\bar{b}b$ taken from Ref. [21]. The results in particular show limits obtained using -ray [22], neutrino [20], and cosmic-ray studies. *Right:* An example of the near-term improvements that will be achieved in γ-ray searches for heavy DM. For this specific channel ($DM \to b\bar{b}$), it is clear that SWGO will considerably improve reach on DM lifetime

such a hierarchy of scales for a TeV scale DM candidate would emerge easily. *Dark matter could be a proton-like state formed out of new light quarks interacting under a new strong dark force.* This new force called *dark colour* (DC), confining at a scale given by $\Lambda_{\rm DC}$, can be parametrized by the coupling constant $\alpha_{\rm DC}(\mu)$. For 3 dark colours and 2 dark flavours, a coupling value of $\alpha_{\rm DC}(\Lambda_{\rm UV}) \sim 2 \times 10^{-2}$ would give the required hierarchy $m_{DM}/\Lambda_{\rm UV} \sim 10^{-14}$ for a TeV scale dark matter. Let us comment also on the mechanism required to produce such a $10 - 100$ TeV scale DM. Thermal freeze-out for such a proton-like DM candidate gives a value of $\Lambda_{\rm DC} \sim 100$ TeV[3]. It is an interesting coincidence that the bound from DM stability on Planck mass suppressed $D = 6$ operators gives the same value of m_{DM} as the one obtained from requiring that such a proton-like DM behaves like a thermal DM candidate. The second part of the thesis explores this theme and the details can be found in Chapters 5 and 6. Note that such a heavy DM candidate will be probed by future indirect detection experiments like CTA and SWGO (see right plot in Fig. 1.2).

II) Hierarchy for conformality

A large separation of energy scales in a theory $\Lambda_{\rm IR} \ll \Lambda_{\rm UV}$, where $\Lambda_{\rm IR}$ is some IR scale while $\Lambda_{\rm UV}$ is some UV scale, would imply that the energy dependence of physical quantities at $\Lambda_{\rm IR} \ll E \ll \Lambda_{\rm UV}$ would be small. This corresponds to approximate scale invariance in the theory.

We could envisage an extension of the SM that has this scale-invariant property. Such a scale-invariant extension of the SM would not have particle-like excitations [24]. In order to experimentally probe such an NP extension, the scale invariance is at most approximate and it must be broken. Any interaction of this NP sector with the non-scale invariant SM would break this symmetry. Introducing a mass gap $\Lambda_{\rm IR}$ in this sector would also imply breaking the scale invariance, below which the spectrum can contain particle degrees of freedom.

A possible dark sector with a large separation of scales $\Lambda_{IR} \ll \Lambda_{UV}$ can be approximated as a scale-invariant sector at energies far from the two scales $\Lambda_{IR} \ll E \ll \Lambda_{UV}$. Production directly in the scale-invariant regime would mean that any energy dependence on the thresholds can be neglected. These sectors interacting via irrelevant portals with the SM can be experimentally probed at various

[3]In the large N limit, baryonic DM mass $\sim N\Lambda_{\rm DC}$ where N is the number of dark colors.

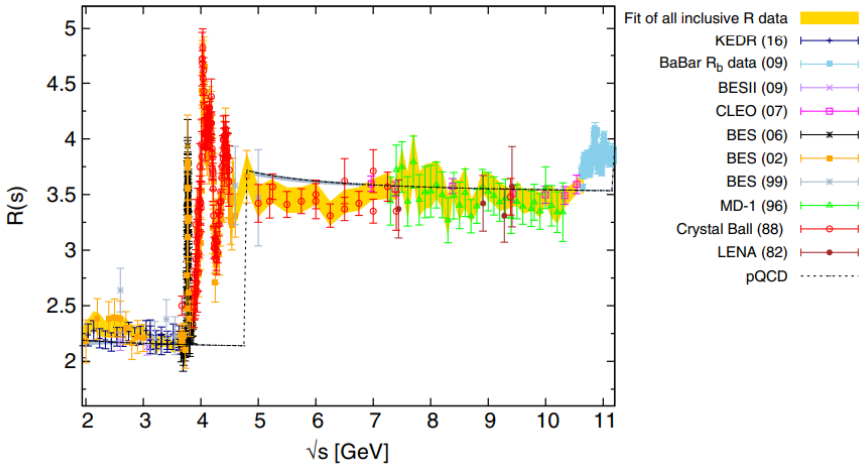

Figure 1.3: Compilation of inclusive data in range for hadronic R-ratio $R(s)$ [23].

terrestrial experiments [25]. In the first part of this thesis, we use such a framework in order to study such approximately scale invariant sectors at neutrino oscillation experiments, details can be found in Chapters 3, and 2.

In this context, we should also highlight another interesting property of QCD: predictability in the $E \to \infty$ limit away from thresholds. The cross-section for $e^+e^- \to$ hadrons in the high energy limit can be written in terms of the hadronic R- ratio:

$$\sigma(e^+e^- \to \text{hadrons}) = R(s) \times \sigma(e^+e^- \to \mu^+\mu^-) \tag{1.10}$$

with $R = N_c \sum_i Q(q_i)^2$ in the high energy limit. This can be seen in Fig. 1.3.

This same idea will form the skeleton of the first part of the thesis, where computing dark sector production cross-section at energies far from the thresholds can be done without many model assumptions.

Overview of this Thesis

The work in this thesis attempts to account for New Physics in two complementary ways. Part I, based on Ref. [26] extends the Standard Model (SM) with a putative new sector which is SM-neutral and light $\sim \mathcal{O}$(MeV). Whereas part II of the thesis, based on Refs. [27, 28], involves extending both the SM matter and SM gauge group with a new QCD-like strong force as well as new SM-charged fermions which gives a dark sector with heavy dark matter $\sim \mathcal{O}$(100 TeV). The backbone of this thesis involves recycling ideas from the SM itself as a way to search for NP, in particular from QCD itself as were highlighted in this chapter.

Part I

How to probe a light dark sector and not care too much about the model

Chapter 2

Introduction to Part I

In this chapter, we will lay out the main foundation for the discussion in Chapter 3. We will introduce hidden sectors and eventually focus on irrelevant portal hidden sectors. We will view the main strategy used for drawing constraints and results in the next chapter, highlighting its strengths and weaknesses.

2.1 Hidden Sectors

Entire "hidden" or dark sectors with very tiny couplings to the SM have the extraordinary potential to address the most pressing problems in particle physics. We already saw in Chapter 1 how such hidden or dark sectors can provide alternative solutions to heavy new physics for solving the hierarchy problem in the SM. Such hidden sectors comprise any new physics with non-SM matter not interacting with any SM force and can arise robustly within the QFT framework. (For complete reviews on motivations and models, see Ref. [29, 30]) In addition, they can also arise in top-down theoretical considerations like string theory. (See [31] for example)

The feeble nature of the couplings of these sectors may lead one to regard them as inconsequential. Interestingly enough, this *feebleness* can be the key to their discovery. The lifetime of any decaying particle $\tau = \Gamma^{-1} \propto \kappa^{-2}$ where Γ is the decay width of the particle and κ is the strength of interaction between the new hidden sector and SM. For a small value of κ, the hidden sector particles would be **long-lived** particles (LLPs). This means such invisible LLPs can be discovered in detectors placed far from the interaction or collision point - free from the SM background. It is already clear that with the plethora of terrestrial experiments including high-energy colliders, high-intensity experiments as well as future-forward experiments, we can hope to explore the entire parameter range for these LLPs (See Fig. 2.1 for an overview of how different experiments cover the LLP parameter space).

These hidden sectors need to be categorized and this can be systematically done in terms of *portals* mediating the SM-DS interaction. Any general portal can be written as:

$$\mathcal{L}_{\text{portal}} = \sum \mathcal{O}_{\text{SM}} \times \mathcal{O}_{\text{DS}} \tag{2.1}$$

where $\mathcal{O}_{\text{SM}}$ is an operator composed of SM fields whereas $\mathcal{O}_{\text{DS}}$ is an operator comprising dark or hidden fields and the summation implies a variety of portals going over many dimensions. In fact, the portals can then be arranged in terms of their dimensionality D. The most common and well-studied lowest-dimension portals are given below:

$D \leq 5$ Portal	NP Particle	Operator
Vector	Dark photon	$-\frac{\varepsilon}{2\cos\theta_W} B^{\mu\nu} F'_{\mu\nu}$
Higgs	Dark scalars	$(AS + \lambda S^2) H^\dagger H$
Axion	Pseudoscalars	$\frac{a}{f_a} F^{\mu\nu}\tilde{F}_{\mu\nu}$, $\frac{a}{f_a} G_{i\mu\nu}\tilde{G}_i^{\mu\nu}$, $\frac{\partial_\mu a}{f_a}\bar{\psi}\gamma^\mu\gamma^5\psi$
Neutrino	Sterile neutrinos	$y_N N L H$

where $B^{\mu\nu} \equiv \partial_\mu B_\nu - \partial_\nu B_\mu$ is the hypercharge field strength tensor, $F'_{\mu\nu} \equiv \partial_\mu A'_\nu - \partial_\nu A'_\mu$ is the field strength tensor of the $U(1)_D$ dark vector boson, H is the SM Higgs doublet, L is a SM lepton doublet of any generation, $F_{\mu\nu}(G_{i\mu\nu})$ are the field-strength tensors of the SM photon (gluon) field while ψ stands for any SM fermion. Each of these SM gauge singlet operators $\mathcal{O}_{\rm SM}$ serves as the *portal* to the DS by coupling to the dark fields (in the table above): a vector A', a scalar S, a pseudoscalar a, a fermion N. All the portals given above are renormalizable except the axion portal which is non-renormalizable with $D = 5$. These minimal renormalizable portals can be generalised to irrelevant or $D \geq 5$ case by picking general operators with higher dimension on the DS side, $\mathcal{O}_{\rm DS}$, instead of single fields.

We will not review these commonly studied portals here. The reader is directed to any of the following comprehensive reviews, and main papers on these portals: See Refs. [32, 33] for dark photon, Ref. [34] for dark scalar case, for axion portal ($D = 5$) Refs. [35–41] (see [42] for a study specific to neutrino experiments), See Ref. [29, 30, 43] for a review on these portals.

In this part of the thesis instead, we concentrate on higher dimension portals with dimension $D > 5$. It is interesting to note that for $D = 4$ portals, for the SM-DS interaction to be weak, the portal coupling should be small: any of the coefficients ε , λ , y_N appearing in the portals in Table 2.1 must have value $\ll 1$. Whereas, for the case of irrelevant or $D \geq 5$ portal, this *interaction coupling is naturally weak* due to suppression coming from the UV scale in the portal.

Next, we will review the main probes to constrain hidden sectors and then discuss the motivations to probe portals with $D > 5$.

2.2 Common Experimental Probes of Dark Sectors

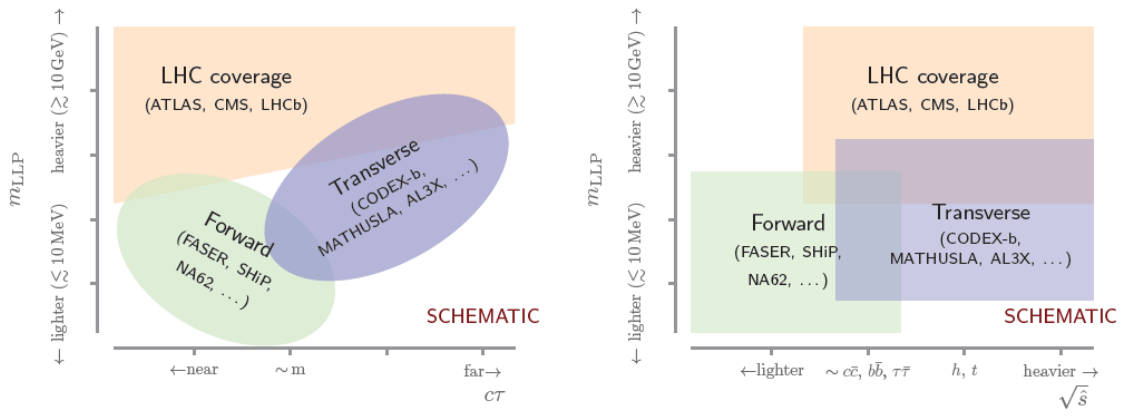

Figure 2.1: Schematic summary of reach and coverage of current, planned or proposed experiments in terms of the LLP mass, lifetime and the required parton center-of-mass energy, $\sqrt{\hat{s}}$ taken from [44].

- *At proton colliders:* Dark sector particles with large branching ratios originating from Higgs, Z boson can be copiously produced at high energy colliders running at large centre-of-mass energies. These probe dark sectors in the GeV range produce very collimated SM jets due to the large boost of the DS particle. For details on search strategies of strongly coupled hidden sectors at LHC, see Ref. [45].

- *At high intensity experiments:* Hidden sector particles below the electroweak scale can be copiously produced at low-cost experiments (with respect to high energy colliders or more futuristic LLP experiments like MATHUSLA which require more capital investment) at the intensity frontier. Such experiments generally have center-of-mass energies much lower than the typical high-energy collider machines. Such high-intensity experiments involve a proton or electron beam (or even muon beam, see ref. [46–48] for future proposals of fixed target experiments with a muon beam) hitting a fixed target, producing a high flux of SM particles alongside a beam of putative DS particles (see ref. [49–54] for general reviews on the capabilities of high-intensity experiments).

- *At neutrino oscillation experiments:* These come under high intensity experiments but due to the huge neutrino experiment program in progress and their multi-purpose nature, we class them as separate probes. Short and long-baseline neutrino experiments happen to be placed behind some of the most powerful proton beams up to date. Thus, they provide an ideal (and low-cost) and pre-existing infrastructure for probing low scale dark sectors. Further, a rich short-baseline experimental program for neutrinos has been planned at Fermilab (e.g. DUNE, SBNP, see ref. [55–57] for experiment details, ref. [58–60] for recent studies on DS search at these experiments). These new proposals will improve upon the current neutrino experiments, using a higher number of protons on target (POT), and better detectors that can help in reducing SM background [61], therefore leading to an increased sensitivity for DS searches.

- *At Forward and future LLP experiments:* Apart from neutrino experiments, a natural setup to probe DS is at future experiments proposed for long-lived particle (LLP) searches (e.g. see [30, 62] for a review). See also [63] for first run results from FASER which reported no signal events for a DS search.

In Fig. 2.1, we see an overview of how the different experiments probe the LLP/hidden sector parameter space. In the next section, we narrow down to irrelevant portal dark sectors - the focus of this part of the thesis and make the cases for probing these scale-suppressed portals with dimensionality $D > 5$.

2.3 Why Look for Irrelevant Dark Sectors

While the case of renormalizable with $D \leq 4$ and axion portals with $D = 5$ has been widely covered in literature, generic non-renormalizable portals with $D \geq 5$ have been covered in a less exhaustive way. Here we will make a case for irrelevant portals. In this section, we will demonstrate the properties of irrelevant portals that will allow us to construct a *model agnostic* strategy - something not possible for the relevant case.

Let us look at two generic DS-SM portals which could be in the new physics Lagrangian:

$$\mathcal{L} \supset \kappa \, \mathcal{O}_{\rm SM} \, \mathcal{O}_{\rm DS} + ... + \frac{\kappa'}{\Lambda^2_{\rm UV}} \mathcal{O}'_{\rm SM} \, \mathcal{O}'_{\rm DS} \, , \tag{2.2}$$

where κ, and κ' are dimensionless couplings, the first term is a marginal portal with $D = 4$ or $[\mathcal{O}_{\rm SM}] + [\mathcal{O}_{\rm DS}] = 4$. This can be mapped onto any of the marginal scenarios discussed previously, for example the dark scalar case would imply $\mathcal{O}_{\rm SM} = H^\dagger H$ and $\mathcal{O}_{\rm DS} = S^2$. Let us look at the last term in this hypothetical NP scenario which has $D = 6$ or $[\mathcal{O}_{\rm SM}] + [\mathcal{O}_{\rm DS}] = 6$. Based on naive dimensional analysis (NDA), we can write the cross-section for production of DS from SM particles for the two cases as:

$$\sigma_{D=6} \sim \sum_{threshold} \frac{4\pi\kappa^2}{\Lambda_{\rm UV}^4} E^2 \qquad \sigma_{D=4} \sim \sum_{threshold} \frac{4\pi\kappa'^2}{E^2} \tag{2.3}$$

where E is the energy at which we are probing this NP scenario. Here $\sum_{threshold}$ sums all the infrared threshold contributions in the total cross-section σ. These contributions can come from weakly coupled single particle states or else bound states (hadronic resonances in the case of a strongly coupled theory or "positronium" like bound states for weakly coupled theory).

It is clear that at low energies $E \ll \Lambda_{\rm UV}$ the DS production cross section from the irrelevant portal will not be significant. Both at high E and for low $\Lambda_{\rm UV}$ however, the $\sigma_{D=6}$ contribution could become important. It is clear that $\sigma_{D=6}$ will clearly *grow with the energy of the experiment.* If we want to translate this to an experimental distribution, this would mean that the bulk of events would be expected at high energies.

Let us look at concrete scenarios of both an irrelevant DS-SM portal and a marginal/relevant portal. For the irrelevant portal scenario, we pick the following portal with overall portal dimension $D = 6$ [25]:

$$\frac{\kappa}{\Lambda_{\rm UV}^2}(\bar{e}_R\gamma^\mu e_R)(\bar{\chi}\gamma_\mu\gamma^5\chi) \tag{2.4}$$

where a free SM-neutral Majorana fermion χ couples to the SM electronic current $(\bar{e}_R\gamma^\mu e_R)$. The dark UV theory has a scalar ϕ which can decay to $\bar{e}_R\chi$ via its Yukawa coupling. [1] The portal in Eq. 2.4 is generated after integrating out the mediator ϕ for $m_\phi \gg m_\chi$. For a stable χ, this portal can be constrained in missing energy searches at LEP2 in e^+e^- collisions by the OPAL [64] and L3 collaborations [65]. Fig. 2.2a taken from Ref. [25] shows the differential number of events for the process $e^+e^- \to DS + \gamma$ as a function of the recoil mass to the photon system [2] for this particular portal. *It is clear from this case that the contribution to the DS production cross-section is larger for large DS invariant mass (or photon recoil mass).*

Let us now contrast this with the case of an *unparticle* hidden sector portal discussed in [66] with overall portal dimension $D \lesssim 4$:

$$(H^\dagger H)(\mathcal{O}_{\rm DS}) \tag{2.5}$$

Here the $\mathcal{O}_{\rm DS}$ is a gauge invariant operator for a hidden sector with N_f scalars so concretely $\mathcal{O}_{\rm DS} = \phi_i^\dagger\phi_j$ with operator dimension close to 2 [3]. This hidden sector could be produced at high energy colliders like LHC via the partonic process $gg \to h^* \to DS$ where the hidden sector is produced via mixing with an off-shell higgs. Fig. 2.2b taken from Ref. [66] shows the production cross section for such a hidden sector and its variation with partonic energy s. *It is clear that the largest contribution to the cross-section comes from small values of s [66] in this case.* Because of the behavior of the total cross-section, threshold corrections cannot be ignored here. This is

[1] This hidden sector is similar to a simplified SUSY model with a neutralino χ and a selectron ϕ.

[2] This final state γ are produced due to initial state radiation (ISR) from the incoming electrons, positrons at LEP.

[3] This is a mass operator which develops small negative anomalous dimension so $[\mathcal{O}_{\rm DS}] \lesssim 2$.

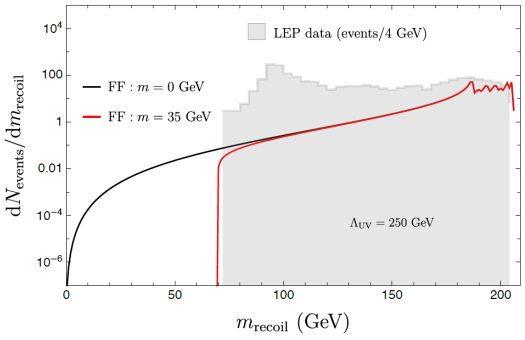

(a)

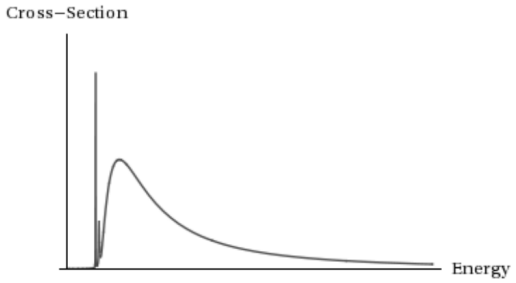

(b)

Figure 2.2: *Left:* Differential number of events for $e^+ + e^- \to \gamma + DS$ as a function of the recoil mass (equal to the DS invariant mass) at LEP. The black and red curves correspond to the DS with one Majorana fermion coupled to the SM through the D = 6 portal of Eq. 2.4. The portal coupling κ has been set to 1 and the mediator mass Λ_{UV} has been set to 250 GeV. The two curves correspond to two different masses of the DS fermion m shown in the plot [25]. *Right:* One possible shape for the cross-section $\sigma(s)$ to produce hidden sector particles given in Eq. 2.5, versus partonic energy taken from Ref. [66].

very different from the irrelevant portal discussed earlier where the total budget of the cross-section allows us to ignore infrared threshold corrections. This leads us to the next question:

Can we exploit this particular property of irrelevant portals to build a model agnostic framework?

Let us envisage a scenario in which the irrelevant dark sector in the example, is scale-invariant much above the mass gap, Λ_{IR} (mass of the dark fermion χ) [4]. If the energy $\sqrt{s}$ of an experiment that probes the DS is such that $\Lambda_{IR} \ll \sqrt{s} \ll \Lambda_{UV}$, the DS states are produced directly in the conformal regime. The cross-section to produce such a dark sector in the conformal regime σ_{DS} can be written in terms of two factorised out matrix elements[5] comprising the SM amplitude and associated phase space and the DS amplitude and phase space as:

$$\sigma_{DS} \propto \int d\Phi_{SM} |\mathcal{M}_{SM}|^2 \times \underbrace{\sum_n \int d\Phi_{DS} \left|\langle\Omega| \mathcal{O}_{DS} |n\rangle\right|^2}_{= 2\,\mathrm{Im}\left(i \langle\Omega| T\{\mathcal{O}_{DS}\mathcal{O}_{DS}\} |\Omega\rangle\right)} \tag{2.6}$$

where the DS operator $\mathcal{O}_{DS}$ interpolates a DS state $|n\rangle$ from vacuum $|\Omega\rangle$ and the integration is over the entire dark sector phase space $d\Phi_{DS}$. Here in the second step in Eq. 2.6, we have used the *optical theorem*. This optical theorem allows us to sum over the DS phase space in an inclusive manner and relates it to the imaginary part of the two-point function of the DS operator, which in the conformal regime is fixed by the scaling dimension of the operator as:

$$\mathrm{Im}\left(i \langle\Omega| T\{\mathcal{O}_{DS}\mathcal{O}_{DS}\} |\Omega\rangle\right) \propto (p^2)^{\Delta-2} \tag{2.7}$$

where Δ is the scaling dimension of the operator $\mathcal{O}_{DS}$. Inclusive DS production rates can be estimated using only the scaling dimension of the DS operator, along with the optical theorem. It is this property of a scale-invariant dark sector that we deem *model agnostic* since computing the

[4]The presence of a mass gap breaks scale invariance in the IR but we can still approximate the dark sector very well as a scale-invariant one at $\Lambda_{IR} \ll E \ll \Lambda_{UV}$

[5]The physics at long-distance scale will decouple from physics at short-distance scales

production cross-section does not require specifying the fields comprising the composite operator $\mathcal{O}_{\rm DS}$ [25, 26]. The next natural question is:

Can we get meaningful constraints for any dark sectors under this framework?

Under the conformal approximation, the E^2 behaviour of the cross-sections given in Eq. 2.3 is captured well, however, the infrared threshold corrections cannot be predicted under this approach.

It is clear that the importance of the infrared threshold contribution depends on the behavior of the cross-section with energy or indirectly on the overall dimensionality of the portal. In the relevant portal case of Fig. 2.2b, the resonances at threshold are given by weakly coupled bound states $\phi^\dagger\phi$. These contributions will become important due to the decreasing behavior of cross-section as seen in Fig. 2.2b. Similar threshold contributions for the irrelevant portal case in Fig. 2.2a will not be important in the total cross-section as the bulk of events is coming from energies much larger than the thresholds.

More information regarding the hidden sector model and conformal symmetry breaking would be required before saying anything meaningful in this case. Thus, we see that *the prediction from conformal dynamics is only reliable if all the kinematics of the hidden sector lies much above the mass gap, or m_S in this case* (See also [66]).

At this point, we can circle back to the irrelevant portal DS we discussed earlier in Eq. 2.4 and also Fig. 2.2a where the distribution is dominated by events from energies much above the two mass gap values, i.e. the conformal regime of the sector. There can be multiple other scenarios for such irrelevant portal dark sectors where the dark dynamics is well-captured by a conformal theory at energies $\Lambda_{\rm IR} \ll E \ll \Lambda_{\rm UV}$ with $\Lambda_{\rm IR}$ being the generic mass gap in the sector (where the conformal approximation is not good) and $\Lambda_{\rm UV}$ is the mediator between the SM and dark sector. Many examples of such sectors have been discussed in [25]. How to probe such sectors at neutrino oscillation experiments will form the first part of this thesis which is mainly based on Ref. [26].

2.4 Caveats in our Strategy

So far we have lauded the conformal approximation approach for its implicit model agnosticism, but in this section, we will elaborate on the possible caveats such *model agnostic* approaches tend to suffer from.

I) Living without mediators ?

Hidden valleys [31] (HV) are a popular scenario of irrelevant portal DS in literature. These involve models of strongly coupled new dynamics that interact with the SM via irrelevant portals. They were theorized with the hope of discovery at LHC (or Tevatron) by the open production of their TeV scale mediators. In Fig. 2.3, the cross-section for the production of hidden valley particles can be seen as a function of the center of mass energy E_{cm}. The production cross section is enhanced due to resonance at the mass of the mediator Z', $m_{Z'} = 1$ TeV. By now Hidden Valley models have come to include a much larger class of models motivated by various BSM scenarios and with a much wider phenomenology (for example see Ref. [45]). The key point here is that *discovery of hidden valley irrelevant dark sectors was anticipated based on the open production of their heavy mediators. Could the discovery of the light hidden sector precede that of the heavy mediators?* This is the question we have tried to address here in this part of the thesis [26] (See also [25]). We will

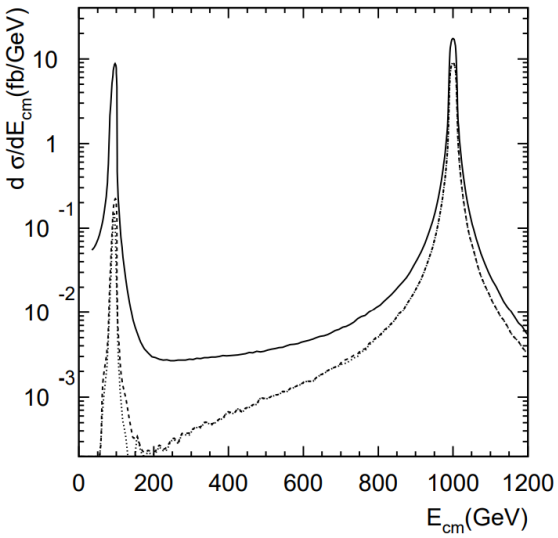

Figure 2.3: Differential cross-sections for hidden valley particles as a function of partonic c.m. energy $\sqrt{s}$. The solid curve represents the inclusive cross-section without acceptance cuts, the dashed is with the trigger requirements [67]

consider DS-SM portals generated after integrating out the heavy mediators and probe the dark sector directly in the scale-invariant regime.

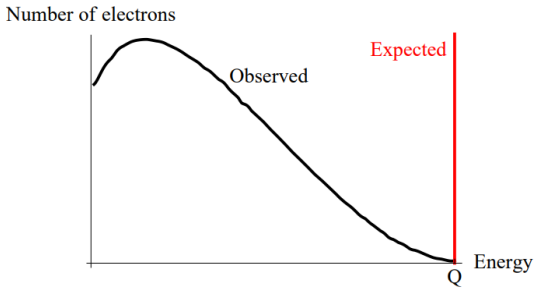

(a) Continuous energy spectrum of electrons emitted in β decay which pointed to the existence of neutrinos - an analogy of discovery of a dark sector in its conformal regime (described in the main text).

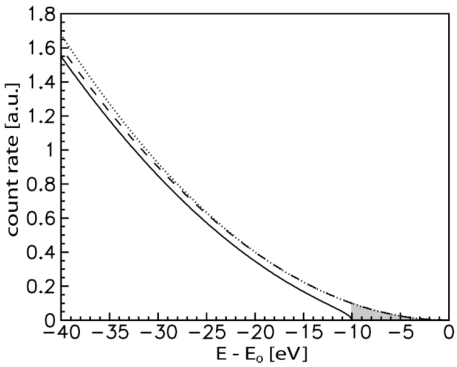

(b) Figure taken from Ref. [68] to show how non-zero mass of neutrino affects the endpoint of the beta spectrum. The dotted and the dashed lines correspond to $m(\nu_e) = 0$, the solid line to $m(\nu_e) = 10$ eV.

Figure 2.4

Living in a world described by an effective field theory (EFT) where the heavy mediators have been integrated out, comes with a disadvantage: constraints tend to become weak (and conservative). Any experimental data must be interpreted under the effective field theoretic perspective bin by bin. The momentum flowing in the contact interaction or DS invariant mass $p_{\rm DS}$ cannot exceed the mass of the mediator $\Lambda_{\rm UV}$. Imposing $\frac{p^2_{\rm DS}}{\Lambda^2_{\rm UV}} \ll 1$ on the experimental data implies getting rid of any possible signal in experimental data bins with energy close to $\Lambda_{\rm UV}$ as our EFT loses validity (See Ref. [25, 69]).

Fermi's theory: Let us draw some parallelisms with the Fermi's theory of weak interactions

and the discovery of neutrinos. The continuous energy spectrum of electrons in the beta decay $n \to p + e^- + \bar{\nu}_e$ (shown in Fig. 2.4a) first led Pauli to postulate the existence of neutrinos in 1930. Infact, neutrinos can be seen as a dark sector produced by a dimension-6 four-fermion operator made of *visible* matter and *invisible* neutrino sector:

$$\bar{p}\gamma^\mu(1-\gamma_5)n\bar{e}\gamma_\mu(1-\gamma^5)\nu_e \equiv \mathcal{O}_{\rm vis}\nu_e$$

Indeed, the neutrino discovery via beta decay can be compared to the production of a conformal dark sector as we now explain. The beta decay energy spectrum and the endpoint of the energy distribution in Fig. 2.4a is dominated by the kinematic phase space information and is limited by $(m_n - m_p)^2$ with m_n and m_p being the mass of neutron and proton respectively. In fact, the endpoint of this energy distribution which led to the discovery of the *then "dark" sector* is much below the UV threshold - for the weak interaction (we now know) that the mediators are W bosons hence $\Lambda_{\rm UV} = m_W = 80$ GeV. The IR scale instead is the neutrino mass so $\Lambda_{\rm IR} = m_\nu$ hence we see that in some sense *the neutrinos were discovered first in their conformal regime* $m_\nu \ll \sqrt{s_\beta} \ll m_W$ where $\sqrt{s_\beta} \sim m_n - m_p$. For a truly conformal neutrino sector $m_\nu = 0$, the non-zero mass can affect the energy spectrum, but this effect is very small as can be seen from the Fig. 2.4b [68]. In this case, the threshold effects do not change the prediction. Thus, the beta decay and the eventual discovery of neutrinos form a toy conformal dark sector, analogous to the dark sectors discussed in the sections in this part.

II) Do distribution functions favour conformal behavior/approximation?

The naive dimensional analysis expectation for an irrelevant portal cross-section points to growth with energy. We can also see this in Fig. 2.5b where we have plotted the differential cross-section for $d\sigma(q\bar{q} \to DS)/dp^2_{\rm DS}$ for a dimension 6 portal of the form

$$(1/\Lambda^2_{\rm UV})\mathcal{O}_{\rm DS}\mathcal{O}_{\rm SM}.$$

Here, $p^2_{\rm DS}$ is the squared invariant DS mass. But note, that at LHC, we observe the process $p\bar{p} \to DS$ meaning the partonic cross-section $\sigma(q\bar{q} \to DS)$ must be folded with the partonic distribution functions (PDFs). The cross-section for $p\bar{p} \to DS$ can be schematically written in terms of the partonic cross-section and PDFs in the standard way as:

$$\sigma_{\bar{p}p\to DS} = \int dp^2_{\rm DS} \frac{d\sigma_{q\bar{q}}}{dp^2_{\rm DS}} \int \frac{dx}{x} f_q\left(\sqrt{p^2_{\rm DS}}, x\right) f_{\bar{q}}\left(\sqrt{p^2_{\rm DS}}, \frac{p^2_{\rm DS}}{xs}\right) \tag{2.8}$$

where $f_q(Q,x)$ and $f_{\bar{q}}(Q,x)$ are the usual partonic distribution functions for the corresponding partons carrying the momentum fraction x at a scale Q. Let us further write the relevant PDFs contribution to $\sigma(pp \to DS)$ as the partonic weight W defined in the usual way in literature (see [70]):

$$W_{\bar{q}q}\left(s, \sqrt{p^2_{\rm DS}}\right) = \int_{p^2_{\rm DS}/s}^1 \frac{dx}{x} f_q\left(\sqrt{p^2_{\rm DS}}, x\right) f_{\bar{q}}\left(\sqrt{p^2_{\rm DS}}, \frac{p^2_{\rm DS}}{xs}\right) \tag{2.9}$$

The partonic differential cross section for an arbitrary $D = 6$ portal producing DS, based on NDA can be written as:

$$\frac{d\sigma_{q\bar{q}}}{dp^2_{\rm DS}} \propto \frac{1}{s}\frac{p^2_{\rm DS}}{\Lambda^4_{\rm UV}} \tag{2.10}$$

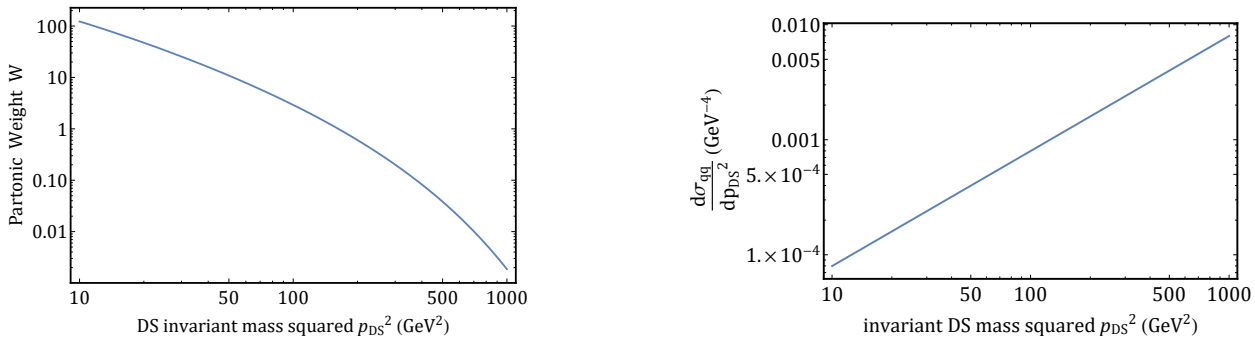

(a) **(b)**

Figure 2.5: *Left:* Partonic distribution functions or partonic weight distribution for the $pp \to DS$ cross-section where $\sqrt{s} = 1$ TeV. *Right:* Differential cross-section for $\bar{q}q \to DS$ as a function of $p_{\rm DS}^2$ for a $D = 6$ portal (we pick Z portal defined later in the thesis) growing with energy.

We can plot both the quantities in Eq. 2.9 and Eq. 2.10 as functions of $p_{\rm DS}^2$ in Figs. 2.5a and 2.5b.

From Fig. 2.5a, we can see that *PDFs tend to bias the lowest accessible energy at high-energy colliders*, thereby a convolution of the partonic cross-section and partonic weight in Eq.2.9 and Eq.2.10 does not truly grow with energy (See also Fig. 3.1 for Drell-Yan production of DS which is the convolution of the two). Thus, the measured cross section or observed events for $pp \to DS$ for irrelevant portal at experiments may not always follow a strict growth with $\sqrt{s}$. Of course, the conformal approximation is much more pathological in the relevant/marginal portal case as we have pointed out so far and as is clear from the Fig. 2.2b. This $pp \to DS$ behavior is also in sharp contrast with measured events at an e^-e^+ collider LEP for the dimension-6 portal shown in Fig. 2.2a which did grow with energy. This strict growth feature is not *visible* at a possible measurement at proton-proton pp colliders or beam dump experiments where the cross-section involves interaction between protons in the beam with protons/neutrons in the target. In our analysis, to consider events only in the conformal regime, we impose a lower cut on the $p_{\rm DS}^2$ such that we only include events compatible with $p_{\rm DS}^2/\Lambda_{\rm IR}^2 > 1$ only. However, note here again that a DS with a mass gap given by $\Lambda_{\rm IR}$ cannot have invariant mass lower than $n\Lambda_{\rm IR}$ where n is the number of lightest DS particles produced in any DS search. We find that this kinematic condition on $p_{\rm DS}^2 > n^2\Lambda_{\rm IR}^2$ almost always takes care that we consider events in the conformal regime. (See also discussion in B.3)

Alternatively, there can be scenarios where due to kinematics, the DS invariant mass or $p_{\rm DS}$ is fixed. This can be the case for Higgs resonant DS production $h \to DS$ where the SM Higgs h can decay to dark sector particles. Infact, Ref. [25] concluded that the strongest constraints at LHC can be derived from such processes for irrelevant portal conformal dark sectors. (See Fig. 5 for example in [25]). Mesons decaying only to DS given by $V \to DS$ is also an example where $p_{\rm DS}$ gets fixed by $p_{\rm DS}^2 = m_V^2$ where m_V is the meson mass. See detailed analysis in Section on Annihilation decays and text around Eq. 3.15. Despite the cross-section growth with $p_{\rm DS}^2$ is not always very obvious in production modes like Drell Yan in Fig. 3.1, note that for the bremsstrahlung production mode, the bulk of the contribution to the cross-section comes from the peaks at $p_{\rm DS} \gg \Lambda_{\rm IR}$ from the mixing with ρ and ω mesons.

At this point, we have outlined how we can construct a model-agnostic framework for constraining scale-suppressed irrelevant portal dark sectors interacting with the SM based on conformal approximation. We have also highlighted why this cannot be used as a probe for relevant portals

using concrete examples. In the next chapter, we will describe our strategy more in detail and give specifics on the particular portals that we constrain at neutrino oscillation experiments.

Chapter 3

Searching for Dark Sectors at Neutrino Experiments

In this chapter based on Ref. [26], we probe SM-neutral dark sectors that interact via irrelevant portals with the SM at neutrino oscillation experiments. On general principles we are led to $D \sim 5$ and $D \sim 6$ portals. Such dark sectors are in general *very elusive* due to the irrelevant nature of the portal. The results presented here are complementary to the constraints from current high energy terrestrial experiments and astrophysical data, presented in [25], and in specific cases, much stronger, as we point out in the relevant sections.

In this chapter we consider various (inclusive) DS production processes. Depending on the DS 4-momentum $p_{\rm DS}$, a different production process can be relevant: meson decays (for $\sqrt{p_{\rm DS}^2} \lesssim {\rm M}$, the parent meson mass), direct partonic production (for $\sqrt{p_{\rm DS}^2} \gtrsim \Lambda_{\rm QCD}$) or dark bremsstrahlung (for $\sqrt{p_{\rm DS}^2} < \Lambda_{\rm QCD}$). We require the DS states to be produced away from any mass thresholds, which allows estimating the rates based on general principles. DS particles once produced are required to decay to SM particles inside the neutrino near-detectors placed generally $\sim \mathcal{O}(100{\rm m})$ downstream from the target[1].

Compared to [39, 71] in this chapter, we study a more complete set of operators, both in production and decay of DS particles. We perform a detailed study of production modes through irrelevant portals, such as dark bremsstrahlung and partonic production, that have either been neglected or only considered partially [71–73]. We find that the bremsstrahlung mode can be comparable to other modes and is necessary for a complete analysis. Compared to [25, 74] we focus on high intensity experiments, particularly on neutrino and other proton dump experiments that were not considered previously in this framework. We do so by adopting the model agnostic strategy outlined in [25]. More importantly, this allows us to put bounds on *strongly coupled* light dark sectors through irrelevant portals, which as far as we know is not a thoroughly studied scenario at high intensity experiments (except in [25]. See [74–77] and references therein for searches at collider experiments). Strongly coupled GeV-scale DS are relevant in frameworks containing composite resonances from a new gauge group, such as composite versions of Asymmetric Dark Matter [78–80], Mirror world models [81, 82], some incarnations of the Twin Higgs paradigm [4] and are a natural realization of the Hidden Valley scenario [31].

The outline of the chapter is as follows: in section 3.1 we describe the dark sector portals and the relevant model agnostic framework for estimating inclusive rates, lifetime and multiplicity of DS particles, also pointing out the mild model dependent assumptions we have to make to proceed.

[1] Far detectors are less constraining due to a very small angle subtended to the interaction point.

In section 3.2 we describe various DS production processes relevant at neutrino experiments, while in section 3.3, we give an overview of the neutrino experiments we use to constrain the parameter space, and describe our strategy for estimating signal events from DS decaying inside the neutrino detector. Our results and bounds can be found in Section 3.4 with a discussion and summary in section 3.5. Appendices A,B,C,C.1 and C.2 contain technical details.

3.1 Portals and Model Agnostic Strategy

In this section we discuss the relevant theoretical details for studying dark sectors with irrelevant portal to the SM. The emphasis is towards being as model agnostic as possible, and only allowing for minimal model dependence where necessary. We point out the assumptions we have to make at various stages for this. This section and the following chapter build upon the model agnostic approach first undertaken in [25], wherein more details can be found.

Dark sectors with portal interactions to the SM from irrelevant operators can be generated in a large class of models, generically by exchange of heavy mediators charged under both the SM and the DS. The general form of such a portal is

$$\frac{\kappa}{\Lambda_{\rm UV}^{D-4}}\mathcal{O}_{\rm SM}\,\mathcal{O}_{\rm DS}\,, \tag{3.1}$$

where $\Lambda_{\rm UV}$ is the mass scale of the heavy mediator, κ is a dimensionless coupling, and $\mathcal{O}_{\rm SM}$ ($\mathcal{O}_{\rm DS}$) are local operators made of SM (DS) degrees of freedom. The dimensionality of portal $D = [\mathcal{O}_{\rm SM}]+[\mathcal{O}_{\rm DS}]$ is greater than 4 for irrelevant portals. States in the DS are further characterized by a mass gap $\Lambda_{\rm IR}$, and the dynamics between the scales $\Lambda_{\rm UV}$ and $\Lambda_{\rm IR}$ is approximately scale invariant. A large hierarchy between these scales is a working assumption of this scenario. In order to avoid strong constraints, we also assume that the portal preserves both CP and flavor symmetries of the SM.

The most constraining portals are expected to be those with lowest dimension D. In concrete examples of such DS, both weakly and strongly coupled, the two lowest dimension DS operators are a scalar operator $\mathcal{O}$ (of dimension $\Delta_{\mathcal{O}} \lesssim 4$) and a conserved current operator $J_\mu^{\rm DS}$ (of dimension 3). While the dimension of a conserved current operator is fixed to be 3 in 4D, the reason to take the scalar slightly marginal is to ensure that the condition $\Lambda_{\rm IR}/\Lambda_{\rm UV} \ll 1$ is realized naturally. We will consider $\Delta_{\mathcal{O}} = 3, 4$ in this chapter. Specific to a given model there can be other operators that generate portals to the SM. However in the absence of a symmetry, their dimension is either unprotected or requires additional assumptions about the DS. We will therefore limit ourselves with only a current and a scalar operator on the DS side. The gauge invariant operators on the SM side that can be used to make a portal operator, with increasing scaling dimension, are $H^\dagger H$ and $J_\mu^{\rm SM} = \bar{f}\gamma_\mu f$, $\bar{f}\gamma_\mu\gamma^5 f$, $f = l, q$ or $J_\mu^{\rm SM} = H^\dagger i\overleftrightarrow{D}_\mu H$ (see table 1 in ref. [25] for a complete list of scenarios) [2]. The lowest dimension Lorentz invariant combinations are then $J_\mu^{\rm DS}\, J_{\rm SM}^\mu$ and $\mathcal{O}\, H^\dagger H$. In the unitary gauge, $H^\dagger i\overleftrightarrow{D}_\mu H \sim Z_\mu$ so that for this portal the interactions with the DS proceed through a Z-boson. We will refer to this as the *Z portal*. At the energy scales relevant at neutrino experiments, Z is never produced on-shell, so we can integrate it out and generate an effective JJ operator where now the SM current is the one that couples to Z. Therefore, considering JJ portals

[2]Note that we do not study the fermionic portal given by coupling the DS with $\mathcal{O}_{\rm SM} \equiv lH$. Such a DS can be realised in a strongly coupled theory (See Ref. [83]) with a gluequark (χ) - an exotic bound state of a dark fermion and dark gluons which can interact with the SM via the portal $(lH)(\mathcal{G}^a_{\mu\nu}\sigma^{\mu\nu}N^a)$ where N is a majorana dark fermion transforming in the adjoint of $SU(N)_{DC}$ with SM quantum numbers $= (1,1)_0$ and $\mathcal{G}_{\mu\nu}$ is the dark gluon field strength tensor. This portal is responsible for the stability of χ - a DM candidate, hence, the $\Lambda_{\rm UV}$ scale suppressing it must be $\sim 10^{18}$ GeV. It is evident that studying this portal requires addressing subtle model dependent issues, thus, we do not pursue this portal in this work.

where the SM current is either generic or the one for Z, we cover all possibilities. We will refer to these as the *generic* JJ portal and the *Z-aligned* JJ portal respectively.

Hence the lowest dimension portals that can be formed are

$$\begin{aligned}\mathcal{L}_{\text{portal}} &= \frac{\kappa_{\mathcal{O}}}{\Lambda_{\text{UV}}^{\Delta_{\mathcal{O}}-2}}\mathcal{O}H^\dagger H + \frac{\kappa_J}{\Lambda_{\text{UV}}^2}J_\mu^{\text{DS}}J_{\text{SM}}^\mu + \frac{\kappa_Z}{\Lambda_{\text{UV}}^2}J_\mu^{\text{DS}}H^\dagger i\overleftrightarrow{D}^\mu H \\ &= \frac{\kappa_{\mathcal{O}}}{\Lambda_{\text{UV}}^{\Delta_{\mathcal{O}}-2}}\mathcal{O}H^\dagger H + \frac{\kappa_J}{\Lambda_{\text{UV}}^2}J_\mu^{\text{DS}}J_{\text{SM}}^\mu + \frac{\kappa_Z}{\Lambda_{\text{UV}}^2}\frac{v_{\text{EW}}}{m_Z}J_\mu^{\text{DS}}J_{\text{SM, Z}}^\mu\,, \end{aligned} \tag{3.2}$$

where $\kappa_{\mathcal{O}}, \kappa_J, \kappa_Z$ are dimensionless coefficients, v_{EW} is the electroweak VEV and in the second line we have integrated out Z, which couples the DS current to $J^\mu_{\text{SM, Z}}$, the SM current that couples to the Z boson where we are including the $g_2/\cos\theta_W$ coupling of the Z boson current in $J^\mu_{\text{SM, Z}}$. The three terms in eq. (3.2) are the Higgs portal, the generic JJ portal and the Z portal respectively. It is clear that a Z-aligned JJ portal can be obtained from the Z-portal with a rescaling: $\kappa_J = \kappa_Z(v_{\text{EW}}/m_Z)$. For $\Delta \lesssim 4$, all these portals are of dimension $D \sim 6$. In principle, a DS described by a local QFT also possesses a stress-energy tensor $T^{\mu\nu}_{\text{DS}}$ of dimension 4, that can be used to build dimension 8 operators with SM dimension 4 operators. However, given a larger suppression compared to the dimension 6 portals in (3.2), the bounds on them are too weak to be of any interest.

If the energy $\sqrt{s}$ of an experiment that probes the DS is such that $\Lambda_{\text{IR}} \ll \sqrt{s} \ll \Lambda_{\text{UV}}$, the DS states are produced directly in the conformal regime. Inclusive DS production rates can be computed using the optical theorem depicted in in Eq. 2.6 described in the previous chapter in Sec. 2.3.

While for irrelevant portals, the matrix element does not decrease with energy (See Fig. 2.5b also)(specific behavior depends on the production mode), this needs to be convolved with the structure functions (e.g. the pdfs/form-factors/splitting functions, depending on the production channel), and this changes where the bulk of events come from (See also discussion around Eq. 2.9 in Sec. 2.3 of the previous chapter). As long as the involved p_{DS} values are away from $\Lambda_{\text{UV}}, \Lambda_{\text{IR}}$, one can ignore the events near the thresholds in a self-consistent manner. Relatedly, the two point function of $\mathcal{O}_{\text{DS}}$ will also depend on the ratio $\Lambda^2_{\text{IR}}/p^2_{\text{DS}}$ and $p^2_{\text{DS}}/\Lambda^2_{\text{UV}}$. For self-consistency, we again need both these ratios to be small. In particular, the condition $p^2_{\text{DS}}/\Lambda^2_{\text{UV}} < 1$ effectively ensures the mediators of mass Λ_{UV} are not directly produced and the effective local operator for the portal is a good description. In ref. [25], this was enforced by ensuring that the obtained bound on Λ_{UV} always satisfies this condition for the highest p^2_{DS} used in the calculation. In practice, this effectively resulted in a lower limit on the parts of Λ_{UV} ruled out, or completely invalidated certain bounds. As we will see, for neutrino experiments, where the involved energy is much smaller than LHC or LEP, this condition is less detrimental. By restricting to $\Lambda_{\text{UV}} \gtrsim 50$ GeV, we are able to get useful bounds as well as be consistent with the EFT condition. The condition on Λ_{IR} on the other hand needs to be imposed, which we do for each production mode.

After production, the DS states will interact and decay among each other, and eventually all the DS degrees of freedom would decay to the *Lightest Dark Sector Particle* (LDSP), which we denote by ψ. We will take the mass of ψ to be of order Λ_{IR} and this can be taken as our definition for the mass gap Λ_{IR}. In the absence of additional symmetry, ψ will decay back to SM states from the portal interactions itself. Since the portal interactions are weak, the typical time for DS states to decay among each other is much smaller than the typical lifetime of ψ, and can be safely ignored. Note that the LDSP is not the DM candidate in the scenario under consideration—a DM candidate would need to be much more long lived, and will have a missing energy signal. In this chapter we will assume that the DS relaxes entirely to LDSPs, and leave the question of considering a fraction of events to be missing energy, for future work.

The signatures of ψ depend on its lifetime, and this is the first place where some assumptions have to be made, which bring some model dependence. At high energy colliders, depending on the lifetime of ψ, one can get missing energy events, displaced vertices, or prompt decays, ordered by decreasing lifetimes. Missing energy events, being most inclusive, need minimal information about the underlying dynamics of DS, while displaced vertices and prompt decays being exclusive, need some information. Note that the requirement $\Lambda_{\rm IR}/\Lambda_{\rm UV} \ll 1$ puts us away from the prompt decay regime, since in this limit, the lifetime increases. Focusing on neutrino experiments, since the detectors are placed some distance from the interaction point, we are in the displaced vertex scenario. It is possible to detect the decay of ψ inside the detector, or its scattering against electrons or nucleons of the detector [84–91]. Both signatures need some knowledge of the IR behaviour of the underlying theory, and are model dependent, however with varying degrees. For these two signatures, the relevant DS matrix elements are:

$$\begin{aligned} \text{Decay}: \ & \langle \Omega | \mathcal{O}_{\rm DS} | \psi \rangle = a\, f\, \Lambda_{\rm IR}^{\Delta_{\mathcal{O}}-2} \,, \\ \text{Scattering}: \ & \langle \psi(p_f) | \mathcal{O}_{\rm DS} | \psi(p_i) \rangle = a\, F(p_i, p_f, \Lambda_{\rm IR}) \,, \end{aligned} \tag{3.3}$$

where $|\Omega\rangle$ is the vacuum, f is a decay constant, F is a form factor and a is an $\mathcal{O}(1)$ number, all of which are model dependent. In this chapter, we will only focus on the decay mode, as we explain this choice now.

The model dependence that enters in the decay case comes in the combination $a\,f$. Scattering process, on the other hand, requires knowing the form factor which can be a complicated function of the momenta (especially for strongly coupled sectors). The functional dependence also influences who ψ recoils against most efficiently. The spin of ψ does not fix the portal, since one can make multiple total spin states using two ψ. Further, depending on the spectrum, an LDSP might up scatter to a close by state, making the scattering inelastic (similar to what happens in inelastic Dark Matter scenarios [92]), leading to a different parametric dependence for the scattering cross-section. These aspects make it clear that scattering processes require additional model dependent assumptions, and we will not consider them here. Moreover, most importantly, the scattering cross-section will be further suppressed by a factor of $(\Lambda_{\rm IR}/\Lambda_{\rm UV})^4$ wrt the DS decay case. A further reason to choose decays over scattering is that they have a larger signal-to-noise ratio, and we will have more to say about it in sec 3.3. Note that while there are weakly coupled models in which all the LDSPs are stable under some accidental symmetry, and therefore can only be studied through scatterings in the experiments under scrutiny (and therefore our analysis will not apply to such scenarios), in strongly coupled models unstable resonances are expected generically.

The lifetime of ψ to decay to SM states, via the portal itself, can be estimated in a straightforward manner. However there are differences when the decay is from mixing with a SM state or a direct decay. For a direct decay from a portal of dimension D, the lifetime can be estimated to be

$$\frac{1}{\tau_\psi} \sim \Lambda_{\rm IR} \frac{\kappa^2}{8\pi} \frac{f^2}{\Lambda_{\rm IR}^2} \left(\frac{\Lambda_{\rm IR}^2}{\Lambda_{\rm UV}^2} \right)^{D-4} , \tag{3.4}$$

where the decay constant f is defined by the matrix element $\langle \Omega | \, \mathcal{O} \, | \psi \rangle = a\, f\, \Lambda_{\rm IR}^{\Delta_{\mathcal{O}}-2}$ and a is an $\mathcal{O}(1)$ number taken to be 1. Further, f can be estimated to be $f = \sqrt{c}\,\Lambda_{\rm IR}/4\pi$, where c is the number of degrees of freedom of the DS. On the other hand, if the LDSP decays through mixing with a SM particle such as Higgs, if the LDSP is spin 0, or Z, if the LDSP is spin 1 (e.g. through

$\mathcal{O}H^\dagger H$ or $J^{\rm DS}_\mu H^\dagger i\overleftrightarrow{D}^\mu H$ respectively), the lifetime in the limit $\Lambda_{\rm IR} \ll m_{Z/h}$ is given as

$$\frac{1}{\tau_\psi} = \Gamma_i \sin^2\theta_i \,, \;\; \tan 2\theta_i = \frac{2\delta_i}{m_i^2} \,, \;\; i = Z, h \,, \tag{3.5}$$

where $\Gamma_{Z/h}$ is the decay width of Z/h evaluated at $m_{Z/h} = \Lambda_{\rm IR}$, and the mixing parameter δ_i is

$$\begin{aligned} \delta_h &= \kappa_{\mathcal{O}}\, v_{\rm EW} f \left(\frac{\Lambda_{\rm IR}}{\Lambda_{\rm UV}}\right)^{\Delta_{\mathcal{O}}-2} \,, \\ \delta_Z &= \kappa_J\, v_{\rm EW} f \frac{m_Z \Lambda_{\rm IR}}{\Lambda_{\rm UV}^2} \,. \end{aligned} \tag{3.6}$$

To model the hadronic decay of the scalar LDSP (that mixes with the Higgs), we use the spectator quark model for $\Lambda_{\rm IR} > 2$ GeV and the dispersive analysis for $\Lambda_{\rm IR} < 2$ GeV, following [93]. For a spin-1 LDSP (mixing with the Z) we again use the spectator quark model for $\Lambda_{\rm IR} > 2$ GeV, and a data-driven approach for $\Lambda_{\rm IR} < 2$ GeV, following [94, 95] for the vector and axial vector component respectively.

The next model dependent assumption needed in order to evaluate the reach at high intensity experiments is how many LDSPs are produced per DS shell, or equivalently how many are excited by the DS operator acting on the vacuum. We will take two benchmark values, $n_{\rm LDSP} = 2$ for weakly coupled dark sectors and $n_{\rm LDSP} = n(p^2_{\rm DS})$ a function of the invariant mass squared $p^2_{\rm DS}$ of the DS system, similar to the case of QCD [96]:

$$n(p^2_{\rm DS}) = A\,(\log x)^B \exp\Big\{C\,(\log x)^D\Big\} \,, \tag{3.7}$$

where $x = p^2_{\rm DS}/\bar{\Lambda}^2$, $\bar{\Lambda} = 0.1\Lambda_{\rm IR}$, $A = 0.06, B = -0.5, C = 1.8, D = 0.5$, and $p^2_{\rm DS}$ is the invariant mass squared of the DS system. Our results are not very sensitive to small changes in $n_{\rm LDSP}$. In particular, as argued in section 3.4, its impact on the exclusion plots will be mostly in regions in which the LDSPs are light and long-lived.

Finally, we need to know the directional distribution of the produced LDSPs, to estimate if they interact with the detector. In the strongly coupled benchmark where typically $n_{\rm LDSP} > 2$, we assume that the LDSPs have a uniform angular distribution in the rest frame of DS (i.e. the frame in which $p_{\rm DS}$ only has a time component), and we can boost it to the lab frame to know its relevant distribution. A uniform distribution in the rest frame is a simplifying choice, and is well motivated, at least for a certain class of strongly coupled theories (e.g. see ref. [97] for such a scenario). Further, even if the distribution is not uniform per event, it can be uniform when all the events are considered. For light enough LDSPs, which are very boosted in the lab frame, small deviations from this assumption do not change our results significantly.

The weakly coupled case is in principle different, and the angular distribution depends on the production mode, spin of produced DS particles and the specific form of the portal. In general we expect $\mathcal{O}(1)$ differences among the possible LDSP angular distributions in the DS rest frame. For example, in DY production the typical LDSP distribution is either proportional to $\sin^2\theta$ or $1+\cos^2\theta$ for scalar and light fermion LDSPs respectively. The difference between the two distributions is that the scalar distribution is more peaked around the most probable LDSP lab angle $\sim 1/\gamma_{\rm DS}$. However, since the LDSP is produced with a high boost, any differences in the distribution are washed out, and we can assume an isotropic distribution in the DS rest frame as before. We have checked this by an explicit computation.

3.2 DS Production Modes at Proton Beam based Experiments

Even though at neutrino experiments the primary process is a proton interacting with a nucleus, depending on the energy scale of the process, there are various production modes to consider. In this chapter, we consider experiments based on 120 and 400 GeV beam energies. For such energies there are three relevant production modes. First of all, the proton nucleus interaction creates mesons, which may decay into lighter mesons and DS states, or completely annihilate into DS states. Denoting the 4-momentum carried by the DS state as $p_{\rm DS}$, this requires $p_{\rm DS}^2 \leq (\mathbf{M}_{\rm heavy} - \mathbf{M}_{\rm light})^2$ for the first scenario and $p_{\rm DS}^2 = \mathbf{M}_{\rm heavy}^2$ for the second. We will refer to these as radiative and annihilation meson decays (MD) respectively. For $p_{\rm DS}^2 \gtrsim \Lambda_{\rm QCD}^2$, the incoming proton is at high enough energies so one has to consider partonic process involving constituents from the incoming proton and the nucleons in the target, and we refer to this as Drell-Yan (DY) production mode. For $p_{\rm DS}^2 \lesssim \Lambda_{\rm QCD}^2$, DS states can be produced from initial state emission, which we will refer to as Dark Bremsstrahlung (DB) mode. For each of these processes, the production cross section has a different differential distribution in $p_{\rm DS}^2$. Fig. 3.1 shows a comparison of the differential DS production cross-section for DY, DB and radiative MD mode, for Z portal, at 120 GeV beam energy. The radiative MD mode is flat in $p_{\rm DS}$, switching off when the phase space for DS production closes, which in turn is set by the parent meson mass. The DB mode switches off around $\Lambda_{\rm QCD}$ beyond which it is not a valid description of the scattering process. The sharp peak in the DB mode is due to meson resonance, as seen in the form factors (see App. A). The switch off of DY mode comes from the drop in the PDFs of constituents of the proton at higher $p_{\rm DS}^2$, given $\sqrt{s}$ of the experiment, and is a slower drop.

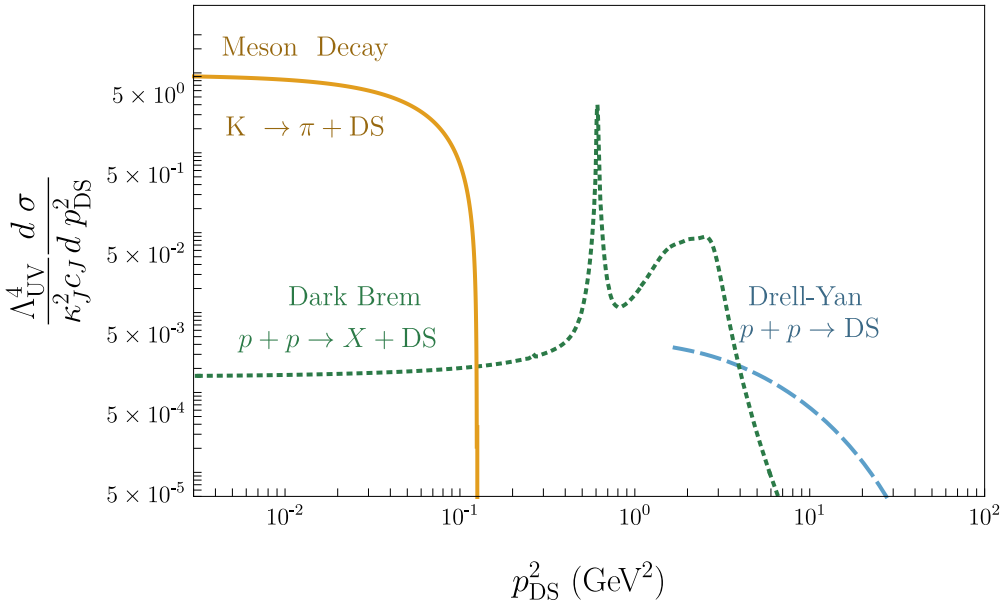

Figure 3.1: Relative importance of various production modes: the scaled differential cross-section for DS production at DUNE-MPD ($E_{\rm beam} = 120$ GeV) as a function of $p_{\rm DS}^2$ for various DS production modes (for Z portal). Solid yellow shows meson decay: $K \to \pi + \text{DS}$ mode, dotted green line shows dark bremsstrahlung mode ($p + p \to X + \text{DS}$), and dashed blue line shows Drell-Yan mode ($p + p \to \text{DS}$). The reported cross-section is per proton-on-target, and is without the geometric acceptance factor $\epsilon_{\rm geom}$ (which at DUNE is approximately 10^{-3} for DY and meson modes and around 10^{-2} for DB mode).

We remark that dependence of the production cross section on the center of mass energy $\sqrt{s}$ of the experiment is not the one given by naive power counting (*i.e.* $\sigma \sim s^{D-5}/\Lambda_{\rm UV}^{2D-8}$), and is general dependent on the production mode. For MD and DB modes, the typical scale of the process is not

set by the center of mass energy of the experiment, but rather by the hadronic resonances. There is a residual dependence on $\sqrt{s}$ in the meson production cross section and in the proton-nucleon cross section respectively, but typically this dependence is much weaker than the expected one above the specific hadronic production threshold. DY production instead is more sensitive on $\sqrt{s}$. These features are easily seen in fig. 3.1.

Independent of the production mode, we need to estimate the number of DS signal events S produced. This is generically given as

$$S = N_{\rm signal} = N_{\rm DS}\, P_{\rm decay}\, \epsilon_{\rm geo}\ , \tag{3.8}$$

where $P_{\rm decay}$ is the probability for at least one LDSP to decay inside the radial location of the detector, $\epsilon_{\rm geo}$ is the geometric acceptance for the LDSP direction to intersect with the detector and $N_{\rm DS}$ is the number of DS states produced. For more than one production mode, a sum is implied. Note that we have defined a signal event as one in which at least one LDSP decays inside the detector. The case of more than one LDSPs can be accounted for by multiplying the single LDSP probability with the number of LDSPs produced, and it's included in the definition of $P_{\rm decay}$ (see App. C for a detailed discussion of this). As the final step to get the number of signal events S, we have to express $N_{\rm DS}$ in eq. (3.8) in terms of the (inclusive) signal cross section $\sigma_{\rm S}$ as

$$N_{\rm DS} = \frac{N_{\rm POT}}{\sigma_{\rm pN}}\sigma_{\rm S}\ , \tag{3.9}$$

where $\sigma_{\rm S}$ is the cross section for DS production, $N_{\rm POT}$ is the total number of proton delivered on target during the duration of the experiment (projected years for future experiments) and $\sigma_{\rm pN}$ is the typical proton-nucleus cross section for the proton beam hitting the target, taken constant for the center of mass energies of the experiments we consider [98]:

$$\sigma_{\rm pN} = A^{0.77}\, 49.2\ {\rm mb}\ , \tag{3.10}$$

with A the target nucleus' atomic weight. In eq. (3.9), we are considering only DS production in the first interaction length of the target (or the dump for beam-dump experiments), neglecting production happening at later lengths with a degraded beam. Our computations are therefore conservative.

Specific to the case of meson decays, for a given meson $\mathbf{M}$ and in a given decay channel C (where the decay channel C stands for any of the various decay modes via which the meson M can decay, we discuss these in detail in the next sections), $N_{\rm DS}$ is given as

$$N_{\rm DS} = N_{\rm POT}\, N_{\rm M} {\rm Br}_{\rm C}\Big(\mathbf{M} \to {\rm DS}\ (+\mathfrak{m})\Big)\ , \tag{3.11}$$

where $N_{\rm M}$ is the number of mesons produced per collision and ${\rm Br}_{\rm C}$ is the branching ratio of the meson $\mathbf{M}$ to the DS (which may be in association with other mesons $\mathfrak{m}$).

Strictly speaking, the various factors that go into the estimation of the number of signal events $N_{\rm signal}$ depend on the kinematic information, the production mode, and the details of the detector (*e.g.* on- vs off-axis). For example, depending on $p^2_{\rm DS}$, the boost of the DS states and therefore its decay probability is different. Further, depending on whether the DS is produced with a non-zero transverse momentum or not, the angle subtended at the detector can be different. The correct procedure would be to consider differential quantities and integrate over the allowed range.[3] This

[3]Note that for meson annihilation decay $\mathbf{M} \to {\rm DS}$, $p^2_{\rm DS}$ is fixed to M^2.

however can obscure the relation between a given experiment and the probed parameter space. As a way out, we use the average value of boost factor for estimating the probability, and compute the average geometric acceptance. In app. C.2 we compare this procedure, referred to as *factorized* approach, with the exact procedure, called the *full* approach, and show that the difference between the two is small.

This simplified strategy to compute bounds is useful for the following reason. While production quantities such as the cross section depend in a trivial way on $\Lambda_{\rm UV}$ and very weakly on $\Lambda_{\rm IR}$ via the kinematic condition $p_{\rm DS}^2 \geq n_{\rm LDSP}^2 \Lambda_{\rm IR}^2$, the decay probability depends on both parameters. By using averages in the production quantities allows factorizing them from the decay probability. This procedure therefore allows an analytic understanding of $\Lambda_{\rm UV}$ dependence on the number of signal events. Given the vast array of cases, coming from different experiments, different production channels (which can depend also on extra parameters like the dimension Δ), different decay channels, and the strongly vs weakly coupled scenario, this factorization allows one to track the $\Lambda_{\rm UV}$ dependence clearly, and also speeds up the computations.

We next briefly outline the details of the three production modes discussed earlier.

3.2.1 Meson Decays

The considered portals between the SM and the DS can cause mesons to decay into DS states. Once the mesons are produced by the incoming proton hitting the target, they can decay in two ways. The first possibility is a heavier meson $\mathbf{M}$ decaying into a lighter SM state (such as another meson $\mathfrak{m}$) along with DS states. This is to be contrasted with the case when the mesons decay just into the DS states and nothing else. These two are the radiative decay and annihilation decay modes respectively. The differential production cross section for radiative decay, as shown in fig. 3.1 for the Z portal, is flat in $p_{\rm DS}$ up to kinematic threshold. The decay width for both modes can be approximately estimated, keeping the portal generic:

$$\Gamma \sim \kappa^2\, g_{\rm SM}^2\, \Phi(\Delta) \left(\frac{f_M}{M}\right)^a \begin{cases} \frac{v^2}{m_h^4}\, \frac{M^{2\Delta_{\mathcal{O}}-1}}{\Lambda_{\rm UV}^{2\Delta_{\mathcal{O}}-4}}\,, & \mathcal{O}H^\dagger H \text{ portal}, \\ \\ \frac{M^5}{\Lambda_{\rm UV}^4}\,, & JJ \text{ portal}. \end{cases} \tag{3.12}$$

where κ is the portal coupling, M is the mass of the parent meson, f_M is the decay constant, $\Delta_{\mathcal{O}}$ is the dimension of $\mathcal{O}$, $g_{\rm SM}$ is a dimensionless coupling built out of dimensionless SM couplings (like the gauge couplings, loop factors, extra SM particles' phase space, and relevant spurions), and $\Phi(\Delta)$ is the phase space factor coming from the integration over the DS degrees of freedoms (e.g. see eq. (3.13)). The exponent of the dimensionless ratio (f_M/M) depends on the process, and is -2 for processes coming from the axial anomaly, $+2$ for tree level processes from the chiral Lagrangian and 0 for processes directly proceeding through the portal (without going through the chiral Lagrangian). In this estimate we have ignored the lighter meson mass for radiative decay, and have not included the meson form factors for simplicity. In our full analysis we include all these effect. We next discuss specific details of the radiative and annihilation decays as DS production modes.

Radiative Decays

For the radiative decay of the form $\mathbf{M} \to \mathfrak{m} + \text{DS}$ proceeding via a flavour violating loop, the DS state is produced either by the quark line, and/or by the internal W loop (which is necessary to

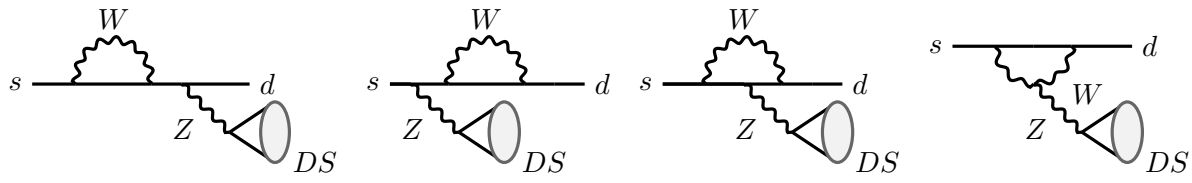

Figure 3.2: The underlying quark level transition in DS production via Z portal in flavour violating decays such as $K \to \pi + \text{DS}$.

change the quark flavor). This depends on the portal operator. For $J^{\rm SM}_\mu J^\mu_{\rm DS}$ portal where $J^{\rm SM}_\mu$ is the quark current, the DS is produced just by the quark lines, whereas for $J^{\rm SM}_\mu = iH^\dagger \overleftrightarrow{D}_\mu H \sim Z_\mu$, the DS states can be produced by attaching a Z to the quarks, or to the W in the loop[4]. The DS states can also be produced by the Higgs portal $\mathcal{O}H^\dagger H$. To understand their relative importance, let's consider the ratio of the branching ratios of the two different portals for DS production:

$$\frac{\text{BR}_{OHH}}{\text{BR}_{JHDH}} \sim \frac{3456\ \Gamma(\Delta_\mathcal{O}+1/2)}{\pi^{1/2}\Gamma(2\Delta_\mathcal{O})\Gamma(\Delta_\mathcal{O}-1)}\frac{M^2}{m_h^4}\frac{(M-m)^{2\Delta_\mathcal{O}-6}}{\Lambda_{\rm UV}^{2\Delta_\mathcal{O}-8}} \tag{3.13}$$

with M (m) being the mass of the heavy (light) meson, $\Delta_\mathcal{O}$ the dimensionality of the operator $\mathcal{O}$, where for the higgs portal case we have used the usual effective lagrangian coupling $C_{ij}\bar{d}^i_L d^j_R h$ between the flavour changing quarks and higgs (see [25] for example) and for the Z portal case, we have considered only the top quark contribution in the loop of the $\mathcal{O}(m_t^2/m_W^2)$. In order to understand this scaling, let us compare the two portals: for the Higgs Portal coupling we integrate the W-top loop which gives the effective coupling $\sim (1/16\pi^2)g_2^2 V_{ts}V_{tb}(m_{q_i}/v)(m_t^2/m_W^2)$, while the QCD matrix element is given by $\langle M|\bar{d}^i_L d^j_R|m\rangle \sim (M^2-m^2)/(m_{q_i}-m_{q_j})$ for the quark level transition $q_i \to q_j$ where we ignore the mass of the light meson/quarks for writing Eq. 3.13. For the Z portal estimate instead, we used factors of m_t^2/m_W^2 for the top quark loop contribution and approximated the matrix element for the meson transition as $\langle M|\bar{d}^i_L\gamma_\mu d^j_L|m\rangle \sim M$. It is clear that for $\Delta_\mathcal{O} \geq 4$, production through the Higgs portal is suppressed with respect to the Z portal and will give weaker bounds. We discuss this in more detail in sec. 3.4.4.

For production through a $\Delta_\mathcal{O} = 3$ Higgs portal, even though the $\Lambda_{\rm UV}$ scale probed is higher than Z portal production case (discussed in more detail in sec. 3.4.4), the bound is still at most only marginally stronger compared to missing energy searches at LHC [25]. In this subsection we will mostly focus only on the Z portal production for mesons, but will make some comments about the Higgs portal case in sec. 3.4.

Examples of radiative meson decay processes are $K^+ \to \pi^+ + \text{DS}$, $B^+ \to K^+ + \text{DS}$ and $D^+ \to \pi^+ + \text{DS}$, and a prototypical diagram (for $K^+ \to \pi^+ + \text{DS}$) is shown in fig. 3.2. In general, these processes proceed through insertion of two CKM entries, so that for flavor i going to j, the amplitude approximately scales as $\sum_k V^{\rm CKM}_{ik}V^{\rm CKM}_{kj} f(m_k/m_W)$, where m_k is the quark mass of flavor k, m_W is the W mass and $f(x)$ is a loop function [99, 100]. For D mesons, for which the underlying process is $c \to u$, there is no top quark in the loop, as opposed to B, K decays, which makes the D-meson process suppressed. As a result, the D decays are not very constraining—e.g. the large number of D mesons expected at SHiP (enhancement by $\sim 10^4$ compared to B meson production, see ref. [101]) is not enough to overcome the GIM and CKM suppression of $\sim 10^{-12}$ wrt $B \to K$ decays.

Due to the abundant number of K mesons produced at neutrino experiments, $K \to \pi + \text{DS}$ decay is an important mode for DS production. For this process, and for the Z portal case, the Feynman diagrams are shown in fig. 3.2. Note that one must include penguin diagrams as well as self-energy

[4]We are working in the unitary gauge.

diagrams [99, 100]. The DS production rates can be obtained from the SM calculation for $d\bar{s} \to \bar{\nu}\nu$, but with some modifications. We can use the SM results if we keep only the penguin diagrams and omit the box diagrams in the $d\bar{s} \to \bar{\nu}\nu$ process, since the latter are specific to the neutrino coupling (e.g. see [100]). This however must be done in the unitary gauge since the box and the penguin diagrams are needed together to make the result gauge invariant in an arbitrary gauge, but their gauge dependent parts vanish individually in the unitary gauge[5] [100]. Once these subtleties are addressed, we can simply replace the neutrino current coupling to Z, $g_{\rm EW}/2\cos\theta_W(\bar{\nu}_L\gamma_\mu\nu_L)$, with the DS current coupling to Z, $(\kappa_J v_{\rm EW} m_Z/\Lambda^2_{\rm UV})J^{\rm DS}_\mu$. This allows us to write the rate of decay of $K^+ \to \pi^+ + \text{DS}$, using the optical theorem, as:

$$\begin{aligned}\Gamma_{K^+\to\pi^++\text{DS}} &= \frac{1}{2M_K}\left(\frac{G_F}{\sqrt{2}}\frac{g_{\rm EW}\cos\theta_W}{8\pi^2}\right)^2 \frac{m_Z^2 v_{\rm EW}^2 \kappa_J^2}{\Lambda^4_{\rm UV}} \\ &\times \left(\sum_{j=c,t} V^*_{js}V_{jd}\bar{D}(x_j, x_u=0)\right)^2 \int \frac{\mathrm{d}^3 p_\pi}{(2\pi)^3}\frac{1}{2E_\pi}\mathcal{M}_\mu\mathcal{M}^*_\nu \\ &\times 2\ \mathrm{Im}\left\langle J^\mu_{DS}(p_{\rm DS})J^\nu_{DS}(p_{\rm DS})\right\rangle\ , \end{aligned} \tag{3.14}$$

where G_F is the Fermi constant, θ_W is the weak mixing angle, $g_{\rm EW}$ is the electroweak gauge coupling, M_K is the mass of the K meson, $v_{\rm EW}$ is the Higgs VEV, m_Z is the Z boson mass, $E_\pi = \sqrt{m_\pi^2 + |\vec{p}_\pi^2|}$, $p_{\rm DS} = p_K - p_\pi$, $\mathcal{M}_\mu = \langle\pi^+|\,\bar{d}\gamma_\mu s\,|K^+\rangle$ is the SM QCD matrix element (see App. B.1 for details), and V_{ij} are CKM matrix elements. The loop functions $\bar{D}(x_j)$, where $x_j = m_j^2/m_W^2$, sum the contributions from various diagrams. The upper limit for p_π integral is fixed by the kinematic requirement $p^2_{\rm DS} \geq n^2_{\rm LDSP}\Lambda^2_{\rm IR}$.

Apart from the decay $K^+ \to \pi^+ + \text{DS}$, one can also consider the decays of K^0_L and K^0_S. We can obtain the partial width of K^0_L from that of K^+ using ref. [99] by replacing $|V^*_{js}V_{jd}|^2$ in eq. 3.14 with $|\mathrm{Im}(V^*_{js}V_{jd})|^2$. The $K^0_S \to \pi^0 + \text{DS}$ decay is less constraining since it has a smaller branching ratio due to the large width of K^0_S (see refs [60, 102]).

We next consider decays of B mesons to DS which is relevant at proton-beam experiments with higher beam energies (e.g. SHiP and CHARM, with $E_{\rm beam} \sim 400$ GeV, $\sqrt{s} \sim 27$ GeV). These high energy proton beam experiments would also have a high K meson production rate but a large number of them get absorbed in the beam dump or target. Unlike B mesons, kaons have a decay length[6] which largely exceeds the hadronic interaction length (l_H) hence they tend to be absorbed in thick targets (for a target length of several l_H s) and only a fraction of them then decay to DS before absorption [93, 103]. For estimating this, we use ref. [103] for SHiP, and ref. [93] for CHARM.

The B meson decays to lighter mesons like K and π take place via Z-penguin diagrams which we already encountered in the case of $K^+ \to \pi^+ + \text{DS}$ (see fig. 3.2) except for the appropriate exchange of external quark flavors ($b \to s/d + \text{DS}$ instead of $s \to d + \text{DS}$). Of all the B decay modes, we find that the largest contribution to signal comes from the decays $B \to K + \text{DS}$ and $B \to K^* + \text{DS}$ [70]. For example, even though the partial width for the decay of $B_s \to \rho + \text{DS}$ is twice of $B \to K + \text{DS}$, the number of signal events from B_s decays are suppressed due to smaller number of B_s mesons produced with respect to $B^\pm$ and B_0 mesons at SHiP [101]. The contribution from $B \to \pi + \text{DS}$ is suppressed with respect to $B \to K + \text{DS}$ by a factor ~ 20 coming from $|V_{ts}|^2/|V_{td}|^2$ that enters in the respective decay widths [99]. This same suppression applies when comparing B meson decays to vector mesons: $B \to \rho + \text{DS}$ is suppressed with respect to $B \to K^* + \text{DS}$. We calculate the partial

[5] If we stayed in arbitrary gauge, the DS would also couple to the longitudinal modes of W and hence the box diagrams would also contribute. In the unitary gauge, $H^\dagger D_\mu H \sim Z_\mu$, the DS does not couple to W, and the box diagrams' contributions vanish.

[6] The decay length of $K^\pm, K^0_L$ is ~ 3 meters $\gg l_H \sim 15.3$ cm for SHiP and CHARM target [93].

decay widths for these B decays in the same way as in eq. (3.14) using the appropriate QCD matrix elements from eq. (B.2) and eq. (B.4) in Appendices B.1 and B.2.

We do not consider DS production from radiative decays of pseudoscalar mesons like π, η, η'. Their radiative decay into $\gamma + \text{DS}$ through a generic JJ portal is suppressed by the loop factor from the chiral anomaly triangle diagram, from the electromagnetic coupling and from the lightness of the meson in the π case [71].[7]

Radiative decays of vector mesons like ρ and ω can also produce DS via decay modes like $\rho^0 \to \pi^0 + \text{DS}$, etc. These decays would occur via flavour conserving transitions producing DS either through Z portal or SM vector quark current. The number of DS events from this mode is sub-leading due to the large width of ρ meson with respect to K meson width ($\Gamma_\rho \sim 10^{-1}$ GeV $\gg \Gamma_K \sim 10^{-17}$ GeV). Moreover, the radiative decays of vector mesons $V \to \text{DS} + P$ where P is a generic pseudo scalar are anyway suppressed since the interaction mediating the process come from the same triangle diagram mediating pseudoscalar radiative decays like $\pi^0 \to \gamma + \text{DS}$. Recently [104] considered three-body leptonic decays of mesons to put bounds on leptophilic ALPs. In our case too, DS can be produced from such leptonic charged meson decays such as from the decay $K^+ \to \mu^+ + \nu + DS$ via Z portal. However we find this mode to be very suppressed with respect to $K \to \pi + \text{DS}$, due to phase space suppression (see also [105]).

Eventually, to calculate the number of DS events from a meson decay, we use eq. (3.11). It is clear from eq. (3.11) that the meson decay mode that gives the strongest bound would depend on N_M, the number of parent mesons produced per POT at a given neutrino experiment. In general, this can be estimated as the ratio of production cross section of the meson to the total cross section between proton beam and target: $N_{\text{M}} = \sigma_{pN\to M}/\sigma_{pN}$. We take these numbers for various experiments from ref. [101] (also see references within) for 400 GeV beam energy and from ref. [58] for 120 GeV beam energy, which are obtained using PYTHIA simulations.

Annihilation decays

DS states can also be produced via annihilation decays of vector mesons through the JJ portal: $V \to \text{DS}$ where V can be $\rho, \phi, \omega, J/\psi$. We do not consider DS production from the annihilation decay of pseudoscalar mesons from this portal since it will not be model-independent under our approach [25]: the pseudoscalar decay matrix element is proportional to its momentum p_μ, which either vanishes when contracted to a conserved DS current, or gives a term proportional to a new, model dependent scale if the DS current is not conserved (corresponding to the internal DS symmetry breaking scale).

In principle the same topology can happen for the Higgs portal and scalar mesons (the matrix element for the spin 1 annihilation through this portal vanishes). However, given the uncertainties in the details of scalar meson production and their subdominance, we do not consider this possibility here. The leading contribution in this topology for the Higgs portal comes from FCNC CP-violating pseudoscalar annihilation decays such as $K \to \text{DS}$ [106], and we will briefly discuss them together with radiative decays in Sec.3.4.

For a general V, and for the case of $V \to \text{DS}$ via Z portal, we can compute the decay width as

[7] For the Z portal case, one external leg of the triangle diagram would produce Z which can couple with DS. This mode can give bounds at LSND due to the huge number of pions ($N_{\pi_0} \sim 10^{22}$), and we find that the Λ_{UV} probed is comparable to CHARM in the Meson Production mode.

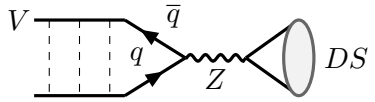

Figure 3.3: DS produced via Z portal in annihilation decays of vector mesons.

before:

$$\begin{aligned}\Gamma(V \to \mathrm{DS}) &= \frac{1}{2\,m_V}\frac{1}{3}g_Z^2\frac{\kappa_J^2 v^2}{m_Z^2\Lambda_{\mathrm{UV}}^4}f_V^2 m_V^2 \sum \epsilon_\mu^*(p)\epsilon_\nu(p)\; 2\;\mathrm{Im}\left\langle J_{\mathrm{DS}}^\mu(p) J_{\mathrm{DS}}^\nu(p)\right\rangle|_{p^2=m_V^2} \\ &= \frac{\kappa_J^2 c_J}{96\pi}\frac{g_Z^2 v^2}{m_Z^2}\frac{m_V^3 f_V^2}{\Lambda_{\mathrm{UV}}^4}\,,\end{aligned} \tag{3.15}$$

where m_V is the mass of the vector meson, f_V is the decay constant defined by $\langle V(p)|\,\bar{q}\gamma_\mu\, q\,|\Omega\rangle = i f_V m_V \epsilon_\mu^*(p)$, $\epsilon_\mu^*(p)$ is the polarization vector for V meson, and g_Z is the coupling of $\bar{q}\gamma_\mu\, q$ to Z boson. Here we have again used the optical theorem to do integration over DS phase space and used the expressions reported in [25] for the imaginary part of the correlators at $m_V \gg \Lambda_{\mathrm{IR}}$. Out of ϕ, ω and J/ψ, the largest branching ratio to DS would be that of J/ψ because of the narrow total width, and a partial width which is enhanced by the mass.

We find that the bounds from $J/\psi \to \mathrm{DS}$ are comparable to those from $B \to K/K^* + \mathrm{DS}$ decays at SHiP. Despite $\mathrm{BR}(J/\psi \to \mathrm{DS})/\mathrm{BR}(B \to K/K^* + \mathrm{DS}) \sim 10^{-2}$, the large number of J/ψ mesons expected at SHiP as compared to B mesons, $N_{J/\psi}/N_B \sim \mathcal{O}(100)$ compensates for this.

For neutrino experiments based on the 120 GeV NuMI beam line, annihilation decays of lighter vector mesons like $\rho,\ \omega,\ \phi$ can give contribution to signal events. Out of the three vector mesons $\rho,\ \omega,\ \phi$, we find that the leading contribution to DS production is via ϕ meson decay to DS. We can compare the branching ratio for ϕ and ω decay to DS via Z portal:

$$\frac{\mathrm{BR}(\phi \to \mathrm{DS})}{\mathrm{BR}(\omega \to \mathrm{DS})} = \frac{\mathrm{BR}(\phi \to e^+e^-)}{\mathrm{BR}(\omega \to e^+e^-)}\frac{m_\phi^4}{m_\omega^4}\frac{\left(-\frac{1}{2}+\frac{2}{3}\sin^2\theta_W\right)^2}{e_s^2\;4\sin^4\theta_W}\,, \tag{3.16}$$

where $e_s = -1/3$ is the EM charge of strange quark. Using this we expect DS produced in ϕ decay to dominate over ω decay to DS by a factor given by: $N_\phi/N_\omega \times \mathrm{BR}(\phi \to \mathrm{DS})/\mathrm{BR}(\omega \to \mathrm{DS}) \sim 0.007/0.03 \times 50 \sim 10$. Here we have used numbers for ϕ meson production at 80 GeV from ref. [107] and ω meson production at 120 GeV from [71]. A similar estimate shows that the case of ρ is also subleading. Therefore we only focus on the ϕ decay and do not consider ρ and ω. Note that ρ and ω annihilation decays overlap with the (vector) bremsstrahlung production mode when p_{DS}^2 hits the resonance peak [90]: not including them avoids over-counting such contributions. We do not consider the annihilation decays of heavier mesons like Υ since its production will be very suppressed at neutrino experiments due to its large mass.

Now we outline how we compute the LDSP boost entering the decay probability and geometric acceptance factors for the meson production mode. More details can be found in the appendix C.1.1. In order to calculate the decay probability of the LDSP, we use the following estimate for the average boost factor for the LDSP produced from meson decays:

$$\langle\gamma\rangle_{\mathrm{LDSP}} \approx \frac{\left\langle E_{\mathrm{DS}}^{\mathrm{lab}}\right\rangle}{\langle n_{\mathrm{LDSP}}\rangle\,\Lambda_{\mathrm{IR}}}\,, \tag{3.17}$$

where $\left\langle E_{\mathrm{DS}}^{\mathrm{lab}}\right\rangle$ is the average energy of the DS produced from parent meson decay in the lab frame. We have checked that an honest average of $\langle\gamma\rangle_{\mathrm{LDSP}}$ matches this estimate very well. To obtain $\left\langle E_{\mathrm{DS}}^{\mathrm{lab}}\right\rangle$,

$E_{\rm beam}^{\rm lab}$ (GeV)	Z portal production						H portal production					
	$\langle\gamma\rangle_{\rm DS}^{\rm weak}$	$\langle\gamma\rangle_{\rm DS}^{\rm strong}$	$\langle\gamma\rangle_{\rm LDSP}^{\rm weak}$	$\langle\gamma\rangle_{\rm LDSP}^{\rm strong}$	$\langle\epsilon_{\rm geo}\rangle^{\rm weak}$	$\langle\epsilon_{\rm geo}\rangle^{\rm strong}$	$\langle\gamma\rangle_{\rm DS}^{\rm weak}$	$\langle\gamma\rangle_{\rm DS}^{\rm strong}$	$\langle\gamma\rangle_{\rm LDSP}^{\rm weak}$	$\langle\gamma\rangle_{\rm LDSP}^{\rm strong}$	$\langle\epsilon_{\rm geo}\rangle^{\rm weak}$	$\langle\epsilon_{\rm geo}\rangle^{\rm weak}$
Drell-Yan												
120 (DUNE-MPD)	12	12	1490	160	0.004	0.004	9	9	1600	150	0.002	0.002
400 (SHiP)	25	25	4310	400	0.63	0.63	17	17	4830	364	0.54	0.54
Dark Bremsstrahlung												
120 (DUNE-MPD)	80	80	4500	655	0.040	0.040	74	74	4630	650	0.039	0.039
400 (SHiP)	270	270	15000	2200	1	1	250	250	15700	2200	0.96	0.97
Meson Radiative Decay $K \to \pi + {\rm DS}$												
120 (DUNE-MPD)	31	26	215	48	0.003	0.004	31	26	215	48	0.003	0.004
400 (SHiP)	55	45	375	84	0.79	0.89	55	45	375	84	0.79	0.89
Meson Annihilation Decay $\phi \to {\rm DS}$												
120 (DUNE-MPD)	8	8	403	61	0.001	0.001	-	-	-	-	-	
400 (SHiP)	14	14	702	107	0.27	0.27	-	-	-	-	-	-

Table 3.1: Average quantities $\langle\gamma\rangle_{\rm DS} = \langle E_{\rm DS}^{\rm lab}/p_{\rm DS}\rangle$, $\langle\gamma\rangle_{\rm LDSP}$ and $\langle\epsilon_{\rm geo}\rangle$ for Z portal and H portal production, for various production modes, and for weak/strong case. The reported numbers are for fixed $\Lambda_{\rm IR} = 10$ MeV. For Higgs portal, we have taken $\Delta_{\mathcal{O}} = 4$. The shown numbers are for DUNE-MPD (at 120 GeV) and SHiP (at 400 GeV) target materials (which sets the target atomic weight and number A, Z respectively). The average DS boost $\langle\gamma\rangle_{\rm DS}$ depends on weak/strong case through the kinematic condition $\sqrt{p_{\rm DS}^2} \geq n_{\rm LDSP}\Lambda_{\rm IR}$ imposed when calculating the average, and is a weak dependence. Annihilation decays of vector mesons does not proceed through the Higgs portal due to mismatch in quantum numbers.

the strategy is as follows: for radiative decays of the form $\mathrm{M} \to \mathrm{m} + \mathrm{DS}$, in the parent meson rest frame, the DS 3-momentum $\vec{p}_{\rm DS}^{\,0} = \{(p_{\rm DS}^0)_T, (p_{\rm DS}^0)_z\}$ can be written using energy conservation as:

$$|\vec{p}_{\rm DS}^{\,0}| = \sqrt{\frac{(M^2 - m^2 + p_{\rm DS}^2)^2}{4M^2} - p_{\rm DS}^2}\,, \tag{3.18}$$

and fixes $(p_{\rm DS}^0)_z = |\vec{p}_{\rm DS}^{\,0}|\cos\theta_{\rm DS}^0$, where $\theta_{\rm DS}^0$ is the angle that the DS makes with the meson flight direction, in its rest frame. For annihilation decays, of the form $\mathrm{M} \to \mathrm{DS}$, the DS 3-momentum in the meson rest frame is zero by momentum conservation. We further assume that 3-momentum of the mesons that decay to DS is perfectly aligned along the beam axis i.e. $\theta_{\rm meson} = 0$.[8]

We next calculate $(E_{\rm DS}^{\rm lab},\, (p_{\rm DS}^{\rm lab})_z)$ from $(E_{\rm DS}^0,\, (p_{\rm DS}^0)_z)$ using the boost and the velocity of the parent meson in the lab (which is along the z-axis), obtained from the average meson momentum values for various experiments from table 6 in ref. [71]. From $(p_{\rm DS}^{\rm lab})_z$, we can obtain $\left|\vec{p}_{\rm DS}^{\,\rm lab}\right|$ by noting that the transverse component is unaffected by the z direction boost, so that everything is a function of $\theta_{\rm DS}^0$ and $p_{\rm DS}^2$. Finally, to get the average value of DS 3-momentum $\left\langle\left|\vec{p}_{\rm DS}^{\,\rm lab}\right|\right\rangle$, we average over $\cos\theta_{\rm DS}^0$, since DS is isotropic in this variable and set $p_{\rm DS}^2$ to its average value for each radiative meson case. We have again checked that this matches a true average.

To get the final number of signal events as in eq. (3.8), we also need the geometric acceptance, which we again compute as an average. See App. C.1.1 for details of these computations, and App. C.2 for a comparison between using this average procedure with a more refined analysis. Some typical values of $\langle\gamma\rangle_{\rm LDSP}$ are given in table 3.1.

3.2.2 Drell-Yan production

If the typical exchanged momentum from the protons to the DS is comparable or larger than $\Lambda_{\rm QCD}$, the process is able to probe the partonic constituents of the nucleon. Given the energy scales involved, the protons are ultra-relativistic, and using the parton distribution functions (PDF) language to model the interaction between the constituents is justified. Notice that in our case, the condition to probe the partonic structure of the nucleon is $p_{\rm DS}^2 \gtrsim 1$ GeV^2, which is a request

[8] A more refined analysis using [58] shows that the most probable value for the ratio between transverse and longitudinal components of 3-momentum of decaying K mesons $|p_{\rm meson}^{\rm T}/p_{\rm meson}^{z}| \sim \theta_{\rm meson} \sim 10^{-2} \ll 1$. Using a non-zero but small value of $\theta_{\rm meson}$ does not change our final results.

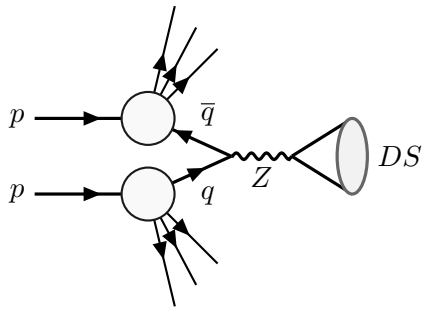

Figure 3.4: Prototypical Drell-Yan process in Z portal for the DS production.

on the total DS system, and not on the mass $\Lambda_{\rm IR}$ of the DS constituents. This is unlike what happens in models in which the mediator is produced on-shell, such as in light dark photon models. The production cross-section is in general dependent on the portal. A general estimate for the amplitude of DY through a given portal can be obtained on dimensional grounds, by assuming the typical momentum to be $\sqrt{p_{\rm DS}^2}$, and integrating over it to get the cross section. For Higgs portal, the partonic cross-section comes from Higgs exchange and is dominated by gluon initial states, while for Z portal, there is a Z exchange, and the initial states are the quarks. For the Z-aligned JJ portal, the results of Z portal apply, once appropriately rescaled, if the couplings are assumed to be Z-aligned (both in axial-vector and isospin space). The Feynman diagram for such a process is shown in fig. 3.4. Due to the similarity with Drell-Yan (DY) annihilation process we dub this production channel DY.

Consider first the Higgs portal. The leading interaction at the constituent level is due to *gluon-gluon fusion* (ggF) processes: indeed light quarks, while abundant in the proton, have a suppressed coupling to the Higgs, while heavy quarks are rare in the proton. Following [70], the effective ggF operator is, after integrating out the Higgs,

$$\mathcal{L} \supseteq F(\hat{s}) \frac{\kappa_{\mathcal{O}}}{\Lambda_{\rm UV}^{\Delta-2}} \frac{\alpha_s}{16\pi m_h^2} G^{\mu\nu\,a} G^a_{\mu\nu} \mathcal{O} \,, \tag{3.19}$$

where $F(\hat{s})$ is a function of the center of mass energy $\hat{s}$ of the process that accounts for the loops of internal quarks. Given that our computation is valid only for $p_{\rm DS}$ above the QCD scale, we retain in F only the contributions coming from the top, bottom, charm and strange quarks. This expression holds for center of mass energies much smaller than the Higgs mass (true for typical neutrino and beam dump experiments).

The cross section to produce a DS shell of total momentum $p_{\rm DS}^2$ can be computed by integrating over the DS phase space using optical theorem:

$$\begin{aligned}\sigma^{\rm DY(Higgs)} = A\,\sigma_{\rm pp}^{\rm DY(Higgs)} = \frac{A\,\alpha_s^2}{1024}\frac{\kappa_{\mathcal{O}}^2 c_{\mathcal{O}}}{m_h^4 \pi^{7/2}} \frac{\Gamma(\Delta_{\mathcal{O}}+1/2)}{\Gamma(2\Delta_{\mathcal{O}})\Gamma(\Delta_{\mathcal{O}}-1)} \\ \times \int_{Q_0^2}^{s} {\rm d}p_{\rm DS}^2 \left|F(p_{\rm DS}^2)\right|^2 \frac{p_{\rm DS}^{2(\Delta_{\mathcal{O}}-1)}}{\Lambda_{\rm UV}^{2\Delta_{\mathcal{O}}-4}} \\ \times \int_{p_{\rm DS}^2/s}^{1} \frac{{\rm d}x}{sx} f_g\left(p_{\rm DS}, x\right) f_g\left(p_{\rm DS}, p_{\rm DS}^2/(sx)\right) \,,\end{aligned} \tag{3.20}$$

where A is the atomic number of the target nucleus, f_g are the gluon PDFs[9], x is the longitudinal

[9]To compute the PDF integral, we used the nCTEQ15 PDF values [108], included in the MANEPARSE Mathematica package [109].

momentum fraction of one of the initial gluons in the CM frame and $\sqrt{s}$ is the center of mass energy of the protons. The lower limit of the integral over $p_{\rm DS}^2$ is cutoff at $Q_0^2 = (1.3\ {\rm GeV})^2$, the lowest for which the PDFs have been fitted, and below which the process does not probe a single parton and the DY picture breaks down. For consistency, Q_0^2 must be more than the minimum invariant mass of the DS system, $(n_{\rm LDSP}\Lambda_{\rm IR})^2$, which we impose internally.

Next consider the Z portal. Since the quark-Z coupling depends only on the up or down type of the quark, the process is dominated by light quark-antiquark annihilations. We will consider only contributions coming from up and down quarks, for which the couplings are given as

$$\begin{aligned} g_u^2 &= \frac{g_{\rm EW}^2}{\cos^2\theta_W}\left(\frac{1}{8} + \frac{4}{9}\sin^4\theta_W - \frac{1}{3}\sin^2\theta_W\right) , \\ g_d^2 &= \frac{g_{\rm EW}^2}{\cos^2\theta_W}\left(\frac{1}{8} + \frac{1}{9}\sin^4\theta_W - \frac{1}{6}\sin^2\theta_W\right) . \end{aligned} \tag{3.21}$$

Unlike the ggF case, the relevant PDFs depend on whether the target nucleon is a proton or a neutron. We approximate the neutron PDFs f_i^n to be the isospin-rotated PDFs of the proton f_i^p:

$$f_u^p = f_d^n\ ,\ \ f_d^p = f_u^n\ ,\ \ f_{\bar{u}}^p = f_{\bar{d}}^n\ ,\ \ f_{\bar{d}}^p = f_{\bar{u}}^n\ . \tag{3.22}$$

The partonic cross section for the pp/pn interaction in the limit of massless quarks reads:

$$\sigma_{pp/pn}^{\rm DY(Z)} = \frac{1}{1152\pi}\frac{g_{\rm EW}^2 v^4 \kappa_J^2 c_J}{m_Z^4\cos^2\theta_W\Lambda_{\rm UV}^4}\int_{Q_0^2}^{s} {\rm d}p_{\rm DS}^2 p_{\rm DS}^2 \ \times \int_{p_{\rm DS}^2/s}^{1}\frac{{\rm d}x}{sx}\ X_{pp/pn}(s,x,p_{\rm DS}^2)\ , \tag{3.23}$$

where

$$\begin{aligned} X_{pp}(s,x,p_{\rm DS}^2) &= 2\sum_{i=u,d}\left(g_i^2 f_i^p(x) f_{\bar{i}}^p(p_{\rm DS}^2/(sx))\right)\ , \\ X_{pn}(s,x,p_{\rm DS}^2) &= g_u^2\, f_u^p(x) f_{\bar{d}}^p(p_{\rm DS}^2/(sx)) + g_u^2\, f_{\bar{u}}^p(x) f_d^p(p_{\rm DS}^2/(sx)) \\ &\quad + g_d^2\, f_d^p(x) f_{\bar{u}}^p(p_{\rm DS}^2/(sx)) + g_d^2\, f_{\bar{d}}^p(x) f_u^p(p_{\rm DS}^2/(sx))\ . \end{aligned} \tag{3.24}$$

In the PDFs used, we have taken the factorization scale to be the exchanged momentum $p_{\rm DS}^2$ and not indicated it explicitly to keep the expressions simpler. Putting the contributions from the protons and neutrons together, the total DY cross section for the Z portal is:

$$\sigma^{\rm DY(Z)} = Z\sigma_{pp}^{\rm DY(Z)} + (A-Z)\sigma_{pn}^{\rm DY(Z)}\ , \tag{3.25}$$

where Z, A are respectively the atomic and weight number of the target nuclei. Notice that in both Higgs and Z portal scenarios the partonic cross section increases with $p_{\rm DS}$ (See also Fig 2.5b), as expected on dimensional grounds. The drop at high $p_{\rm DS}$ seen in fig. 3.1 is due to the PDF convolutions.

In order to estimate the decay probability, we estimate the average boost of the LDSP in the lab frame (not to be confused with the boost of the total DS system) as given in eq. (3.17). The value for these averaged quantities is given in table 3.1.

In principle, the boost should take into account the angle in the DS frame: while particles in the DS frame have roughly the same energy, in the lab frame particles emitted along the beam are more boosted with respect to particles emitted in the opposite direction. We have checked that this effect is negligible, when restricting to particles hitting the detector. For the geometric acceptance, we notice that in the DY production mode, the DS system has no transverse momentum and is

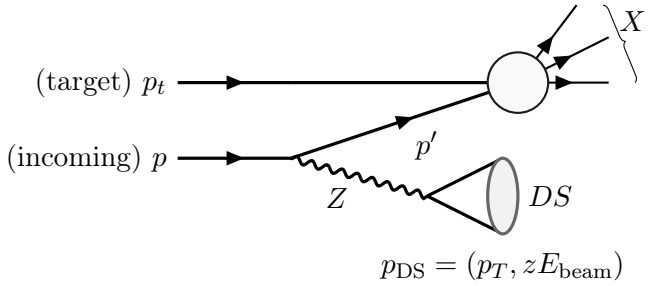

Figure 3.5: DS produced via Z portal in the Bremsstrahlung production mode.

collinear to the beam axis. After boosting the LDSP momentum in the DS frame we compute the angles that corresponds to the detector. To estimate $\epsilon_{\rm geo}^{\rm DY}$, we follow the prescription given in App. C.1.

In general, in the DY production mode, events are produced with larger $p_{\rm DS}^2$ compared to other modes (see fig. 3.1). We also find that the average energy of the DS system in the lab frame is not as high as in bremsstrahlung. These lead to lower γ of the DS system, a larger LDSP angular spread and therefore a slightly smaller $\epsilon_{\rm geo}$ for on-axis detectors.

3.2.3 Dark Bremsstrahlung ($pp \to \mathbf{DS} + X$)

Another possibility is for the DS states to be produced directly from proton as an initial state radiation. In this case, the exchanged momentum $p_{\rm DS}^2$ is not hard enough to probe the partonic structure. Following [110], we model the process using the initial state radiation (ISR) splitting function formalism. The idea is to treat the DS as incoming from the leg of the initial beam proton, which then becomes slightly virtual—an almost on-shell particle participating in the rest of the process. In the following, we will use the standard jargon: p_T for the transverse momentum of the DS system (in the plane orthogonal to the beam direction) and $z\,E_{\rm beam}$ for its longitudinal momentum, where $E_{\rm beam}$ is the beam longitudinal momentum (in the lab frame).

The splitting function formalism works well when the virtual particle is almost on shell. This means that in order to get reasonable cross sections, we must integrate the variables p_T and z in a sub-region of their kinematically allowed values, in which the virtual proton is not too off-shell. Denoting the momentum of the proton after DS emission as p', concretely, we will consider the region in which the virtuality is small:

$$\frac{-p'^{\,2} + m_p^2}{E_{p'}^2} = \frac{z^2 m_p^2 + (1-z)p_{\rm DS}^2 + p_T^2}{z(1-z)^2 E_{\rm beam}^2} < 0.1\,. \tag{3.26}$$

The choice of 0.1 is arbitrary and our results are not sensitive to small changes in this. In order to compute the splitting functions, we need to compute the vertex between the proton and the Z or Higgs. For the Higgs, by using low energy theorems [111] we can compute the coupling between the Higgs and nucleon at zero momentum to be $g_{hNN} h\bar{N}N$, where $g_{hNN} = 1.2 \times 10^{-3}$. To model the momentum dependence of the form factor, we employ a generalization of the *extended Vector Meson Dominance* (eVMD) model, in which the DS state interacts with the hadron by mixing with the scalar, CP even hadronic resonances. The resonances' propagators are taken to be Breit-Wigners (BW), and the mixing coefficients are fixed by using sum rules and by fitting the zero momentum values. The form factor is taken from [110] and the specific values used are reported in appendix A.1.

We also need to take into account the fact that for too high virtuality the quasi-real proton

stops interacting with the target proton as a coherent object, and the bremsstrahlung computation breaks down. To do this we multiply the previous form factor by a smooth cutoff [112]:

$$F_D(Q^2) = \frac{\Lambda_p^4}{\Lambda_p^4 + Q^4} \,, \tag{3.27}$$

where $\Lambda_p = 1.5$ GeV is the cutoff, taken to be near the proton mass, and Q^2 is the virtuality of the intermediate proton:

$$Q^2 \equiv -p'^2 + m_p^2 = \frac{z^2 m_p^2 + (1-z)p_{\rm DS}^2 + p_T^2}{z} \,. \tag{3.28}$$

Finally, the cross section for the process is calculated by factorizing the total cross section into the Bremsstrahlung part and a proton-nucleus (after Bremsstrahlung) part. The proton-nucleus cross section $\sigma_{pN}^{\rm nTSD}$ is calculated using the difference between the total inelastic proton-nucleus cross section and the *target single diffractive* (TSD) contribution, in which the target nucleus is diffracted but not disintegrated. This choice allows neglecting possible interference between the initial state and the final state radiation [98, 110]. According to [98, 113], $\sigma_{pN}^{\rm nTSD}$ is a slowly varying function of energy, and for the energies involved, we can approximate it as a constant

$$\sigma_{pN}^{\rm nTSD} = 762\,(A/56)^{0.71}\left(1 - 0.021\,(56/A)^{0.36}\right) \,, \tag{3.29}$$

where A is the target atomic weight. We will now generalize the results of [70, 110] to higher dimensional portals.

So far the discussion applies to any of the portals. However, once a portal is specified, the involved form factors change. Consider first the Higgs portal. Putting everything together, the inclusive production cross section is given as

$$\begin{aligned}\sigma_{pN}^{\rm Brem(Higgs)} = \sigma_{pN}^{\rm nTSD} g_{hNN}^2 \frac{v^2}{16\pi^{9/2} m_h^4} \frac{\Gamma(\Delta_{\mathcal{O}} + 1/2)}{\Gamma(\Delta_{\mathcal{O}} - 1)\Gamma(2\Delta_{\mathcal{O}})} \frac{\kappa_{\mathcal{O}}^2 c_{\mathcal{O}}}{\Lambda_{\rm UV}^{2\Delta_{\mathcal{O}}-4}} \\ \times \int {\rm d}p_{\rm DS}^2 {\rm d}p_T^2 {\rm d}z\, |F_H|^2 \times \; z\left((2-z)^2 m_p^2 + p_T^2\right) \\ \times \left(\frac{1}{m_p^2 z^2 + (1-z)p_{\rm DS}^2 + p_T^2}\right)^2 p_{\rm DS}^{2\Delta_{\mathcal{O}}-4} \,,\end{aligned} \tag{3.30}$$

where F_H is the Higgs bremsstrahlung form factor built as outlined before, and can be found in App. A.1. The limits of integration are chosen to respect the kinematic condition $p_{\rm DS}^2 \geq n_{\rm LDSP}^2 \Lambda_{\rm IR}^2$.

Next consider the Z portal case. The only difference is in the form factors of the axial and vector current of the proton. For the vector case, the production cross section is given as

$$\begin{aligned}\sigma_{pN}^{\rm Brem(Z,\ Vector)} = \sigma_{pN}^{\rm nTSD} \frac{\kappa_J^2 c_J}{2^{11}\pi^4} \frac{v^4}{m_Z^4 \Lambda_{\rm UV}^4} \frac{g_{\rm EW}^4}{\cos\theta_W^4} \times \int {\rm d}p_{\rm DS}^2 {\rm d}p_T^2 {\rm d}z \left|F_Z^{\rm V}\right|^2 \\ \times \left(\frac{2}{z} + \frac{4p_{\rm DS}^2 z\,\left(p_T^2 + m_p^2(z^2+2z-2)\right)}{\left(m_p^2 z^2 + (1-z)p_{\rm DS}^2 + p_T^2\right)^2}\right) \,.\end{aligned} \tag{3.31}$$

The vector form factor $F_Z^V(p_{\rm DS}^2)$ is modeled by ρ (iso-triplet) and ω (iso-singlet) exchange. We take three states for each tower. Details are given in App A. For the axial case, the cross section is given

as

$$\begin{aligned}\sigma_{pN}^{\text{Brem(Z, Axial)}} = \sigma_{pN}^{\text{nTSD}} \frac{\kappa_J^2 c_J}{2^{11}\pi^4} \frac{v^4}{m_Z^4 \Lambda_{\text{UV}}^4} \frac{g_{\text{EW}}^4}{\cos\theta_W^4} \times \int \mathrm{d}p_{\text{DS}}^2 \mathrm{d}p_T^2 \mathrm{d}z \left|F_Z^{\text{A}}\right|^2 \\ \times \frac{2}{z}\left(\frac{1}{m_p^2 z^2 + (1-z)p_{\text{DS}}^2 + p_T^2}\right)^2 \\ \times \left(p_{\text{DS}}^2(1-z)^2 + \left(p_T^2 + z^2 m_p^2\right)^2 + 2p_{\text{DS}}^2 \right. \\ \left. \times \left(m_p^2 z^2 \left(5 + (z-5)z + p_T^2(1+z^2-z)\right)\right)\right) \,. \end{aligned} \tag{3.32}$$

Similar to the vector case, for the axial form factor we take the respective iso-triplet axial vector exchange (there is no contribution from the axial iso-singlet resonances). Details about the axial form factor $F_Z^A(p_{\text{DS}}^2)$ are in App A. Combining the vector and the axial pieces we get

$$\sigma_{pN}^{\text{Brem, (Z)}} = \sigma_{pN}^{\text{Brem, (Z, Vector)}} + \sigma_{pN}^{\text{Brem, (Z, Axial)}} \,. \tag{3.33}$$

Notice that in eq. 3.33 the interference term between the vector and axial piece vanishes, due to the different quantum numbers under parity of the two possible states.

The vector contribution to the cross section is subdominant with respect to the axial one, due to an accidental cancellation in the vectorial quark coupling. The vector contribution has a more narrow distribution in p_{DS}^2 than the axial one, and it's peaked at m_ω^2: this is because ω is much more narrow than the iso-triplet vectors and axial vectors resonances mixing with the Z. Notice that the same exact computation holds for a JJ portal aligned (in both Lorentz and flavor space) to the Z quantum numbers. For different coupling structure of J_{SM} for a generic JJ portal, we can decompose the proton vector and axial form factors in their iso-singlet and iso-triplet components to get the correct form factor, shown in App. A.

An estimate for the cross section can be given by exploiting the fact that the cross section is dominated by the Breit-Wigner (BW) peaks in the form factors. The p_{DS}^2 integral of the BW associated with an intermediate meson $\mathfrak{m}$ can be estimated as $\pi f_{\mathfrak{m}}^2 m_{\mathfrak{m}}^3/(2\Gamma_{\mathfrak{m}})$, where we have used the notation of App. A. Therefore, using the splitting function to give the correct momentum scaling, upto an $\mathcal{O}(1)$ factor, the cross section for radiating DS particles through a dimension D portal made of a SM operator and a dimension $\Delta_{\mathcal{O}}$ DS operator can be estimated as:

$$\sigma \sim \sigma_{pN} g_{\text{SM}}^2 \Phi(\Delta) f_{\mathfrak{m}}^2 \begin{cases} \frac{v^2}{m_h^4} \frac{m_{\mathfrak{m}}^{2\Delta_{\mathcal{O}}-1}}{\Lambda_{\text{UV}}^{2\Delta_{\mathcal{O}}-4}\Gamma_{\mathfrak{m}}} & : \mathcal{O}H^\dagger H \text{ portal}\,, \\ \\ \frac{m_{\mathfrak{m}}^5}{\Lambda_{\text{UV}}^4 \Gamma_{\mathfrak{m}}} & : JJ \text{ portal}\,, \end{cases} \tag{3.34}$$

where, as in the meson case, g_{SM} is a dimensionless SM factor built out of dimensionless couplings (like the gauge couplings), $\Phi(\Delta)$ is the phase space factor coming from the integration over the DS degrees of freedoms, $f_{\mathfrak{m}}$ is the coupling of proton to the meson $\mathfrak{m}$ and $\Gamma_{\mathfrak{m}}, m_{\mathfrak{m}}$, is its decay width and mass respectively (see App A). In presence of multiple resonances, the estimate can be done by restricting to the leading contribution of the BW. For both the Higgs and Z portals the DS is produced as a collimated state forming an angle with the beam $\theta_{\text{DS}} \sim p_T/E_{\text{DS}}^{\text{lab}} = p_T/(zE_{\text{beam}})$. The average acceptance $\epsilon_{\text{geo}}^{\text{brem}}$ is computed by averaging over all the kinematic variables, and it doesn't differ much from the one obtained by replacing θ_{DS} with its average. Details of the computation of the geometric acceptance are given in App C.1. To estimate the average decay probability, we use the average LDSP boost, as defined in eq. (3.17) (see also table 3.1 for typical values), with the

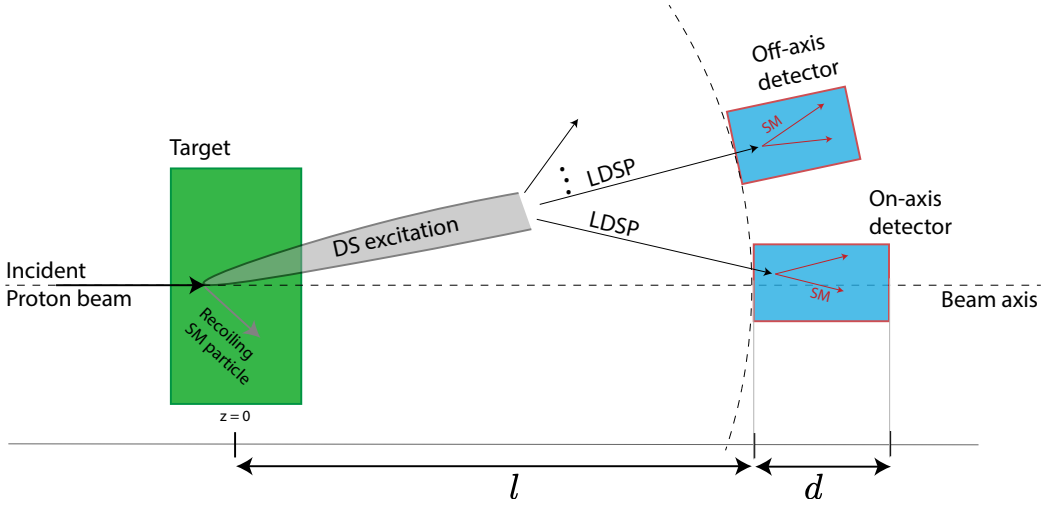

Figure 3.6: A cartoon of DS events produced at a typical neutrino detector (drawn not to scale): both on-axis and off-axis cases are shown. In general the DS state may not be produced along the beam-axis, as shown, though this is dependent on the production mode: annihilation decays of Mesons and DY production modes produce DS along the beam-axis, while radiative decays of Mesons and DB production mode produce DS at a small angle from the beam-direction.

only difference being that the probability distribution is given by the splitting function. The typical energy of the DS system in the lab frame is roughly $(3/4)E_{\rm beam}$ for all the portals considered, larger than in DY case.

3.3 Experimental Setup, Signal, and Background Estimation

In this section we briefly discuss the experiments we consider for obtaining the bounds on the $\Lambda_{\rm UV}$ and $\Lambda_{\rm IR}$ scales, and the assumptions we make when obtaining these bounds.

As explained in Sec. 3.1, the relevant characteristics of high intensity experiments are their beam energy $E_{\rm beam}$, their integrated luminosity (reported as the total protons on target $N_{\rm POT}$) and geometric details of the experimental setup. Further, the detectors in these experiments can be placed on-axis (i.e. along the line of the incoming beam) or off-axis (see fig. 3.6 for a cartoon of the experimental setup), which can change the geometric acceptance if certain production modes are forward peaked. Specific to the MD production mode, the number of meson $N_{\rm M}$ produced at a given experiment is an additional input, as seen from eq. (3.11). This depends on the target details as well as the energy in the centre of mass frame, $\sqrt{s} \approx \sqrt{2E_{\rm beam}m_p}$.

In this chapter we consider a representative set of past, present and future experiments. Table 3.2 gives the list of considered experiments with the relevant parameters.

We show bounds from recasts of BSM search results from past and current experiments, and projections from current and upcoming experiments, considering a few representatives from each category. We will also consider a future dedicated LLP search experiment, SHiP, for comparison, since it has a broad reach in typical DS models (e.g. see ref. [114]). We will take the SHiP parameters to be very optimistic, to have a conservative comparison with the neutrino experiments. A more comprehensive analysis that also considers other dedicated LLP experiments can be useful, and will be done in future. The best bounds from the high intensity experiments that we consider are from the currently under construction DUNE experiment and the proposed SHiP experiment. We also

show bounds coming from other experiments running at the same beam energies of these two (120 GeV and 400 GeV respectively).

Out of past experiments, we show CHARM, a beam dump experiment that ran on the CERN SPS (400 GeV) beamline in the 1980s. CHARM searched for the decay of axion-like particles (ALPs) into a pair of photons, electrons and muons and found no events [115], and we will recast this search for our bounds. Our choice of the past experiments are representative, and not based on the strongest bounds, but rather on considering similar beam energies as DUNE and SHiP (e.g. PS191 and νCAL, with beam energy of 19.2 GeV and 70 GeV respectively, can give a slightly better bound than CHARM, but are much weaker than the advocated future experiment DUNE. We will comment in sec. 3.4 about these two experiments).

We do not recast Heavy Neutral Lepton decay searches of CHARM or other past experiments like BEBC, or dark particle scatterings as done for example in [116, 117], given the different final state topology.

From existing experiments, we choose the MicroBooNE and ICARUS experiments, based on the 120 GeV NuMI beamline. These are two of the three detectors of Fermilab's Short-Baseline Neutrino program (SBNP) [55].[10] For MicroBooNE, we will use the analysis in ref. [118] for dark scalars decaying into electron-positron pairs. For ICARUS, we will use the results in [60], which studied DS coupled through the renormalizable Higgs portal.[11] DM searches at another current experiment, MiniBooNE, based on 8 GeV BNB beamline, use scattering [85, 119], and as explained in Sec. 3.1, they require additional model dependent assumptions, so we will not consider them here. Another currently running NuMI-based experiment is NOνA. We are not aware of any search for DS decays done at this experiment (for a scattering analysis, see [85, 120], based on [121]). Since NOνA is currently running, we show a possible prospect of such a search. We assume that it will be possible to reduce the backgrounds to negligible amounts, given the good angular resolution of the detector.

For future experiments we look at the Deep Underground Neutrino Experiment (DUNE). Ref. [58] has proposed the use of the multipurpose, high pressure gaseous chamber- the Multi-Purpose Detector (MPD) present in DUNE near detector complex for DS searches. We show projections for our DS scenario for the future DUNE-MPD as well.

Another class of future and existing experiments that are worth considering are the ones that are built in a region directly forward of the beam interaction point at LHC, like the already running FASER [122] and FASERν [123] (see [124] for the recent analysis) and SND [125], and the proposed experiments at the Forward Physics Facility (FPF) [126]. These experiments are in spirit similar to proton beam dumps, given that unlike traditional collider experiments they are put directly in the forward region, but have a much higher beam energy. This can potentially be relevant for non-renormalizable portals. The reach of these detectors have been thoroughly studied in the recent past in the context of Dark Sectors: a non-exhaustive list of works includes [102, 127–129] for renormalizable portals at FASER, [130] for ALPS at FASER, [131] for SND prospects, [132] for a strongly coupled dark sector at the FPF, [133, 134] for renormalizable portals at the FPF and [70] for FASER2 prospects. We will briefly comment on their reach on these models in Sec.3.4.

In order to estimate the sensitivity of the selected current and future experiments, an assessment

[10]The third detector, SBND, is too far off-axis with respect to the NuMI beamline and therefore its geometric acceptance is too low to give meaningful constraints. These three detectors also run on the 8 GeV Booster Neutrino Beam (BNB), which is at a lower energy than the NuMI energy, 120 GeV. We find the bounds to be subleading compared to DUNE (but better than other detectors), and do not consider it.

[11]Since the target specifications for NuMI beamline experiments are the same as that of proposed DUNE-LBNF beamline, we recycle the meson production numbers for DUNE-LBNF [58] also for the NuMI beamline experiment ICARUS.

Experiment	N_{POT} (total)	E_{beam} (GeV)	l (m)	d (m)	Off-axis angle, θ_{det} (rad)	θ_{acc} (rad)
CHARM [115, 135, 136]	2.4×10^{18}	400	480	35	0.01	0.003
NOνA-ND [85, 121]	3×10^{20}	120	990	14.3	0.015	0.002
MicroBooNE (KDAR) [118]	1.93×10^{20}	120	100	10.4	-	0.013
ICARUS-NuMI [55, 60]	3×10^{21}	120	803	19.6	0.097	0.005
DUNE-MPD[58, 137]	1.47×10^{22}	120	579	5	0	0.004
SHiP [103, 114]	2×10^{20}	400	64	50	0	0.078

Table 3.2: The relevant parameters for the experiments considered in this chapter. The quantities l and d are defined in fig. 3.6. θ_{det} stands for the position of the detector centre with respect to the beam line, with the origin taken at the interaction point. Entries with zero θ_{det} indicate that the detector is placed along the beam axis. θ_{acc} stands for the detector half angular opening. Note that for MicroBoone KDAR analysis, the K mesons are produced at rest (in the lab frame) so that θ_{det} is irrelevant. The angle θ_{acc} for this case is measured with the origin at the NuMI hadron absorber, placed $\mathcal{O}(600)$ m from the interaction point [118].

of the background is needed. We assume that beam dump experiments can be made background free by imposing cuts with $\mathcal{O}(1)$ signal efficiencies, as seen in past searches, e.g. at CHARM [115]. On the other hand, at neutrino experiments, the neutrino beam itself can be a source of background events. At these experiments the typical mass of the LDSPs probed is $\mathcal{O}$(10-100) MeV, therefore the available channels for the LDSP decay to the SM are mostly photons and electron-positron pairs, which produce electromagnetic showers in the detector. Heavier decay products, such as muons, will be reconstructed as tracks (but for all practical purposes, we will treat them similar to the showers in this section). The following discussions hold for any of the decay products.

In principle, the two shower signature has no irreducible background. Reducible background events come from hard radiation of a single photon, or from neutral-current ν scattering against a nucleus producing a π^0, which then decays into $\gamma\gamma$. The produced photons then can convert into e^+e^- pairs, that mimic the signal. However, it's not guaranteed that the two daughter particles will be reconstructed as separate showers.

The typical condition in order to reconstruct the two particles involves an isolation cut between the decay products, or in other words an angular separation cut. The specific implementation depends on the specific detector and analysis strategy. We will briefly review what has been suggested in previous works. However many of the relevant aspects can be understood more generally, which we will elaborate with a relevant prototypical experiment in mind.

For the ICARUS experiment, as suggested in [60], an angular separation of 10° is enough to be able to separate the two showers. Background events instead have a narrow separation between the charged particles, or potentially two showers that do not originate from the same vertex. The angular cut reduces the background events to a negligible amount. In [84] the authors elaborate on an analysis with less stringent cuts but with $\mathcal{O}(100)$ background events. Indeed a strong isolation cut has low efficiency for lighter, and therefore more boosted, LDSPs. This is especially true for the models under consideration here, in which DB and DY production modes are non-negligible and generate LDSPs more boosted than the ones coming from meson decays. For example, in DB, for the weakly coupled case $n_{\text{LDSP}} = 2, \Lambda_{\text{IR}} = 100$ MeV, we expect the daughter particles to be separated by an angle of $1/\gamma_{\text{LDSP}} \approx 0.15°$, which is smaller or comparable to the angular resolutions of some of the detectors. This highlights a potential problem in our framework, when reconstructing the signal. For this reason, we suggest that at ICARUS, it might be better to avoid a stringent cut in angular separation and work with $\mathcal{O}(100)$ background events [84], possibly reduced with an energy

cut and a cut on the direction of the DS system with respect to the beam. Interestingly, for strongly coupled DS we expect the angular separation condition to be less stringent on the signal. Because of a larger $n_{\rm LDSP}$, the energy is split among more LDSPs, leading to a suppression of the single LDSP boost factor. For such sectors, assuming an average $n_{\rm LDSP}$ of $\mathcal{O}(10)$, the average separation angle is typically $\mathcal{O}(1^\circ)$ for DB and 100 MeV masses, and less for other production modes. Since this is of the order of the angular resolution of ICARUS, it should be feasible to reconstruct the signal events as separated tracks for masses not too light.

Specific to the DUNE-MPD detector, in [58, 138, 139] it has been shown that boosted signal events have a narrower angular separation compared to the more isotropic background distributions. Due to this difference the search can effectively be rendered background free. Even in this case the two decaying particles must be reconstructed as separate particles, which these references claim to achieve. In these studies, the typical opening angle between the decay products is comparable to the weakly coupled scenarios we consider in this work. Therefore we take this search to be background free.

If instead the two decay products are not separated, the event will be reconstructed as a single electron event. The background to this kind of event comes from ν_e charged-current scattering, from ν-e elastic scattering events or ν neutral-current quasi-elastic events. The idea of decaying particle hiding behind the single electron signature has been explored in [140, 141]. In these works it is shown how to recast the analysis of the LSND experiment (with a beam energy of 0.8 GeV) that looked for ν_e charged-current scattering [142, 143] to put bounds on BSM particles decaying into e^-e^+, hiding as single electron events. In particular, the decaying particle would present as an excess of high energy electron events near the maximum value of the energy analyzed (200 MeV)[12]

Considering now a higher beam energy experiment, searches for charged-current at NuMI based experiment (with beam energy 120 GeV) typically look for neutrino with GeV energies, a bit lower than the typical LDSP energy (see for example [144]). Other scattering analysis typically look for ν-e elastic scattering. The cuts imposed require a low energy recoil, and a very forward electron. It's unclear whether or not they can be used to put stringent bounds on misidentified e^-e^+ pairs. It will be very interesting to explore this signature of single electron hiding in the high energy tail of scattering events at high beam energy experiments, but we will not study this signature here.

We would like to point out that it should be possible to run the neutrino experiments in a beam dump mode, essentially removing all the background, while keeping almost all the signal (except the one coming from charged meson decays). A beam dump proposal for DUNE has been studied in [145], showing that indeed running in the beam dump mode allows neglecting all the SM backgrounds in the DUNE detector, albeit at a reduced luminosity of roughly two orders of magnitude (one order of magnitude, for the optimistic scenario). The idea to suppress neutrino background by steering the beam off the target (as in the beam dump mode) has been already implemented at MiniBooNE [119] (although looking for DM scattering events) and MicroBooNE experiments. We will recast the MicroBooNe search, which however is quite different in spirit from the typical beam dump search, as it is optimized to look for Kaon Decay At Rest (KDAR). The idea is to look for the decay products of Kaons decaying at rest in the NuMI hadron absorber, which have a very peculiar directionality: in usual cases, the decay products of produced kaons are collected by a detector placed further down the beamline, whereas here the MicroBooNE detector is placed on the back side of the NuMI hadron absorber (e.g. see fig. 1 in ref. [118]). This peculiarity allows

[12]We do not recast LSND bounds in the DB and DY modes, even if the intensity is one of the highest. For DY, due to a very low beam energy of 0.8 GeV, the integration range of the partonic center of mass energy is very small. For DB, the condition on the integration domain of eq. (3.26) is very constraining. Relaxing the condition, by setting the RHS of eq. (3.26) to 1, the bounds are still worse than DUNE.

the signal events to be easily distinguished from background events, with an estimated efficiency of 0.14 on signal selection.

In addition to the backgrounds discussed so far, there is an extra component coming from *neutrino trident events*, in which a neutrino scatters against a nucleus in a purely electroweak process, to produce a lepton-antilepton pair. As argued in [58, 146], the expected number of events is $\mathcal{O}(10)$ events at DUNE-MPD, while it is lower in other liquid Argon detectors like ICARUS. In more conventional detectors like NOνA, $\mathcal{O}(10)$ e^-e^+ trident events are expected [61]. Given the rather peculiar kinematics, it's possible to bring down these background events and neglect them in the analysis [58].

For all these reasons, we will compute the signal yield contours for 10 and 100 event lines when discussing prospects for DUNE-MPD. Indeed 10 events represent a reasonable proxy for an almost background free search in the presence of $\mathcal{O}(1)$ experimental efficiency, although this number could be brought down in specific experiments by a more careful analysis of the reducible backgrounds. The 100 event lines instead can be representative of some signal loss due to selection cuts (which could be present for example in the weakly coupled case due to a small angular separation) or for a reduction in $N_{\rm POT}$, for example due to running in dump mode for a limited amount of time.

From the experimental analysis we recast, we use 95% confidence level, including the signal efficiencies reported. For CHARM [115] which observed 0 event, we set a bound at 95% confidence level of $N_{\rm signal} < 3$, using efficiency of 0.51 and 0.85 for the e^+e^- and $\mu^+\mu^-$ modes respectively. For MicroBooNE KDAR [118] which observed 1 event compared to a background expectation of 1.9 events, we require $N_{\rm signal} < 3.8$ at 95% confidence level, with a signal reconstruction efficiency of 0.14.

3.4 Analysis Results and Discussion

In this section we present our bounds on the parameters $\Lambda_{\rm UV}, \Lambda_{\rm IR}$. As we have argued before, the dominant production mode is through the Z-portal, but the decay can proceed through either Z-portal or Higgs portal. As discussed in section 3.2, there are three production modes for DS states, each of which has a different distribution in $p_{\rm DS}$ and therefore contributes differently depending on the energy and the detector geometries. In fig. 3.7 we show the exclusion regions individually for the three production modes, keeping to the Z portal decay for simplicity, for both weakly and strongly coupled benchmark scenarios. We will assume that the LDSP has spin 1 in order to fix the decay parametrics. In fig. 3.8, we show the combined bounds from this work, for both Z and Higgs portal decays, and compare against bounds from LHC and LEP from ref. [25]. The bounds for the Z-aligned $J^{\rm SM}_\mu J^\mu_{\rm DS}$ portal can be obtained from the Z portal bounds simply by re-scaling the signal cross section as $\sigma^Z_{\rm S}/\sigma^{JJ}_{\rm S} \sim (\kappa^2_Z/\kappa^2_{JJ})\,(v^2/m^2_Z)$. The case of generic JJ portal is obtained from the Z-portal by an appropriate combination vector/axial parts of the current and a rescaling of the couplings.

One can understand the general features of the excluded regions. The right edge of excluded region (on the high $\Lambda_{\rm IR}$ side) is due to the LDSPs being too short lived. Therefore the bound is roughly set by $\beta\gamma c\tau \sim \ell_{\rm detector}$. Given that typically for high $\Lambda_{\rm IR}$, $n_{\rm LDSP}$ for the weakly and strongly coupled cases are very similar, the right edge of the excluded region is almost identical for the weakly and strongly coupled cases. The left edge of the excluded region is instead due to the LDSPs being too long lived, $\beta\gamma c\tau \gg \ell_{\rm detector}$. In this case the exponentials appearing in the decay probability (eq. (C.2)) can be expanded to linear order and it's possible to get the slope of the left edge. For example, in the weakly coupled case with both production and decay through Z portal (or

any generic 6D operator) the left edge is set by a constant ($\Lambda_{\rm IR}^6/\Lambda_{\rm UV}^8$) line, where the factors come from the exponential expansion to linear order and the $1/\Lambda_{\rm UV}^4$ in the production cross-section. For the strongly coupled case the $n_{\rm LDSP}^2$ factors have a non trivial dependence on $\Lambda_{\rm IR}$, and in general it is not possible to get the slope. Its effect is to increase the total signal events since the number of LDSPs is larger than in the weakly coupled scenario considered. This enhancement asymptotes to the weakly coupled case when $\Lambda_{\rm IR}$ is close to threshold due to the behaviour of the chosen function.

In all these exclusion plots, regions bounded by solid lines show the excluded parameter space from recasts of past and recent DS searches (CHARM [115] and MicroBooNE [118]). The region bounded by dashed contours in our plots show the potential of current and future upcoming neutrino experiments: NOνA-ND and ICARUS (current), and DUNE-MPD (near future). To compare their potential with future DS experiments, we also show the projections coming from the future beam dump experiment SHiP. For these projected exclusions, we have shown the 10 signal events line assuming 100% reconstruction and detection efficiency. Following our discussion in section 3.3, for DUNE-MPD, we also show the 100 events line in fig. 3.8.

There are several features of the bounds which make the neutrino experiments a very powerful probe for dark sectors, in the parametrization considered in this work. First of all, we find that the bounds from current and upcoming neutrino experiments are comparable to dedicated DS experiments, with a reach of $\Lambda_{\rm UV}$ in multiple TeV range, for $\Lambda_{\rm IR}$ in the MeV-GeV range. This is similar to the ranges probed in high energy experiments like LHC and LEP (as done in ref. [25]). The typical scale l at which the detectors are placed is much larger than the corresponding scale in the LHC DV searches, and the typical boosts involved are also different, which together select a somewhat larger τ and hence a smaller $\Lambda_{\rm IR}$ region compared to LHC. Importantly, neutrino experiments fill the gaps in the parameter space coming from trigger[13] and event selection requirements at LHC and LEP, since they are sensitive to much lower energy activity in the detector. Even more importantly, in portals which are not enhanced by a resonant production, the EFT condition $(p_{\rm DS}^2)_{\rm max} < \Lambda_{\rm UV}^2$ makes LHC and LEP bounds inconsistent, an issue which is again alleviated at neutrino experiments due to a smaller $\sqrt{s}$ involved. All these features are seen in the bounds in fig. 3.7, 3.8.

In the following subsections, we will discuss in detail how prospective DS searches at neutrino experiments can complement current bounds for different portals considered in this work. We will also emphasize the difference between the production modes, especially on how a particular detector geometry can favor one mode over the other.

3.4.1 Z Portal Production

Consider first the MD production mode through the Z portal (fig. 3.7 first row), where we show bounds from various experiments. We also show bounds coming from the MicroBooNE KDAR analysis [118] which is only relevant for the MD mode. We find that for neutrino experiments based at 120 GeV proton beam, in general the strongest bounds come from radiative decays of K meson ($K \to \pi + \text{DS}$) due to the large number of K mesons produced with respect to other mesons. However, for the strongly coupled DS case where the kinematic condition on $p_{\rm DS}^2$ is stronger due to a larger $n_{\rm LDSP}$, we find that at DUNE and ICARUS, $\phi \to$ DS decays can give a stronger bound on $\Lambda_{\rm UV}$ as compared to K meson bounds. For experiments based on 400 GeV proton beam, heavier mesons like B, J/ψ can be produced in large numbers and can contribute to bounds at CHARM and SHiP. These heavier mesons can in principle probe larger $\Lambda_{\rm IR}$ due to the relaxed kinematic condition $n_{\rm LDSP}\Lambda_{\rm IR} \lesssim M$, where M is the mass of the decaying meson. The $\Lambda_{\rm IR}$ reach is correlated

[13]This could be improved with dedicated trigger designs, as done in [147] for CMS in a different lifetime region than the typical one of the gap

with the $\Lambda_{\rm UV}$ reach, for fixed lifetime. At SHiP, we indeed find that J/ψ decays probe the highest $\Lambda_{\rm UV}$ scales as opposed to K meson decays which suffer from the kinematic condition. However, we find that K mesons can still improve reach on lower $\Lambda_{\rm IR}$ values relative to J/ψ, B mesons due to larger geometric acceptance for $K \to \pi + \text{DS}$ and larger number of K mesons. At CHARM, we find that $J/\psi \to$ DS decays give the leading bounds which dominate those coming from $K \to \pi + \text{DS}$ decays.

For the Drell-Yan (direct partonic) production mode (fig. 3.7 middle row), the best bounds come from SHiP, and the other experiments only give subleading bounds. Within them, due to the collinear nature of the produced DS beam, detectors of the on-axis type are more sensitive to this mode. Note that compared to the DB mode, the average DS boost is smaller for the DY mode, so that the LDSP spread is more and the off-axis detectors are penalized less.

For the case of dark bremsstrahlung (fig. 3.7 bottom row), the DS is produced very collimated along the beam line, favoring detector geometries closer to it. We find that the best bounds from neutrino experiments for this mode come from DUNE-MPD. These are comparable in $\Lambda_{\rm UV}$ and only probe slightly smaller $\Lambda_{\rm IR}$ values, as compared to the future beam dump experiment SHiP. This is because in bremsstrahlung the typical $p^2_{\rm DS}$ is cut roughly around QCD scales, and an increase in $\sqrt{s}$ at SHiP as compared to DUNE does not lead to a large increase in the production cross section. The other experiments shown, ICARUS-NUMI, NOνA and CHARM give subleading reach in both $\Lambda_{\rm UV}$ and $\Lambda_{\rm IR}$. Despite an increase in the number of POTs with respect to NOνA, ICARUS still has lower sensitivity due to a reduced angular coverage. Both ICARUS and CHARM, due to their off-axis nature, miss out signal events from the forward DS beam, characteristic of the dark bremsstrahlung mode.

Combining all the production modes, in fig. 3.8 we show the final excluded parameter space, for both weakly and strongly coupled benchmarks. We also show the results from [25] which studied resonant DS production through Z portals at high energy colliders and presented exclusion regions from ATLAS monojet search [148], displaced vertex search [149, 150], and from total Z width bounds from LEP [151]. The bounds presented here probe different parts of the parameter space, in particular in $\Lambda_{\rm IR}$, even if the $\Lambda_{\rm UV}$ reach is comparable to before, and also probe gaps in parameter space in earlier work which came from trigger requirements. The complementarity of the bounds at neutrino experiments, as compared to missing energy and displaced searches at LHC is due to the peculiar position of the near detectors of neutrino experiments, placed at $\mathcal{O}(10^2)$ meters. We also find that the bounds are stronger than past beam dump searches like E137 and NA64 (whose results can be found in [25, 71]) due to a larger $N_{\rm POT}$, and in some cases, a larger beam energy.

From fig. 3.8 we see that one of the *current* strongest bounds for Z portal DS still comes from the indirect Z width measurement at LEP, $\Lambda_{\rm UV} > 525(k_J^2 c_J)^{1/4}$ GeV [25] which is independent of $\Lambda_{\rm IR}$ till the kinematic threshold. This bound is stronger than CHARM and MicroBooNE. Additionally, CHARM and MicroBooNE are also weaker than the LHC monojet and displaced vertex bounds except for the strongly coupled case (fig. 3.8 top right) where they probe slightly higher $\Lambda_{\rm IR}$ values. Prospective DS searches at current Fermilab neutrino facilities, ICARUS and NOνA-ND, improve on CHARM and MicroBooNE, but they are still weaker than the LEP bound.

Most importantly however, we find that future neutrino detector DUNE-MPD will be sensitive to $\Lambda_{\rm IR}$ in the range $\mathcal{O}(0.1 - 1)$ GeV for $\Lambda_{\rm UV}$ of few TeVs, a region not covered by LHC exclusions. Future LLP experiment SHiP based on 400 GeV proton beam would further improve sensitivity with respect to DUNE-MPD and LHC searches. These improvements are either due to a higher geometric acceptance from being on-axis or from having a wider detector, or due to a higher beam energy.

Another past proton beam dump experiment νCAL, with a beam energy of 70 GeV, has searched

for the decay of a scalar particle [152, 153]. Recasting this search [154, 155] gives bounds slightly better than CHARM, excluding in roughly the same $\Lambda_{\rm IR}$ region, and with $\Lambda_{\rm UV}$ up to 1 TeV. This is due to the fact that the bremsstrahlung cross section for this energy is the same as of CHARM, given the proton virtuality cutoff, the experiment has a similar luminosity, but it is closer to the beam and target. The bounds are still weaker than DUNE and SHiP. Recasting the Heavy Neutral Lepton search of PS191 [156, 157], as suggested in [158, 159], gives bounds better than CHARM but worse than νCAL and DUNE. We do not show these bounds to keep the plots uncluttered.

Emphasizing the complementarity of neutrino experiments with respect to the LHC searches, we note that for the strongly coupled case (fig. 3.8 top right), the LHC (ATLAS) searches are not sensitive in a gap of parameter space values close to $\Lambda_{\rm UV} \sim 500$ GeV $- 2$ TeV and $\Lambda_{\rm IR} \sim 0.1 - 0.5$ GeV. We find that both future neutrino experiment DUNE-MPD and dedicated LLP experiment SHiP would remarkably fill this gap in the Z portal DS parameter space. These gaps were due to trigger and event selection requirements.

So far we have only considered decay through the Z-portal, but the decay can also proceed through the Higgs portal. Before proceeding with that, a couple of comments about the interplay of the quantum numbers of LDSPs and the relevant decay portals is in order. According to the Landau-Yang theorem [160, 161], a massive spin-1 particle cannot decay into two massless spin-1 particles. This implies that if the LDSP is a spin-1 particle then for values of $\Lambda_{\rm IR} < 2m_e$, it will not decay into any visible SM particles, so that the only signal is a missing energy. If instead the LDSP is a spin-0 particle, there is no such condition. However for such small values of $\Lambda_{\rm IR}$, the LDSPs are too long lived and cannot be efficiently constrained at the experiments considered here. For this reason it's crucial to realize that while production from the Higgs portal is very suppressed, it might be relevant for decays if its the only available decay mode. We should clarify that if multiple portals are available for decay, one has to consider the dominant one. When considering the LDSP decay through the Higgs portal, we are assuming it to be dominant compared to other portals. Note that a spin-1 LDSP cannot decay through the Higgs portal due to quantum numbers.

In the bottom row of fig. 3.8 we show the bounds where the LDSP decay occurs through the $\Delta = 4$ Higgs portal. The longer lifetime of the LDSPs, due to a very small coupling to leptons and the extra $\Lambda_{\rm IR}^2/m_h^2$ suppression factor, effectively shifts the exclusion regions to higher $\Lambda_{\rm IR}$ regions. However, bounds from such values of $\Lambda_{\rm IR}$ can be suppressed due to being too close to the edge of allowed phase space, effectively chopping off the bounded region. This makes these bounds typically weaker than colliders, in their $\Lambda_{\rm UV}$ reach, although they still cover regions unconstrained by Z portal decays at higher $(\Lambda_{\rm IR}/\Lambda_{\rm UV})$ ratio.

Finally, for completeness, we will now tabulate constraints coming from invisible meson decays where the LDSP is long-lived enough to escape detectors. Overall, we find that these bounds are weaker in their $\Lambda_{\rm UV}$ reach than the ones coming from both LHC and neutrino detectors.

For the Z portal (both production and decay), the strongest constraints from invisible meson decay come from flavour changing decays of B and K mesons (updated w.r.t ref. [25]). We take the BaBAR upper limit for $B^+ \to K^+$ decays [162]: $\mathcal{B}(B^+ \to K^+ \bar{\nu}\nu) < 1.6 \times 10^{-5}$, which gives

$$\begin{aligned} &\frac{\Lambda_{\rm UV}}{\rm GeV} > 60\,(\kappa_J^2\, c_J)^{1/4}, \\ &\frac{\Lambda_{\rm IR}}{\rm MeV} \ll 108\,(\kappa_J^2 c_J)^{-0.2}\,(\text{weak})\,, 65\,(\kappa_J^2 c_J)^{-0.2}\,(\text{strong}) \end{aligned} \tag{3.35}$$

For the case of $K \to \pi +$ DS, we take the upper limit from the NA62 Collaboration [163]:

$\mathcal{B}(K^+ \to \pi^+ + \bar{\nu}\nu) < 1.06 \times 10^{-10}$ which gives

$$\frac{\Lambda_{\rm UV}}{\rm GeV} > 68.8\,(\kappa_J^2\,c_J)^{1/4},$$
$$\frac{\Lambda_{\rm IR}}{\rm MeV} \ll 83\,(\kappa_J^2 c_J)^{-0.2}\ \text{(strong)} \tag{3.36}$$

The bounds for a weakly coupled DS are similar. For the case in which the LDSP decay is via $\Delta_{\mathcal{O}} = 4$ Higgs portal instead, the bounds for the B and K meson decays respectively are:

$$\frac{\Lambda_{\rm UV}}{\rm GeV} > 60\,(\kappa_J^2\,c_J)^{1/4},\ \text{for}\ \frac{\Lambda_{\rm IR}}{\rm GeV} \ll 1.6\,(\kappa_J^2 c_J)^{-0.14} \tag{3.37}$$
$$\frac{\Lambda_{\rm UV}}{\rm GeV} > 68.8\,(\kappa_J^2\,c_J)^{1/4},\ \text{for}\ \frac{\Lambda_{\rm IR}}{\rm MeV} \ll 77\,(\kappa_J^2 c_J)^{-0.14} \tag{3.38}$$

In the above, the condition on $\Lambda_{\rm IR}$ has been calculated assuming a strongly coupled DS, and they do not change significantly for the weakly coupled case.

The invisible decays from J/ψ which have been searched for by the BES Collaboration [164] set an upper limit on $\mathcal{B}(J/\psi \to \bar{\nu}\nu) < 7.2 \times 10^{-4}$. However, we found the resulting bound on $\Lambda_{\rm UV}$ to be weaker than those coming from the BaBar and NA62 limits on B, K decays, and we do not report it here.

A preliminary study of FASER and SND, using an integrated luminosity of $\mathcal{L} = 150$ fb^{-1} and 3 signal event exclusion, shows that the exclusion power of these experiment comes mostly from the decays of SM forward object like mesons or on-shell Z, whose spectra can be taken from the FORESEE package [165]. For the decay through Z portal, the bounds are comparable to DUNE but are in a slightly different $\Lambda_{\rm IR}$ region due to a different boost, and a different distance at which the detectors are located, while for decays through Higgs portal ($\Delta = 4$) they can improve the bounds up to $\Lambda_{\rm UV}$ 1 TeV: this is because for resonant production through Z portal, $p_{\rm DS}^2 \simeq m_z^2$, allowing for larger LDSP masses to be produced and tested. Future experiments like FASER2 can exclude up to 10 TeV given the larger luminosity and the dimensions of the detector, compared to its predecessor. These will be studied in detail in a future work, together with other experiments at the lifetime frontier such as MATHUSLA and Codex-b.

3.4.2 JJ Portal (Z-aligned) Production

Even though the Z-aligned JJ portal and Z-portal are equivalent at neutrino experiments after an appropriate rescaling of the κ, there is a distinction between them at high energy experiments that can produce a Z on-shell. Contrary to Z-portal case, for the Z-aligned JJ portal, the LHC bounds are generally weaker due to the lack of resonant production and EFT consistency condition on $\Lambda_{\rm UV}$. For the same reason, there is no bound coming from Z-width. In this scenario, the bounds on $\Lambda_{\rm UV}$ come only from LEP missing energy searches (see fig. 8 in ref. [25]). Therefore regions in the parameter space with too short lifetimes are not tested due to the requirement for the LDSP to decay outside the detector. On the other hand, the bounds coming from high-intensity experiments such as neutrino experiments are essentially unchanged with respect to the Z-portal case, so that all the discussion from before applies: they are able to exclude a larger portion of $\Lambda_{\rm UV}$ by roughly one order of magnitude in the large lifetime region (low $\Lambda_{\rm IR}$), compared to the LEP/LHC detector size, while it excludes a completely unexplored region at small lifetime (or large $\Lambda_{\rm IR}$).

3.4.3 JJ Portal (generic) Production

The previous sections can give us an insight on how high-intensity experiments can put a bound on a generic $J_\mu^{\rm SM} J_{\rm DS}^\mu$ portal, where $J_\mu^{\rm SM}$ is a generic flavor-conserving SM current. Missing-energy bounds coming from LHC will still hold provided $\mathcal{O}(1)$ couplings to light quarks, although as explained in the previous section they are limited by the EFT condition. If these are absent, (e.g. for $\bar{e}\gamma^\mu e\, J_\mu^{\rm DS}$ portal) the leading bounds come from LEP mono-photon searches ($\Lambda_{\rm UV} \gtrsim 10^2$ GeV for $\Lambda_{\rm IR} \lesssim 100$ MeV), while electron beam dump experiments like E137 and missing energy searches at NA64 put weaker bounds, see ref. [25].

Proton-beam based neutrino experiments cannot probe hadrophobic current interactions given that couplings to quarks are essential for all production modes. Since neutrino experiments typically exclude LDSP masses for $\Lambda_{\rm IR} \lesssim 2m_\pi$, if the decay proceeds through generic JJ portal, we need non-zero couplings to electrons. If that is small, the Higgs portal may be relevant depending on couplings. This feature is not present in missing energy searches at high energy colliders and high intensity experiments, which only probe the production mode. This problem can be circumvented if instead of looking at displaced vertex signatures (where LDSP decays inside the detector), in which both DS production and DS decay into SM are required, scattering events are also considered. As mentioned in previous sections, we do not look at such signatures due to the extra assumptions needed with respect to LDSP decays.

We remark that no big difference is expected from changing the axial or vector nature of the SM current as long as their coupling is of the same order. While for Z portal the axial contribution to bremsstrahlung is larger than the vector counterpart, due to the accidentally small coupling of the vector component, this is not necessary for a generic case. A similar argument also hold for DY mode, while for MD mode the quantum numbers of the SM current select the relevant meson processes (see App B for details). To conclude, as long as DS has a coupling to proton and electrons in $J_{\rm SM}^\mu$, we expect the results to not change dramatically at fixed magnitude of the couplings: the bounds presented in sec. 3.4.1 apply.

3.4.4 Higgs Portal Production

The bounds at neutrino experiment for production through $\Delta_\mathcal{O} = 4$ Higgs portal $\mathcal{O}H^\dagger H$ are very weak: assuming decay through Z portal $\Lambda_{\rm UV} \ll 10^2$ GeV for DB and DY modes since these modes are suppressed by a small Higgs coupling. Only radiative meson decays happening through a top loop do not suffer from such a problem. The strongest bounds for this case then come from meson decay $\mathrm{K} \to \mathrm{DS}$ where for DUNE-MPD, we get $\Lambda_{\rm UV} \lesssim 12$ GeV. This exclusion is much weaker than the bounds coming from missing energy searches at LHC and Higgs coupling fits [25], $\Lambda_{\rm UV} \gtrsim 450$ GeV. For $\Delta \geq 4$ the rate is suppressed with respect to the Z portal as explained in Sec. 3.2.1. The situation is slightly improved for high-energy beam experiments like SHiP (where $\Lambda_{\rm UV} \lesssim 74$ GeV is excluded for the $\mathrm{B} \to \mathrm{K} + \mathrm{DS}$ meson decay), but is still not competitive with the ones coming from Higgs resonant production at LHC. For this reason, we do not show any plots for production through the Higgs portal.

For a $\Delta_\mathcal{O} = 3$ Higgs portal, at DUNE-MPD, $\mathrm{K} \to \mathrm{DS}$ decay gives the leading bound, $\Lambda_{\rm UV} \lesssim 540$ GeV. At SHiP, we find that the leading bounds come from $\mathrm{B} \to \mathrm{K} + \mathrm{DS}$ decays which give $\Lambda_{\rm UV} \lesssim 10$ TeV for $\Lambda_{\rm IR} \sim 1.8 - 2.8$ GeV. The DUNE-MPD bounds are weaker than the LHC missing energy searches (which exclude $\Lambda_{\rm UV} \lesssim 8$ TeV) whereas the SHiP bounds are stronger.

The forward experiment FASER does not put strong constraint on DS production and decay through resonant Higgs portal. Only FASER2, due to a higher luminosity and geometric acceptance,

can put bounds that are comparable with the conventional LHC searches in a narrow lifetime regions: up to $\Lambda_{\rm UV} = 10$ TeV for $\Delta = 3$, while up to $\Lambda_{\rm UV} = 1$ TeV for $\Delta = 4$.

3.5 Summary

Secluded sectors that interact very feebly with the SM have the potential to be probed at the high-intensity frontier, particularly at neutrino experiments (as has been previously explored in refs. [58, 60, 89, 166], see also refs. [154, 155]). Most of the past work has focused on the case of relevant portals, while the case of irrelevant portal DS scenario has only recently been explored [25, 71, 74, 139, 167]. In this work, we have considered the sensitivity of DS that interacts with SM through a dimension 6 irrelevant portal, at past and current neutrino experiments, and its prospective discovery in both existing and future neutrino experiments based on proton beams.

We have performed a detailed study of the possible production mechanisms of DS through non-renormalizable portals: meson decays ($M \to m + DS$, $V \to \text{DS}$), direct partonic production ($\bar{q}q \to \text{DS}$, $gg \to \text{DS}$), and dark bremsstrahlung ($pp \to \text{DS} + X$). The interplay between the various production mechanisms as a function of the DS invariant mass squared $p^2_{\rm DS}$ can be summarized in the plot shown in fig. 3.1. Compared to previous works on irrelevant portals, we have added production details, and also considered strongly coupled dark sectors, and done so in a model agnostic framework. Further, we have constrained such dark sectors using past and current analyses at beam dump/neutrino experiments, also showing projections for prospective searches at existing and future neutrino experiments. In order to emphasize the importance of these bounds, we have also compared our results with previous bounds on such portals.

In an earlier work of this scenario [25], the most stringent bounds on DS excitations produced from the decay of Z bosons was set by LHC monojet searches [148] and LHC displaced vertex search [149, 150], in a range of $(\Lambda_{\rm UV}, \Lambda_{\rm IR})$ values dictated by various factors such as the energy of the experiment and the lifetime of the DS etc. In the present work, we have tried to address the question if neutrino experiments, being placed farther from the interaction point (as compared to say the ATLAS detector at LHC) could probe a lower $\Lambda_{\rm IR}$ range, thereby testing a complementary parameter space with respect to high energy colliders for such elusive dark sectors. Our main summary plots can be found in fig. 3.8.

While the present work focuses on the utility of neutrino experiments for probing dark sectors, we would like to mention the status of other probes of the dark sectors considered here, for completeness. Colliders and beam-dump probes produce the DS states directly. Other setups that also produce DS states directly result in astrophysical bounds from Supernova cooling, from lifetime of horizontal branch stars and from positronium lifetime. Due to kinematics, bounds coming from astrophysical objects such as Supernovae can't probe the $\Lambda_{\rm IR} \gtrsim 100$ MeV given the lower typical temperature. Therefore they are subleading in the region in which neutrino experiments are competitive with respect to LHC bounds, and we will not show them. However in the much lower $\Lambda_{\rm IR}$ regime, they can become the most competitive bounds, as can be seen for example by recasting the results of [168]. Complementary to those are indirect probes where the initial and final states are SM states, and DS degrees of freedom propagate internally. Examples of such probes are electroweak precision tests (EWPT), fifth-force constraints, torsion balance experiments, molecular spectroscopy, etc. Depending on the process, these indirect probes are UV sensitive (and in that case they do not probe the dark dynamics directly) or give weaker constraints. A careful analysis of all these direct and indirect effects was already carried out in ref. [25] and we refer the reader to there.

In this work, for the case of Z portal DS production, we find that past analyses and prospective

DS searches at current neutrino experiments give weaker bounds when compared with the current bounds from LHC and LEP in resonant production scenarios. However, future neutrino experiments such as DUNE-MPD would improve on this, and will be sensitive to $\Lambda_{\rm IR}$ in the range $0.1-1$ GeV for $\Lambda_{\rm UV}\sim 1$ TeV. The current displaced vertex searches at LHC are already probing $\Lambda_{\rm UV}$ as high as few TeVs, but only in the $\Lambda_{\rm IR}$ range $\sim 0.6-2.5$ GeV for the strongly coupled DS case. The ATLAS DV searches lose sensitivity in the range of $\Lambda_{\rm IR}\sim 0.1-0.6$ due to trigger requirements (as can be seen from the gap on the right plot in fig. 3.8).[14] Future neutrino experiment DUNE-MPD will have a unique sensitivity to access this gap in the parameter space for a range of $\Lambda_{\rm IR}\sim 0.1-1$ GeV for $\Lambda_{\rm UV}$ of a few TeVs.

We have also compared these results with projections from the proposed experiment SHiP which serves as a benchmark for LLP experiments. As can be seen from fig. 3.8, SHiP will improve on the reach of DUNE-MPD by probing $\Lambda_{\rm UV}$ of few TeVs for a range of $\Lambda_{\rm IR}\sim 0.1-2$ GeV. This is mainly due to its higher proton beam energy of 400 GeV and larger geometric acceptance ($\epsilon_{\rm geo}\sim 1$ for the production modes bremsstrahlung and DY and $\epsilon_{\rm geo}\sim 0.1-0.9$ for K and J/ψ decays).

As we have described in the previous section, we can recycle our bounds at neutrino experiments on Z portal also for the case of $J^{\rm SM}_\mu J^\mu_{\rm DS}$ portal where $J^{\rm SM}_\mu=\bar f\gamma_\mu f,\bar f\gamma_\mu\gamma^5 f, f=l,q$. The earlier work in [25] found no bounds from LHC for this portal, once EFT considerations were taken into account. The only constraint presented is the one for $J^{\rm SM}_\mu=\bar e\gamma_\mu e$ from monophoton searches at LEP (see fig. 8 in ref. [25]) where the excluded space is restricted to $\Lambda_{\rm UV}\lesssim 200$ GeV for $\Lambda_{\rm IR}\lesssim 0.1$ GeV. These bounds are much weaker than the bounds we get at neutrino experiments. Therefore neutrino experiments are a useful tool to study DS that do not directly mix with the Z and that are not enhanced by resonant production at colliders. We have already explained how our Z portal bounds can be recycled for a JJ portal, since a JJ portal can be obtained from Z portal after integrating out Z mediator.

For the case of the Higgs portal $\mathcal{O}H^\dagger H$ production (for $\Delta_\mathcal{O}=4$) the bounds from neutrino experiments are very weak, and are limited to values of $\Lambda_{\rm UV}$ much below the electroweak scale. Whereas, in comparison, bounds from Higgs resonant production derived in ref. [25] coming from missing energy and displaced vertex searches at high energy colliders are much stronger.

To map our results to the dark photon (DP) portal results, we can make the DS emission diagrams for the Z portal case by replacing the dark photon field A'_μ as

$$(e\epsilon)A'_\mu\to(\kappa_Z/\Lambda^2_{\rm UV})(g_Z v/m_Z)J^{DS}_\mu \tag{3.39}$$

(See also [25, 167] for similar a rescaling discussion). This rescaling can allow us to see Z portal in a very crude way as a dark photon portal with an effective mixing parameter given by

$$\epsilon_{eff}=\frac{p^2_{\rm DS}}{\Lambda^2_{\rm UV}}\frac{\sqrt{\frac{\kappa^2_Z g^2_Z v^2}{m^2_Z}c_J}}{4\pi e} \tag{3.40}$$

In Fig. 3.9 we show the parameter space for the dark photon scenario excluded by the past experiments, as well as projected sensitivities from various operating and future experiments. In Fig. 3.9, DUNE will be sensitive to ϵ in the range $\sim 5\times10^{-8}-3\times10^{-7}$ for mass of dark photon $m_{A'}\sim 0.2-1$ GeV. Using Eq. 3.40 and the bounds we get for the Z portal scenario in our

[14] The trigger requirements imposed in [25] depend on the $n_{\rm LDSP}$ distribution. Events where the number of LDSPs produced has a downward fluctuation can loosen the cut, but will also affect the total cross-section, the decay probability and the geometric efficiency. Including this effect systematically will reduce the un-probed region but not entirely.

($\log_{10}(\Lambda_{\rm IR}/\Lambda_{\rm UV}), \Lambda_{\rm UV}$) parameter space (See Fig.3.8), we can very crudely translate our constraints to constraints on ϵ_{eff}. For DUNE[15], we find that the projected reach would be constraining an $\epsilon_{eff} \sim 2 \times 10^{-6}$ for $\Lambda_{\rm IR} \sim 1$ GeV (where $\Lambda_{\rm IR}$ is the DS mass gap). This rescaling allows us to effectively check our model-dependent bounds against bounds given in literature.

The bounds presented in this chapter here are derived under a model agnostic approach and are applicable to a large class of DS models (see [25] for explicit examples). Knowledge of the underlying dark dynamics can be used to study other possible signatures like DS scatterings with SM particles, but will need to be done on a case-by-case basis, and hence is out of the scope of this work. We have discussed in detail our assumptions and limitations of our approach in section 3.1. Our results are conservative and can be improved if the full theory is defined explicitly. Despite this, we claim that our approach can be very useful in giving a qualitative picture.

The point of this work is to convey the usefulness of a model agnostic approach to exploring dark sectors, and the potential of neutrino experiments (both current and future) as unique probes of irrelevant DS-SM portals. Future proposed LLP experiments at LHC interaction points like MATHUSLA, CODEX-b, ANUBIS are designed to improve reach on $\Lambda_{\rm IR}$ scales for such elusive DS. However, future neutrino experiment DUNE Multi-Purpose Detector (MPD) [137] running at the LBNF (Long Baseline Neutrino Facility) would probe low $\Lambda_{\rm IR}$ scales in a shorter timescale. The forward LHC detectors like FASER and SND (see [169] for a recent status report), built for searching feebly interacting particles would be taking data during the LHC Run 3, and could also give useful bounds for our DS. We hope our study would motivate analyses of neutrino-detector data for the search of such elusive dark sectors.

[15]here to get ϵ_{eff} we are plugging $g_Z = g_u$ defined in Eq. 3.21

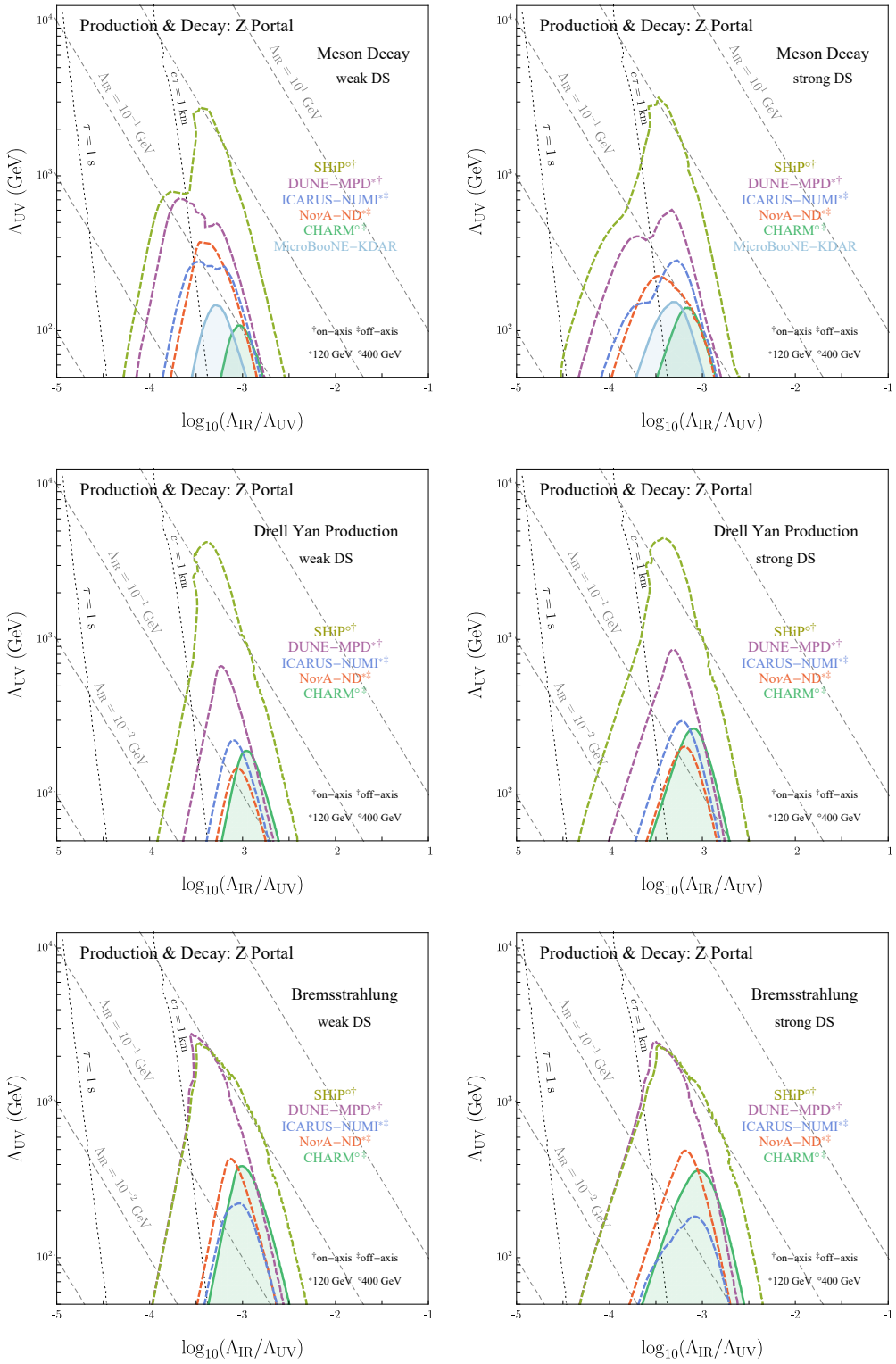

Figure 3.7: Constraints on DS production and decay from $D = 6$ Z portal for various production modes: Meson Decay (top row), Drell-Yan (mid row) and Dark Bremsstrahlung (bottom row), for weakly coupled (left) and strongly coupled (right) benchmark cases. Exclusions are shown in solid lines, while future projections are shown in dotted lines. The superscripts indicate the beam energy and the on/off axis nature of detectors for each of the experiments considered. The black dotted lines show the LDSP lifetime τ isocurves, while the gray dashed lines show $\Lambda_{\rm IR}$ isocurves. The region with $\tau > 1$ s is excluded by constraints coming from BBN (cosmology). The bounds assume $p_{\rm DS}^2/\Lambda_{\rm UV}^2 < 0.1$ for EFT validity which is satisfied by restricting to $\Lambda_{\rm UV} > 50$ GeV. All plots assume $\kappa_i^2 c_i = 1$, where i labels the portal, κ is the portal coupling and c is a measure of degrees of freedom of the DS.

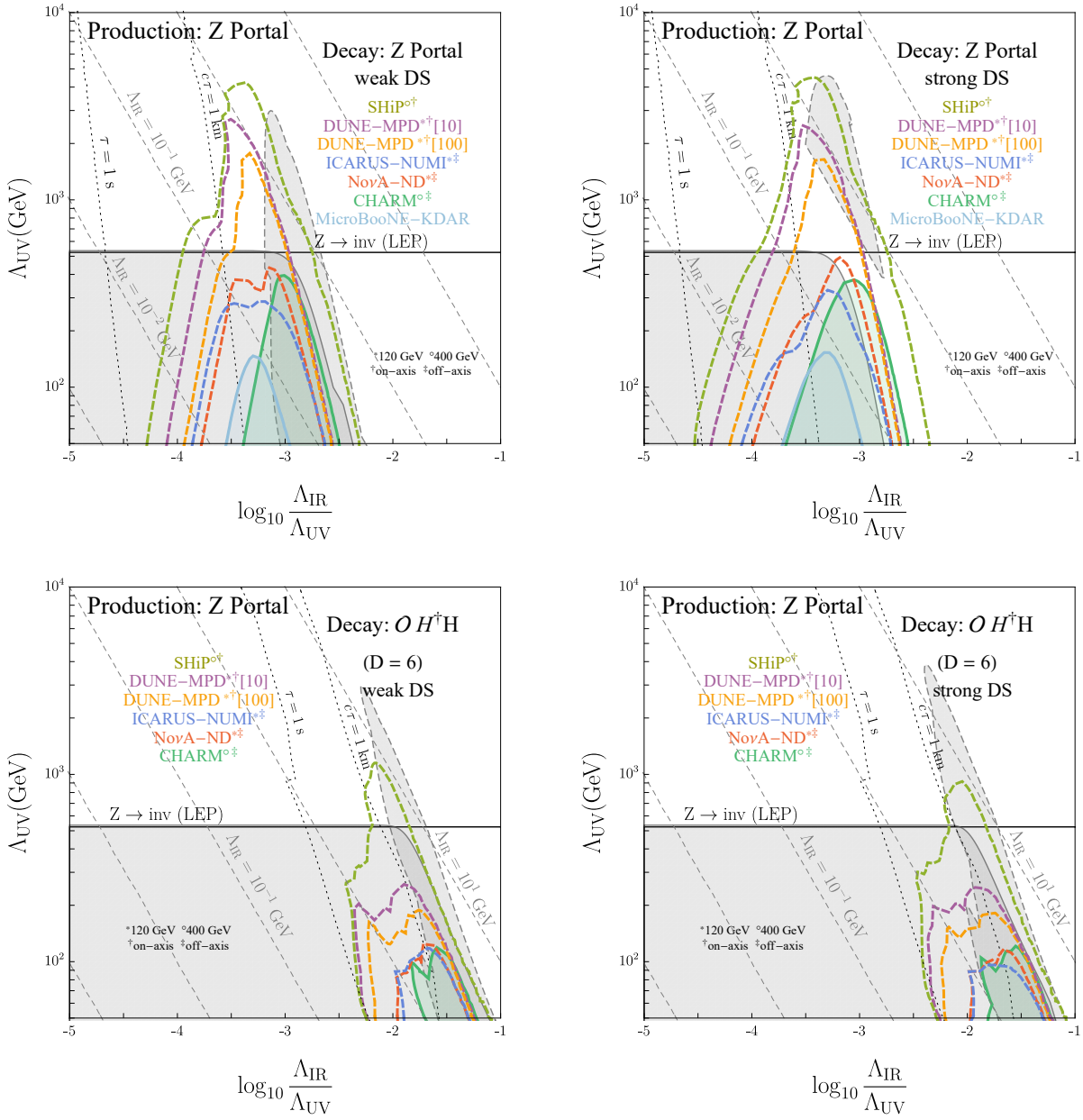

Figure 3.8: Constraints on DS production through the $D = 6$ Z portal, and decay through the same Z portal (top), or through $D = 6$ $\mathcal{O}H^\dagger H$ portal (bottom), at various neutrino experiments. We have shown both the 10 event and the 100 event lines for DUNE. For comparison, bounds from high-energy colliders (obtained in ref. [25]) are also shown in gray (monojet searches with solid boundary and displaced vertex searches with dashed boundary). The left (right) plots assume weakly coupled (strongly coupled) dark dynamics. The exclusion from the Z invisible width measurement at LEP is shown by the horizontal solid black line. We restrict to $\Lambda_{\rm UV} > 50$ GeV for EFT validity. All plots assume $\kappa_i^2 c_i = 1$, where i labels the portal, κ is the portal coupling and c is a measure of degrees of freedom of the DS.

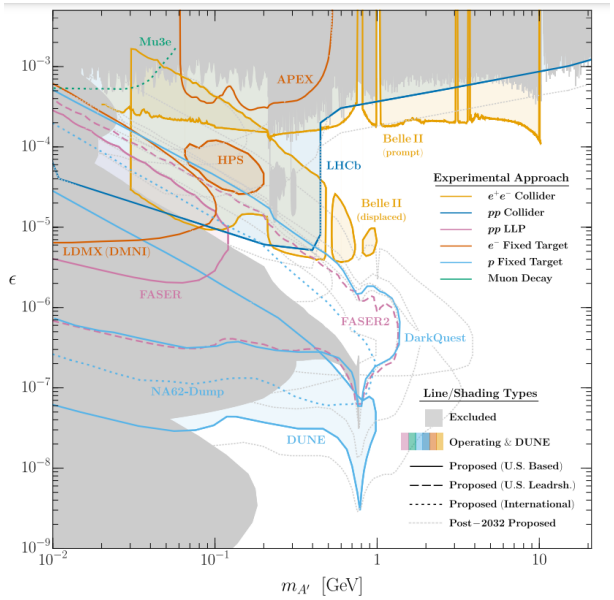

Figure 3.9: Constraints on the visible dark-photon parameter space taken from Ref. [53]: Nearterm and future opportunities to search for visibly decaying dark photons interacting through the vector portal displayed in the dark photon mass (m'_A) – kinetic mixing (ϵ) parameter space. Constraints from past experiments (gray shaded regions) and projected sensitivities from operating and fully funded experiments and DUNE (colored shaded regions). Line coloring indicates the key experimental approach used (e^+e^-collider, pp collider, LHC LLP detector, electron fixed target, proton fixed target, muon decay), highlighting one aspect of the complementarity between different facilities/experiments. Collectively, these experiments are poised to cover large regions of open dark photon parameter space

Part II

How to hope for grand unification and not overclose the universe with dark matter

Chapter 4

Introduction to Part II

In this chapter, we introduce new physics that is heavy $\sim \mathcal{O}(100$ TeV) and charged under the SM - a composite dark matter model with an $SU(5) - GUT$ UV completion [27, 28]. This introduction gives the main motivations for this work, drawing some analogies with bound states in QCD.

4.1 Composite Dark Matter

The Standard Model (SM) can be considered paradigmatic for many of its remarkable properties. In particular, global symmetries in the SM arise accidentally in the infrared and explain conservation laws violated only by UV-suppressed higher-dimension operators. A minimal solution to the cosmological stability of dark matter can be given using accidental symmetries in analogy with the proton stability arising due to baryon number conservation in the SM. This was demonstrated in Chapter 1. Such models are free from any ad-hoc symmetries (like R-parity or Z_2) generally imposed by hand in many DM models. A simple way to get an accidentally stable DM state is to extend the SM gauge group with a new confining gauge force. (See [170] for an example where SM accidental symmetries make the DM stable instead). Such *composite dark matter* models (See [171] for review and references within) can give a variety of possible DM candidates which are either: "meson-like", "baryon-like", "glueball-like" or even more exotic states like the "gluequark" [83].

In this part of the thesis, we follow this possibility that has been explored previously in [83, 172, 173] where the dark sector content comprises new **dark** quarks transforming as real or vectorlike representations under the SM gauge group and as fundamentals under the new dark gauge group. This framework - dubbed *vectorlike confinement* was first introduced in [174] and allows mass terms for the dark fermions without much impact on electroweak precision observables. [1] We concentrate on a baryonic DM which is more robust due to its stability (wrt mesonic DM candidates - See section 5.1 for more details on this). In addition to getting a stable SM-neutral DM candidate, we also want the SM gauge couplings to unify.

4.2 Gauge Coupling unification

The trajectories of the Standard Model gauge couplings at low energies when extrapolated using Renormalization Group Equations (RGE) come close to each other in value at a high energy scale $M_{\rm GUT} \sim 10^{14}$ GeV as shown in Fig. 4.1. This experimental observation can hint at the intriguing possibility that the SM gauge group unifies under a Grand Unified Theory (GUT) (See [176] for a

[1] Adding chiral dark fermions, in contrast, is much trickier due to non-trivial anomaly cancellation (See Ref. [175] for example).

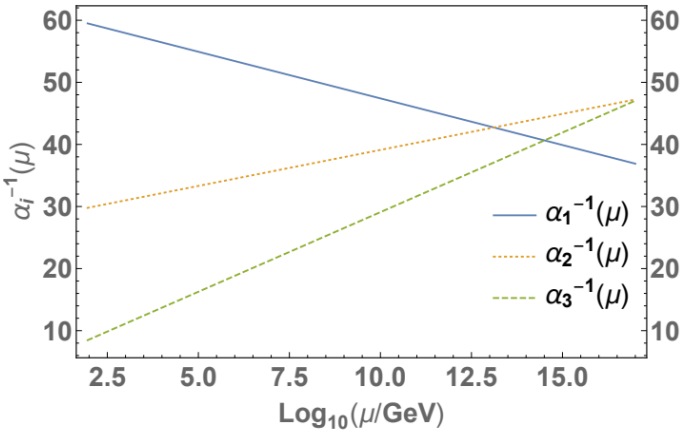

Figure 4.1: SM Renormalization Group Evolution (RGE) of gauge couplings gi at 1-loop written in terms of $\alpha_i \equiv g_i^2/4\pi$. The label "$i = 1, 2, 3$" denotes the $U(1)$, $SU(2)$ and $SU(3)$ SM subgroups respectively with the normalization $g_1 = \sqrt{5/3}g'$ where g' is the SM hypercharge coupling.

review). The simplest scenario of non-supersymmetric (SUSY) minimal $SU(5)$ GUT where the SM matter is unified in the $\bar{5}$ and 10 SU(5) representations has been already excluded [177]. The GUT gauge bosons lead to the prediction of proton decay and the proton lifetime bounds put a lower constrain on the M_{GUT} scale of around $M_{\text{GUT}} \gtrsim 10^{15}$ GeV.

The evolution of the SM gauge couplings is sensitive to any new fields with quantum numbers under the SM gauge group $SU(3) \times SU(2) \times U(1)$. Unification, thus, can be used as a guiding principle to parametrise any new physics (NP) content (see [178] for example). As is evident, there is a vast number of theories and models that can arise to give composite DM states. However, *we will find that demanding that any new particles mitigate (and not worsen) gauge coupling unification in the SM puts severe restrictions on these models.* In fact, we find that very few models pass our criteria (see details on benchmark model in Chapter 6) for gauge coupling unification under our unification criteria (See sec 5.2).

4.3 Dark Spectrum

In this section, we discuss the various mass scales that appear in the dark sector and how they appear from both top-down and bottom-up considerations.

The non-Abelian dark gauge group ($SU(N)_{\text{DC}}$ or $SO(N)_{\text{DC}}$) confines in the IR at the dark confinement scale given by Λ_{DC}. We consider the regime where the dark fermions are lighter than the confinement scale with mass $m < \Lambda_{\text{DC}}$. Requiring that the stable dark baryons formed from these light fermions reproduce all the observed dark matter relic abundance [17] gives $\Lambda_{\text{DC}} \sim 80$ TeV [172] (See also Sec. 6.3.4). This scale can vary by $\mathcal{O}(30$ TeV) if uncertainties on the non-perturbative cross-section for baryonic annihilation $\langle \sigma_{\text{ann}} v \rangle$ are considered.

These dark fermions come as $SU(5)$ GUT fragments. In a consistent $SU(5)$-GUT theory, the *GUT* partner fermions of these dark fermions would be introduced. These GUT partners have mass of scale $M_H > \Lambda_{\text{DC}}$. This mass scale M_H is fixed from gauge coupling unification considerations and can vary within a range of values under our *optimistic unification criteria.* (See section 5.1.2 for more details).

It is evident at this point that such a strongly coupled dark sector with both light $m < \Lambda_{\text{DC}}$ and heavy $M_H > \Lambda_{\text{DC}}$ fermions would have a rich spectrum of bound states below confinement.

The spectrum comprises light baryons (also the DM candidate) with mass $M \sim N_{\rm DC}\Lambda_{\rm DC}$, light mesons with $M < \Lambda_{\rm DC}$, heavy mesons with mass $M \sim M_H > \Lambda_{\rm DC}$, heavy baryons with mass $M \sim M_H > \Lambda_{\rm DC}$, heavy-light mesons with mass $M > \Lambda_{\rm DC}$, heavy-light-light baryons with mass $M > \Lambda_{\rm DC}$, and some more states. For more details on the interplay and the impact of these bound states, see Chapter 6.

Analogy with QCD bound states

Let us look in parallel at QCD now: bottom and charm quarks with masses m_Q are very distinguished from light strange, up, and down quarks. In fact, the hierarchy $m_Q \gg \Lambda_{\rm QCD}$ leads to simplified dynamics for these quarks. However, they are still light enough to have a rich spectrum of bound states given by heavyonium, heavy-light mesons (mesons formed of one heavy and one light quark) and so on. Indeed, the top quark is too heavy to have this effect since it decays too quickly. Bound states formed by these heavy quarks bottom, charm share many rich interactions in the SM.

In the dark sector discussed in this part of the thesis, the cosmological history and dark matter phenomenology are controlled by the GUT partner mass M_H (See section 6.3 for details). The M_H value also controls in addition the spectrum of the theory. For the bound states with mass $M_H \gg \Lambda_{\rm DC}$, we rely on heavy quark effective theory for modeling the mass of the bound states (See Sec. H.2 for details). In order to describe the dynamics below the dark confinement scale, we rely on lattice QCD results.

In the dark theory, we find that for very large M_H, the fermions are short-lived and cannot survive till dark confinement. This leads to no cosmological consequences for the DM phenomenology and we reproduce the standard light baryonic DM picture. This is in analogy with the SM top quark which decays too quickly to give interesting bound states in QCD.

For lower M_H mass values, the GUT partners can form dark bound states with light dark fermions which leads to a *recombination* period during the cosmological history (See details in Sec. 6.3.2).

4.4 Why GUT completion?

Demanding gauge coupling unification from composite dark matter models introduces an additional theory prior - we will find that this is very constraining on the number of theories that give a viable baryonic DM candidate. In addition to this, the impact of GUT partners is non-trivial on the DM cosmology as we show in Sec. 6.3.4. We find that to accommodate a realistic GUT model, we need non-trivial reheating dynamics such that the GUT partner abundance is suppressed. In addition to this, another crucial prediction of the benchmark model is the production of SM-colored dark mesons (NGBs) in the theory (See Sec. 6.2 for more details on the meson spectrum).

Imposing $SU(5) - GUT$ UV completion also leads to systematic classification of composite dark matter models from an EFT point of view. In the low-energy dark effective theory at scales much below the GUT scales, the decay of bound states relies on non-renormalizable operators breaking symmetries. For any viable model with a baryonic DM candidate, this implies operators that will make other bound states decay fast enough. Working in a GUT UV completion, we find that these higher-dimension operators in the IR Lagrangian must be generated *at the renormalizable level in the GUT Lagrangian.* We use this to systematically classify all viable models and write their *parent GUT theory.* A full list and more details on this GUT approach of model building can be found in

Sec. 5.1.2.

Chapter 5

Composite Dark Matter in $SU(5)$ Grand Unified Theory

In this chapter and in chapter 6 based on [27, 28], we explore scenarios of extending the SM by the *addition of dark fermions that can give SM gauge coupling unification and give a baryonic dark matter stable due to the dark baryon number.* An effort in this direction was already made in [172].

The main motivation of this chapter is to systematically describe the $SU(5)$-GUT UV completion of composite dark matter models. The dark fermions added transform as fundamentals under the dark color gauge group $\mathcal{G}_{DC}$ ($SU(N)_{\rm DC}$ or $SO(N)_{\rm DC}$) and are light with masses below the dark confinement scale, $\Lambda_{\rm DC}$. These dark fermions come as $SU(5)$ fragments. In a consistent $SU(5)$-GUT theory, the GUT partners of these dark fermions are introduced. We are thus led to ask the following question: *how relevant are the GUT partners*[1] *of these dark fermions and how do they impact the low-energy model building and dark matter cosmology?* We systematically address this question in this chapter and in chapter 6.

The dark sector in the UV is invariant under $\mathcal{G}_U \times \mathcal{G}_{DC}$ with $\mathcal{G}_U$ being the unified group $SU(5)$. At $M_{\rm GUT}$, the unified group giving $\mathcal{G}_U \to \mathcal{G}_{\rm SM}$. From $M_{\rm GUT}$ down to the dark confinement scale $\Lambda_{\rm DC}$, the theory is then invariant under $\mathcal{G}_{\rm SM} \times \mathcal{G}_{DC}$.

The requirement for SM gauge coupling unification would set the mass scale of the GUT partners which would imply the following hierarchy of mass scales in our dark theory:

$$m \lesssim \Lambda_{\rm DC} < M_H < M_{\rm GUT}.$$

Here m is the mass of the light dark fermions, M_H is the mass of their GUT partners and $M_{\rm GUT}$ is the scale at which the SM couplings *unify*.

Before describing our dark sector, we would like to discuss previous works that have performed studies similar to ours. We are not aware of many works in the literature that consider accidentally stable dark matter models in the context of $SU(5)$ unification, apart from Ref. [172]. In [172], the authors perform a classification of viable DM models that give an accidentally stable light baryonic DM in strongly coupled theories. Models are characterised as either *golden class* - models where all species symmetries are broken at the renormalizable level, or *silver class* - models which can be made viable either by requiring higher dimension operators to break species symmetries or via additional model building. Instead, our model classification is done from an $SU(5)$-GUT approach and it systematically classifies all viable models based on allowed symmetry-breaking operators.

[1] embedding low energy dark fermions in $SU(5)$ multiplets would mean they come alongside the remaining SM fragments or GUT partners.

Indeed, we reproduce the silver class models of Ref. [172] and find them to be viable models giving an accidentally stable DM baryon. We describe this process in detail in Sec. 5.1.1. Moreover, Ref. [172] studies gauge coupling unification, relying on perfect unification, and analyses only three viable models. Our criteria for unification discussed in Sec. 5.2 is much more relaxed and not based on perfect unification (where the three couplings meet at a point in the $(\alpha_i^{-1}, \log\mu)$ plane). Infact, we also consider SM extensions that simply improve upon the unification found with the minimal SM content. This implies that for some scenarios the GUT partner scale or M_H can be as low as $\Lambda_{\rm DC} \sim 10^5$ GeV. Moroever, when discussing unification, Ref. [172] considers a common mass scale for the GUT partners. We on the other hand, also consider some scenarios of mass splitting between the GUT partners, this can be found in Sec. 5.2.3. Finally, Ref. [172] does not study the impact of GUT partners on DM cosmology. We study this in detail and details can be found in the next chapter.

For models raising the question of SM gauge coupling unification in the context of technicolor theories, see Ref. [179] for example. There are also other models that aim at solving the DM problem and unification in literature [180–183]. However, none of these models utilize accidental symmetries to stabilize DM.

Our benchmark model for unification (See Sec. 6.1) and DM coincides with the model in Refs. [172, 183]. In Ref. [183], the SM is extended by a new multiplet $\chi \equiv (3,2)_{1/6}$ charged under a new confining $SU(3)_H$ gauge group. The DM is a composite state called *GUTZilla DM* with masses much above the scale of 10^7 GeV. Such a high scale DM is not thermal and is produced before the end of reheating. The stability of DM is guaranteed by imposing a $\mathbb{Z}_2$ symmetry. Our thermal DM candidate instead is stable due to accidental symmetry which is much more elegant.

In the proceeding sections and chapters, it will become evident that our analysis extends the analysis done in Ref. [172] relying on a more comprehensive model-building approach. With respect to DM models given in [180, 182, 183], our analysis adopts a different approach utilizing accidental symmetries for stabilizing DM.

In this chapter, we give the details about the classification of viable models (Sec. 5.1) and the analysis of SM gauge coupling unification (Sec. 5.2) for each of these models. The lists of all viable models can be found in Appendix 5.1 and the analysis of unification under our unification criteria can be found in Appendix E.

5.1 Model Building and Classification

We consider an extension of the SM with a new confining gauge group $\mathcal{G}_{\rm DC}$ (*dark colour*) and new Dirac fermions $\mathcal{Q}$ (*dark fermions*) which transform as fundamentals under $\mathcal{G}_{\rm DC}$ and as vector-like representations R (possibly reducible) under the SM gauge group $\mathcal{G}_{\rm SM}$.

Adding vector-like SM representations takes care of $\mathcal{G}_{\rm SM}$ anomaly cancellation and allows us to write a mass term for the dark fermions.

The dark fermions come as $SU(5)$ fragments, thus, at $M_{\rm GUT}$, they are unified with the remaining SM representations in the $SU(5)$ multiplet or their *GUT partners*. The masses of these GUT partners can be in the range $m < M_H < M_{\rm GUT}$, more precise reasons for this will be explained in the later sections. The only scalar we consider at energies much below the GUT scale is the elementary Higgs boson[2]. We can write the renormalizable lagrangian in the dark sector at energies much below the $M_{\rm GUT}$ scale:

[2]Note that in our UV theory which is an $SU(5)$ theory, we have a scalar transforming as an adjoint of $SU(5)$ to spontaneously break $SU(5) \to SM$

$$\mathcal{L} = \mathcal{L}_{\rm SM} - \frac{1}{4g_{\rm DC}^2}\mathcal{G}_{\mu\nu}^2 + \sum_{i=1}^{N_{\rm S}} \bar{\mathcal{Q}}^i(i\not{D} - m_{\mathcal{Q}})\mathcal{Q}^j + y_{ij}^L \bar{\mathcal{Q}}^i H P_L \mathcal{Q}^j + y_{ij}^R \bar{\mathcal{Q}}^i H P_R \mathcal{Q}^j + \text{h.c.} \tag{5.1}$$

where $\mathcal{G}_{\mu\nu}$ is the dark gluon field strenth and $g_{\rm DC}$ is the dark gauge coupling. The index i in $\mathcal{Q}^i$ denotes the different *dark species* (or multiplets of the SM gauge group) in the models and we show a summation over all the dark species from $i = 1, ... N_{\rm S}$. Each dark model will be further distinguished by the total *dark flavours* $N_{\rm DF}$ which is the total number of representations which are fundamentals under dark colour (this is analogous to flavour in QCD).

The total number of dark flavours $N_{\rm DF}$ and dark colours $N_{\rm DC}$ in a dark model is restricted due to the perturbativity of SM coupling as well as asymptotic freedom of dark colour. We will describe this in detail in the next section on model classification Sec. 5.1.2. Depending on the SM quantum numbers of the dark fermions $\mathcal{Q}^i$, yukawa couplings with the Higgs boson can be written, as can be seen from Eq. 5.1.

It is evident that the renormalizable $\mathcal{L}$ in Eq. (5.1) is left invariant under a phase rotation of all dark fermions. This is the *dark baryon number* symmetry, $U(1)_{\rm DB}$ which can make the lightest baryon stable (see also [172]). In addition to the dark baryon number, the renormalizable Lagrangian in Eq. (5.1) can also have additional accidental symmetries which can lead to the stability of other bound states. For example, dark mesons $\bar{\mathcal{Q}}^i\mathcal{Q}^j$ have been considered in the literature [172], stable due to the accidental symmetry called species symmetry (which rotates each dark fermion species $\mathcal{Q}^i$ by one phase).

Next, we discuss the suitable nonrenormalizable operators that can be written to break all the accidental symmetries arising in Eq. 5.1.

5.1.1 Breaking of Accidental Symmetries

Each dark theory comprising dark fermions can have a certain set of accidental symmetries, as is evident from Eq. 5.1. One or more of these are required to stabilise the DM. Determining the level at which these symmetries are violated implies classifying the non-renormalizable operators that break these symmetries. This also allows us to classify the dark bound states that can be viable DM candidates.

Let us consider a bound state of mass M that decays to SM through a generic higher dimension operator of overall dimension D given by

$$\frac{k}{\Lambda_{\rm UV}^{D-4}}\mathcal{O}_{\rm DS}\mathcal{O}_{\rm SM} \tag{5.2}$$

where k is a dimensionless coupling and $\Lambda_{\rm UV}$ is the UV scale suppressing the symmetry-breaking interaction. Here, $\mathcal{O}_{\rm DS}$ is the combination of dark fields and $\mathcal{O}_{\rm SM}$ is the combination of SM fields. The decay width of such a dark bound state via this operator in Eq. 5.2 can be estimated to be:

$$\Gamma \sim \frac{k^2}{8\pi}\frac{N_{\rm DC}}{16\pi^2} M \left(\frac{M}{\Lambda_{\rm UV}}\right)^{2D-8} \tag{5.3}$$

Indirect detection DM searches [22, 184, 185] imply a lower bound on the DM lifetime of

$$\tau_{\rm DM} \gtrsim 10^{28}\ \text{s}. \tag{5.4}$$

This translates to a lower bound on the $\Lambda_{\rm UV}$ scale suppressing the nonrenormalizable interactions responsible for spoiling the DM stability. For thermal DM, the mass of DM in our model should be ~ 100 TeV. We can now get the bounds on $\Lambda_{\rm UV}$ scale for the symmetry-breaking operator that destabilises DM. These bounds for dimension-5 and dimension-6 operators are:

$$\text{For D} = 5 \qquad \Lambda_{\rm UV} \gtrsim 6 \times 10^{31}\ \text{GeV} \times (k^2 N_{\rm DC})^{1/2} \left(\frac{M_{\rm DM}}{100\ \text{TeV}}\right)^{3/2} \tag{5.5}$$

$$\text{For D} = 6 \qquad \Lambda_{\rm UV} \gtrsim 2.5 \times 10^{18}\ \text{GeV} \times (k^2 N_{\rm DC})^{1/4} \left(\frac{M_{\rm DM}}{100\ \text{TeV}}\right)^{5/4} \tag{5.6}$$

To ensure the stability of DM in our theory, from Eqs. (5.5)-(5.6), it is clear that only $D = 6$ operators are appropriate. We will now discuss why a good DM candidate is given by the lightest dark baryon and not light meson.

Why can light mesons not be good DM candidates if the dark sector is seen as an EFT?

The lightest bound states in any dark sector that are neutral under the SM $(1,1)_0$ are considered to be *good DM candidates* provided their lifetime does not violate indirect detection bounds given in Eq. 5.4. An SM gauge singlet light meson can either be *i*) neutral under species number $\bar{\mathcal{Q}}^i \mathcal{Q}^i$ or *ii*) charged under species number $\bar{\mathcal{Q}}^i \mathcal{Q}^j$. Ref. [172] considered light mesons stable due to "G-parity" (See also Ref. [186] for the first discussion of this model) as a good DM candidate in the $SU(3)_{\rm DC}$ dark model V where V denotes the dark fermions with the SM charges $(1,3)_0$. We explain now why such gauge singlet mesons cannot be robust DM candidates. For all these scenarios, symmetry-breaking dimension-5 operators of the following type can be written:

$$\bar{\mathcal{Q}}^i \mathcal{Q}^i H^\dagger H, \qquad \bar{\mathcal{Q}}^i \mathcal{Q}^j H^\dagger H, \qquad \bar{\mathcal{Q}}^i \sigma^{\mu\nu} \mathcal{Q}^j B_{\mu\nu} \tag{5.7}$$

Here the last operator is responsible for breaking G-parity.

It is evident that meson-stabilising accidental symmetries (species symmetries or G-parity) can always be broken by dimension-5 $M_{\rm P}$-suppressed operators.[3] From the $\Lambda_{\rm UV}$ bound in Eq. 5.5, it is evident that mesons are never good DM candidates in a viable dark model.

Infact, Ref. [186] comments on the G-parity breaking operator given in Eq. 5.7 noting that extra suppression must be imposed to guarantee the cosmological stability of the meson. Indeed, some additional symmetry arguments can be imposed to prohibit the operators of Eq. 5.7 from appearing in the dark Lagrangian , thereby making the light meson cosmologically stable. For our dark theory which we consider as an EFT, light mesons cannot be good DM candidates.

Dark baryons, in our scheme, are stable due to dark baryon number which can only be broken by dimension-6 or higher operators [4] making them a good DM candidate. We can thus identify, the lightest dark baryon as a *robust DM candidate*.

How can we deal with other long-lived dark bound states?

[3] For our dark sector, we restrict ourselves to dark fermions that are fragments of $SU(5)$ representations which are at most rank 2. There could be more exotic higher dimensional $SU(5)$ representations that prohibit such symmetry-breaking dimension-5 operators.

[4] for example for $N_{\rm DC} = 3, \mathcal{Q}^3 \psi_{\rm SM}/\Lambda^2_{\rm UV}$ breaks $U(1)_{\rm DB}$ where the $SU(N)_{\rm DC}$ indices are contracted and $\psi_{\rm SM}$ is an SM fermion required to write an SM gauge invariant $\mathcal{O}^{(6)}$.

In every dark theory, in addition to the DM candidate, accidental symmetries can also give rise to other long-lived bound states. These can be characterized as (*i*) light mesons (at the light-dark fermion level $\sim \Lambda_{\rm DC}$), (*ii*) heavy baryons, and heavy mesons (at the GUT partner level $\sim M_H$). All these bound states are metastable (due to species symmetries) and hence subject to strong cosmological constraints coming from BBN i.e. $\tau_{\text{non-DM}} \lesssim 1$ s where $\tau_{\text{non-DM}}$ is the lifetime of the meta-stable bound state. The decay of these bound states via the symmetry-breaking operators can be generated at any of the following scales:

1. Reduced Planck scale $M_{\rm P}$ (for operators appearing in the UV-GUT Lagrangian),
2. GUT scale $M_{\rm GUT}$ (for operators generated by integrating out GUT bosons $\mathcal{X}_\mu$ and GUT scalars H_3),
3. GUT partner scale $M_{\rm H}$ scale where $\Lambda_{\rm DC} < M_H \lesssim M_{\rm GUT}$ (for operators generated by integrating out GUT partner fermions).

We now begin with discussing the $\Lambda_{\rm UV}$ bounds on the operators responsible for the decay of the light mesons. The lightest mesons in the dark theory can have mass $m \lesssim \Lambda_{\rm DC} \sim 100$ TeV (See also discussion in Sec. 6.2 on the mass spectrum of light mesons). Imposing the BBN bound on the lifetime of these light mesons of $\tau_{\text{non-DM}} \lesssim 1$ s, we can use Eq. 5.3 to get the following lower bounds on the $\Lambda_{\rm UV}$ scale as:

$$\text{For D} = 5 \qquad \Lambda_{\rm UV} \lesssim 6 \times 10^{17}\ \text{GeV} \times (k^2 N_{\rm DC})^{1/2} \left(\frac{M_{\rm meson}}{100\ \text{TeV}}\right)^{3/2} \tag{5.8}$$

$$\text{For D} = 6 \qquad \Lambda_{\rm UV} \lesssim 2.5 \times 10^{11}\ \text{GeV} \times (k^2 N_{\rm DC})^{1/4} \left(\frac{M_{\rm meson}}{100\ \text{TeV}}\right)^{5/4} \tag{5.9}$$

where $M_{\rm meson}$ is the mass of the long-lived light meson. From Eq. 5.8, it follows that accidental symmetries broken by $M_{\rm P}$ suppressed dimension-5 operators can mediate a fast enough decay for light mesons, with mass $m \lesssim 100$ TeV.

However, following Eq. 5.9, accidental symmetries broken by dimension-6 operators cannot be generated at a scale $\Lambda_{\rm UV} = M_{\rm GUT},\ M_{\rm P}$. Such $D = 6$ interactions should be generated by the exchange of GUT partners at a scale $\Lambda_{\rm UV} = M_{\rm H} \ll M_{\rm GUT}$ to mediate a fast enough decay for light mesons.

In addition to this, we can also have $D = 6$ interactions generated at the $M_{\rm H}$ scale via the exchange of GUT partners and an insertion of a dimension-5 operator. For such operators, the $\Lambda_{\rm UV}$ scale can be written as $\Lambda_{\rm UV} = (M_{\rm P} M_{\rm H})^{1/2}$ or $\Lambda_{\rm UV} = (M_{\rm GUT} M_{\rm H})^{1/2}$ depending on the scale suppressing the dimension-5 operator, $M_{\rm P}$ or $M_{\rm GUT}$. For such operators, we find that the BBN bound on long-lived states is not violated only if $M_{\rm H} < 10^6$ GeV. Since this $M_{\rm H}$ scale is too close to $\Lambda_{\rm DC} \sim 100$ TeV, we do not consider the generation of such operators.

We can now concentrate on the possibility of $D = 6$ and other higher dimension operators generated by the exchange of GUT partners $\mathcal{H}$ at the $M_{\rm H}$ scale. As explained[5], such operators are always generated at $\Lambda_{\rm UV} = M_{\rm H}$ through diagrams involving only renormalizable couplings i.e. Yukawa couplings between the SM Higgs boson h and dark fermions. Examples of these diagrams

[5]Note that our dark theory does not have any additional dark coloured scalars, hence the only possibility for nonrenormalizable interactions generated at $\Lambda_{\rm UV} \ll M_{\rm GUT}$ are those obtained after integrating out GUT partners at $M_{\rm H}$ scale.

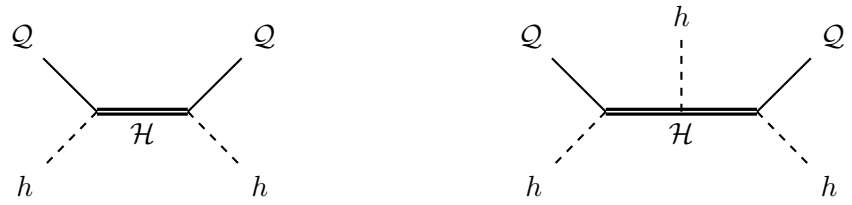

Figure 5.1: Tree level exchange diagrams of GUT partners $\mathcal{H}$ involving Yukawa couplings which will give $D = 6$ operators generated at $\Lambda_{\rm UV} = M_{\rm H}$ after integrating out the GUT partners. Here h is the SM Higgs boson and $\mathcal{Q}$ are the light dark fermions.

are shown in Fig. 5.1 and they will give the resulting corresponding $D = 6$ operators [6]:

$$\frac{y^2}{M_{\rm H}^2}\bar{\mathcal{Q}}^i\gamma_\mu\mathcal{Q}^j H^\dagger D^\mu H \qquad \frac{y^3}{M_{\rm H}^2}\bar{\mathcal{Q}}^i\mathcal{Q}^j HHH \tag{5.10}$$

Here, y denotes either of the Yukawa coupling in the dark sector y_L or y_R shown in the dark sector Lagrangian in Eq. 5.1.

The $D = 6$ operators above can be generalized for any $D > 6$ operator with n couplings with the Higgs and we can write even higher dimension operators suppressed by powers of $M_{\rm H}$:

$$\frac{y^{2n}}{M_{\rm H}^{6n-1}}\bar{\mathcal{Q}}^i\mathcal{Q}^j(HD^\mu H)^{2n} \qquad \frac{y^{2+n}}{M_{\rm H}^{n+1}}\bar{\mathcal{Q}}^i\mathcal{Q}^j H^2 H^n \tag{5.11}$$

Such $M_{\rm H}$ scale suppressed $D > 6$ operators can lower the $\Lambda_{\rm UV}$ bound for symmetry-breaking nonrenormalizable interactions required for fast enough decay of long-lived states.

In fact, we can have a $D = 9$ operator given by $\bar{\mathcal{Q}}^i\mathcal{Q}^j(HD_\mu H)^2/M_{\rm H}^5$breaking species symmetries. Such a $D = 9$ operator will allow long-lived mesons to decay fast enough. Imposing $\tau < 1$ s will give the upper bound on $\Lambda_{\rm UV}$ as:

$$\Lambda_{\rm UV} = M_{\rm H} \lesssim 3.6 \times 10^7 \text{ GeV} \times (k^2 N_{\rm DC})^{1/10}\left(\frac{M_{\rm meson}}{100 \text{ TeV}}\right)^{11/10} \tag{5.12}$$

This M_H value is allowed under our assumption that $M_H/\Lambda_{\rm DC} \gtrsim \mathcal{O}(10^2)$ and is also compatible with the EFT description.

We do not need to classify any $D > 9$ species symmetry-breaking operators, we comment on this now. Since such operators contain a single dark quark bilinear, it follows that to break all the relevant species symmetries it is sufficient to consider operators with at most four SM Higgs h. Indeed, let us consider the dark fermion bilinear made by the $SU(3)_c$ color singlet T (See Table 5.1 having the EW quantum numbers $(3, 1)$ under the $SU(2)_L \otimes U(1)_Y$. The bilinear $\overline{T}\tilde{T}$ then gives the largest electroweak quantum numbers $\supset (5, 2)$ under $SU(2)_L \otimes U(1)_Y$ out of all the dark fermions considered in this work. This $\overline{T}\tilde{T}$ should be coupled with H^4 to make an SM gauge invariant operator in the dark Lagrangian. We can see now that increasing the dimensionality of the operator would imply adding $(H^\dagger H)^n$, which does not break any new dark species symmetries. Hence, we can conclude that no additional species symmetries are broken by $D > 9$ operators.

With this, we can conclude the discussion on the issue of the metastability of light mesons. In addition to light mesons, as we noted earlier, we can also have heavy baryons and mesons formed

[6]Note that these $D = 6$ operators will only be relevant when a $D = 5$ operator $\bar{\mathcal{Q}}^i\mathcal{Q}^j HH$ breaking the same species symmetries cannot be written. This occurs for models in which the $D = 5$ operator vanishes identically for example, when the HH forms an isosinglet with unit hypercharge.

$\mathcal{Q}^i$	$SU(5)$	SM Quantum Numbers
N	1	$(1,1,0)$
$D \oplus L$	$\bar{5}$	$(\bar{3},1,1/3) \oplus (1,2,-1/2)$
$U \oplus E \oplus Q$	10	$(\bar{3},1,-2/3) \oplus (1,1,1) \oplus (3,2,1/6)$
$Q \oplus T \oplus S$	15	$(3,2,1/6) \oplus (1,3,1) \oplus (6,1,-2/3)$
$V \oplus G \oplus X \oplus N$	24	$(1,3,0) \oplus (8,1,0) \oplus (\bar{3},2,5/6) \oplus (1,1,0)$

Table 5.1: All dark fermions $\mathcal{Q}^i$ and their corresponding quantum numbers under the SM gauge group $SU(3)_c \times SU(2)_L \times U(1)_Y$ along with the $SU(5)$ representations embedding them.

from GUT partners. In general, GUT partners can be long-lived due to accidental symmetries since they can introduce new species symmetries in the dark theory. Bound states made by these GUT species could be SM-charged hence, their abundance will be subject to constraints from BBN as well. This would impose a constraint on their lifetime τ_H. Thus, a hierarchy between the GUT partner mass and the mass of dark fermions forming DM, i.e. $M_H > \Lambda_{\rm DC}$, is crucial. We address the issue of metastability of these GUT partner states in Sec. 6.1

The higher dimension operators generated by the exchange of heavy GUT partners also influence the UV-GUT model or *parent GUT theory*. We discuss this in detail in the next section (Sec. 5.1.2).

5.1.2 Classification of Models

In this Section, we outline the general procedure to classify viable models that can give an accidentally stable baryonic DM. Each viable dark sector model is identified by a set of species of degenerate dark fermions $\mathcal{Q}^i$ having mass $m \lesssim \Lambda_{\rm DC}$. The choices of dark species and dark colours are determined by the dark coupling and SM coupling behaviour in the UV as we will describe next. At $M_{\rm GUT}$ these low energy dark fermions unify with their GUT partners whose mass scale $\Lambda_{\rm DC} < M_{\rm H} < M_{\rm GUT}$ is dictated by the requirement for unification (see Section 5.2). Each low energy dark sector model thus can be embedded in a dark $SU(5)$-GUT model, we also describe the procedure for this. In Table 5.1, we show the notation for the dark fermions $\mathcal{Q}^i$ we use throughout the thesis and their respective SM quantum numbers.

SU$(N)_{DC}$ Models

For a (Weyl) dark fermion $\mathcal{Q}_L$ ($\mathcal{Q}_L^c$) transforming as a fundamental (anti-fundamental) of $SU(N)_{\rm DC}$ and as a (possibly reducible) representation of SM, we extend the SM by adding:

$$\mathcal{Q}_L \oplus \mathcal{Q}_L^c \equiv (\square,\ R_{\rm SM}) \oplus (\bar{\square},\ \bar{R}_{\rm SM}), \tag{5.13}$$

Note that in our notation the dark fermions $\mathcal{Q}^i$ transforming in the conjugate SM representation are denoted with tilde $\tilde{\mathcal{Q}}^i$, however, they transform as a fundamental under $SU(N)_{DC}$. For the case in which representations are real under SM, like for V, G and N, we have $V = \tilde{V}$, $G = \tilde{G}$, $N = \tilde{N}$.

The classification of accidentally stable composite dark matter in this section described has an overlap with all the models listed in Ref. [172]. Our classification procedure results, however, in also additional models obtained after relaxing some simplifying assumptions made in Ref. [172][7]. In the following, we describe our general procedure for the case in which the dark gauge group

[7] In [172] the so-called silver class models that were considered have at most two flavors of dark fermions, this leaves out many viable models.

$\mathcal{G}_{\rm DC} = SU(N)_{\rm DC}$ while in Section 5.1.2 we cover the scenario in which the dark gauge group $\mathcal{G}_{\rm DC} = SO(N)_{\rm DC}$.

We begin with a *'bottom-up'* approach which allows us to identify the light dark fermionic content in each dark sector model. This selection is done by scanning all dark fermions made by the SM fragments of $SU(5)$ representations given in Table 5.1 subject to the following requirements:

1. **Dark Colour Confinement**: The dimension of the SM representation R i.e. the allowed number of dark flavors $N_{\rm DF}$ and the numbers of dark colors $N_{\rm DC}$ dictate the UV behaviour of each dark sector model. These have to be fixed in order to not break the perturbativity of both $SU(N)_{\rm DC}$ and SM. A lower bound on $N_{\rm DC}$ of light dark fermions comes from requiring that the dark fermions preserve the asymptotic freedom of the dark color coupling $\alpha_{\rm DC}$. Using renormalization group equation $\mathrm{d}\alpha_i^{-1}/d\log Q = -\beta_i/2\pi$ to define gauge the $\beta-$function coefficients, we get the following requirement for $SU(N)_{\rm DC}$ gauge group:

$$\beta_{DC} = -\frac{11}{3}N_{\rm DC} + \frac{2}{3}N_{DF} < 0 \tag{5.14}$$

   This, however, is not a sufficient condition for confinement. For the dark colour gauge group to confine, the number of dark flavours $N_{\rm DF}$ in the theory should be below the lower edge of the conformal window or $N_{\rm conf}$ i.e. $N_{\rm DF} < N_{\rm conf}$. This value of $N_{\rm conf}$ is a non-perturbative value and has been calculated by lattice simulations for QCD [187] to be equal to $N_{\rm conf} = 12$. Following [175], we generalise this lattice result for a generic number of dark colours $N_{\rm DC}$ and require that our $SU(N)_{\rm DC}$ models have:

$$N_{\rm DF} \leq 4N_{\rm DC} \tag{5.15}$$

   for dark colour confinement.

2. **Perturbativity of SM couplings**: We want the selection of light-dark fermions to be such that the SM couplings do not develop Landau poles below the SM *"GUT scale"* where we take this scale for to be $M_{GUT}^{SM} = 6.5 \times 10^{14}$ GeV. At the GUT scale, the heavy GUT gauge bosons provide a further negative contribution to the β-function of SM couplings β_i thus improving the perturbativity of the unified model. These conditions are met if the additional contributions from the new physics content to the β_i function coefficients satisfy:

$$\Delta\beta_Y \lesssim 18, \qquad \Delta\beta_2 \lesssim 12, \qquad \Delta\beta_3 \lesssim 11 \tag{5.16}$$

   which translates into an upper bound both on the number of colors $N_{\rm DC}$ and dark flavors $N_{\rm DF}$ of dark fermions.

3. **Presence of DM candidate**: We select the models with at least one viable DM candidate. This for us is the lightest stable dark baryon with no color, no EM charge and no hypercharge. For example, for $N_{\rm DC} = 3$ these DM candidates for the case of $SU(3)_c$ colored dark fermions are given by:

$$QQ\tilde{D},\ DDU \tag{5.17}$$

   or for the case in which the dark fermions have only SM EW charges, we can have:

$$LLE,\ LLT,\ VE\tilde{E},\ VL\tilde{L},\ NE\tilde{E},\ NL\tilde{L},\ VVV,\ VVN,\ VNN,\ NNN \tag{5.18}$$

4. **All species symmetries must be broken:** We select the models in which all species symmetries are broken either by Yukawa couplings or by the allowed higher dimensional operators discussed in section 5.1.1. In Table 5.2 we provide the full list of operators for the $SU(N)_{\rm DC}$ case.

operator	type	dim
$H\bar{Q}\tilde{D}$, $H\bar{Q}\tilde{U}$, $H\bar{L}\tilde{E}$, $H\bar{L}\tilde{T}$, $HL\bar{N}$, $HL\bar{V}$	Yukawa	4
$\overline{\tilde{L}}LH^{c\dagger}H$, $\overline{N}V^iH^\dagger\sigma^iH$, $\overline{E}V^iH^{c\dagger}\sigma^iH$, $\overline{E}T^iH^\dagger\sigma^iH$, $\overline{T}^iNH^{c\dagger}\sigma^iH$	$\bar{\mathcal{Q}}_i\mathcal{Q}_jHH$	5
$\overline{N}\sigma^{\mu\nu}V^iW^i_{\mu\nu}$, $\overline{E}\sigma^{\mu\nu}T^iW^i_{\mu\nu}$, $\overline{G}^a\sigma^{\mu\nu}NG^a_{\mu\nu}$, $\overline{S}\sigma^{\mu\nu}UG_{\mu\nu}$	Dipole	5
$\overline{L}EHHH$, $\overline{L}THHH$	$\bar{\mathcal{Q}}_i\mathcal{Q}_jHHH$	6
$\overline{D}\gamma^\mu UH^{c\dagger}D_\mu H$, $\overline{E}\gamma^\mu NH^{c\dagger}D_\mu H$	$\bar{\mathcal{Q}}_i\gamma^\mu\mathcal{Q}_jHD_\mu H$	6
$\overline{T}^i\tilde{T}^j(H^{c\dagger}\sigma^iH)(H^{c\dagger}\sigma^jH)$	$\bar{\mathcal{Q}}_i\mathcal{Q}_jHHHH$	7
$\overline{E}\tilde{E}(H^{c\dagger}D_\mu H)^2$	$\bar{\mathcal{Q}}_i\mathcal{Q}_j(HD_\mu H)^2$	9

Table 5.2: List of operators for $SU(N)_{\rm DC}$ models breaking species symmetries in viable models.

We note that in our classification no operator couples an $SU(3)_c$ colored dark fermion to one with purely SM electroweak quantum numbers (under $SU(2)_L \times U(1)_Y$). This can be verified from the list of operators in Table 5.2. Regarding $SU(3)_c$ charged dark fermions, we note that the operators generate couplings only among $\tilde{Q}$, D and U (or Q, $\tilde{D}$ and $\tilde{U}$). This means that any viable model must be either a combination of $SU(3)_c$ singlet dark fermions or a combination of $\tilde{Q}$, D and U (or Q, $\tilde{D}$ and $\tilde{U}$).

Identifying minimal parent GUT theory: In order to determine the UV completion of each viable model, we must identify the corresponding *minimal parent GUT theory*. The higher dimension operators required in any low energy viable model to destabilise the light mesons (discussed in Sec. 5.1.1) impact this. These higher dimension operators are generated by integrating out GUT partners at M_H scale. The minimal set of $SU(5)$ GUT representations required to embed both the light-dark fermions as well as these integrated out GUT partners at $M_{\rm H}$ define the parent GUT theory. We will next see that by our intrinsic definition of minimal parent GUT theory, there are no accidental species symmetries in the dark GUT lagrangian. We will demonstrate this using the example of the $L \oplus E$ model given below.

In Appendix D, we provide the list of all viable models along with their parent GUT theories. Note that the same minimal parent GUT theory may be the origin of many low-energy models. Now we discuss two examples of $SU(3)_{DC}$ models to clarify how we identify the parent GUT theory:

- $Q \oplus \tilde{D}$ model: Here the DM candidate is $QQ\tilde{D}$ where all the species symmetries are broken by the Yukawa $\overline{Q}\tilde{D}H$ in the low energy theory. The parent GUT theory for this model is given by $5 \oplus 10$ where the GUT level Yukawa couplings are:

$$\mathcal{L}_{\rm GUT} \ni \bar{\Psi}_5\phi_5^\dagger\Psi_{10}. \tag{5.19}$$

  Here, Ψ_5 and Ψ_{10} are the GUT multiplets that embed Q and $\tilde{D}$, whereas ϕ_5 is the GUT representation that embeds the SM Higgs.

- $L \oplus E$ model: In this model, the gauge singlet DM candidate is given by LLE. Unlike the $Q+\tilde{D}$ case, in this scenario, the simplest GUT representation embedding L and E fragments, given

by $\bar{5} \oplus 10$, cannot be identified as a viable parent GUT theory. Additional GUT multiplets must be added to this to introduce Yukawa couplings which can generate higher dimensional operators in the low energy theory. These operators are crucial for destabilizing the light mesons in any theory that can violate the BBN bound as we discussed in Sec. 5.1.1. Indeed, the parent GUT theory for this model is identified as $\bar{5} \oplus 10 \oplus 5 \oplus 1/24$. The GUT multiplets 5 and 10 must be added to break all GUT species symmetries as:

$$\mathcal{L}_{\rm GUT} \ni \bar{\Psi}_{10}\phi_5\Psi_5 + \bar{\Psi}_{1/24}\phi_5\Psi_{\bar{5}} + \bar{\Psi}_5\phi_5\Psi_{1/24} \tag{5.20}$$

The additional GUT multiplets 5 and 24 embed the *auxiliary* GUT fragment fields given by $\tilde{L}$ and N which must be integrated at M_H to generate the higher dimension operator (See also Fig. 5.1) in the low energy theory, $\bar{L}EHHH$. As we hinted earlier, the same parent GUT theory can be the origin of many low-energy models. This parent GUT theory can indeed, also give rise to the low energy model given by $L \oplus E \oplus \tilde{L} \oplus N$.

In order to further clarify how we characterise the parent GUT theory, let us use another embedding for this $L \oplus E$ model to demonstrate how it will not fulfill the criteria we demand. We can envisage a scenario where $L \oplus E$ is embedded in $5 \oplus \bar{5} \oplus 10$ where the auxiliary GUT multiplet 5 has been added to break the accidental species symmetry. At the GUT level, we can now write the following gauge invariant terms:

$$\mathcal{L}_{\rm GUT} = \bar{\Psi}_{10}\phi_5\Psi_5 + \frac{1}{M_{\rm P}}\bar{\Psi}_5\Psi_{\bar{5}}\phi_5\phi_5 \tag{5.21}$$

It is evident from Eq. 5.21 that in this parent GUT theory, the GUT species symmetry associated with $\bar{5}$ remains unbroken at the renormalizable level and is broken only by the $M_{\rm P}$ suppressed dimension-5 operator. To attain the $L \oplus E$ model, we must now integrate out the auxiliary GUT fragment embedded in 5, in this case, given by $\tilde{L}$. This would result in the higher dimension operator in the low energy theory given by:

$$\mathcal{O}^{(6)} \simeq \frac{1}{M_{\rm P}M_H}\bar{L}EHHH \tag{5.22}$$

This dimension-6 operator would mediate the decay of the light meson $\bar{L}E$. However, it was already shown in Sec. 5.1.1 (See also Eq. 5.9) that such dimension-6 operators can only mediate the meson decay complying with the BBN bound for $M_H < 10^6$ GeV. Considering this M_H scale is too close to $\Lambda_{\rm DC}$, such operators are not considered to be generated in our low energy dark theory. Note that in this example the addition of operators with the GUT breaking scalar ϕ_{24} will lead to a contribution to the mass matrix. In principle, a higher dimension GUT invariant operator of the type $\bar{\Psi}_5\Psi_{10}\phi_{24}\phi_5^\dagger$ can be written, however, it will not break any additional GUT species symmetries.

Theorem: By our definition of parent GUT theory, any unbroken GUT species symmetry will be inherited by the low energy model. If there is an unbroken species number at the renormalizable level in the GUT Lagrangian (like in Eq. 5.21, the GUT theory will not provide the necessary embedding for the low energy model complying with bounds on higher dimension operators already discussed in Sec. 5.1.1.

In section 5.2, we discuss the possibility of gauge coupling unification in the models found in our classification. We distinguish between the two groups of dark fermions as: (i) light dark fermionic content of the low energy model at a mass $m \lesssim \Lambda_{\rm DC}$, (ii) the heavy dark fermionic content at a mass scale M_H, comprising both the remaining GUT representations or GUT partners and the additional heavy quarks integrated out for the generation of the nonrenormlizable interactions.

$\mathbf{SO}(N)_{DC}$ Models

In this section we identify the viable models for $\mathcal{G}_{\rm DC} = SO(N)_{\rm DC}$. The dark fermions transforming under (fundamental) vector representations of $SO(N)_{\rm DC}$ are real. This leads to two consequences: (i) there is no difference between baryons and antibaryons, (ii) dark mesons can be $\mathcal{Q}_i\mathcal{Q}_j$ states.

In this case we can write the dark sector matter content added to the SM as:

$$\begin{aligned} &\mathcal{Q} \equiv (\square, R_{\rm SM}) \oplus (\square, \bar{R}_{\rm SM}) && \text{if } R_{\rm SM} \text{ is a complex representation under SM} \\ &\mathcal{Q} \equiv (\square, R_{\rm SM}) && \text{if } R_{\rm SM} \text{ is a real representation under SM} \end{aligned} \tag{5.23}$$

Both species numbers corresponding to $R_{\rm SM}$ and $\bar{R}_{\rm SM}$ must be broken now to enable the decay of stable, dangerous mesons, since now both $\mathcal{Q}_i\mathcal{Q}_j$ and $\mathcal{Q}_i\bar{\mathcal{Q}}_j$ states exist.

Similar to the case of $SU(N)_{\rm DC}$ case, we identify all the possible species symmetry breaking operators including the allowed nonrenormalizable interactions.

The Yukawa interactions now are given by:

$$HQ(D \text{ or } U), \quad HL(E \text{ or } T \text{ or } N \text{ or } V), \quad HDX \tag{5.24}$$

The higher dimension operators between the electroweak charged dark fermions remain the same as in the case of $SU(N)_{\rm DC}$ given by Table 5.2 where $\bar{\bar{L}}LH^{c\dagger}H$ and $\overline{E}\tilde{E}(H^{c\dagger}D_\mu H)^2$ are replaced respectively with $LLH^{c\dagger}H$ and $\bar{E}\bar{E}(H^{c\dagger}D_\mu H)^2$ for the $SO(N)_{\rm DC}$ case.

As for $SU(N)_{\rm DC}$ case, the $SO(N)_{\rm DC}$ dark fermion flavours $N_{\rm DF}$ and the number of dark colours $N_{\rm DC}$ are constrained by demanding the asymptotic freedom of the dark color coupling. For $SO(N)_{\rm DC}$ case the condition on the one-loop beta function will be given by:

$$\beta_{DC} = -\frac{11}{3}(N_{\rm DC} - 2) + \frac{2}{3}N_{\rm DF} < 0 \tag{5.25}$$

where we have used the normalization for $\mathrm{Tr}(T^aT^b) = \delta^{ab}$ for the generators in the fundamental of $SO(N)_{\rm DC}$. Given the dark fermionic flavours, this imposes a lower limit on the number of dark colors. We do not impose the stronger bound on the number of dark flavours $N_{\rm DF}$ coming from confinement i.e. $N_{\rm DF} < N_{\rm conf}$ for the $SO(N)_{\rm DC}$ case. We are not aware of any lattice studies evaluating $N_{\rm conf}$ for $SO(N)$ theories.

5.1.3 Mass Splitting

In this section, we address the issue of producing a natural hierarchy between the mass of dark fermions and their GUT partners given by $m \lesssim \Lambda_{\rm DC} < M_H$ where m is the mass of the light-dark fermions, and M_H is the GUT partner mass. Note that $\Lambda_{\rm DC} \sim 100$ TeV to account for the thermal DM abundance. The hierarchy $M_H > \Lambda_{\rm DC}$ is required as already mentioned in Sec. 5.1.1 due to bounds on the GUT partner lifetime coming from BBN (See also discussion in Sec. 6.1). Moreover, the hierarchy of $M_H > \Lambda_{\rm DC}$ is also necessary (as we will discuss in the next section on unification Sec. 5.2) for gauge coupling unification. Thus, a hierarchy $M_H > m$ is crucial for our dark sector.

In this section, we find that there is no way to get the hierarchy $M_H > m$ at tree level without tuning the GUT parameters. We further verify if the tuning is maintained by including higher dimension operators to the mass spectrum. In the second half of this section, we use a spurionic argument to demonstrate that the tuning is not technically natural.

For our demonstration, we consider the $SU(3)_{\rm DC}$ model with dark fermions given by $Q \oplus \tilde{D}$ model and the GUT partners given by the fragments U, E, and $\tilde{L}$. The following hierarchy is

required:

$$m_Q, m_{\tilde{D}} \ll m_U, m_E, m_{\tilde{L}}.$$

We can explicitly compute the tree-level mass spectrum of dark fermions for this model:

$$5 = \begin{cases} m_{\tilde{D}} & = m_5 + \frac{2}{\sqrt{30}} y_5 v_{\rm GUT} \\ m_{\tilde{L}} & = m_5 - \frac{3}{\sqrt{30}} y_5 v_{\rm GUT} \end{cases} \qquad 10 = \begin{cases} m_U & = m_{10} + \frac{2}{\sqrt{30}} y_{10} v_{\rm GUT} \\ m_E & = m_{10} - \frac{3}{\sqrt{30}} y_{10} v_{\rm GUT} \\ m_Q & = m_{10} - \frac{1}{\sqrt{30}} y_{10} v_{\rm GUT} \end{cases} \tag{5.26}$$

where m_5, y_5, y_{10} are GUT mass and Yukawas appearing in the $SU(5)$ invariant Lagrangian (See Eq. F.3 in Appendix), and $v_{\rm GUT}$ is the SM-preserving vacuum expectation value of the GUT breaking scalar. This tree-level spectrum above was computed for the scenario in which the GUT breaking scalar transforms under the adjoint 24 of $SU(5)$. (See Appendix F for details on this computation). We can also consider various possibilities of $SU(5)$ GUT breaking scalars in addition to the minimal 24 case (see Appendix F for these scenarios).

The desired hierarchy $m_Q, m_{\tilde{D}} \ll m_U, m_E, m_{\tilde{L}}$ can be obtained at the renormalizable level (only) if $m_{5,10} \approx y_{5,10} v_{\rm GUT} \sim M_H$. This requires the introduction of two tunings in this model: one tuning between m_5 and $y_5 v_{\rm GUT}$ and a second tuning between m_{10} and $y_{10} v_{\rm GUT}$.

The next question is whether the required tuning is natural or not, *i.e.* if it is stable under radiative corrections.

Spurionic argument:

In this subsection, we demonstrate that the tuning of $SU(5)$ mass parameters needed for mass splitting in the model $Q \oplus \tilde{D}$ is not technically natural.

Let us consider the mass terms and Yukawa couplings for the $Q + \tilde{D}$ model embedded in $5 \oplus 10$ of $SU(5)$ (with scalars in 24 and 5):

$$\mathcal{L} = -m_5 \overline{\psi}\psi - m_{10} \overline{A} A - y_5 \overline{\psi} \phi_{24} \psi - y_{10} \overline{A} \phi_{24} A - y_L \overline{\psi}_L \phi_5^\dagger A_R - y_R \overline{\psi}_R \phi_5^\dagger A_L + \text{h.c.} \tag{5.27}$$

where $\psi \in 5$, $A \in 10$ of SU(5). In the following, we focus on $\psi \in 5$ and we consider the generation of a large hierarchy between the mass of $\tilde{D}$ and $\tilde{L}$. The desired hierarchy $m_{\tilde{D}} \ll m_{\tilde{L}}$ can be achieved by setting m_5 and $y_5 v$ to large values, as already explained. We will see that such a choice is not radiatively stable.

The mass matrix for ψ can be decomposed as two SU(5) structures given by $\bar{5} \times 5 = 1 + 24$:

$$5^\dagger \mathcal{M}_5 5, \quad \mathcal{M}_5 = m_1 \cdot \mathbb{I} + m_{24} \cdot 24 \tag{5.28}$$

where $\mathbb{I}$ is the identity matrix and we consider the matrix structure of 24 to be aligned to $\langle \Phi_{24} \rangle$ where $\langle \Phi_{24} \rangle$ is the GUT-breaking vev (See F.2). We can now write m_1 and m_{24} in terms of the bare Lagrangian mass terms in Eq. 5.27:

$$\begin{aligned} m_1 &= m_5 + ... \\ m_{24} &= y_5 v_{\rm GUT} + ... \end{aligned} \tag{5.29}$$

where ... contains all contributions encompassing both tree-level and higher dimension operators

and their respective radiative corrections. For example, diagrams such as those shown in Fig. 5.2 can contribute to these effective terms m_1, and m_{24}.

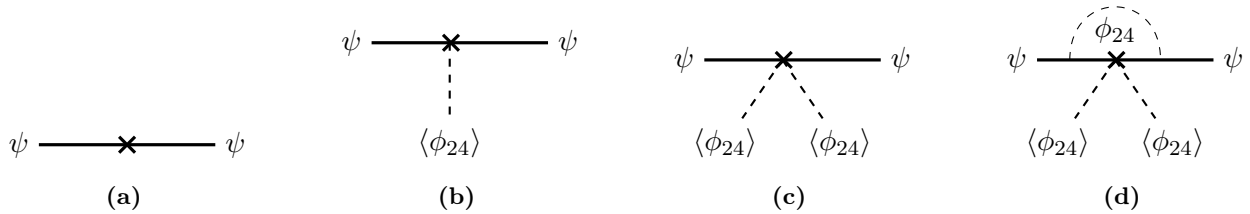

Figure 5.2: (a) Example of diagram contributing to the mass term m_1 of Eq. 5.29 for the fermion $\psi \in 5$ of SU(5). (b) Example of diagram contributing to the mass term m_{24} of Eq. 5.29 for the fermion $\psi \in 5$ of SU(5). (c) Example of diagram contributing to both m_1 and m_{24} mass terms for the fermion $\psi \in 5$ of SU(5). (d) Radiative correction to the diagram in (c) contributing to both m_1 and m_{24} mass terms for the fermion $\psi \in 5$ of SU(5).

In the same spirit, we can write the mass matrix for $A \in 10$ using the SU(5) structures given by $\bar{10} \times 10 = 1 + 24 + 75$:

$$\mathcal{M}_{10} = m_1 \cdot \mathbb{I} + m_{24} \cdot 24 + m_{75} \cdot 75 \tag{5.30}$$

where we can write m_1, m_{24} and m_{75} in terms of the bare Lagrangian mass terms:

$$m_1 = m_{10} + ... \tag{5.31}$$
$$m_{24} = y_{10} v_{\rm GUT} + ... \tag{5.32}$$
$$m_{75} = 0 + ... \tag{5.33}$$

where from Eq. 5.27 it is evident that the tree-level contribution to m_{75} is 0 for the minimal SU(5) case in which the SU(5)-breaking scalar is in the adjoint.

Let us now focus on the case of hierarchy between $m_{\tilde{D}} \ll m_{\tilde{L}}$. After SU(5) symmetry breaking (see also Eq. F.4), we can write the mass of the SM fragments in ψ in terms of effective masses m_1 and m_{24} as:

$$\begin{aligned} m_{\tilde{D}} &= m_1 + \frac{2}{\sqrt{30}} m_{24} \\ m_{\tilde{L}} &= m_1 - \frac{3}{\sqrt{30}} m_{24} \end{aligned} \tag{5.34}$$

To get a hierarchy of $m_{\tilde{D}} \ll m_{\tilde{L}}$, solving Eq. (5.34) in terms of m_1 and m_{24} gives

$$\frac{\sqrt{30}\ m_1}{m_{24}} = \frac{\sqrt{30}\ (m_5 + ...)}{(y_5 v + ...)} = -2 - 5 \cdot \frac{m_{\tilde{D}}}{m_{\tilde{L}}} \tag{5.35}$$

For perfect gauge coupling unification, we find (see also next sec. 5.2) that $m_{\tilde{L}} \approx 10^{11}$ GeV for $m_{\tilde{D}} = 10^5$ GeV implying a small value of the ratio $m_{\tilde{D}}/m_{\tilde{L}}$ in Eq. 5.35 of $\mathcal{O}(10^{-6})$.

Any tuning between two parameters is technically natural if it is respected at all orders. Indeed, if loop contributions to the ratio in Eq. 5.35 are less than $\mathcal{O}(10^{-6})$, the tuning would be technically natural. Radiative corrections from diagram (d) in Fig. 5.2 will contribute to both m_1 and m_{24}, thereby, spoiling the tuning given in Eq. 5.35.

A similar argument can be repeated for the case of tuning in $A \in 10$.

5.2 Gauge Coupling Unification

In this Section, we describe our procedure for analysing the viable models for successful SM gauge coupling unification. As hinted earlier, in our analysis we diverge from *point-like* coupling unification where the SM coupling constants α_i unify at one point in the $(\alpha_i^{-1}, \log\mu)$ (this was also used in Refs. [172, 183]). We analyze the viable composite dark matter models requiring that they minimally *mitigate* the coupling unification achieved with the SM (shown in the left Fig. 5.3) Our approach described in the next subsection despite being very optimistic shows that assessing composite dark matter models from a *GUT* point of view greatly reduces the number of viable theories - our main results of this section can be found in the summary plot in Fig. 5.4.

Below the unification scale for any two SM couplings μ, the SM couplings α_i evolve as per the usual RGE. We do not consider any contributions coming from the strong dynamics below the dynamical $\Lambda_{\rm DC}$ scale. Considering the contribution of light dark fermions above $\Lambda_{\rm DC}$ and those of the GUT partners above $M_H > \Lambda_{\rm DC}$, at 1-loop, we can write:

$$\frac{1}{\alpha_i(\mu)} = \frac{1}{\alpha_i(M_z)} - \frac{\beta_i^{SM}}{2\pi}\log\frac{\mu}{M_z} + \Delta_i - \frac{\Delta\beta_i^{L}}{2\pi}\log\frac{M_H}{\Lambda_{DC}} - \frac{\Delta\beta^{SU(5)}}{2\pi}\log\frac{\mu}{M_H} \tag{5.36}$$

where $\beta_i^{SM} = (\frac{41}{10}, -\frac{19}{6}, -7)$ are the three 1-loop SM beta functions (with the notation $g_1 = \sqrt{5/3}g_Y$ where g_Y is the SM hypercharge coupling), Δ_i encapsulate all the IR and UV threshold corrections [8] which we will ignore in our calculations, $\Delta\beta_i^L$ is the 1-loop beta-function contribution coming from the light-dark fermions in each model and $\Delta\beta^{SU(5)}$ is the corresponding $SU(5)$ invariant contribution coming from the 1-loop beta function of the entire $SU(5)$ multiplet.

The main part of this analysis was done assuming a common mass scale M_H for all the GUT partners of the $SU(5)$ multiplets. However, we also checked a few models, namely $\Psi = L \oplus E$ and $\Psi = V$, assuming non-degenerate mass scales for heavy GUT fermions (see Sec. 5.2.3) to quantify unification in these models.

5.2.1 Unification Criteria

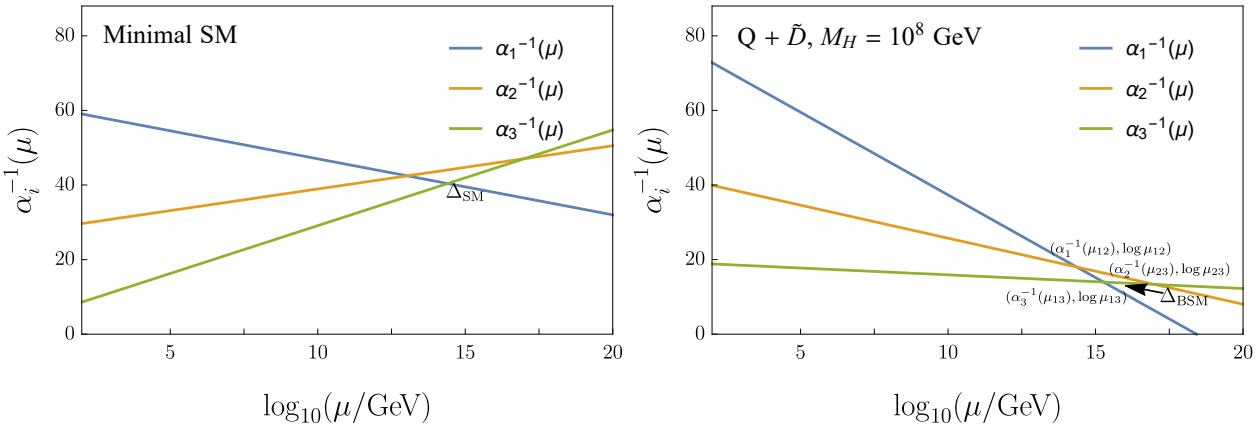

Figure 5.3: We show the one-loop renormalization group evolutions of the gauge coupling constants in the SM *(left)* and in the BSM model *(right)* to depict our definitions of the SM triangle $\Delta_{\rm SM}$ and the BSM triangle $\Delta_{\rm BSM}$ defined in the main text. For the BSM model, we consider the $SU(3)_{\rm DC}$ model $Q + \tilde{D}$ where the GUT partner scale is fixed to 10^8 GeV.

[8] in our effective theory we have integrated out the GUT states, so on matching our effective theory with the full GUT theory at the GUT scale, we would have threshold corrections which can be easily ignored.

Instead of accepting only scenarios that give a perfect gauge coupling unification after running with the BSM model content i.e. the dark fermions as well as their $SU(5)$ GUT counterparts, we accept a triangle formed in the (α_i^{-1} versus $\log\mu$) plane (for an example, see Fig. 5.3 (right)). We only aim at achieving a unification scenario better than the one obtained in the SM thereby excluding a necessary requirement of "perfect" unification.

Here we note that minimal SM unification has already been ruled out [177]. The non-observation of proton decay puts a lower bound on the GUT scale of $M_{\rm GUT} \gtrsim 10^{15}$ GeV which is higher than the SM GUT scale of $M_{GUT}^{SM} = 6.5 \times 10^{14}$ GeV.

Under our optimistic approach of achieving unification, we do not exclude the SM for unification and cast a net wide enough to not lose any composite DM model for SM coupling unification. Once we get a model that can better the unification in the SM, we then require that more precise threshold corrections would improve the unification scale bound.

Our unification basis can be parametrised in terms of three degrees of freedom: the area of the unification triangle, the value of unified coupling α_{GUT}, and the value of the unification scale $\tilde{M}_{GUT}$. These were used to scan for any possible viable models giving a DM candidate and successful (albeit imperfect) gauge coupling unification and to constrain the mass scale of heavy GUT partners M_H. We now expand on these constraints further:

- **Quality Constraint:** we require that the area of the triangle $\mathcal{A}_\Delta$ formed in the $(\alpha_i^{-1}, \log\mu)$ plane be lesser or equal to the one obtained in the SM $\mathcal{A}_{SM}$. We use the barycentre of this "unification triangle" to define the values of GUT coupling $\alpha_{GUT}(M_H)$ and unification scale $\tilde{M}_{GUT}(M_H)$ for a range of values of the mass of GUT partners, M_H.

- **Vertical Constraint:** requiring perturbativity of the GUT coupling $\alpha_{GUT} < 4\pi$ constrains the centre of the triangle to be always above $\alpha_{GUT}^{-1} = 1/4\pi$.

- **Horizontal Constraint :** we require that the barycentre of the unification triangle, $\tilde{M}_{GUT}$ be above its SM value $M_{GUT}^{SM} = 6.5 \times 10^{14}$ GeV (to be less excluded by proton decay than the SM). Additionally, we do not want the unification scale $\tilde{M}_{GUT}$ to exceed the Planck scale M_P, so we allow for corresponding M_H values for which $\tilde{M}_{GUT}(M_H) \leq M_P$.
  In addition to these three unification degrees of freedom, we also impose an additional fourth constraint:

- $\alpha_{\rm GUT}$ **Landau Poles:** We do not want the GUT theory to have landau poles below the Planck Scale $M_{\rm P}$.

An additional requirement for model consistency is imposed by the requirement that the dark coupling $\alpha_{\rm DC}$ does not lose its asymptotic freedom even after adding the heavy GUT partners. This would imply that $\beta_{DC}^{SU(5)} < 0$ where $\beta_{DC}^{SU(5)}$ is the 1-loop beta function contribution to $\alpha_{\rm DC}$ coming from the entire $SU(5)$ multiplet.

5.2.2 Unification Check for Viable Models

SU$(N)_{DC}$ Models

We analyse gauge coupling unification for all the viable $SU(N)_{\rm DC}$ models under our three criteria listed above under the assumption that the heavy GUT partners have a common mass scale M_H. The results are presented in table E.1 in Appendix E.

We find that only two models are viable candidates after this check. These are:

- $\mathbf{Q} \oplus \tilde{\mathbf{D}}$: For $N_{DC} = 3$, our basis for unification requires that the mass scale of the heavy GUT partners (U, E and $\tilde{L}$) be 6.5×10^6 GeV $< M_H < 5 \times 10^{14}$ GeV giving a unification scale 3×10^{15} GeV $< \tilde{M}_{GUT} < M_P$. The lower bound on M_H comes from imposing the proton decay bound on the GUT scale. This model, in addition, gives a perfect gauge coupling unification at a scale $\tilde{M}_{GUT} = 1 \times 10^{17}$ GeV for $M_H = 1 \times 10^{11}$ GeV. (See also Refs. [172])

- $\mathbf{N}$: This model satisfies our unification requirements trivially since this model gives unification as good as the SM giving $\tilde{M}_{GUT} = 6.5 \times 10^{14}$ GeV. Requiring $\alpha_{GUT} < 4\pi$ puts a lower bound on the mass scale of the heavy GUT partners (V, X and G) requiring $M_H > 1.2 \times 10^9$ GeV for $N_{\rm DC} = 3$, assuming the GUT parent theory to be given by 24.

To investigate why such few models make it past our relaxed unification criteria, we show a plot of various low energy viable models in the plane ($\delta_{12},\ \delta_{32}$) in Fig. 5.4 where $\delta_{ij} \equiv \delta_i - \delta_j$. Here, δ_i for any SM extension contains the running from both the light dark fermions and their GUT partners:

$$\delta_i = -\frac{\Delta\beta_i^L}{2\pi} \log \frac{M_H}{\Lambda_{DC}} - \frac{\Delta\beta^{SU(5)}}{2\pi} \log \frac{\mu}{M_H} \tag{5.37}$$

In Fig. 5.4, the grey region shows the universal region in the plane ($\delta_{12},\ \delta_{32}$) in which we mitigate SM coupling unification with respect to the SM following our criteria described earlier. For a fixed value of M_H this represents a point in the plane ($\delta_{12},\ \delta_{32}$).

The degree of unification in a BSM viable model can also be parametrized in terms of the size of the threshold corrections required at the unification scale (See [180] for example). We use the common definition used in unification literature for this and define the threshold correction required at the $M_{\rm GUT}$ scale $N_{\rm th}$ as [180]:

$$\alpha_1^{-1}(M_{\rm GUT}) - \alpha_3^{-1}(M_{\rm GUT}) = \frac{N_{\rm th}}{2\pi} \tag{5.38}$$

In order to get unification in the SM at a scale of $M_{\rm GUT} \approx 10^{15}$ GeV, $|N_{\rm th}| \approx 15$.

From Fig. 5.4, it is evident that models like $L \oplus E$ perform very poorly even under our relaxed unification criteria. The size of threshold corrections $N_{\rm th}$ required in this case at $M_{\rm GUT} \approx 10^{15}$ is ≈ 60 (where to compute this we fixed the scale of the GUT partners at 10^{10} GeV).

SO$(N)_{DC}$ Models

We perform a check for $SU(5)$ unification for all the SO$(N)_{DC}$ viable models under our three criteria listed above under the assumption that the heavy GUT partners have a common mass scale M_H. The results are presented in Table E.2 in Appendix E.

No SO$(N)_{DC}$ model compatible with our criteria of unification is found assuming a common mass for GUT partners. However, we will see in the next section how assuming non-degenerate masses between GUT partners can give good unification in the SO(3) V model.

5.2.3 Case for Non-Degenerate Heavy Masses

We extend our unification analysis for two models, namely SU$(3)_{DC}$ models $\Psi = L \oplus E$, and $\Psi = V$ as well as SO$(3)_{DC}$ $\Psi = V$ considering non-degenerate masses for the heavy GUT partners. This analysis clarifies the conditions needed to improve the gauge coupling unification in these scenarios.

- $SU(3)_{DC}$ $\mathbf{L} \oplus \mathbf{E}$: This $SU(3)_{DC}$ model giving DM candidate LLE does not give unification under our criteria with one common heavy mass scale M_H. The parent GUT theory for this

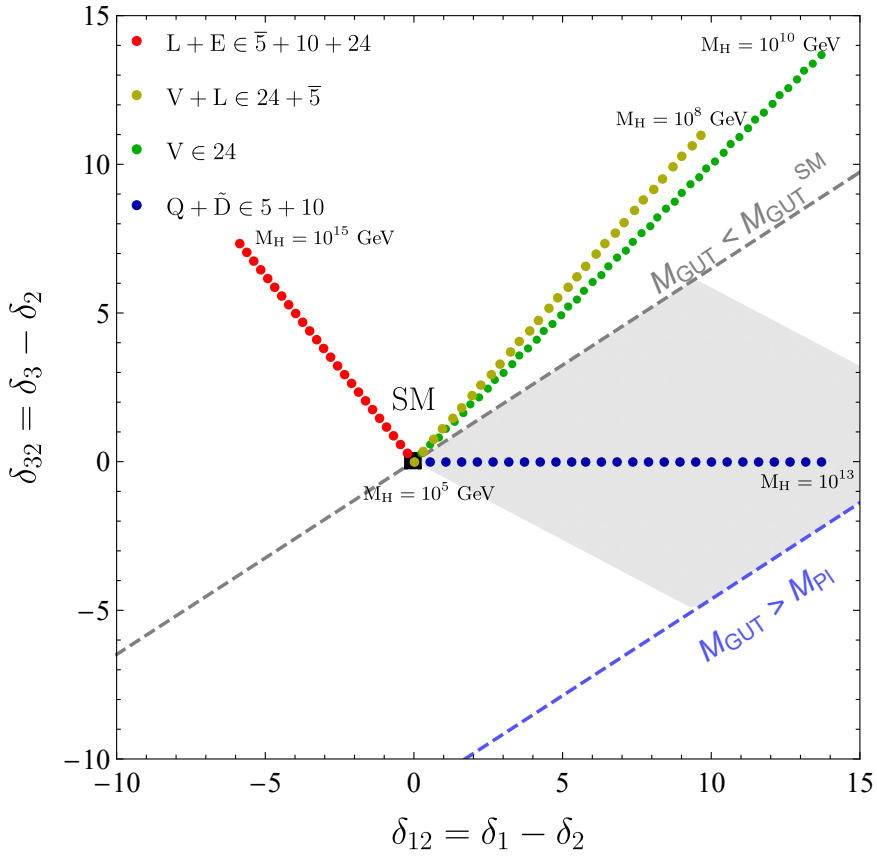

Figure 5.4: Summary plot showing some viable composite dark matter models and their respective positions in the $(\delta_{12}, \delta_{32})$ plane for different values of heavy fermion mass $M_{\rm H}$. This plot is drawn for fixed $N_{\rm DC} = 3$. The gray shaded region shows the universal allowed region under our unification conditions that gives unification better than the SM. The black point marks the SM for $\delta_{12} = 0$, $\delta_{32} = 0$. In red, olive, green, and blue we show the δ_{12}, δ_{32} contribution for the models $L + E$, $V + L$, V, and $Q + \tilde{D}$ coming from the running of light dark fermions and the heavy GUT partners at M_H. At $M_{\rm H} = 10^5$ GeV, all models give unification as in SM due to running of the complete GUT multiplet from $M_{\rm H}$. The region above (below) the light gray dashed (light blue) line shows the region constrained due to a too fast proton decay (GUT scale $> M_{\rm P}$).

model is given by $\bar{5} \oplus 10 \oplus 5 \oplus 24$. Using different combinations of splittings between heavy partners, we find that splitting them as $H_1 = \tilde{L} \oplus U$ and $H_2 = D \oplus \tilde{D} \oplus Q$ gives us an allowed region in the parameter space of the two heavy scale masses M_{H_1} and M_{H_2}. Fig 5.5 shows the allowed values of M_{H_1} and M_{H_2} which give successful unification for this case.

- $SU(3)_{DC}$ **V**: Introducing two heavy mass scales for the V model does not improve unification for any combinations of mass splitting between the GUT partners. Further, we find that even with three mass splittings, we are unable to achieve successful unification under our criteria. Fig 5.5 shows the unification region for this model in the (M_{H_1}, M_{H_2}) parameter space, in which $H_1 = G \oplus X$, and $H_2 = X^\dagger$.

- $SO(3)_{DC}$ **V**: Non-degeneracy between masses of GUT partners gives successful unification in this model as compared to the $SU(N)_{\rm DC}$ case. In Fig. 5.6 we show a comparison between the two mass splittings for the V model in the case of $SU(N)_{\rm DC}$ and $SO(N)_{\rm DC}$ respectively. For the $SU(N)_{\rm DC}$ case, no allowed region is found in the (M_{H_1}, M_{H_2}) plane since α_{GUT} is not perturbative for low values of M_{H_2} (where $G = H_2$). For the $SO(N)_{\rm DC}$ case G is a Majorana fermion and hence $\alpha_{\rm GUT}$ remains perturbative also for lower values of M_{H_2} unlike

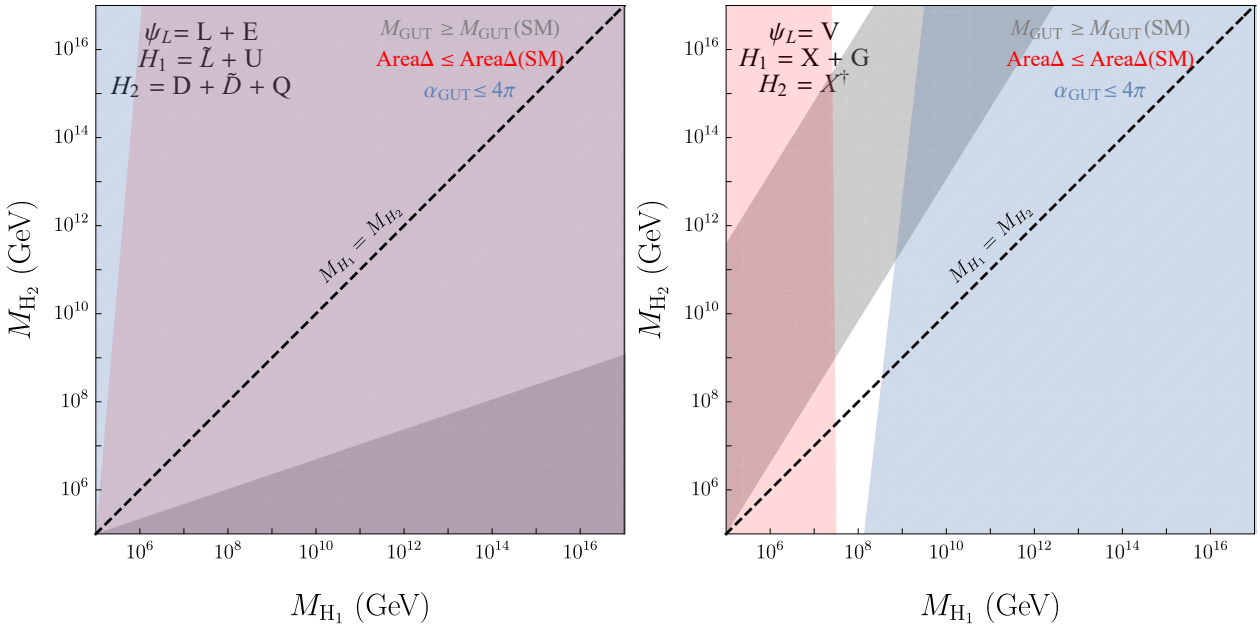

Figure 5.5: *Left:* Allowed region for gauge coupling unification for non-degenerate masses under our basis for $L \oplus E$ model in the M_{H_1}, M_{H_2} parameter space. *Right:* No overlapping region under our unification basis for model V for any of the cases of non-degenerate heavy fermion groupings. Shown here in the case in which $H_1 = X + G$ and $H_2 = X^\dagger$.

in the $SU(N)_{\rm DC}$ case.

We note here that despite in the $L \oplus E$ model we improve unification by splitting the heavy quarks, we also introduce more number of tunings needed. With non-degenerate GUT partners, we will now have the following scales in the theory: m, M_{H_1}, M_{H_2}, $\tilde{M}_{GUT}$.

With the degenerate GUT partner scenario, as described in Sec. 5.1.3 we must fine-tune the parameters to create the hierarchy between dark fermions and their GUT partners $m < M_H$. Introducing more hierarchies would make the tuning more pathological.

5.3 Summary

In this chapter, we have systematically studied and classified $SU(5) - GUT$ completions for composite dark matter models where the DM candidate arises as an accidentally stable dark baryon. These are gauge theories where the SM matter is extended with *dark* fermions that transform as fundamentals under the dark color gauge group $SU(N)_{\rm DC}$ or $SO(N)_{\rm DC}$ and as vector-like representations under the SM gauge group $\mathcal{G}_{\rm SM}$. We assume that the dark quarks are light with masses below the dark confinement scale $\Lambda_{\rm DC}$, at which the dark colour gauge group confines. An effort in this direction was already made in Refs. [172].

Due to the GUT nature of the dark theory, the dark fermions come with their GUT partners where the mass of the GUT partners M_H is set by gauge coupling unification. Ref. [172] considers perfect gauge coupling unification which sets M_H to one particular value that corresponds to the unification scale of the theory given by $M_{\rm GUT}$. In this work with respect to Ref. [172], we have used a less conservative requirement for gauge coupling unification and required that the viable dark model only mitigates the coupling unification achieved in the SM. We have given details of this unification criteria in Sec. 5.2. With respect to Ref. [172], we have included a much more detailed classification of viable models based on an analysis of higher dimension operators generated by GUT partners. Our

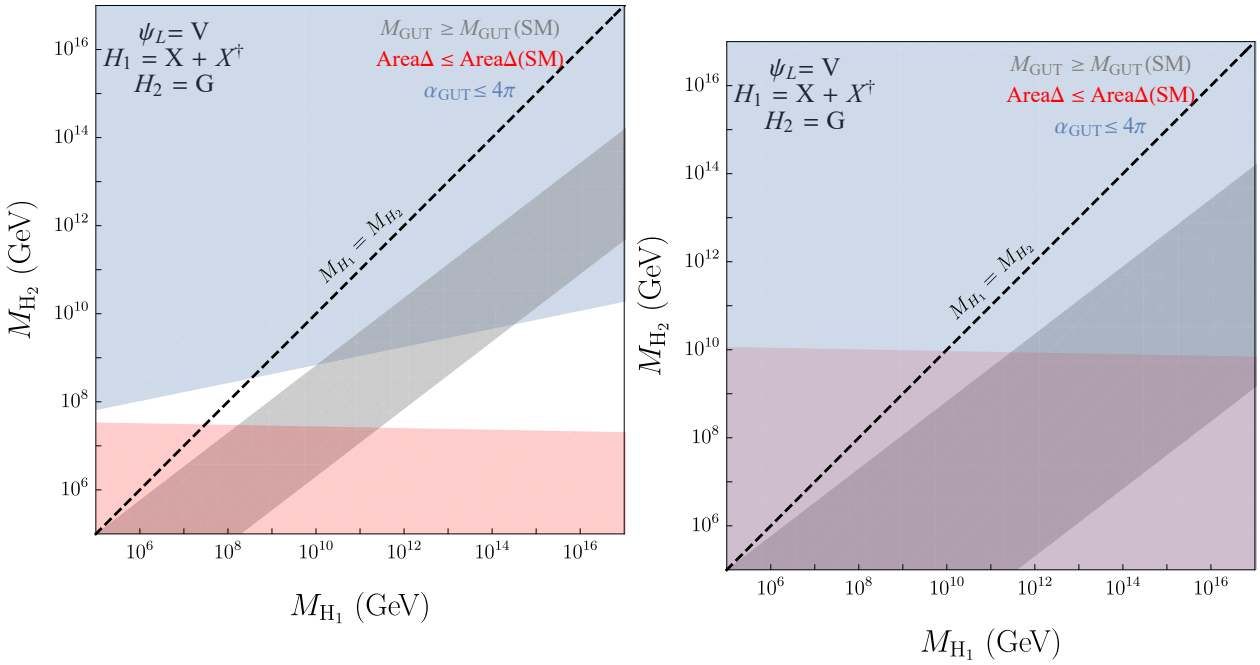

Figure 5.6: Comparison between $SU(3)_{DC}$ V model and $SO(3)_{DC}$ V model on the allowed region for unification with splitting in mass between GUT partners. *Left:* Shows $SU(3)_{DC}$ V model in the M_{H_1}, M_{H_2} parameter space with grouping as $H_1 = X + X^\dagger$ and $H_2 = G$ showing no allowed region for good unification. *Right:* Shows the same V model with dark colour group $SO(3)_{DC}$ and allowed region for good unification.

rigorous analysis of operators and classifying these models can be found in Sec. 5.1. Moreover, with respect to Ref. [172], we have also addressed the question of creating a natural hierarchy between the light-dark fermions and their GUT partners i.e. $M_H > m$. Our discussion can be found in Sec. 5.1.3. We find that the GUT mass and Yukawa parameters, m_5, m_{10}, $y_5 v_{GUT}$, $y_{10} v_{GUT}$ must be tuned to obtain the required hierarchy $m_{\tilde{D}}, m_Q \ll m_{\tilde{L}}, m_E, m_U$ at tree level. We further clarify that this tuning is spoiled when radiative corrections are included.

In this chapter, we conclude that requiring gauge coupling unification in viable composite dark matter models highly restricts the number of theories. We find only two viable models: a trivial scenario with SM singlet N, and our benchmark model with SM-colored dark fermions $Q + \tilde{D}$. Note that these two are the viable models for the case in which all the GUT partners are at the same mass scale M_H. In addition to these two models, we also find that the two models $SU(3)_{DC}$ model $L \oplus E$ and the $SO(3)_{DC}$ V model can give good unification for non-degenerate GUT partners masses M_{H_1} and M_{H_2}. This, however, implies, introducing more number of tunings to get the split spectrum, hence we will not discuss the phenomenology of these scenarios any further. Our main results of this section can be found in the summary plot in Fig. 5.4 and Figs. 5.6-5.5 (see also appendix E).

In the next chapter, we discuss the details of the benchmark model $Q \oplus \tilde{D}$. With regard to this model, we will describe the phenomenology of NGBs as well as the dark matter cosmology in the light of GUT partners.

Chapter 6

Benchmark Model: Symmetries and Cosmology

In this Chapter based on work in prepartion (with R. Contino, S. Bottaro) [27, 28] we discuss the NGB spectrum and the relevant cosmological details of the benchmark model: $Q + \tilde{D}$. The detailed analysis of the methodology for picking this model can be found in the last chapter. In this chapter, we first discuss how considering the GUT partners enhances the overall accidental symmetries of the renormalizable dark sector leading to charged long-lived bound states (See Sec. 6.1). We then further discuss the dark matter cosmology of this model in the presence of GUT partners in Sec. 6.3. We are not aware of any other study that considers the impact of GUT partners on composite baryonic dark matter phenomenology in such detail.

6.1 Benchmark Model: $Q \oplus \tilde{D}$

To write the $SU(5)-$GUT theory for a composite dark matter model, we first define the content of the theory in terms of $SU(5)$ multiplets. The SM matter fields are unified in the usual way in the $\bar{\mathbf{5}}$ and $\mathbf{10}$ representations. The scalar sector is composed of the minimal representations required for the spontaneous breaking of $SU(5) \to \mathcal{G}_{\rm SM}$ in addition to the SM higgs: $\mathbf{24_H}$ and $\mathbf{5_H}$. Our dark theory has no dark coloured scalars. By implementing the UV completion in a GUT, we introduce the doublet-triplet splitting problem between the SM Higgs and the GUT colored partner H_3, we do not try to address it here.[1] Finally, we can embed the dark fermions Q and $\tilde{D}$ (where we use the nomenclature as in Ref. [172]) into the following irreps of $\mathcal{G}_{DC} \times \mathrm{SU}(5)$:

$$\begin{aligned} \mathbf{5}_F^{\rm DS} = (\square, 5) &= \underbrace{(\square, 1, 2, 1/2)}_{\tilde{L}} \oplus \underbrace{(\square, 3, 1, -1/3)}_{\tilde{D}} \\ \mathbf{10}_F^{\rm DS} = (\square, 10) &= \underbrace{(\square, 3, 2, 1/6)}_{Q} \oplus \underbrace{(\square, \bar{3}, 1, -2/3)}_{U} \oplus \underbrace{(\square, 1, 1, 1)}_{E} \end{aligned} \tag{6.1}$$

Here, the dark gauge group $\mathcal{G}_{\rm DC}$ is $SU(N)_{\rm DC}$ and as denoted, the dark fermions transform in the fundamental representation of $\mathcal{G}_{\rm DC}$. Note that the $SU(5)$ breaking scalar is a singlet under the dark color gauge group. As is evident from Eq. 6.1, the dark fermions Q and $\tilde{D}$ are accompanied by their GUT partners - $\tilde{L}$, U and E.

[1] This can be potentially solved by embedding the dark model in an extra-dimensional GUT, we leave this for a future work.

	Dark Species				
	5		10		
Symmetry	$\tilde{L}$	$\tilde{D}$	Q	U	E
$U(1)_{\rm DB}$	$+1$	$+1$	$+1$	$+1$	$+1$
$U(1)_{\rm DL}$	$+1$	0	0	0	$+1$
$U(1)_{\rm U}$	0	0	0	$+1$	0

Table 6.1: Quantum number assignments for the dark matter fields for the accidental symmetries $U(1)_{\rm DB}, U(1)_{\rm DL}, U(1)_{\rm U}$ to arise at the renormalizable level in the dark lagrangian. For the conjugate fields, the assignments are opposite to the ones in the table.

The most general gauge invariant lagrangian describing the SM matter fields and dark fields of Eq. 6.1 can be written as:

$$\mathcal{L}_{\rm SM} \supset y_5^{SM} \bar{5}_{SM} 5_H^\dagger 10_{SM} + y_{10}^{SM} 10_{SM} 5_H 10_{SM} + h.c. \tag{6.2}$$

$$\begin{aligned}\mathcal{L}_{\rm DS} \supset & -m_5 \bar{5}_F 5_F - m_{10} \bar{10}_F 10_F - y_5 \bar{5}_F 24_H 5_F - y_{10} \bar{10}_F 24_H 10_F \\ & - y_L \bar{5}_F P_R 5_H^\dagger 10_F - y_R \bar{5}_F P_L 5_H^\dagger 10_F + h.c.\end{aligned} \tag{6.3}$$

where $P_{L,R}$ are the left, right projectors. Note that in Eq. 6.2 and Eq. 6.3 we have only written the mass and Yukawa terms for simplicity. Once $SU(5)$ is broken down to $\mathcal{G}_{SM}$, we can write the Yukawa terms between the dark fields in terms of the broken phase SM fragments:

$$\begin{aligned}\mathcal{L}_{\rm Y} = & \, y_L(H_3^\dagger \bar{\tilde{D}}_L U_R + H_3^\dagger \bar{\tilde{L}}_L Q_R) + y_L(H^\dagger \bar{\tilde{D}}_L Q_R + H^\dagger \bar{\tilde{L}}_L E_R) \\ & + y_R(H_3^\dagger \bar{\tilde{D}}_R U_L + H_3^\dagger \bar{\tilde{L}}_R Q_L) + y_R(H^\dagger \bar{\tilde{D}}_R Q_L + H^\dagger \bar{\tilde{L}}_R E_L) + \text{h.c.}\end{aligned} \tag{6.4}$$

where H denotes the SM higgs weak doublet whereas H_3 is its GUT colored partner. Integrating H_3 out, the dark theory at scales $\mu \ll M_{\rm GUT}$ will be given by:

$$\begin{aligned}\mathcal{L}_{\rm Y} = & \, y_L(H^\dagger \bar{\tilde{D}}_L Q_R + H^\dagger \bar{\tilde{L}}_L E_R) + y_R(H^\dagger \bar{\tilde{D}}_R Q_L + H^\dagger \bar{\tilde{L}}_R E_L) \\ & - \frac{y_L y_L^*}{M_{H_3}^2}(\bar{\tilde{D}}_L U_R)(\tilde{L}_L \bar{Q}_R) - \frac{y_R y_R^*}{M_{H_3}^2}(\bar{\tilde{D}}_R U_L)(\tilde{L}_R \bar{Q}_L) + \text{h.c.}\end{aligned} \tag{6.5}$$

At the renormalizable level, it is evident that there are accidental symmetries in addition to dark baryon number that leave the dark $\mathcal{L}$ invariant. These are:

- **U-number $\mathbf{U(1)_U}$**: Rotating the U dark quark field by a phase clearly leaves the dark $\mathcal{L}$ invariant due to the absence of U-number breaking yukawa terms in eq. 6.5. As is evident from the second line in Eq. (6.5), this symmetry is broken by dim-6 operators obtained after integrating out $M_{H_3} (\sim M_{\rm GUT})$.
- **Dark lepton number $\mathbf{U(1)_{DL}}$**: This symmetry acts only on leptonic (QCD singlet) dark fields. As is evident, the second Yukawa term in Eq. 6.5 involving dark leptonic fields conserves this number. This is broken by dim-6 operators as the one shown in eq. 6.5.

We summarise the dark field assignments of quantum numbers under these accidental symmetries in Table 6.1.

Figure 6.1: Heavy GUT partners H can decay to the light d.o.f.s (dark fermions L and SM) via tree level exchange of the GUT colored higgs H_3 and GUT gauge bosons $\mathcal{X}$.

Due to these accidental symmetries, the lightest heavy hadrons carrying these charges are long-lived. They can decay through higher dimensional operators violating the accidental symmetry. The abundance of dark baryonic states (non-DM) made of GUT partners ($\tilde{L}$, E or U fields dark fields) with long lifetimes τ_H would be disfavoured due to cosmological constraints. Constraints from Big Bang Nucleosynthesis (BBN) would exclude lifetimes $\tau_H > 1$ s. The GUT partners can decay to the lighter degrees of freedom (SM d.o.fs as well as dark fermions) via the exchange of GUT leptoquarks $\mathcal{X}$ and the SU(3) triplet GUT scalar H_3. For example, for the exchange of H_3 ($\sim M_{\rm GUT}$), we can write the tree level DL−number and U−number violating operator as:

$$\frac{y_L^* y_5^{\rm SM}}{M_{\rm GUT}^2}(\tilde{D}_L \bar{U}_R)(d_R^c u_R^c) \tag{6.6}$$

$$\frac{y_L^* y_5^{\rm SM}}{M_{\rm GUT}^2}(\bar{Q}_R \tilde{L}_L)(q_L l_L) \tag{6.7}$$

where d_R, u_R is the SM $R-H$ down type quark and up type quark, q_L is the SM $L-H$ quark doublet, and l_L is the SM $L-H$ lepton doublet. From the BBN bound which requires $\tau_H \lesssim 1$ s, we can obtain a lower bound on the mass scale of the GUT partners M_H:

$$\tau_H \lesssim 1\text{s} = 1\ \text{sec}\left(\frac{0.1}{y_L}\right)^2\left(\frac{1}{y_5^{\rm SM}}\right)^2\left(\frac{10^9}{M_H}\right)^5\left(\frac{M_{\rm GUT}}{10^{17}}\right)^4 \tag{6.8}$$

Here, we have used the value of $M_{\rm GUT} = 10^{17}$ GeV for perfect unification in this model.

These accidental symmetries can also be broken by tree-level exchange of GUT $\mathcal{X}_\mu$ bosons. An example of such a dim-6 U-number breaking operator is:

$$\frac{g_{GUT}^2}{M_{\rm GUT}^2}\left(\bar{Q}_R \gamma^\mu U_R\right)\left(u_R \gamma_\mu q_L\right) \tag{6.9}$$

This would lead to a similar lower bound on M_H as in Eq.6.1. Dim-6 operators leading to box diagrams with an exchange of both H_3 and $\mathcal{X}$ would lead to less stringent bounds on M_H due to the loop suppression.

6.2 Spectrum of Dark Mesons

The lightest states in our dark theory are the mesons (pseudo) NGBs resulting from the SU$(N_{DF})_L \times$ SU$(N_{DF})_R \to$ SU$(N_{DF})_V$ breaking of the dark flavour symmetry after dark confinement where for the benchmark model $N_{DF} = 9$. These light dark mesons transform under the adjoint representation 80 of the unbroken SU$(9)_V$ group. The phenomenology of dark mesons charged under $SU(2)_L \times U(1)_Y$ was recently studied in Ref. [188] (See also [172, 174]). Dark mesons (depicted by π_D) in the benchmark model $Q + \tilde{D}$ are shown in Table 6.2. In this model, there are no accidental symmetries

protecting the dark mesons, thus, light mesons cannot be long-lived. Depending on their quantum numbers under the SM (see first column in Table 6.2), these dark mesons can decay to two SM gauge bosons via anomalous couplings of the form:

$$\frac{N_{\rm DC}}{16\pi^2}\frac{c^{ij}_{\pi_D}}{f}\sum_{i,j} g^i_{\rm SM} g^j_{\rm SM}\pi_D F^{(i)}_{\mu\nu}\tilde{F}^{\mu\nu\ (j)} \tag{6.10}$$

where c^{ij}_{π} is the anomaly coefficient, $F^{(i)}_{\mu\nu}$ is the field strength tensor of the SM gauge boson A^i_μ to which the dark pions decay and $g^i_{\rm SM}$ is the SM gauge coupling. Here f is the dark pion decay constant given in the large-$N_{\rm DC}$ limit by $f \sim \frac{\sqrt{N_{\rm DC}}}{4\pi}\Lambda_{\rm DC}$. In the following Table 6.2, we classify the dark mesons according to the quantum numbers under the SM gauge group and decay modes to SM gauge bosons:

SM quantum numbers	dark meson	decay mode to SM
$(1,1)_0$	$\bar{Q}Q - \tilde{\bar{D}}\tilde{D}$	$BB,\ WW$
$(1,2)_{\pm 1/2}$	$\bar{Q}\tilde{D} +$ conj	$\bar{f}_{SM} f_{SM}$
$(1,3)_0$	$\bar{Q}Q$	WB
$(8,1)_0$	$\bar{Q}Q,\ \tilde{\bar{D}}\tilde{D}$	gB
$(8,2)_{\pm 1/2}$	$\bar{Q}\tilde{D} +$ conj.	hg
$(8,3)_0$	$\bar{Q}Q$	Wg

Table 6.2: Table showing all the NGBs and their SM quantum numbers along with their decay modes to the SM. Note that the dark meson $\bar{Q}\tilde{D}$ is a composite Higgs and will mix with the SM Higgs, we describe this in the main text.

6.2.1 NGB Spectrum

Here we describe the NGB spectrum using the NGB potential for the $Q + \tilde{D}$ model. In the absence of weak gauging and Yukawa couplings, the dark Lagrangian is invariant under $G \equiv SU(9)_L \times SU(9)_R \times U(1)_{DB}$ symmetry which will be explicitly broken by the dark fermion mass terms. We can promote the parameters in the dark Lagrangian to spurions. Indeed, we can associate three spurions of the broken global symmetry and write their transformation rules:

1. **Dark fermion mass:** We can write the mass matrix M_q as

$$\mathcal{L}_{\rm mass} \ni \bar{\psi}_L M_q \psi_R + \bar{\psi}_R M_q^\dagger \psi_L \tag{6.11}$$

   Here $\psi_L \to L\ \psi_L$ where $L \in SU(9)_L$ and $\psi_R \to R\ \psi_R$ where $R \in SU(9)_R$. $\psi_{L,R}$ contains all the 9 dark flavours. Under G, we can write the transformation rule for M_q:

$$M_q \to L M_q R^\dagger \tag{6.12}$$

2. **Gauge couplings of $\mathcal{G}_{SM}$**: We can write the SM gauge couplings that appear in the kinetic term of the dark lagrangian as:

$$\mathcal{L}_{kinetic} \ni g_{SM} T^a A^a_\mu = T^A (g_{SM}\delta^{Aa}) A^a_\mu \equiv T^A \chi^{Aa} A^a_\mu \tag{6.13}$$

where the spurion $(g_{SM}\delta^{Aa}) \equiv \chi^{Aa}$ transforms as i) an adjoint of the global dark symmetry group G and as ii) an adjoint of the SM (gauge) symmetry group $\mathcal{G}_{SM}$. This spurion breaks the symmetry group down to the diagonal group.

3. **Yukawa couplings:** Finally, the Yukawa couplings in the dark Lagrangian can be written as 9×9 matrices $Y^a_{L,R}$:

$$\mathcal{L}_{\text{Yukawa}} \ni \bar{\psi}_L Y^a_L H^a \psi_R + \bar{\psi}_R Y^a_R H^a \psi_L + h.c. \tag{6.14}$$

Above, a is the $SU(2)_L$ index and the spurion $Y^a_{L,R}$ transforms as:

$$\text{Under G}: \quad Y^a_L \to L\, Y^a_L\, R^\dagger; \quad Y^a_R \to R\, Y^a_R\, L^\dagger \tag{6.15}$$

$$\text{Under } \mathcal{G}_{\text{SM}}: \quad Y^a_{L,R} \quad \text{transforms as} \quad (\bar{2},1)_{-1/2} \tag{6.16}$$

Let us construct the NGB potential at lowest order using the spurionic transformation rules described above. This will allow us to write the mass contributions to the NGBs. We will construct the effective potential by adopting the standard non-linear representation for the NGB fields

$$\Sigma(x) \equiv \exp\left\{\frac{2i\pi^A(x)T^A}{f}\right\} \tag{6.17}$$

At the lowest order in M_q the NGB potential is the same as that of the QCD pion. We can write the $G \times \mathcal{G}_{SM}$ invariant potential term using M_q and the scalars:

$$V^{(M_q)} = B_0(\text{Tr}(\Sigma^\dagger M_q) + \text{Tr}(\Sigma M_q^\dagger)) \tag{6.18}$$

Under G, $\Sigma \to L\Sigma R^\dagger$. The coefficient B_0 has dimension 3 and can be estimated using NDA:

$$B_0 \sim \frac{N_{\text{DC}}}{16\pi^2}\Lambda^3_{\text{DC}} \tag{6.19}$$

B_0 will be fixed to this value from the vacuum energy contribution to the quark mass in the UV theory. Expanding Eq. 6.18 around $\pi = 0$, we can read off the meson mass contribution from the dark quark masses which scales linearly (exactly like for the QCD pion):

$$\delta m^2_{\pi_D} \sim \Lambda_{\text{DC}} \cdot m \tag{6.20}$$

where m is the dark fermion mass. Let us now compute the contribution to the NGB mass from the SM gauge bosons using the spurion introduced earlier χ^{Aa}. The leading contribution from χ^{Aa} only arises at $\mathcal{O}(\chi^2)$, exactly like in the case of composite Higgs (See Ref. [189] for a review). We can once again write the invariant potential term as:

$$V^{(g)} = c^{(g)}\text{Tr}[\Sigma^\dagger\, T^A_L\, \Sigma\, T^B_R]\chi^{Aa}\chi^{Ba} \tag{6.21}$$

Here, $c^{(g)}$ can be estimated to be:

$$c^{(g)} \sim \frac{N_{\text{DC}}}{(16\pi^2)^2}\Lambda^4_{\text{DC}} \tag{6.22}$$

Thus, the SM gauge fields contribute to the mass of NGBs as:

$$\delta m^2_{\pi_D} \sim \frac{g^2}{16\pi^2}\Lambda^2_{\text{DC}} \tag{6.23}$$

Finally, we can write the NGB potential terms using the Yukawa spurion $Y^a_{L,R}$. The Yukawas can directly contribute to the NGB mass by a direct contribution from the NGB potential terms arising at $\mathcal{O}(Y^2)$:

$$\begin{aligned} V^{(Y)} &= c_1^{(Y)}\mathrm{Tr}[\Sigma\, Y_R^a\, \Sigma\, Y_L^{a\dagger}] + \mathrm{h.c.} \\ &+ c_2^{(Y)}\mathrm{Tr}[\Sigma^\dagger Y_L^a]\ \mathrm{Tr}[\Sigma Y_L^{a\dagger}] + \mathrm{Tr}[\Sigma Y_R^a]\ \mathrm{Tr}[\Sigma^\dagger Y_R^{a\dagger}] \\ &+ c_{2LR}^{(Y)}\mathrm{Tr}[\Sigma Y_R^a]\mathrm{Tr}[\Sigma Y_L^{a\dagger}] + \mathrm{h.c.} \end{aligned} \tag{6.24}$$

The potential in Eq. 6.24 is the most general potential at $\mathcal{O}(Y^2)$ which is invariant under $\mathcal{G}_{SM}$ and formally invariant under parity. Under parity the transformation rules of the fields and spurions are given by:

$$P: \quad \psi_L \leftrightarrow \psi_R \quad \Rightarrow \Sigma \leftrightarrow \Sigma^\dagger \tag{6.25}$$

The Yukawa terms of Eq. 6.24 will preserve parity if the spurion transforms as:

$$P: \quad Y_L^a \leftrightarrow Y_R^a \tag{6.26}$$

The coefficients $c^{(Y)}$ can be estimated as:

$$c^{(Y)} \sim \frac{N_{\mathrm{DC}}}{(16\pi^2)^2}\Lambda_{\mathrm{DC}}^4 \tag{6.27}$$

Finally, we can write the contribution to the NGB mass coming from the Yukawa couplings as:

$$\delta m^2_{\pi_D} \sim \frac{y^2}{16\pi^2}\Lambda^2_{\mathrm{DC}} \tag{6.28}$$

where the coefficient y^2 conserves parity and can be written as:

$$y^2 \sim \mathrm{Re}[y_L y_R^*] + (|y_L|^2 + |y_R|^2) \tag{6.29}$$

We can finally write the NGB mass as a sum of all these contributions given in Eq. 6.28,Eq. 6.23 and Eq. 6.20 as:

$$m^2_{\pi_D} \sim \Lambda_{\mathrm{DC}}\, m + \frac{g^2_{SM}}{16\pi^2}\Lambda^2_{\mathrm{DC}} + \frac{y^2}{16\pi^2}\Lambda^2_{\mathrm{DC}} \tag{6.30}$$

Mixing with SM Higgs: In addition to contributing directly to the mass of the NGBs, the Yukawas can lead to a mixing term with the SM Higgs. In order to derive the mixing angle between the composite Higgs NGB given by $\bar{Q}\tilde{D}$ and SM Higgs, let us consider the low-energy effective lagrangian for NGBs and Higgs H:

$$\begin{aligned} \mathcal{L}_{\pi-H} &= c_H\{\mathrm{Tr}[\Sigma^\dagger Y_L^a] + \mathrm{Tr}[\Sigma Y_R^a]\}H^a \\ &+ \mathrm{h.c.} + \mathcal{O}(H^2) \end{aligned} \tag{6.31}$$

Expanding to the lowest order, we can write the mixing terms between the NGBs and Higgs as:

$$\mathcal{L}_{\pi-H} \sim \frac{c_H}{f}(y_L - y_R)\pi_{(1,2)}H + \frac{c_H}{f^2}(y_L + y_R)\pi_{(1,2)}\pi_{(1,1)}H \tag{6.32}$$

where $\pi_{(1,2)}$ is the composite higg NGB while $\pi_{(1,1)}$ is the SM singlet NGB. Finally, the coefficient c_H can be estimated using NDA as:

$$c_H \sim \frac{N_{\rm DC}}{16\pi^2}\Lambda_{\rm DC}^3 \sim \Lambda_{\rm DC} \cdot f^2 \tag{6.33}$$

As is evident, the first term in Eq. 6.32 implies a mixing between the NGB $\pi_{(1,2)}$ and the SM higgs. Finally, the mixing angle can be written as:

$$\theta \approx \frac{y_- \Lambda_{\rm DC} f}{m_{\pi_D}^2 - m_h^2} \tag{6.34}$$

where we have defined $y_- = (y_L - y_R)$. In the limit in which the dark fermions are massless, and $y_- \ll 1$, the NGB mass in Eq. 6.30 will be dominated by the SM gauge contribution term, thus we can write the mixing angle as:

$$\theta \approx 4\pi\sqrt{N_{\rm DC}}\frac{y_-}{g_{SM}^2} \tag{6.35}$$

where we have used $m_{\pi_D}^2 \approx (g_{SM}^2/16\pi^2)\Lambda_{\rm DC}^2$. Thus, we can expect a large mixing angle between the NGB and SM Higgs for $y_- \approx \mathcal{O}(1)$.

6.2.2 Production and Decay of NGBs

In this subsection we will comment briefly on the production and decay modes of NGBs at colliders. In our parameter space for the dark sector, the most plausible value for $\Lambda_{\rm DC}$ (compatible with DM abundance) is $\sim$ 100 TeV. For these large values of $\Lambda_{\rm DC}$, the NGBs will be too heavy and thus, cannot be probed at colliders. For lower values of $\Lambda_{\rm DC}$, however, the value of GUT partner mass M_H is very tuned (as can be seen from our result plot in Fig. 6.4). In this tuned part of the parameter space, one can hope to produce NGBs at future colliders.
NGBs with anomalous couplings with SM gauge bosons can be produced at colliders via vector boson fusion. The neutral component of the composite higgs $\bar{Q}\tilde{D}$ NGB $\pi^0_{(1,2)}$ will be produced from the SM Higgs via processes such as ggF (gluon gluon fusion). The charged component instead $\pi^+_{(1,2)}$ will be produced via associated $t\bar{t}$ production at colliders. The SM singlet NGB will be very weakly coupled and light in the limit of $y_- \ll 1$, to be produced at colliders.
Let us now comment on the various decay modes of NGBs and the respective partial decay widths. The decay modes of NGBs to SM gauge bosons have been summarised in the Table 6.2. Note that the NGBs can also decay in addition to other (lighter) NGBs alongside an SM field - gauge boson V or Higgs h. For example, a decay $\pi^0_{(1,2)} \to h + \pi^0_{(1,1)}$ can occur. The coupling for the case of an associated gauge boson V will be derivative suppressed, while for the case of associated h production, the coupling will be proportional to the Yukawa couplings in the dark sector as can be seen from the second term in Eq. 6.32.

The decay width for the dark mesons decaying to 2 SM gauge bosons can be written as:

$$\Gamma_{\pi_D \to VV} \simeq (c^{ij}_{\pi_D})^2 \frac{\alpha^i_{\rm SM}\alpha^j_{\rm SM}}{8\pi}\frac{m^3_{\pi_D}}{\Lambda^2_{\rm DC}} \tag{6.36}$$

For prompt decays of the SM-singlet pion to $\gamma\gamma$, we expect the dark mesons to have the lifetime τ given by:

$$\tau = \Gamma^{-1}_{\pi_D} \simeq 10^{-15}\ {\rm s}\left(\frac{c}{0.17}\right)^2\left(\frac{\alpha_{\rm EM}}{0.007}\right)^2\left(\frac{m_{\pi_D}}{500\ {\rm GeV}}\right)^3\left(\frac{80\ {\rm TeV}}{\Lambda_{\rm DC}}\right)^2 \tag{6.37}$$

The SM-singlet pions do not receive any SM gauge contribution in the mass term. In the limit in which the dark quarks are massless $m \approx 0$, the only contribution to the singlet mass comes from the Yukawa term. For $y_- \ll 1$, the mass of the $\pi_{(1,1)}$ can be as light as 500 GeV for $\Lambda_{\rm DC} \sim 80$ TeV.

The decay of the meson $\pi^0_{(1,2)}$ will instead occur via mixing with the elementary SM Higgs h as :

$$\Gamma_{\bar{Q}\tilde{D}} \simeq (\sin^2\theta)\ \Gamma_h|_{m_h=m_{\pi_D}} \tag{6.38}$$

where Γ_h is the total decay width of the SM Higgs (defined as the sum of the partial decay widths into the accessible SM final states) evaluated at $m_h = m_{\pi_D}$. Here $\sin\theta$ is the mixing angle between the pion $\bar{Q}\tilde{D}$ and the SM higgs which was derived in Eq. 6.34. Notice that the mixing of the SM Higgs with an NGB violates parity. For $y_L = y_R$, parity will be conserved, and the mixing will vanish. The largest decay rate for the neutral component of composite Higgs meson will be to pairs of SM top quarks. We can get the lifetime of this meson as:

$$\tau = \Gamma^{-1}_{\pi_D} \simeq 10^{-26}\ \text{s} \left(\frac{y_-}{0.1}\right)^2 \left(\frac{\Lambda_{\rm DC}}{80\ \text{TeV}}\right)^4 \left(\frac{m_{\pi_D}}{4\ \text{TeV}}\right)^4 \left(\frac{\Gamma_h}{50\ \text{GeV}}\right) \tag{6.39}$$

where we have used the partial width of SM Higgs to $\bar{t}t \sim 50$ GeV. For the mass of $\pi_{(1,2)}$ meson in the massless dark quark limit, we are considering only the SM gauge contributions given by $m_{\pi_D} \sim (g_{EW}/4\pi)\Lambda_{\rm DC}$, where g_{EW} is the weak coupling at $\mu = 80$ TeV given by ≈ 0.6.

Finally, the $SU(3)$ octet $\bar{Q}\tilde{D}$ meson in Table 6.2 cannot decay to SM gauge bosons via anomalous couplings. It can decay via its non-renormalizable coupling to the SM Higgs and gluon given by the operators:

$$y_- g_3 \frac{f}{\Lambda^3_{\rm DC}} D_\mu \pi_D D_\nu H G^{\mu\nu}, \qquad y_+ g_3 \frac{f}{\Lambda^3_{\rm DC}} D_\mu \pi_D D_\nu H \tilde{G}^{\mu\nu}. \tag{6.40}$$

where $y_+ = (y_L + y_R)$. Note that the two couplings y_+, y_- of the respective operators follow the transformation rules under parity for their respective operators in Eq. 6.40. The decay width of the octet meson via this dimension-6 coupling can be written as:

$$\Gamma_{\bar{Q}\tilde{D}\to hg} \simeq \frac{N_{\rm DC}}{8\pi} \frac{(y_-^2 + y_+^2)}{4\pi} \frac{g_3^2}{4\pi} \frac{m^5_{\pi_D}}{\Lambda^4_{\rm DC}} \tag{6.41}$$

We can get the lifetime for this octet meson as:

$$\tau = \Gamma^{-1}_{\pi_D} \simeq 10^{-19}\ \text{s} \left(\frac{y_-^2 + y_+^2}{0.02}\right) \left(\frac{\alpha_S}{0.118}\right) \left(\frac{\Lambda_{\rm DC}}{100\ \text{TeV}}\right)^4 \left(\frac{m_{\pi_D}}{5\ \text{TeV}}\right)^5 \tag{6.42}$$

For the mass of $\pi_{(8,2)}$ meson in the massless dark quark limit, we consider only the SM gauge contributions given by $m_{\pi_D} \sim (g_S/4\pi)\Lambda_{\rm DC}$, where g_S is the strong coupling at $\mu = 80$ TeV given by ≈ 0.8.

Now we comment on light mesons in models other than the benchmark model that are protected by accidental symmetries. For example, in the $SU(3)_{DC}$ model given by the light fermions $L \oplus E$, the light mesons in the theory can decay only via dimension-6 operators. Note that this model can also give good unification under our criteria for non-degenerate GUT partner mass (See discussion in Sec. 5.2.3)

For the decay of the $\bar{L}E$ meson via the dimension-6 operator $(\kappa/\Lambda^2_{\rm UV})\bar{L}EHHH$, the decay width

will be given by:

$$\Gamma_{\pi_D} \sim \frac{k^2}{8\pi}\frac{N_{\rm DC}}{16\pi^2}\frac{\Lambda_{\rm DC}^4}{\Lambda_{\rm UV}^4} m_\pi \tag{6.43}$$

Using this, we get the lifetime for this meson in the case of $L \oplus E$ model as :

$$\tau = \Gamma_{\pi_D}^{-1} \simeq 0.5 \text{ s} \left(\frac{k^2 N_{\rm DC}}{3}\right)\left(\frac{m_{\pi_D}}{4 \text{ TeV}}\right)\left(\frac{\Lambda_{\rm DC}}{80 \text{ TeV}}\right)^4\left(\frac{10^{11} \text{ GeV}}{\Lambda_{\rm UV}}\right)^4 \tag{6.44}$$

where we have only considered SM gauge contribution to the mass of the $\bar{L}E$ meson in the massless dark quark limit. Such dimension-6 operators (as was already discussed in Sec. 5.1.1) should be suppressed by $\Lambda_{\rm UV} \gtrsim 10^{11}$ GeV to not violate the bound on the lifetime of these mesons coming from BBN, $\tau \lesssim 1$ s.

In the next section, we discuss the cosmological history of the benchmark model given by the dark fermions $Q \oplus \tilde{D}$. In the benchmark model case, in this section, we have clarified the mass spectrum of the dark mesons and demonstrated that they will be short-lived. During the cosmological evolution of the dark sector with temperature, the dark mesons will thus be in equilibrium.

6.3 Cosmological History

In this section, we clarify the cosmology of theories with a light baryonic DM candidate (already considered in Ref. [172]), focusing on the role of GUT partners.

The Universe can undergo different thermal histories in the two different cosmological histories, either with a 1) large reheating temperature at the end of inflation wrt GUT partner mass such that $T_{RH} > M_H$ or a 2) low reheating temperature such that $T_{RH} < M_H$. Here we give an overview of the first case and postpone a brief discussion of the second scenario for Sec. 6.4.

The universe first undergoes a phase of perturbative freeze-out for the free H quarks at a temperature of $T_{F.O.}^{pert} = M_H/\mathcal{O}(10)$. As the universe cools down, *dark confinement* occurs at a temperature $T = T_{DC}$ where $T_{DC} \sim \Lambda_{\rm DC}$. In the following discussion, we will generically refer to light DM forming fermions with mass $m \lesssim \Lambda_{\rm DC}$ as L and their GUT partners as H with mass $M_H > \Lambda_{\rm DC}$. Due to the much larger abundance of L at T_{DC}, we expect that the bound states are majorly comprised of hadrons formed purely of light dark fermions - light baryons LLL and light dark mesons $\bar{L}L$ with masses:

$$m_{LLL} \sim N_{\rm DC}\Lambda_{\rm DC}, \qquad m_{\bar{L}L}^2 \sim m_L\Lambda_{\rm DC} + \frac{\alpha_{\rm SM}}{4\pi}\Lambda_{\rm DC}^2 \tag{6.45}$$

In addition to these usual states typical of the light-dark fermion regime [172], we also have hybrid states involving the GUT partner fermions H. The frozen-out population of H type quarks at $T \sim \Lambda_{\rm DC}$ can combine with light fermions forming hybrid baryons HLL and hybrid mesons $\bar{H}L$ at dark confinement. These are peculiar heavy states with large masses m_{hyb} and large size r_{hyb} given by (See also discussions of similar bound states in Refs. [83, 190–192] and in Refs. [193, 194] which studied them in the context of supersymmetric gauge theories):

$$m_{hyb} \sim \mathcal{O}(M_H), \qquad r_{hyb} \sim \mathcal{O}(\Lambda_{\rm DC}^{-1}) \tag{6.46}$$

Due to the large radii and low binding energy $B_{HLL} \sim \mathcal{O}(1)\ \Lambda_{\rm DC}$, these hybrid baryons and mesons can collide among each other and with other purely light states - LLL, $\bar{L}L$, with a large geometric cross-section of order $\sigma_{\rm rec} \sim 1/\Lambda_{\rm DC}^2$.

There are also other bound states in our dark sector containing more than one H such as HHH, $\bar{H}H$. These states with large negative binding energy are perturbative and well described by the Coulombic potential of Eq. H.7 (see also [173]). This is only true for bound states in the regime when the following inequality is valid:

$$\Lambda_{DC} \ll |B_\chi| \ll a_\chi^{-1}. \tag{6.47}$$

Here $|B_\chi|$ is the binding energy of the perturbative bound state $\sim \alpha_{\rm DC}^2(M_H)M_H$, and a_χ is the Bohr radius of the state given by roughly $\sim (\alpha_{\rm DC}(M_H)M_H)^{-1}$. In our GUT dark sector, from unification constraints, the benchmark model $Q + \tilde{D}$ can allow for GUT partner masses in the following range: 6×10^6 GeV $\lesssim M_H \lesssim 10^{14}$ GeV. We find that for this entire M_H range the condition in Eq. 6.47 is always true hence the Coulombic approximation is a good one for the higher H hadrons.

At a temperature of $T \lesssim \Lambda_{\rm DC}$, right after dark confinement, a very busy *epoch of recombination* occurs. This involves various recombining processes favoring the formation of unbreakable hadronic states containing more than one H. A similar mechanism has been recently described in Refs. [83, 192, 195] (See also Refs. [190, 191, 196] which first described this).

The recombination reactions populate the higher hybrid states like HHH, $\bar{H}H$, HHL and are efficient only in the forward direction due to energy conservation (See Appendix H for more details). At the end of this epoch, we find that an almost negligible abundance of initial hybrid states HLL and $H\bar{L}$ is left (See also discussion in Ref. [191, 192]). We report our systematic calculations and solutions for this in Sec. 6.3.2 and Appendix H.

Further, it was first shown in Refs. [197–199], and much more recently in Refs. [83, 175, 200–202] that any long-lived non-relativistic matter with an out-of-equilibrium energy density can dominate the energy density of the universe, and inject entropy into it by its decay. In our GUT dark sector as well, a *matter-dominated (MD) era* can be set by the abundance of long-lived H quarks and their bound states. This can lead to a further dilution of the DM density due to the non-standard scaling of the scale factor given by, $a \propto T^{-8/3}$, instead of the standard $a \propto T^{-1}$ scaling during MD era. We discuss the details and the scenarios in which this dilution is relevant in Sec. 6.3.3.

Finally, the DM candidate in our dark theory: the light baryon LLL, undergoes thermal freeze-out at $T_{F.O}^{DM}$. Here, $T_{F.O.}^{DM} \sim \Lambda_{\rm DC}/\mathcal{O}(10)$ is the temperature at which the baryonic annihilations keeping the DM in equilibrium freeze-out[2]. In addition to this thermal contribution, we find that the DM relic abundance can have a non-thermal contribution from the decay of heavy H baryons such as $HLL \to LLL$, if the decay occurs at $T < T_{F.O}^{DM}$. We discuss this in detail in Sec. 6.3.4.

6.3.1 Thermal Freeze-out (of GUT partners)

At scales much above the dark confinement scale $\Lambda_{\rm DC}$, the dark coupling constant $\alpha_{\rm DC}$ is perturbative $\alpha_{\rm DC} \ll 1$. Using renormalization group equation, we can write $\alpha_{\rm DC}$ as:

$$\alpha_{\rm DC}(M_H) = \left(\frac{\beta_{\rm DC}}{2\pi} \log \frac{\Lambda_{\rm DC}}{M_H}\right)^{-1} \tag{6.48}$$

with $\beta_{\rm DC}$ defined in Eq. 5.14. For the benchmark $Q + \tilde{D}$ model, $\beta_{\rm DC} = -5$.

In this unconfined phase at temperature $T \sim M_H \gg \Lambda_{\rm DC}$, free H quarks annihilate with each other to dark gluons and SM particles. The freeze-out temperature for this annihilation reaction is

[2]DM freeze-out is set by rearrangement reactions between baryons giving mesons [172, 203].

of order $T_{F.O}^{pert} \sim M_H/\mathcal{O}(10)$. A general expression for the annihilation cross-section is given by:

$$\langle \sigma_{\rm ann} v_{\rm rel} \rangle \simeq \frac{\pi \alpha_{\rm DC}^2(M_H)}{M_H^2} \tag{6.49}$$

Here we would like to note that only GUT partner quarks H would undergo a thermal freeze-out, while the light dark fermions L will remain in equilibrium with the thermal bath. Once the rate of the $\bar{H} + H$ annihilation reaction drops below the expansion rate H, the thermal freeze-out occurs. An estimate for this "frozen-out" number density of free H quarks can be given by:

$$n_H(T_{F.O.}^{pert}) \sim \frac{H(T_{F.O.}^{pert})}{\langle \sigma_{\rm ann} v_{\rm rel} \rangle} \tag{6.50}$$

where $H(T_{F.O.}^{pert})$ is the Hubble parameter at $T_{F.O.}^{pert}$. Since entropy is conserved in this phase (we will discuss this more in detail in Sec. 6.3.3), we can use $Y = n/s$, the number density per comoving volume, to track the free H abundance. This allows us to write the abundance of H quarks Y_H at the dark confinement temperature T_{DC} as:

$$Y_H(T_{\rm DC}) = \frac{3.79\, x_f^{pert}}{g_*^{1/2} M_{Pl} M_H \sigma_0} \tag{6.51}$$

where g_* is the relativistic d.o.f.s at $T_{F.O.}^{pert}$ (including both the dark d.o.f.s as well as the SM d.o.fs), $M_{Pl} = 1.2 \times 10^{19}$ GeV, σ_0 is the s-wave annihilation cross-section equal to $\langle \sigma_{\rm ann} v_{\rm rel} \rangle$ and given by Eq. 6.49, x_f^{pert} is defined in the usual way as M_H/T_{FO}^{pert} and we compute it in the standard way (see for example [204]).

6.3.2 Dark Confinement and Recombination

As the universe cools down, the dark theory undergoes confinement at $T = T_{\rm DC}$ at which all the free dark d.o.f.s bind into dark color singlets. Here and in the following discussion we assume $N_{\rm DC} = 3$. These dark bound states can either be formed from purely light fermions L or else be hybrid states containing one H quark:

$$\bar{L}L,\ LLL,\ H\bar{L},\ HLL \tag{6.52}$$

We ignore any initial abundance of hadrons with more than one H since $Y_H \ll 1$, hence the formation of such hadrons will be very suppressed (for example $Y_H \sim 10^{-6}$ for $M_H = 10^{10}$ GeV).

At this point, it is important to discuss why we are keeping track of hadrons containing GUT partners H. Any H containing baryon can decay via dimension-6 operator such as those given in Eq. 6.9 (See details in Sec. 6.1) to a purely light baryon LLL. Thus, the fraction of total H abundance in heavy baryons HHL, HHH given by $f_H^{\mathcal{B}}$ would then lead to a non-thermal contribution to the DM abundance. In this section, we describe the processes that impact this fraction of abundance, $f_H^{\mathcal{B}}$.

We will now describe our assumptions on modelling the various hybrid bound states. We assume the following hierarchy of masses between the hybrid meson and hybrid baryons of $M_{HLL} \gtrsim M_{\bar{H}L}$ in analogy with the SM B-meson-baryon system (See Ref. [205] and detailed discussion in Appendix H.2). The masses for these hybrid states can be written similarly to the heavy quark systems in QCD as sums of their constituent "partons" (M_H) and the binding energy of the non-perturbative "muck" $B \sim \mathcal{O}(\Lambda_{\rm DC})$ [205] (See also [191]).

At $T = T_{DC}$, the light mesons will be still relativistic and in equilibrium and the light baryons

LLL being thermal DM also follow the equilibrium distribution before freeze-out at temperature $T > T_{F.O.}^{DM}$.

Since the light hadrons LLL, $\bar{L}L$ are much more abundant than hybrid hadrons, hybrids are much more likely to collide with light hadrons than collide among themselves [190]. These reactions between hybrids and light hadrons are:

$$HLL + \bar{L}L \rightleftharpoons LLL + H\bar{L}, \qquad HLL + \bar{L}\bar{L}\bar{L} \rightleftharpoons H\bar{L} + n\bar{L}L \tag{6.53}$$

These reactions proceed in either direction with a geometric cross-section given by [190, 191]:

$$\sigma_{\rm rec} \sim \frac{\pi}{\Lambda_{\rm DC}^2} \tag{6.54}$$

due to the large radii of HLL, $\bar{L}H$ states, $r \sim \mathcal{O}(\Lambda_{\rm DC}^{-1})$. Note that the baryonic annihilations that set the freeeze-out abundance of LLL proceed via a similar geometric cross-section till they freeze-out at $T \sim T_{F.O.}^{DM}$. These annihilation reactions can be written as:

$$LLL + \overline{LLL} \rightleftharpoons n\bar{L}L \tag{6.55}$$

We now begin the discussion on the busy *epoch of recombination* that begins at $T \lesssim T_{DC}$.

The reactions involving the *type I* hybrids HLL, $H\bar{L}$ in Eq. 6.53 have a much-enhanced rate due to the larger abundance of LLL, $\bar{L}L$. It is, however, likely that the hybrid mesons and baryons *recombine* also among themselves and form bound states with two H. Such bound states are a tower of states with varying angular momentum l. The excited states are larger in size with $r \sim \Lambda_{\rm DC}^{-1}$ and have binding energies given by $B \sim \mathcal{O}(\Lambda_{\rm DC})$. These *breakable* bound states can be either broken by the dark mesons in the thermal bath or else can de-excite to the ground state via the emission of dark radiation. The ground state, instead, is a perturbative state with large (negative) binding energy given by $|B| \sim \alpha_{\rm DC}^2 M_H$. Such states cannot be destroyed by the bath since the probability of finding a meson $\bar{L}L$ in the bath with energy B is Boltzmann suppressed by a factor $e^{-B/T}$. Let us comment further on the role of light mesons $\bar{L}L$ in the breaking of these bound states like HHL, $\bar{H}H$, HHH. Since the light mesons are short-lived (see discussion on NGBs in Sec. 6.2), they follow their equilibrium distribution, hence their abundance is suppressed. This greatly suppresses the breaking rate of the hybrids HHL by the mesons $\bar{L}L$[3].

In the following, we will collectively denote the unbreakable states with binding energy $B \sim \alpha_{\rm DC}^2 M_H$ with u. The rest of the tower of states with binding energy $B \sim \Lambda_{\rm DC}$ are considered to be breakable and denoted with a $*$. We solve for these two groups of bound states as opposed to tracking each bound state at each l level.

We will now discuss the various recombination reactions for the formation of these bound states: HHL, $\bar{H}H$, HHH.

For example, an unbreakable (denoted with u) HHL^u state - a *type II* baryon hybrid can be formed via reactions such as:

$$HLL + H\bar{L} \to HHL^u + n\bar{L}L, \tag{6.56}$$

$$HLL + HLL \to HHL^u + LLL. \tag{6.57}$$

[3]Note that our scenario of suppressed breaking rate of HHL, $\bar{H}H$, HHH by the mesons $\bar{L}L$ in the bath is similar to the case discussed in the Colored dark matter scenario of Ref. [192]. In Ref. [192], the breaking rate of the $\mathcal{Q}\mathcal{Q}$ state by QCD pions is suppressed. This should be contrasted instead with the Gluequark dark matter scenario of Ref. [175] where the out-of-equilibrium abundance of glueballs Φ can contribute substantially to the breaking of bound state $\mathcal{Q}\mathcal{Q}^*$ back to the gluequark χ.

As shown (see also discussion in appendix H.2), these reactions proceed only in the forward direction. The cross-section for the formation of these states at large temperature T is much smaller than the geometric cross-section, $\sigma_{\rm fall}(T) \ll \sigma_{\rm rec}$. For our computation, we use the analytical estimate for $\sigma_{\rm fall}$ given in [192], details of which can be found in the Appendix H.2. There will also be a fraction of type I hybrids that recombine forming *breakable* HHL^* states (denoted by $*$).

Reactions for the formation of breakable HHL^* can be written as:

$$HLL + H\bar{L} \rightleftharpoons HHL^* + n\bar{L}L \tag{6.58}$$

$$HLL + HLL \rightleftharpoons HHL^* + LLL \tag{6.59}$$

where HHL^* depicts any state in the tower of breakable HHL states that can be broken back to the initial states by the thermal bath. Despite the large cross-section for this process $\sigma_{break} \sim \sigma_{rec}$, we find that the abundance of breakable HHL^* states is negligible at the end of recombination (See appendix H for details and Fig. H.1). In addition to HHL, recombination can also proceed leading to the formation of *type II* mesons $\bar{H}H$ made of purely H quarks via the reactions:

$$HLL + \bar{H}L \to \bar{H}H^u + LLL \tag{6.60}$$

$$H\bar{L} + \bar{H}L \to \bar{H}H^u + n\bar{L}L \tag{6.61}$$

$$HLL + \overline{HLL} \to \bar{H}H^u + n\bar{L}L \tag{6.62}$$

Each of the above reactions for $\bar{H}H^u$ formation will also have counterparts leading to the formation of breakable $\bar{H}H^*$ state similar to the HHL^* case given in Eq. 6.59.

Once a significant abundance of HHL has accumulated, recombination can occur forming *type III* baryons made of purely H quarks. These reactions can be written as:

$$HHL + H\bar{L} \to HHH^u + n\bar{L}L \tag{6.63}$$

$$HHL + HLL \to HHH^u + LLL \tag{6.64}$$

Once again, each of the above reactions can be written for the formation of the breakable HHH^* state, active in both backward and forward directions.

We solve the Boltzmann equations for the co-moving abundances Y_i of each of these bound states details of which can be found in the appendix H. Here, we give a summary of our main numerical results at the end of the epoch of recombination.

At T_{DC}, the initial conditions for the epoch of recombination are set by the abundance of free H quarks $Y_H(T_{\rm DC})$ in Eq. 6.51 where a fraction f of Y_H condenses to form type I mesons $H\bar{L}$, and a fraction $(1-f)$ condenses into type I baryons HLL. Turning on the recombination reactions in Eq. 6.53 between hybrids HLL, $H\bar{L}$ and LLL, $\bar{L}L$, we find that the ratio of the abundances of the hybrid baryon HLL, Y_{HLL} to hybrid meson $\bar{L}H$, $Y_{H\bar{L}}$ follows the ratio of their equilibrium distributions and is exponentially suppressed. Thus, at $T \lesssim \Lambda_{\rm DC}$:

$$\frac{Y_{HLL}}{Y_{\bar{L}H}} \simeq \frac{Y^{eq}_{HLL}}{Y^{eq}_{H\bar{L}}} = \frac{g_{HLL}}{g_{H\bar{L}}} e^{-(m_{HLL}-m_{H\bar{L}})/T} \tag{6.65}$$

We find that the above result is very robust against any initial value of f. Further, as soon as the type II and III recombination reactions of Eqs. 6.56- 6.64 come into play, we find that the unbreakable type II and III hybrids: $\bar{H}H^u$, HHL^u, HHH^u are rapidly populated leaving behind a negligible abundance of type I HLL and $\bar{L}H$ at $z \sim 1$ where $z = \Lambda_{\rm DC}/T$. This apparent *de-population* of type I hybrids soon after confinement implies that type I recombination reactions of Eq. 6.53 are inactive

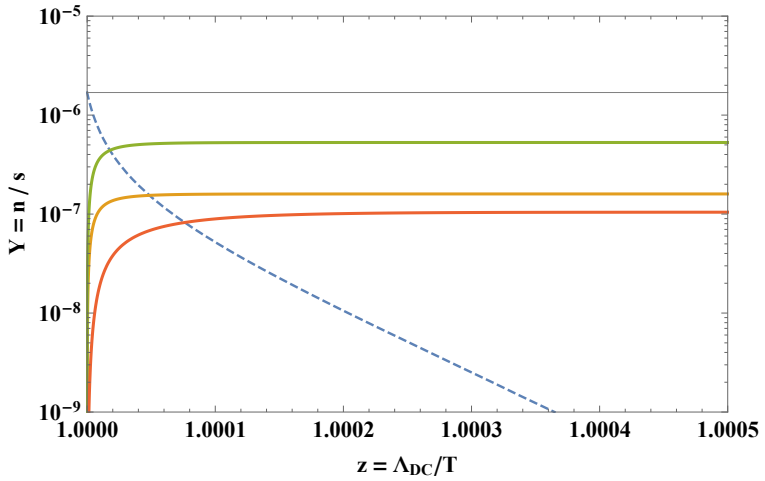

Figure 6.2: Plot showing the comoving abundances Y_i of the various bound states for $M_H = 10^{10}$ GeV after switching on type II and type III recombination reactions (see main text). The solid green, yellow and red lines show the abundances Y of unbreakable $\bar{H}H$, HHL, HHH respectively. The dashed blue contour shows the depleting abundance of type I meson $H\bar{L}$ after the recombination reactions are turned on. The thin gray constant line shows the total H abundance Y_H which will remain conserved throughout the recombination process for H that are sufficiently long-lived.

at the time of DM freeze-out at $T = T^{DM}_{F.O.}$. Note that the type II and type III recombination reactions saturate the higher hybrids soon after confinement at around $z \sim 1$ as can be seen from Fig. 6.2. This depletes the abundance of type I hybrids, thus, all recombination reactions go out of equilibrium by DM freeze-out. Thus, the only relevant reaction for DM abundance at freeze-out is the baryonic annihilation reaction from Eq. 6.55[4]. At $T^{DM}_{F.O.} \sim \Lambda_{\rm DC}/10$, these annihilations go out of equilibrium and this sets the thermal freeze-out abundance of DM.

At the end of recombination, we numerically solve the Boltzmann equations for the abundances of HHL, HHH, $\bar{H}H$ to calculate the fraction of total H abundance in heavy baryons, $f^{\mathcal{B}}_H$. We find this number to be $\sim \mathcal{O}(0.1)$. The details of our numerical set-up and computations can be found in Appendix H.

As we mentioned earlier, the heavy baryons can give a non-thermal contribution to the DM abundance. Depending on the time in which the decay chain

$$HHH \to HHL \to HLL \to LLL \tag{6.66}$$

occurs, we can have the following two possibilities:

1. If the time t_{steps} for the chain reaction above is smaller than t^{DM}_{FO} where t^{DM}_{FO} is the time at which the baryonic DM freezes-out, there will no non-thermal contribution to the DM relic density $\Omega_{\rm DM}$ from GUT partners H. This is because $LLL - LLL$ annihilation are still in equilibrium at $t < t^{DM}_{FO}$ and thus, they wash out any LLL abundance originating from the GUT partner decays.

2. If the decay chain in Eq. 6.66 occurs after DM freeze-out $t_{steps} > t^{DM}_{FO}$, in addition to the thermal abundance of LLL, there will be a non-thermal contribution to Ω_{DM} from GUT partners H. This contribution can overclose the universe, we will discuss this in detail in Sec. 6.3.4.

[4]In the absence of type II and III recombination reactions, type I recombination reactions involving LLL are perilous for DM freeze-out. After DM freeze-out, the almost constant $H\bar{L}$ population starts depleting LLL as LLL can recombine with $H\bar{L}$ to give HLL with a large rate controlled by $\sigma_{\rm rec}$.

Heavy mesons $\bar{H}H$, on the other hand, cannot contribute via their decay to DM abundance. In the benchmark model some of the heavy mesons (such as $\bar{U}\tilde{L}$) can be long-lived due to accidental symmetries. They will eventually decay to light mesons $\bar{L}L$ or else to SM d.o.f.s via GUT scale suppressed dimension-6 operators. Thus, the H abundance that gets *trapped* in heavy mesons $\bar{H}H$ cannot contribute to the DM relic abundance $\Omega_{\rm DM}$.

It was also pointed out in Ref. [173] that a weakly coupled baryon like $\mathcal{B} = HHH$ can have a large annihilation cross-section proceeding via re-arrangement given by:

$$\sigma^{\bar{\mathcal{B}}\mathcal{B}}_{ann} v_{rel} \sim \frac{1}{\sqrt{N_{DC}} C_N \alpha_{DC}} \frac{\pi}{m_H^2} \tag{6.67}$$

which can vastly exceed the annihilation cross-section between the constituents given by $\sim \pi\alpha_{\rm DC}^2/m_H^2$. However, we find that in our dark sector, these annihilations are not efficient at $T \sim \Lambda_{\rm DC}$ in depleting the heavy baryonic population. In order to understand if these annihilation processes are active at T_{DC}, the rate $n_{\mathcal{B}}\langle\sigma^{\bar{\mathcal{B}}\mathcal{B}}_{ann} v_{rel}\rangle$ should be compared to the Hubble rate at T_{DC}, $H(T_{DC})$. For, the annihilation to be active, we want the following condition to be satisfied

$$\frac{n_{\mathcal{B}}\langle\sigma^{\bar{\mathcal{B}}\mathcal{B}}_{ann} v_{rel}\rangle}{H(T_{DC})} > 1 \tag{6.68}$$

Note that only a fraction of total H abundance will form HHH in our dark sector, unlike in Ref. [173]. We can estimate the abundance of heavy baryons at T_{DC} as $n_{\mathcal{B}} \sim f_H^{\mathcal{B}} n_H(T_{DC})$ where $n_H(T_{DC})$. We can now write the H abundance at T_{DC} in terms of the abundance at $T_{F.O.}^{pert}$ using

$$n_H(T_{DC}) = n_H(T_{F.O.}^{pert}) \left(\frac{T_{DC}}{T_{F.O.}^{pert}}\right)^3.$$

Using Eq. 6.50 and Eq. 6.49, we can write the Eq. 6.68 as:

$$\frac{n_{\mathcal{B}}\langle\sigma^{\bar{\mathcal{B}}\mathcal{B}}_{ann} v_{rel}\rangle}{H(T_{DC})} = \frac{f_H^{\mathcal{B}}}{\sqrt{N_{DC}} C_N} \frac{1}{\alpha_{\rm DC}^3} \frac{\Lambda_{\rm DC}}{M_H} \mathcal{O}(10) \tag{6.69}$$

From Eq. 6.69, it is evident that annihilation of baryons is efficient in a very small range of parameter values, given by $\Lambda_{\rm DC}/M_H \sim \mathcal{O}(1)$ (See also Ref. [173]) In our model, since $f_H^{\mathcal{B}} \sim 0.1$, the ratio in Eq. 6.69 is always smaller than 1. Note that in our dark sector, M_H additionally cannot be too low or $\sim \Lambda_{\rm DC} \sim 10^5$ GeV due to constraints from BBN on the long lifetime of these states.

In the next section, we will discuss how long-lived H states can set an early matter-dominated era.

6.3.3 Dilution

The long-lived GUT partners H once frozen out can give rise to an early Matter-Dominated era (MD). They can inject entropy via their decay which can change the DM density with respect to the usual radiation dominated era (RD) by a suppression or dilution factor.

We should contrast this with the heavy dark quark regime discussed in Ref. [173]. In Ref. [173], the heavy dark quarks form the baryonic DM, hence they cannot decay. Moreover, the glueballs in their dark sector dilute the abundance of the heavy dark quarks, such that the matter-dominated era where the dark quark energy density is large, never occurs.

In our dark sector, the suppression factor due to entropy injection from H decay can be approximated for very long-lived H as (for detailed derivation see appendix G) [83, 175]:

$$\mathcal{F} = \frac{4.8}{g_*^{1/4}} \frac{\sqrt{\Gamma_M M_{Pl}}}{T_{MD}} \tag{6.70}$$

where $\Gamma_M = 2/3\ \Gamma_H$ accounts for the fraction of H going to only SM d.o.f.s[5]. T_{MD} is the temperature at which non-relativistic matter energy density in the form of H given by ρ_M becomes equal to the energy density of the SM radiation, ρ_R giving

$$\rho_M(T_{MD}) = \rho_R(T_{MD}).$$

We can use Eq. 6.50 to write ρ_M at T_{MD} as:

$$\rho_M(T_{MD}) = M_H\ n_H(T_{F.O.}^{pert}) \left(\frac{T_{MD}}{T_{F.O.}^{pert}}\right)^3 \tag{6.71}$$

Moreover, since radiation is thermal at temperature T we can write:

$$\rho_R = \frac{\pi^2}{30} g_*(T) T^4 \tag{6.72}$$

where $g_*(T)$ are the relativistic d.o.f. at temperature T. Using Eq 6.71 and Eq. 6.72 and Eq. 6.50 gives us the temperature T_{MD}:

$$T_{MD} = \frac{4\sqrt{5}\ x_{F.O}^{pert}}{g_*^{1/2} \pi^{3/2} \alpha_{DC}^2(M_H)} \frac{M_H^2}{M_{Pl}} \tag{6.73}$$

As the MD era evolves, it eventually enters the non-adiabatic phase in which the radiation energy density ρ_R is dominated by radiation coming from H decays [201]. During this phase, the usual scale factor scaling with temperature $a \propto T^{-1}$ is modified to $a \propto T^{-8/3}$. (We review this and the relevant derivations in Appendix G). The temperature at which this non-standard scaling begins T_i is given by:

$$T_i = T_{MD} \left(\frac{\Gamma_M M_{Pl}}{4.15 (g_*(T_{MD}))^{1/2} T_{MD}^2 + \Gamma_M M_{Pl}}\right)^{2/5} \tag{6.74}$$

The MD era eventually ends at $T \sim T_D$ when the H decays after which the usual radiation dominated (RD) era re-begins. The temperature T_D can be written as:

$$T_D = \sqrt{\frac{\Gamma_M M_{Pl}}{g_*(T_D)^{1/2} 1.67}} \tag{6.75}$$

We can see the various relevant temperatures during MD era plotted as a function of M_H in Fig. 6.3. For the parameter space in M_H, the following hierarchy of the relevant temperatures for MD holds:

$$T_{MD} \gg T_i > T_D \tag{6.76}$$

[5]Following $H \to L + SM + SM$, we can assume that the energy, (or mass of the decaying particle in its rest frame) is evenly distributed to the fermions coupled to the decaying vertex (four-fermion operator), while the spectator quarks (in the baryon) carry a negligible fraction of it. If that is true, then the fraction of H energy going into SM particles is 2/3.

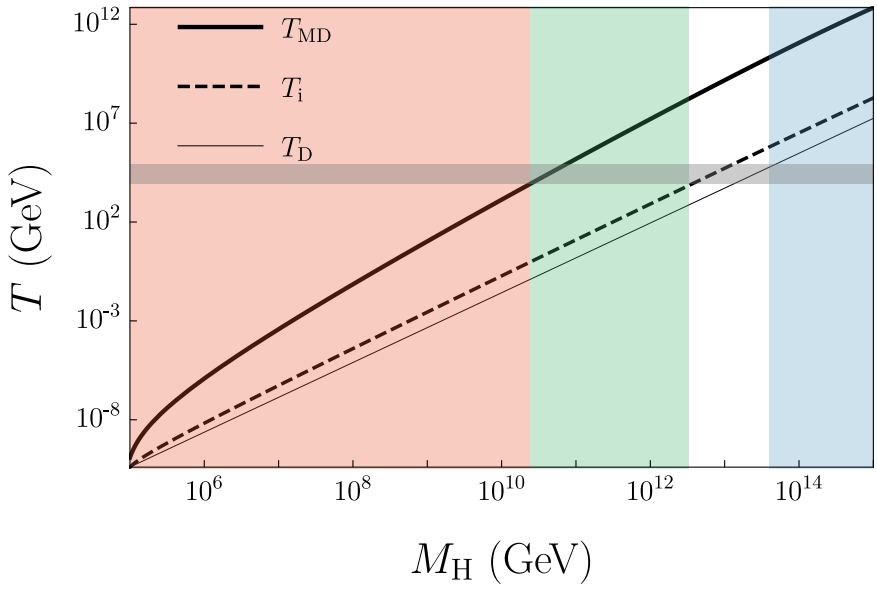

Figure 6.3: Hierarchy of temperatures relevant for the MD era - T_{MD}, temperature at which matter density ρ_M becomes equal to radiation density ρ_R, T_i, temperature at which ρ_R is dominated by the radiation from H decays, T_D, temperature at which all H decays and RD recommences. The various scenarios discussed in the text depend on the M_H value. The gray horizontal band (upper limit) is where confinement occurs at $T = \Lambda_{\rm DC}$ and the lower edge is where DM freeze-out occurs at $T \sim \Lambda_{\rm DC}/10$. In this plot, we are fixing $\Lambda_{\rm DC} = 80$ TeV. The blue band (1) depicts $T_D > T_{DC}$ scenario, the red band scenario (2) where $T_{MD} < T_{FO}^{DM}$ while the green band depicts scenario (3) with $T_i < T_{FO}^{DM}$, the white band depicts (4) where our computation has been extrapolated.

Note that we find for very small values of $M_H \sim 10^5$ GeV, $T_D \gtrsim T_i$. This implies that there will be no extra suppression for these values of M_H.

Depending on these temperatures and their hierarchy with respect to $T \sim \Lambda_{\rm DC}$, we can have various possibilities as illustrated in Fig. 6.3:

1. $T_D > T_{DC}$: (blue region) For $M_H \gtrsim 4\times10^{13}$ GeV (with $\Lambda_{\rm DC}$ fixed to ~ 80 TeV) (see Fig. 6.3), the early MD era has no effect on dark confinement and DM freeze-out. The H quarks decay before dark confinement after which the conventional RD era begins and confinement and freeze-out follow the standard RD evolution described in Sec 6.3.2.

2. For $T_{MD} < T_{FO}^{DM}$: (red region) For $M_H \lesssim 10^{10}$ GeV (see Fig. 6.3), the MD era begins only after DM freeze-out. Entropy injection at $T < T_{FO}^{DM}$ due to the H decay results in a non-standard scaling of the scale factor as $a \propto T^{-8/3}$. This modifies the relation between the number density of DM particles today and the number density of DM particles at freeze-out as:

$$n_{DM}(T_0) = n_{DM}(T_{FO})\left(\frac{T_0}{T_{FO}}\right)^3 \mathcal{F} \tag{6.77}$$

   where $\mathcal{F}$ is given by Eq. 6.67. Note that for our main results in Sec. 6.3.4, we use the full expression for $\mathcal{F}$ given in Appendix G.

3. $T_i < T_{FO}^{DM}$: (green region) For 2×10^{10} GeV $< M_H \lesssim 3\times10^{12}$ GeV (see Fig. 6.3), despite being in the MD era, the comoving entropy $S = sa^3 \propto a^3\rho_R^{3/4}$ is still conserved during recombination and DM freeze-out. At $T > T_i$, when the radiation energy density ρ_R is still dominated by the red-shifted initial radiation (See Eq. G.6), scale factor follows the standard RD scaling for the scale factor given by $a \propto T^{-1}$. This means that $s \propto a^{-3}$ implying a constant comoving

number density given by $Y = n/s$ for this range of M_H. Note, however, that during this adiabatic phase of MD, the Hubble parameter will also include ρ_M and can be written for $T_i < T < T_{MD}$ as (See also [201]):

$$H(T) = \left(\frac{8\pi^3 g_*(T_{MD})}{90}\right)^{1/2} \frac{\sqrt{(T^4 + T_{MD}T^3)}}{M_{Pl}} \tag{6.78}$$

For this range of M_H values, we solve the Boltzmann equations for the recombination era and DM with this modified $H(T)$ (See Appendix G for our solutions). We find that our numerical solution for $f_H^{\mathcal{B}}$ and T_{FO}^{DM} in this MD era does not change significantly with respect to the RD era.

4. $T_{F.O.}^{DM} < T_i$: (white region) For 3×10^{12} GeV GeV $< M_H < 4 \times 10^{13}$ GeV (see Fig. 6.3), comoving entropy sa^3 is not constant anymore during DM freeze-out and recombination since the scale factor scales in a non-standard way given by $a \propto T^{-8/3}$ now. Since $s \not\propto a^{-3}$, $Y = n/s$ is not a good quantity, hence all the Boltzmann equations for recombination and DM should be written in terms of na^3. Since this occurs only for a small window of M_H values, we will simply extrapolate our results from other scenarios for this M_H range. (For more details and a more precise computation on solving equations for such a non-iso-entropic universe, see [201])

6.3.4 Dark Matter Relic Density

The DM density is determined by the various cosmological processes described in the previous sections and depends on the two parameters of our dark theory: the dark confinement scale $\Lambda_{\rm DC}$, and the mass of the GUT partners M_H. The DM density can be written in a condensed form for all scenarios as:

$$\Omega_{\rm DM} = \frac{M_{\rm DM} T_0^3}{\rho_{crit}} \left(Y_{LLL}^{F.O.} + f_H^{\mathcal{B}} Y_H(T_{DC}) e^{-t_{F.O.}\Gamma_H}\right) \mathcal{F} \tag{6.79}$$

where $M_{\rm DM} = m_{LLL} \sim N_{\rm DC}\Lambda_{\rm DC}$, T_0 is the present temperature, ρ_{crit} is the critical energy density $= 3H_0^2/8\pi G$. We defined $Y_H(T_{DC})$ in Eq. 6.51. The DM abundance at freeze-out is given by $Y_{LLL}^{F.O.}$, and is computed numerically. Since at the time of DM freeze-out $\sim \Lambda_{\rm DC}/\mathcal{O}(10)$, the only process active are baryonic annihilations, the Boltzmann equation for DM reduces to:

$$\frac{dY_{LLL}}{dz} = -\frac{\langle\sigma_{ann} v\rangle s}{Hz}\left(Y_{LLL}^2 - (Y_{LLL}^{eq})^2\right) \tag{6.80}$$

with $\langle\sigma_{ann} v\rangle = c\ 4\pi/\Lambda_{\rm DC}^2$ where we vary c for our numerical solution. We compute the fraction of H abundance in H baryons $f_H^{\mathcal{B}}$ numerically for all scenarios (See appendix H). In Eq. 6.79, $e^{-t_{F.O.}\Gamma_H}$ accounts for the heavy baryons decaying after the time at which freeze-out occurs or $t_{F.O.}$. Depending on whether freeze-out occurs during the RD era or the MD era, $t_{F.O.}$ can be written in terms of $T_{F.O.}^{DM}$ as:

$$t_{F.O.} = \begin{cases} \frac{0.3\ M_{Pl}}{g_*^{1/2}(T_{F.O.}^{DM})^2} & T_{MD} < T_{F.O.}^{DM} \\ \frac{0.6}{g_*(T_{MD})^{1/2}} \frac{M_{Pl}}{T_{MD}^{1/2}(T_{F.O.}^{DM})^{3/2}} & T_{MD} > T_{F.O.}^{DM} > T_i \end{cases} \tag{6.81}$$

The dilution factor, $\mathcal{F}$ (See also Eq. 6.70) can be written in terms of the scale-factor a as:

$$\mathcal{F} = \begin{cases} 1 & T_D > T_{DC} \\ \left(\frac{a(T_i)}{a(T_D)}\frac{T_i}{T_D}\right)^3 = \left(\frac{T_D}{T_i}\right)^5 & T_i < T_{F.O.}^{DM} \end{cases} \tag{6.82}$$

where in writing $\mathcal{F}$ we have considered the non-standard scaling of scale factor $a \propto T^{-8/3}$ between the temperature intervals T_i and T_D, which arises due to the non-adiabatic matter dominated era set by H.

We show the estimate of the DM abundance in the parameter space $(M_{\rm H}, \Lambda_{\rm DC})$ in Fig. 6.4 along with other cosmological and unification constraints in our theory. The black contour shows the isocurve for $\Omega_{DM}h^2 = 0.12$ [17] which reproduces the observed DM relic density. The thermal abundance for the light baryons is set by a non-perturbative annihilation cross section $\sigma_{\rm ann} = 4\pi c/\Lambda_{\rm DC}^2$ where c is an order 1 coefficient. We capture this uncertainty in the parameter c by varying it between $0.2 \leq c \leq 1$ in the vertical gray band shown in Fig. 6.4 for large values of M_H.

We will now describe the different scenarios and the relic density estimate for each of them:

1. For $T_D > T_{DC}$, which corresponds to roughly $M_H \gtrsim 10^{13}$ GeV (see Fig. 6.4), the GUT partners H are short-lived enough that they decay before dark confinement. Thus, at $T = T_{DC}$, only light hadrons LLL, $\bar{L}L$ form. Moreover, the MD era ends with the H decay at T_D thus, confinement and DM freeze-out occur in the standard RD era. In this scenario, the observed DM relic density is reproduced for $\Lambda_{\rm DC} \simeq 80$ TeV for $\sigma_{ann} = 4\pi/\Lambda_{\rm DC}^2$ reproducing the DM density in the light quark regime for baryonic DM models given in [172]. It is also clear from Eq. 6.79 that for large M_H (hence large width Γ_H), the contribution from the second term tends to 0. This behavior is well-captured in Fig. 6.4 by the right black contour line for $\Omega_{\rm DM}$ for large M_H values. The contour is almost vertical due to the exponential dependence of $\Omega_{\rm DM}$ with M_H.

2. For $T_i < T_{MD} \lesssim T_{F.O.}^{DM}$, heavy baryons containing H are long-lived enough such that they can give a non-thermal contribution to the relic density by decaying to light baryons LLL after LLL freeze-out. We find that this non-thermal (NT) contribution or $\Omega_{\rm NT}$ (coming from the second term in Eq. 6.79) can overclose the universe resulting in $\Omega_{\rm DM}h^2 \gg 0.12$. Here $\Omega_{\rm NT}$ is given by

$$\Omega_{\rm NT} = \frac{M_{\rm DM}T_0^3}{\rho_{crit}}\left(f_H^{\mathcal{B}} Y_H(T_{DC}) e^{-t_{F.O.}\Gamma_H}\right).$$

   However, note that for these values of M_H and $\Lambda_{\rm DC}$, the DM abundance gets a suppression from the dilution factor $\mathcal{F}$ described in Eq. 6.82, on account of the non-standard scaling of $a \propto T^{-8/3}$ during the MD era. The inclusion of this dilution factor can suppress $\Omega_{\rm NT}$ to reproduce the observed DM relic abundance as can be seen from Fig. 6.4 for values of $M_H < 10^{10}$ GeV. Note that in this case since the MD era begins after freeze-out at T_{MD}, all the processes involving recombination and DM freeze-out occur in the RD era following the standard $a \propto T^{-1}$ scaling.

   Note that a large part of the parameter space in Fig. 6.4 for $M_H \lesssim 10^{10}$ GeV (see Fig. 6.4) is constrained heavily from BBN and unification constraints (We discuss these in detail later in this section).

3. For $T_i < T_{F.O.}^{DM} < T_{MD}$, corresponding to values of roughly 10^{10} GeV $\lesssim M_H \lesssim 10^{12}$ GeV (see Fig. 6.4), the DM freeze-out and recombination processes occurring at $T \sim T_{DC}$ are

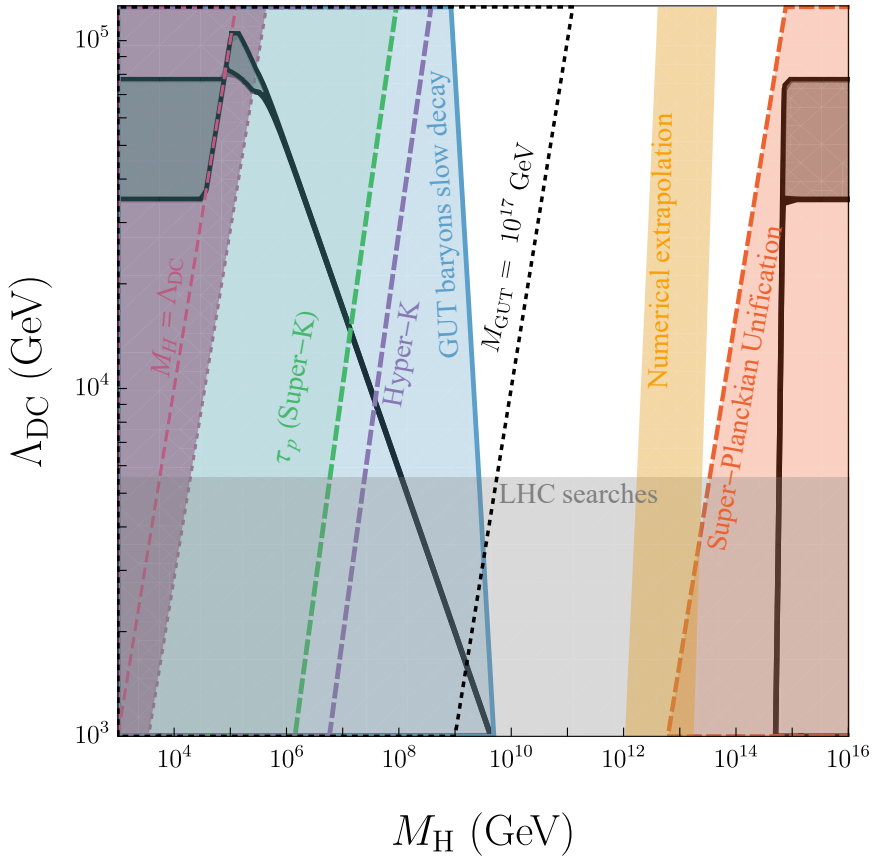

Figure 6.4: The black solid contour line shows the parameters $\Lambda_{\rm DC}$ and $M_{\rm H}$ which produce the correct observed DM abundance $\Omega_{\rm DM}h^2 = 0.12$ with the vertical gray band showing the uncertainty in the non-perturbative baryonic annihilation cross-section as described in the main text. The excluded regions from unification requirements are shown in orange for unification occurring above the Planck Scale, while in green we show the proton lifetime bound from Super-Kamiokande. We also show the projection for the proton lifetime from Hyper-Kamiokande. Finally, the blue region shows the parameter space excluded due to stable or long-lived H hadrons which spoils BBN. The light gray exclusion for $\Lambda_{\rm DC} \lesssim 5$ TeV is indicative, and has been derived using the exclusion from collider searches for dark mesons $m_{\pi_D} \lesssim 500$ GeV (see Ref. [188] for more details). The shaded pink region shows the region in which our DM abundance calculations cannot be considered valid since α_{DC} is no longer perturbative. Finally, the vertical yellow band on the right shows the parameter values where we used extrapolation for the dilution scenario occurring during recombination (See point 4 above in this section and in Sec. 6.3.3 in the main text).

unaffected by the non-standard scaling beginning much later at T_i. However, since the MD era begins earlier than confinement, the recombination equations of section H must be solved with the Hubble parameter H for the MD era given in Eq. 6.78. We find that the result for recombination even in this case is similar to the conclusions applicable for the RD era. The DM relic density estimate and suppression factor conclusion are similar to the scenario in point (2) where the GUT state contribution overcloses the universe. In Fig. 6.4, this scenario corresponds to the values of M_H that are unconstrained from BBN and correspond to "good" unification at $M_{\rm GUT} \sim 10^{17}$ GeV.

4. For $T_{FO}^{DM} < T_i < T_{MD}$, our DM relic density computation cannot be trusted (See also discussion in Sec. 6.3.3 point 4). It is evident from Fig. 6.4 that this case only describes a small window of parameters in the space $(M_H, \Lambda_{\rm DC})$, for 10^{12} GeV $\lesssim M_H \lesssim 10^{13}$ GeV (shown in the vertical yellow band in Fig. 6.4). To get the relic density in this small region, we have simply extrapolated the results from other scenarios and computed the DM abundance using the dilution factor.

Further, some comments about the black contour for $\Omega_{\rm DM}$ for small M_H values are in order. For GUT partners with mass values $M_H \sim \Lambda_{DC}$, the dark coupling constant α_{DC} is not perturbative anymore (pink region in Fig. 6.4), thus, implying that the GUT partners cannot undergo a perturbative freeze-out. The DM abundance computation for this part of the parameter space cannot be trusted. If the GUT partners are as light as the dark fermions with mass $M_H \lesssim \Lambda_{\rm DC}$, the GUT partner contribution to the thermal DM abundance $\Omega_{\rm DM}$ is set to 0. In this $M_H < \Lambda_{\rm DC}$ scenario, all the dark baryons are light. In addition to the baryonic DM candidate given by $QQ\tilde{D}$, the lightest component of the baryons UUU and $\tilde{L}\tilde{L}\tilde{L}$ will be as long-lived as DM due to their accidental symmetries. This will imply three Boltzmann equations for the three baryonic species given by Eq. 6.80. Each of these baryons will annihilate by rearranging among themselves into their respective mesons. These additional baryonic annihilations do not disturb the DM annihilation. The mesons from GUT partners are in chemical equilibrium due to their large scattering cross-section at any temperature T given by $\sigma \sim (1/8\pi)(T^2/f^4)$. These mesons will decouple around the same time as the DM freeze-out temperature and eventually decay to the light d.o.f.s.

Note that despite this, this part of the parameter space for the model is not viable due to severe constraints on the lifetime of SM-charged states coming from Big Bang Nucleosynthesis (BBN). Any H hadron with very long lifetimes $\tau_H \gtrsim 1$ sec would spoil BBN and this excludes low values of M_H in Fig. 6.4 (exclusion shown in blue).

The constraints from our unification requirement exclude (in orange in Fig. 6.4) large $M_{\rm H}$ values for which the $M_{\rm GUT} > M_P$ where M_P is the reduced Planck Scale. The strongest prediction of minimal $SU(5)$ unification in the SM is proton decay $p \to \pi^0 e^+$ via the effective dimension-6 operator below the GUT scale given by:

$$\frac{g_{\rm GUT}^2}{M_X^2} uude \tag{6.83}$$

with M_X being the mass of the GUT bosons X, Y which we set to be equal to the GUT scale $M_{\rm GUT}$. Super-Kamiokande has set an upper bound on the proton lifetime τ_p given by [177]:

$$\tau_p > 1.6 \times 10^{34} \text{ years} \tag{6.84}$$

This translates to an exclusion on the scale of unification in our parameter space which we show in green. In addition, we also show the expected sensitivity (in purple dashed) of Hyper-

Kamiokande [206] which will improve the bound as $\tau_p > 1.3 \times 10^{35}$ years.

The lowest-lying states in the spectrum of our dark theory are dark NGBs that can decay to SM gauge bosons after being produced at high energy colliders. Collider searches thus, can be used to exclude dark meson masses of $m_{\tilde{\pi}} \lesssim 500$ GeV (shown in light gray in Fig. 6.4) [188].

6.4 Summary

In this chapter, we have studied the model-building aspects and cosmology for the benchmark IR (UV) model $Q + \tilde{D}$ $(5 + 10)$. We find that dark quarks cannot come in almost degenerate GUT multiplets since the GUT partners enhance the accidental symmetries in the IR dark sector in addition to dark baryon number $U(1)_{\rm DB}$. These new accidental symmetries are broken at the dimension-6 level via tree exchange of GUT bosons, implying metastable bound states made of GUT partners (See Sec. 6.1 for details). Due to SM charges of the bound states made of GUT fragments, they should decay before BBN $\tau < 1$ s. Moreover, we find that depending on their mass M_H value (which is set by unification), they can heavily influence the thermal history by initiating a matter dominated era as well as an epoch of recombination as we summarise below.

The thermal freeze-out of light baryonic DM is set by $\Lambda_{\rm DC} \sim 80$ TeV to reproduce the observed DM density. We find that in the presence of GUT partner states with mass M_H, we overproduce DM for a large part of the parameter space $(M_H, \Lambda_{\rm DC})$ (See Fig. 6.3.4) as the GUT bound states can decay to DM and contribute to the DM abundance. These values of M_H also correspond to a unification scale of $\sim 10^{17}$ GeV (See Sec. 6.3.4). Larger values of M_H result in short-lived GUT partners which decay too quickly to have any impact on the DM abundance, implying only the usual freeze-out contribution from light baryons. These values of M_H, however, are largely excluded in the theory since the $M_{\rm GUT}$ scale in the model is above the Planck Scale for these M_H values.

Note that this conclusion in Sec. 6.3.4 implicitly assumes that the perturbative freeze-out of the GUT partners (as described in Sec. 6.3.1) occurs in the standard radiation-dominated Universe. If the mass of the heavy GUT partners is large enough, however, freeze-out can occur during the reheating phase that precedes the onset of the radiation dominated era. The idea of the production of massive particles during reheating was first considered in Refs. [207–210]. During reheating the energy density of the Universe is dominated by the coherent oscillations of a scalar field ϕ around the minimum of its potential. At the same time, the scalar ϕ decays into relativistic particles (either SM or dark sector), thus injecting entropy in the Universe. During this period, the temperature T of the plasma does not follow the standard scaling $T \propto a^{-1}$ as in the RD era, but first reaches a maximum temperature given by $T_{MAX} \approx (H_I M_P)^{\frac{1}{4}} T_{RH}^{\frac{1}{2}}$ and then decreases as $T \propto a^{-3/8}$ with the scale factor a due to entropy injection from the decay of the scalar ϕ. Here, H_I is the Hubble scale at inflation, $T_{\rm RH}$ is the temperature at which RD era begins or the reheating phase ends. Such a non-adiabatic MD era led to the dilution of the DM density in our model as described in Sec. 6.3.3. Similarly, if the GUT partners freeze-out during the reheating phase, their final abundance can be suppressed by a similar dilution factor as in Eq. (6.82). This mechanism can be used to make the parameter space $(M_H, \Lambda_{\rm DC})$ viable for both good unification as well as the correct DM abundance in our dark sector model.

In this chapter, we have also studied the spectrum of NGBs in detail in Sec. 6.2. Our dark sector predicts SM-colored NGBs which can decay to SM gauge bosons due to anomalous couplings. In addition, our dark sector also predicts an $SU(2)$ doublet dark meson, which can mix with the SM Higgs with a large mixing angle. We have discussed the production modes and decay of these NGBs in detail in Sec. 6.2. Our parameter space for low $\Lambda_{\rm DC}$ can be constrained by future collider

searches for dark mesons. The mass of the DM in the theory is of the order of 80 TeV which makes it difficult to test produce DM at present or future colliders.

The low energy dynamics involved below the confinement scale and the spectrum of various bound states are non-perturbative in nature. To study the abundances below the confinement scale we have used an extensive system of Boltzmann equations to track the various abundances of all the bound states and compute the values of parameters for computing the observed DM density (See Appendix H). These results heavily rely on lattice QCD studies. More precise lattice results on the spectra of heavy-light states would give more precision to our analysis. A precise non-perturbative computation of the baryonic annihilation cross-section could also lead to an improvement in the limit on the confinement scale $\Lambda_{\rm DC}$.

An alternative probe for such a dark GUT-theory could come from the "Cosmological Collider" program [211, 212]. Since the Hubble Scale during inflation can be as high as $H_I \sim 10^{13}$ GeV during the inflationary era, the GUT partners with masses $M_H \lesssim H_I$ with a possible coupling to the inflaton could leave on-shell signatures via primordial Non-Gassianities (NG). This has been studied for the case of an orbifold GUT theory in Ref. [213] (See also Ref. [214] for a study of NP particles leaving NGs). We leave this for a future direction.

Chapter 7

Conclusions and Outlook

In this thesis, we have asked the broad question:
How can we account for dark sectors and dark matter using what we have learned so far from QCD?

In order to address this question, we have followed *two complementary strategies.*

Part I of this thesis, based on Ref. [26], focuses on the scenario where a putative dark sector interacts with the Standard Model via irrelevant portals. In particular, we have considered the sensitivity of DS that interacts with SM through a dimension 6 irrelevant portal, at past and current neutrino experiments, and its prospective discovery in both existing and future neutrino experiments based on proton beams. This dark sector is neutral under the Standard Model and is characterized, under a simplifying assumption, by only two energy scales: $\Lambda_{\rm UV}$, which is the mass of the mediator exchanged between the dark sector and SM, and $\Lambda_{\rm IR}$, the mass of the lightest state in the DS. At energies far away from these two scales, i.e. $\Lambda_{\rm IR} \ll E \ll \Lambda_{\rm UV}$, the dark sector is approximately scale invariant. This scale invariance can be exploited to construct a framework we call "*model agnostic*". The framework and the assumptions have been discussed in detail in Chapter 2 and Section 2.3.

In chapter 3, we have performed a detailed study of the possible production mechanisms of DS through non-renormalizable portals: meson decays ($M \to m + DS$, $V \to$ DS), direct partonic production ($\bar{q}q \to$ DS, $gg \to$ DS), and dark bremsstrahlung ($pp \to {\rm DS} + X$). The interplay between the various production mechanisms as a function of the DS invariant mass squared $p^2_{\rm DS}$ can be summarized in the plot shown in fig. 3.1. Compared to previous works on irrelevant portals, we have added production details and also considered strongly coupled dark sectors, and done so in a model agnostic framework (See Ref. [215] for a recent model independent framework). For the case of Z portal DS production, we find that past analyses and prospective DS searches at current neutrino experiments give weaker bounds when compared with the current bounds from LHC and LEP in resonant production scenarios. However, future neutrino experiments such as DUNE-MPD would improve on this, and will be sensitive to $\Lambda_{\rm IR}$ in the range $0.1 - 1$ GeV for $\Lambda_{\rm UV} \sim 1$ TeV. Our main result plots can be seen in Fig, 3.8.

Part II of this thesis based on [27, 28] instead focuses on a new physics scenario where the SM gauge group and matter are both extended under the vectorlike confinement framework. New dark fermions lighter than the dark confinement scale come along with their GUT partners in a dark sector with an $SU(5)$-GUT-UV completion. In such theories, the dark matter candidate is the light baryon stable under the dark baryon number. Imposing gauge coupling unification strongly

constrains the number of these models giving a composite dark matter. In this work, with respect to Ref. [172], we have used a less conservative requirement for gauge coupling unification and required that the viable dark model only mitigates the coupling unification achieved in the SM. We have given details of this unification criteria in Sec. 5.2. With respect to Ref. [172], we have included a much more detailed classification of viable models based on an analysis of higher dimension operators generated by GUT partners. From our analysis on unification, we find only two viable models: a trivial scenario with Majorana SM singlet N, and our benchmark model with SM-colored dark fermions $Q + \tilde{D}$. These two are the viable models for the case in which all the GUT partners are at the same mass scale M_H. In addition to these two models, we also find two that the models: $SU(3)_{DC}$ $L \oplus E$ and the $SO(3)_{DC}$ V can give good unification for non-degenerate GUT partners masses M_{H_1} and M_{H_2}. This, however, implies, introducing more tunings to get the split spectrum.

Our dark sector predicts SM-colored NGBs which can decay to SM gauge bosons due to anomalous couplings. The mass spectrum of these mesons has been described in detail in Sec. 6.2.

The cosmology of light baryonic dark matter is heavily influenced by the presence of GUT partners whose abundance can change cosmological evolution. The details on the cosmology of such dark GUT theories can be found in Chapter 6 and the main plot can be found in Fig. 6.4. We find that in the presence of GUT partner states with mass M_H, we overproduce DM for a large part of the parameter space $(M_H, \Lambda_{\rm DC})$ in Fig. 6.3.4. These values of M_H also correspond to a unification scale of $\sim 10^{17}$ GeV. In order to make a larger part of the parameter space viable, the relic abundance of GUT partners must be suppressed with a lower reheating temperature.

In Part II of the thesis, we have chosen to not address the problems that plague four-dimensional (4D) minimal $SU(5)$ unification in SM: namely proton decay, and the doublet-triplet splitting problem between the Higgs and its colored partner H_3 (See Ref. [216] for a review and some possible solutions). The extra-dimensional framework of orbifold-GUTs (See [217–219]) can offer solutions to these. A possible future direction of our work in part II of the thesis would then be to consider an extra-dimensional $SU(5)$ embedding of the dark sector. We leave this possibility for future work.

Another possibility for extension of part II of this thesis is to study the regime in which the dark fermions are heavier than the confinement scale. This would serve as an extension of the analysis already done in Ref. [173].

An interesting direction for part II of this thesis could be in the "Cosmological Collider" program [211]. The GUT partners with masses $M_H \lesssim H_I$ can couple to the inflaton and leave a signature via primordial Non-Gassianities (NG) (See Ref. [213] for example).

Bibliography

[1] C. Csáki, S. Lombardo and O. Telem, *TASI Lectures on Non-supersymmetric BSM Models*. 1811.04279.

[2] R. Sundrum, *Unfolding Particle Physics Hierarchies with Supersymmetry and Extra Dimensions*, in *Theoretical Advanced Study Institute in Elementary Particle Physics : Aspects of Symmetry*, 6, 2023, 2306.07173.

[3] ATLAS collaboration, M. Aaboud et al., *Search for top-squark pair production in final states with one lepton, jets, and missing transverse momentum using 36 fb^1 of $\sqrt{s} = 13$ TeV pp collision data with the ATLAS detector*, *JHEP* **06** (2018) 108 [1711.11520].

[4] Z. Chacko, H.-S. Goh and R. Harnik, *The Twin Higgs: Natural electroweak breaking from mirror symmetry*, *Phys. Rev. Lett.* **96** (2006) 231802 [hep-ph/0506256].

[5] N. Craig, A. Katz, M. Strassler and R. Sundrum, *Naturalness in the Dark at the LHC*, *JHEP* **07** (2015) 105 [1501.05310].

[6] C. Antel et al., *Feebly Interacting Particles: FIPs 2022 workshop report*, in *Workshop on Feebly-Interacting Particles*, 5, 2023, 2305.01715.

[7] J. Cooley et al., *Report of the Topical Group on Particle Dark Matter for Snowmass 2021*, 2209.07426.

[8] M. Milgrom, *A modification of the Newtonian dynamics as a possible alternative to the hidden mass hypothesis.*, **270** (1983) 365.

[9] J. Zuntz, T. G. Zlosnik, F. Bourliot, P. G. Ferreira and G. D. Starkman, *Vector field models of modified gravity and the dark sector*, *Phys. Rev. D* **81** (2010) 104015 [1002.0849].

[10] C. Skordis, D. F. Mota, P. G. Ferreira and C. Boehm, *Large Scale Structure in Bekenstein's theory of relativistic Modified Newtonian Dynamics*, *Phys. Rev. Lett.* **96** (2006) 011301 [astro-ph/0505519].

[11] M. Lisanti, M. Moschella, N. J. Outmezguine and O. Slone, *Testing Dark Matter and Modifications to Gravity using Local Milky Way Observables*, *Phys. Rev. D* **100** (2019) 083009 [1812.08169].

[12] V. C. Rubin, N. Thonnard and W. K. Ford, Jr., *Rotational properties of 21 SC galaxies with a large range of luminosities and radii, from NGC 4605 /R = 4kpc/ to UGC 2885 /R = 122 kpc/*, *Astrophys. J.* **238** (1980) 471.

[13] V. C. Rubin and W. K. Ford, Jr., *Rotation of the Andromeda Nebula from a Spectroscopic Survey of Emission Regions*, *Astrophys. J.* **159** (1970) 379.

[14] A. Bosma, *21-cm line studies of spiral galaxies. 2. The distribution and kinematics of neutral hydrogen in spiral galaxies of various morphological types.*, *Astron. J.* **86** (1981) 1825.

[15] D. Clowe, M. Bradac, A. H. Gonzalez, M. Markevitch, S. W. Randall, C. Jones et al., *A direct empirical proof of the existence of dark matter*, *Astrophys. J. Lett.* **648** (2006) L109 [astro-ph/0608407].

[16] P. Natarajan et al., *Mapping substructure in the HST Frontier Fields cluster lenses and in cosmological simulations*, *Mon. Not. Roy. Astron. Soc.* **468** (2017) 1962 [1702.04348].

[17] Planck collaboration, N. Aghanim et al., *Planck 2018 results. VI. Cosmological parameters*, *Astron. Astrophys.* **641** (2020) A6 [1807.06209].

[18] T. R. Slatyer and C.-L. Wu, *General Constraints on Dark Matter Decay from the Cosmic Microwave Background*, *Phys. Rev. D* **95** (2017) 023010 [1610.06933].

[19] K. K. Boddy et al., *Snowmass2021 theory frontier white paper: Astrophysical and cosmological probes of dark matter*, *JHEAp* **35** (2022) 112 [2203.06380].

[20] IceCube collaboration, M. G. Aartsen et al., *Search for neutrinos from decaying dark matter with IceCube*, *Eur. Phys. J. C* **78** (2018) 831 [1804.03848].

[21] D. Carney et al., *Snowmass2021 Cosmic Frontier White Paper: Ultraheavy particle dark matter*, 2203.06508.

[22] T. Cohen, K. Murase, N. L. Rodd, B. R. Safdi and Y. Soreq, *γ -ray Constraints on Decaying Dark Matter and Implications for IceCube*, *Phys. Rev. Lett.* **119** (2017) 021102 [1612.05638].

[23] A. Keshavarzi, D. Nomura and T. Teubner, *Muon $g-2$ and $\alpha(M_Z^2)$: A new data-based analysis*, *Phys. Rev. D* **97** (2018) 114025.

[24] H. Georgi, *Unparticle physics*, *Phys. Rev. Lett.* **98** (2007) 221601 [hep-ph/0703260].

[25] R. Contino, K. Max and R. K. Mishra, *Searching for elusive dark sectors with terrestrial and celestial observations*, *JHEP* **06** (2021) 127 [2012.08537].

[26] M. Costa, R. K. Mishra and S. Verma, *Model Agnostic Probes of Dark Sectors at Neutrino Experiments*, 2211.13253.

[27] S. Verma, S. Bottaro and R. Contino, *Accidental composite dark matter in SU(5)-GUT theories*, *To Appear* .

[28] S. Verma, S. Bottaro and R. Contino, *Accidental composite dark matter in SU(5)-GUT theories*, *PoS* **ICHEP2022** (2022) 306.

[29] J. Alexander et al., *Dark Sectors 2016 Workshop: Community Report*, 8, 2016, 1608.08632.

[30] J. Beacham et al., *Physics Beyond Colliders at CERN: Beyond the Standard Model Working Group Report*, *J. Phys. G* **47** (2020) 010501 [1901.09966].

[31] M. J. Strassler and K. M. Zurek, *Echoes of a hidden valley at hadron colliders*, *Phys. Lett. B* **651** (2007) 374 [hep-ph/0604261].

[32] B. Holdom, *Two U(1)'s and Epsilon Charge Shifts*, *Phys. Lett. B* **166** (1986) 196.

[33] P. Galison and A. Manohar, *TWO Z's OR NOT TWO Z's?*, *Phys. Lett. B* **136** (1984) 279.

[34] C. P. Burgess, M. Pospelov and T. ter Veldhuis, *The Minimal model of nonbaryonic dark matter: A Singlet scalar*, *Nucl. Phys. B* **619** (2001) 709 [hep-ph/0011335].

[35] B. Döbrich, J. Jaeckel, F. Kahlhoefer, A. Ringwald and K. Schmidt-Hoberg, *ALPtraum: ALP production in proton beam dump experiments*, *JHEP* **02** (2016) 018 [1512.03069].

[36] B. Döbrich, J. Jaeckel and T. Spadaro, *Light in the beam dump - ALP production from decay photons in proton beam-dumps*, *JHEP* **05** (2019) 213 [1904.02091].

[37] W. Altmannshofer, S. Gori and D. J. Robinson, *Constraining axionlike particles from rare pion decays*, *Phys. Rev. D* **101** (2020) 075002 [1909.00005].

[38] K. Asai, S. Iwamoto, Y. Sakaki and D. Ueda, *New physics searches at the ILC positron and electron beam dumps*, *JHEP* **09** (2021) 183 [2105.13768].

[39] E. Bertuzzo, A. L. Foguel, G. M. Salla and R. Z. Funchal, *New limits on leptophilic ALPs and Majorons from ArgoNeuT*, 2202.12317.

[40] L. Harland-Lang, J. Jaeckel and M. Spannowsky, *A fresh look at ALP searches in fixed target experiments*, *Phys. Lett. B* **793** (2019) 281 [1902.04878].

[41] P. deNiverville, H.-S. Lee and M.-S. Seo, *Implications of the dark axion portal for the muon $g-2$, B factories, fixed target neutrino experiments, and beam dumps*, *Phys. Rev. D* **98** (2018) 115011 [1806.00757].

[42] R. T. Co, S. Kumar and Z. Liu, *Enhancing Searches for Heavy QCD Axions via Dimuon Final States*, 2210.02462.

[43] R. Essig et al., *Working Group Report: New Light Weakly Coupled Particles*, in *Community Summer Study 2013: Snowmass on the Mississippi*, 10, 2013, 1311.0029.

[44] G. Aielli et al., *Expression of interest for the CODEX-b detector*, *Eur. Phys. J. C* **80** (2020) 1177 [1911.00481].

[45] G. Albouy et al., *Theory, phenomenology, and experimental avenues for dark showers: a Snowmass 2021 report*, *Eur. Phys. J. C* **82** (2022) 1132 [2203.09503].

[46] Y. Kahn, G. Krnjaic, N. Tran and A. Whitbeck, *M^3: a new muon missing momentum experiment to probe $(g-2)$ and dark matter at Fermilab*, *JHEP* **09** (2018) 153 [1804.03144].

[47] H. Sieber, D. Banerjee, P. Crivelli, E. Depero, S. N. Gninenko, D. V. Kirpichnikov et al., *Prospects in the search for a new light Z' boson with the NA64μ experiment at the CERN SPS*, *Phys. Rev. D* **105** (2022) 052006 [2110.15111].

[48] C. Cesarotti, S. Homiller, R. K. Mishra and M. Reece, *Probing New Gauge Forces with a High-Energy Muon Beam Dump*, 2202.12302.

[49] B. Batell, N. Blinov, C. Hearty and R. McGehee, *Exploring Dark Sector Portals with High Intensity Experiments*, in *2022 Snowmass Summer Study*, 7, 2022, 2207.06905.

[50] B. Batell et al., *Dark Sector Studies with Neutrino Beams*, in *2022 Snowmass Summer Study*, 7, 2022, 2207.06898.

[51] G. Krnjaic et al., *A Snowmass Whitepaper: Dark Matter Production at Intensity-Frontier Experiments*, 2207.00597.

[52] J. Berger et al., *Snowmass 2021 White Paper: Cosmogenic Dark Matter and Exotic Particle Searches in Neutrino Experiments*, in *2022 Snowmass Summer Study*, 7, 2022, 2207.02882.

[53] S. Gori et al., *Dark Sector Physics at High-Intensity Experiments*, 2209.04671.

[54] P. Coloma, L. W. Koerner, I. M. Shoemaker and J. Yu, *Neutrino Frontier Topical Group Report (NF03): Physics Beyond the Standard Model*, 2209.10362.

[55] MicroBooNE, LAr1-ND, ICARUS-WA104 collaboration, M. Antonello et al., *A Proposal for a Three Detector Short-Baseline Neutrino Oscillation Program in the Fermilab Booster Neutrino Beam*, 1503.01520.

[56] MicroBooNE collaboration, R. Acciarri et al., *Design and Construction of the MicroBooNE Detector*, *JINST* **12** (2017) P02017 [1612.05824].

[57] P. A. Machado, O. Palamara and D. W. Schmitz, *The Short-Baseline Neutrino Program at Fermilab*, *Ann. Rev. Nucl. Part. Sci.* **69** (2019) 363 [1903.04608].

[58] J. M. Berryman, A. de Gouvea, P. J. Fox, B. J. Kayser, K. J. Kelly and J. L. Raaf, *Searches for Decays of New Particles in the DUNE Multi-Purpose Near Detector*, *JHEP* **02** (2020) 174 [1912.07622].

[59] G. Chauhan, P. S. B. Dev and X.-J. Xu, *Probing the ν_R-philic Z' at DUNE near detectors*, 2204.11876.

[60] B. Batell, J. Berger and A. Ismail, *Probing the Higgs Portal at the Fermilab Short-Baseline Neutrino Experiments*, *Phys. Rev. D* **100** (2019) 115039 [1909.11670].

[61] P. Ballett, M. Hostert, S. Pascoli, Y. F. Perez-Gonzalez, Z. Tabrizi and R. Zukanovich Funchal, *Neutrino Trident Scattering at Near Detectors*, *JHEP* **01** (2019) 119 [1807.10973].

[62] D. Curtin et al., *Long-Lived Particles at the Energy Frontier: The MATHUSLA Physics Case*, *Rept. Prog. Phys.* **82** (2019) 116201 [1806.07396].

[63] FASER collaboration, B. Petersen, *First Physics Results from the FASER Experiment*, in *57th Rencontres de Moriond on Electroweak Interactions and Unified Theories*, 5, 2023, 2305.08665.

[64] OPAL collaboration, G. Abbiendi et al., *Photonic events with missing energy in e+ e- collisions at S**(1/2) = 189-GeV*, *Eur. Phys. J. C* **18** (2000) 253 [hep-ex/0005002].

[65] L3 collaboration, P. Achard et al., *Single photon and multiphoton events with missing energy in e^+e^- collisions at LEP*, *Phys. Lett. B* **587** (2004) 16 [hep-ex/0402002].

[66] M. J. Strassler, *Why Unparticle Models with Mass Gaps are Examples of Hidden Valleys*, 0801.0629.

[67] T. Han, Z. Si, K. M. Zurek and M. J. Strassler, *Phenomenology of hidden valleys at hadron colliders*, *JHEP* **07** (2008) 008 [0712.2041].

[68] E. W. Otten and C. Weinheimer, *Neutrino mass limit from tritium beta decay*, *Rept. Prog. Phys.* **71** (2008) 086201 [0909.2104].

[69] R. Contino, A. Falkowski, F. Goertz, C. Grojean and F. Riva, *On the Validity of the Effective Field Theory Approach to SM Precision Tests*, *JHEP* **07** (2016) 144 [1604.06444].

[70] I. Boiarska, K. Bondarenko, A. Boyarsky, V. Gorkavenko, M. Ovchynnikov and A. Sokolenko, *Phenomenology of GeV-scale scalar portal*, *JHEP* **11** (2019) 162 [1904.10447].

[71] L. Darmé, S. A. R. Ellis and T. You, *Light Dark Sectors through the Fermion Portal*, *JHEP* **07** (2020) 053 [2001.01490].

[72] E. Bertuzzo and M. Taoso, *Probing light dark scalars with future experiments*, *JHEP* **03** (2021) 272 [2011.04735].

[73] A. Berlin, P. deNiverville, A. Ritz, P. Schuster and N. Toro, *Sub-GeV dark matter production at fixed-target experiments*, *Phys. Rev. D* **102** (2020) 095011 [2003.03379].

[74] H.-C. Cheng, L. Li and E. Salvioni, *A Theory of Dark Pions*, 2110.10691.

[75] E. Bernreuther, K. Böse, T. Ferber, C. Hearty, F. Kahlhoefer, A. Morandini et al., *Forecasting dark showers at Belle II*, 2203.08824.

[76] P. Schwaller, D. Stolarski and A. Weiler, *Emerging Jets*, *JHEP* **05** (2015) 059 [1502.05409].

[77] A. Carmona, C. Scherb and P. Schwaller, *Charming ALPs*, *JHEP* **08** (2021) 121 [2101.07803].

[78] D. E. Kaplan, M. A. Luty and K. M. Zurek, *Asymmetric Dark Matter*, *Phys. Rev. D* **79** (2009) 115016 [0901.4117].

[79] K. M. Zurek, *Asymmetric Dark Matter: Theories, Signatures, and Constraints*, *Phys. Rept.* **537** (2014) 91 [1308.0338].

[80] K. Petraki and R. R. Volkas, *Review of asymmetric dark matter*, *Int. J. Mod. Phys. A* **28** (2013) 1330028 [1305.4939].

[81] R. Foot, H. Lew and R. R. Volkas, *A Model with fundamental improper space-time symmetries*, *Phys. Lett. B* **272** (1991) 67.

[82] R. Foot, *Mirror dark matter: Cosmology, galaxy structure and direct detection*, *Int. J. Mod. Phys. A* **29** (2014) 1430013 [1401.3965].

[83] R. Contino, A. Mitridate, A. Podo and M. Redi, *Gluequark Dark Matter*, *JHEP* **02** (2019) 187 [1811.06975].

[84] B. Batell, J. Berger, L. Darmé and C. Frugiuele, *Inelastic dark matter at the Fermilab Short Baseline Neutrino Program*, *Phys. Rev. D* **104** (2021) 075026 [2106.04584].

[85] P. deNiverville and C. Frugiuele, *Hunting sub-GeV dark matter with the NOνA near detector*, *Phys. Rev. D* **99** (2019) 051701 [1807.06501].

[86] L. Buonocore, C. Frugiuele and P. deNiverville, *Hunt for sub-GeV dark matter at neutrino facilities: A survey of past and present experiments*, *Phys. Rev. D* **102** (2020) 035006 [1912.09346].

[87] P. deNiverville, M. Pospelov and A. Ritz, *Observing a light dark matter beam with neutrino experiments*, *Phys. Rev. D* **84** (2011) 075020 [1107.4580].

[88] B. Batell, P. deNiverville, D. McKeen, M. Pospelov and A. Ritz, *Leptophobic dark matter at neutrino factories*, *Physical Review D* **90** (2014) .

[89] B. Batell, M. Pospelov and A. Ritz, *Exploring Portals to a Hidden Sector Through Fixed Targets*, *Phys. Rev. D* **80** (2009) 095024 [0906.5614].

[90] P. deNiverville, C.-Y. Chen, M. Pospelov and A. Ritz, *Light dark matter in neutrino beams: production modelling and scattering signatures at MiniBooNE, T2K and SHiP*, *Phys. Rev. D* **95** (2017) 035006 [1609.01770].

[91] P. deNiverville, D. McKeen and A. Ritz, *Signatures of sub-GeV dark matter beams at neutrino experiments*, *Phys. Rev. D* **86** (2012) 035022 [1205.3499].

[92] D. Tucker-Smith and N. Weiner, *Inelastic dark matter*, *Phys. Rev. D* **64** (2001) 043502 [hep-ph/0101138].

[93] M. W. Winkler, *Decay and detection of a light scalar boson mixing with the Higgs boson*, *Phys. Rev. D* **99** (2019) 015018 [1809.01876].

[94] P. Ilten, Y. Soreq, M. Williams and W. Xue, *Serendipity in dark photon searches*, *JHEP* **06** (2018) 004 [1801.04847].

[95] C. Baruch, P. Ilten, Y. Soreq and M. Williams, *Axial vectors in DarkCast*, 2206.08563.

[96] B. R. Webber, *Average Multiplicities in Jets*, *Phys. Lett. B* **143** (1984) 501.

[97] C. Cesarotti, M. Reece and M. J. Strassler, *Spheres To Jets: Tuning Event Shapes with 5d Simplified Models*, *JHEP* **05** (2021) 096 [2009.08981].

[98] N. Blinov, E. Kowalczyk and M. Wynne, *Axion-like particle searches at DarkQuest*, *JHEP* **02** (2022) 036 [2112.09814].

[99] A. J. Buras, *Weak Hamiltonian, CP violation and rare decays*, in *Les Houches Summer School in Theoretical Physics, Session 68: Probing the Standard Model of Particle Interactions*, pp. 281–539, 6, 1998, hep-ph/9806471.

[100] T. Inami and C. S. Lim, *Effects of Superheavy Quarks and Leptons in Low-Energy Weak Processes k(L) —> mu anti-mu, K+ —> pi+ Neutrino anti-neutrino and K0 <—> anti-K0*, *Prog. Theor. Phys.* **65** (1981) 297.

[101] SHiP collaboration, C. Ahdida et al., *Sensitivity of the SHiP experiment to Heavy Neutral Leptons*, *JHEP* **04** (2019) 077 [1811.00930].

[102] J. L. Feng, I. Galon, F. Kling and S. Trojanowski, *Dark Higgs bosons at the ForwArd Search ExpeRiment*, *Phys. Rev. D* **97** (2018) 055034 [1710.09387].

[103] D. Gorbunov, I. Krasnov, Y. Kudenko and S. Suvorov, *Heavy Neutral Leptons from kaon decays in the SHiP experiment*, *Phys. Lett. B* **810** (2020) 135817 [2004.07974].

[104] W. Altmannshofer, J. A. Dror and S. Gori, *New Insights Into Axion-Lepton Interactions*, 2209.00665.

[105] V. Barger, C.-W. Chiang, W.-Y. Keung and D. Marfatia, *Constraint on parity-violating muonic forces*, *Phys. Rev. Lett.* **108** (2012) 081802 [1109.6652].

[106] M. Hostert, K. Kaneta and M. Pospelov, *Pair production of dark particles in meson decays*, *Phys. Rev. D* **102** (2020) 055016 [2005.07102].

[107] NA61/SHINE collaboration, A. Aduszkiewicz et al., *Measurement of ϕ meson production in $p+p$ interactions at 40, 80 and* 158 *GeV/c with the NA61/SHINE spectrometer at the CERN SPS*, *Eur. Phys. J. C* **80** (2020) 199 [1908.04601].

[108] K. Kovarik et al., *nCTEQ15 - Global analysis of nuclear parton distributions with uncertainties in the CTEQ framework*, *Phys. Rev. D* **93** (2016) 085037 [1509.00792].

[109] D. B. Clark, E. Godat and F. I. Olness, *ManeParse : A Mathematica reader for Parton Distribution Functions*, *Comput. Phys. Commun.* **216** (2017) 126 [1605.08012].

[110] S. Foroughi-Abari and A. Ritz, *Dark Sector Production via Proton Bremsstrahlung*, 2108.05900.

[111] M. Shifman, A. Vainshtein and V. Zakharov, *Remarks on higgs-boson interactions with nucleons*, *Physics Letters B* **78** (1978) 443.

[112] T. Feuster and U. Mosel, *Photon- and meson-induced reactions on the nucleon*, *Physical Review C* **59** (1999) 460–491.

[113] A. S. Carroll et al., *Absorption Cross-Sections of $\pi^{\pm}$, $K^{\pm}$, p and $\bar{p}$ on Nuclei Between 60 GeV/c and 280 GeV/c*, *Phys. Lett. B* **80** (1979) 319.

[114] SHiP collaboration, M. Anelli et al., *A facility to Search for Hidden Particles (SHiP) at the CERN SPS*, 1504.04956.

[115] CHARM collaboration, F. Bergsma et al., *Search for Axion Like Particle Production in 400-GeV Proton - Copper Interactions*, *Phys. Lett. B* **157** (1985) 458.

[116] G. Marocco and S. Sarkar, *Blast from the past: Constraints on the dark sector from the BEBC WA66 beam dump experiment*, *SciPost Phys.* **10** (2021) 043 [2011.08153].

[117] R. Barouki, G. Marocco and S. Sarkar, *Blast from the past II: Constraints on heavy neutral leptons from the BEBC WA66 beam dump experiment*, 2208.00416.

[118] MicroBooNE collaboration, P. Abratenko et al., *Search for a Higgs Portal Scalar Decaying to Electron-Positron Pairs in the MicroBooNE Detector*, *Phys. Rev. Lett.* **127** (2021) 151803 [2106.00568].

[119] MiniBooNE DM collaboration, A. A. Aguilar-Arevalo et al., *Dark Matter Search in Nucleon, Pion, and Electron Channels from a Proton Beam Dump with MiniBooNE*, *Phys. Rev. D* **98** (2018) 112004 [1807.06137].

[120] NOvA collaboration, P. P. Filip, *Hunting for Light Dark Matter with the NOvA Detector*, in *International Conference on Neutrinos and Dark Matter*, 2020, DOI.

[121] J. Bian, *Measurement of Neutrino-Electron Elastic Scattering at NOvA Near Detector*, in *Meeting of the APS Division of Particles and Fields*, 10, 2017, 1710.03428.

[122] FASER collaboration, A. Ariga et al., *FASER's physics reach for long-lived particles*, *Phys. Rev. D* **99** (2019) 095011 [1811.12522].

[123] FASER collaboration, H. Abreu et al., *Detecting and Studying High-Energy Collider Neutrinos with FASER at the LHC*, *Eur. Phys. J. C* **80** (2020) 61 [1908.02310].

[124] FASER collaboration, H. Abreu et al., *First Direct Observation of Collider Neutrinos with FASER at the LHC*, 2303.14185.

[125] SND@LHC collaboration, G. Acampora et al., *SND@LHC: The Scattering and Neutrino Detector at the LHC*, 2210.02784.

[126] L. A. Anchordoqui et al., *The Forward Physics Facility: Sites, experiments, and physics potential*, *Phys. Rept.* **968** (2022) 1 [2109.10905].

[127] J. L. Feng, I. Galon, F. Kling and S. Trojanowski, *ForwArd Search ExpeRiment at the LHC*, *Phys. Rev. D* **97** (2018) 035001 [1708.09389].

[128] F. Kling and S. Trojanowski, *Heavy Neutral Leptons at FASER*, *Phys. Rev. D* **97** (2018) 095016 [1801.08947].

[129] A. Berlin and F. Kling, *Inelastic Dark Matter at the LHC Lifetime Frontier: ATLAS, CMS, LHCb, CODEX-b, FASER, and MATHUSLA*, *Phys. Rev. D* **99** (2019) 015021 [1810.01879].

[130] J. L. Feng, I. Galon, F. Kling and S. Trojanowski, *Axionlike particles at FASER: The LHC as a photon beam dump*, *Phys. Rev. D* **98** (2018) 055021 [1806.02348].

[131] A. Boyarsky, O. Mikulenko, M. Ovchynnikov and L. Shchutska, *Searches for new physics at SND@LHC*, *JHEP* **03** (2022) 006 [2104.09688].

[132] T. Kuwahara and S.-R. Yuan, *Dark Vector Mesons at LHC Forward Detector Searches*, 2303.03736.

[133] B. Batell, J. L. Feng, M. Fieg, A. Ismail, F. Kling, R. M. Abraham et al., *Hadrophilic dark sectors at the Forward Physics Facility*, *Phys. Rev. D* **105** (2022) 075001 [2111.10343].

[134] B. Batell, J. L. Feng and S. Trojanowski, *Detecting Dark Matter with Far-Forward Emulsion and Liquid Argon Detectors at the LHC*, *Phys. Rev. D* **103** (2021) 075023 [2101.10338].

[135] CHARM collaboration, J. Dorenbosch et al., *A search for decays of heavy neutrinos in the mass range 0.5–2.8 gev*, *Physics Letters B* **166** (1986) 473.

[136] S. N. Gninenko, *Constraints on sub-GeV hidden sector gauge bosons from a search for heavy neutrino decays*, *Phys. Lett. B* **713** (2012) 244 [1204.3583].

[137] DUNE collaboration, B. Abi et al., *Deep Underground Neutrino Experiment (DUNE), Far Detector Technical Design Report, Volume II: DUNE Physics*, 2002.03005.

[138] V. Brdar, B. Dutta, W. Jang, D. Kim, I. M. Shoemaker, Z. Tabrizi et al., *Axionlike Particles at Future Neutrino Experiments: Closing the Cosmological Triangle*, *Phys. Rev. Lett.* **126** (2021) 201801 [2011.07054].

[139] K. J. Kelly, S. Kumar and Z. Liu, *Heavy axion opportunities at the DUNE near detector*, *Phys. Rev. D* **103** (2021) 095002 [2011.05995].

[140] R. Essig, R. Harnik, J. Kaplan and N. Toro, *Discovering new light states at neutrino experiments*, *Physical Review D* **82** (2010) .

[141] S. Foroughi-Abari and A. Ritz, *LSND constraints on the higgs portal*, *Physical Review D* **102** (2020) .

[142] LSND collaboration, C. Athanassopoulos et al., *Evidence for muon-neutrino —> electron-neutrino oscillations from pion decay in flight neutrinos*, *Phys. Rev. C* **58** (1998) 2489 [nucl-ex/9706006].

[143] LSND collaboration, A. Aguilar-Arevalo et al., *Evidence for neutrino oscillations from the observation of $\bar{\nu}_e$ appearance in a $\bar{\nu}_\mu$ beam*, *Phys. Rev. D* **64** (2001) 112007 [hep-ex/0104049].

[144] NOvA collaboration, M. A. Acero et al., *Measurement of the ν_e-Nucleus Charged-Current Double-Differential Cross Section at $\langle E_\nu \rangle = 2.4$ GeV using NOvA*, 2206.10585.

[145] A. Bhattarai, V. Brdar, B. Dutta, W. Jang, D. Kim, I. M. Shoemaker et al., *BSM Targets at a Target-less DUNE*, 2206.06380.

[146] W. Altmannshofer, S. Gori, J. Martín-Albo, A. Sousa and M. Wallbank, *Neutrino Tridents at DUNE*, *Phys. Rev. D* **100** (2019) 115029 [1902.06765].

[147] Y. Gershtein, S. Knapen and D. Redigolo, *Probing naturally light singlets with a displaced vertex trigger*, *Phys. Lett. B* **823** (2021) 136758 [2012.07864].

[148] ATLAS collaboration, M. Aaboud et al., *Search for dark matter and other new phenomena in events with an energetic jet and large missing transverse momentum using the ATLAS detector*, *JHEP* **01** (2018) 126 [1711.03301].

[149] ATLAS collaboration, M. Aaboud et al., *Search for long-lived particles produced in pp collisions at $\sqrt{s} = 13$ TeV that decay into displaced hadronic jets in the ATLAS muon spectrometer*, *Phys. Rev. D* **99** (2019) 052005 [1811.07370].

[150] ATLAS collaboration, G. Aad et al., *Search for long-lived neutral particles produced in pp collisions at $\sqrt{s} = 13$ TeV decaying into displaced hadronic jets in the ATLAS inner detector and muon spectrometer*, *Phys. Rev. D* **101** (2020) 052013 [1911.12575].

[151] ALEPH, DELPHI, L3, OPAL, SLD, LEP Electroweak Working Group, SLD Electroweak Group, SLD Heavy Flavour Group collaboration, S. Schael et al., *Precision electroweak measurements on the Z resonance*, *Phys. Rept.* **427** (2006) 257 [hep-ex/0509008].

[152] J. Blumlein et al., *Limits on neutral light scalar and pseudoscalar particles in a proton beam dump experiment*, *Z. Phys. C* **51** (1991) 341.

[153] J. Blumlein et al., *Limits on the mass of light (pseudo)scalar particles from Bethe-Heitler e+ e- and mu+ mu- pair production in a proton - iron beam dump experiment*, *Int. J. Mod. Phys. A* **7** (1992) 3835.

[154] J. Blumlein and J. Brunner, *New Exclusion Limits for Dark Gauge Forces from Beam-Dump Data*, *Phys. Lett. B* **701** (2011) 155 [1104.2747].

[155] J. Blümlein and J. Brunner, *New Exclusion Limits on Dark Gauge Forces from Proton Bremsstrahlung in Beam-Dump Data*, *Phys. Lett. B* **731** (2014) 320 [1311.3870].

[156] G. Bernardi, G. Carugno, J. Chauveau, F. Dicarlo, M. Dris, J. Dumarchez et al., *Search for neutrino decay*, *Physics Letters B* **166** (1986) 479.

[157] G. Bernardi, G. Carugno, J. Chauveau, F. Dicarlo, M. Dris, J. Dumarchez et al., *Further limits on heavy neutrino couplings*, *Physics Letters B* **203** (1988) 332.

[158] S. N. Gninenko, *Stringent limits on the $\pi^0 \to \gamma X, X \to e + e-$ decay from neutrino experiments and constraints on new light gauge bosons*, *Phys. Rev. D* **85** (2012) 055027 [1112.5438].

[159] D. Gorbunov, I. Krasnov and S. Suvorov, *Constraints on light scalars from PS191 results*, *Phys. Lett. B* **820** (2021) 136524 [2105.11102].

[160] C. N. Yang, *Selection rules for the dematerialization of a particle into two photons*, *Phys. Rev.* **77** (1950) 242.

[161] L. D. Landau, *On the angular momentum of a system of two photons*, *Dokl. Akad. Nauk SSSR* **60** (1948) 207.

[162] BaBar collaboration, J. P. Lees et al., *Search for $B \to K^{(*)}\nu\overline{\nu}$ and invisible quarkonium decays*, *Phys. Rev. D* **87** (2013) 112005 [1303.7465].

[163] NA62 collaboration, E. Cortina Gil et al., *Measurement of the very rare $K^+ \to \pi^+\nu\overline{\nu}$ decay*, *JHEP* **06** (2021) 093 [2103.15389].

[164] BES collaboration, M. Ablikim et al., *Search for the invisible decay of J / psi in psi(2S) — pi+ pi- J / psi*, *Phys. Rev. Lett.* **100** (2008) 192001 [0710.0039].

[165] F. Kling and S. Trojanowski, *Forward experiment sensitivity estimator for the LHC and future hadron colliders*, *Phys. Rev. D* **104** (2021) 035012 [2105.07077].

[166] P. Ballett, T. Boschi and S. Pascoli, *Heavy Neutral Leptons from low-scale seesaws at the DUNE Near Detector*, *JHEP* **03** (2020) 111 [1905.00284].

[167] H.-C. Cheng, L. Li, E. Salvioni and C. B. Verhaaren, *Light Hidden Mesons through the Z Portal*, *JHEP* **11** (2019) 031 [1906.02198].

[168] A. Caputo, H.-T. Janka, G. Raffelt and E. Vitagliano, *Low-Energy Supernovae Severely Constrain Radiative Particle Decays*, *Phys. Rev. Lett.* **128** (2022) 221103 [2201.09890].

[169] J. L. Feng et al., *The Forward Physics Facility at the High-Luminosity LHC*, 2203.05090.

[170] C. Cheung and D. Sanford, *Effectively Stable Dark Matter*, 1507.00828.

[171] G. D. Kribs and E. T. Neil, *Review of strongly-coupled composite dark matter models and lattice simulations*, *Int. J. Mod. Phys. A* **31** (2016) 1643004 [1604.04627].

[172] O. Antipin, M. Redi, A. Strumia and E. Vigiani, *Accidental Composite Dark Matter*, *JHEP* **07** (2015) 039 [1503.08749].

[173] A. Mitridate, M. Redi, J. Smirnov and A. Strumia, *Dark Matter as a weakly coupled Dark Baryon*, *JHEP* **10** (2017) 210 [1707.05380].

[174] C. Kilic, T. Okui and R. Sundrum, *Vectorlike Confinement at the LHC*, *JHEP* **02** (2010) 018 [0906.0577].

[175] R. Contino, A. Podo and F. Revello, *Composite Dark Matter from Strongly-Interacting Chiral Dynamics*, *JHEP* **02** (2021) 091 [2008.10607].

[176] Particle Data Group collaboration, M. Tanabashi et al., *Review of Particle Physics*, *Phys. Rev. D* **98** (2018) 030001.

[177] Super-Kamiokande collaboration, K. Abe et al., *Search for proton decay via $p \to e^+\pi^0$ and $p \to \mu^+\pi^0$ in 0.31 megaton·years exposure of the Super-Kamiokande water Cherenkov detector*, *Phys. Rev. D* **95** (2017) 012004 [1610.03597].

[178] G. F. Giudice and A. Romanino, *Split supersymmetry*, *Nucl. Phys. B* **699** (2004) 65 [hep-ph/0406088].

[179] N. D. Christensen and R. Shrock, *On the unification of gauge symmetries in theories with dynamical symmetry breaking*, *Phys. Rev. D* **72** (2005) 035013 [hep-ph/0506155].

[180] M. Ibe, *Small steps towards Grand Unification and the electron/positron excesses in cosmic-ray experiments*, *JHEP* **08** (2009) 086 [0906.4667].

[181] T. Aizawa, M. Ibe and K. Kaneta, *Coupling Unification and Dark Matter in a Standard Model Extension with Adjoint Majorana Fermions*, *Phys. Rev. D* **91** (2015) 075012 [1411.6044].

[182] R. Mahbubani and L. Senatore, *The Minimal model for dark matter and unification*, *Phys. Rev. D* **73** (2006) 043510 [hep-ph/0510064].

[183] K. Harigaya, T. Lin and H. K. Lou, *GUTzilla Dark Matter*, *JHEP* **09** (2016) 014 [1606.00923].

[184] S. Ando and K. Ishiwata, *Constraints on decaying dark matter from the extragalactic gamma-ray background*, *JCAP* **05** (2015) 024 [1502.02007].

[185] M. Cirelli, E. Moulin, P. Panci, P. D. Serpico and A. Viana, *Gamma ray constraints on Decaying Dark Matter*, *Phys. Rev. D* **86** (2012) 083506 [1205.5283].

[186] Y. Bai and R. J. Hill, *Weakly Interacting Stable Pions*, *Phys. Rev. D* **82** (2010) 111701 [1005.0008].

[187] T. DeGrand, *Lattice tests of beyond Standard Model dynamics*, *Rev. Mod. Phys.* **88** (2016) 015001 [1510.05018].

[188] D. Barducci, S. De Curtis, M. Redi and A. Tesi, *An almost elementary Higgs: Theory and Practice*, *JHEP* **08** (2018) 017 [1805.12578].

[189] R. Contino, *The Higgs as a Composite Nambu-Goldstone Boson*, in *Theoretical Advanced Study Institute in Elementary Particle Physics: Physics of the Large and the Small*, pp. 235–306, 2011, 1005.4269, DOI.

[190] C. Jacoby and S. Nussinov, *The Relic Abundance of Massive Colored Particles after a Late Hadronic Annihilation Stage*, 0712.2681.

[191] J. Kang, M. A. Luty and S. Nasri, *The Relic abundance of long-lived heavy colored particles*, *JHEP* **09** (2008) 086 [hep-ph/0611322].

[192] V. De Luca, A. Mitridate, M. Redi, J. Smirnov and A. Strumia, *Colored Dark Matter*, *Phys. Rev. D* **97** (2018) 115024 [1801.01135].

[193] K. K. Boddy, J. L. Feng, M. Kaplinghat, Y. Shadmi and T. M. P. Tait, *Strongly interacting dark matter: Self-interactions and keV lines*, *Phys. Rev. D* **90** (2014) 095016 [1408.6532].

[194] K. K. Boddy, J. L. Feng, M. Kaplinghat and T. M. P. Tait, *Self-Interacting Dark Matter from a Non-Abelian Hidden Sector*, *Phys. Rev. D* **89** (2014) 115017 [1402.3629].

[195] K. Harigaya, M. Ibe, K. Kaneta, W. Nakano and M. Suzuki, *Thermal Relic Dark Matter Beyond the Unitarity Limit*, *JHEP* **08** (2016) 151 [1606.00159].

[196] N. Arkani-Hamed and S. Dimopoulos, *Supersymmetric unification without low energy supersymmetry and signatures for fine-tuning at the LHC*, *JHEP* **06** (2005) 073 [hep-th/0405159].

[197] R. J. Scherrer and M. S. Turner, *Decaying Particles Do Not Heat Up the Universe*, *Phys. Rev. D* **31** (1985) 681.

[198] M. Kamionkowski and M. S. Turner, *THERMAL RELICS: DO WE KNOW THEIR ABUNDANCES?*, *Phys. Rev. D* **42** (1990) 3310.

[199] J. McDonald, *WIMP Densities in Decaying Particle Dominated Cosmology*, *Phys. Rev. D* **43** (1991) 1063.

[200] G. F. Giudice, E. W. Kolb and A. Riotto, *Largest temperature of the radiation era and its cosmological implications*, *Phys. Rev. D* **64** (2001) 023508 [hep-ph/0005123].

[201] R. T. Co, F. D'Eramo, L. J. Hall and D. Pappadopulo, *Freeze-In Dark Matter with Displaced Signatures at Colliders*, *JCAP* **12** (2015) 024 [1506.07532].

[202] M. Cirelli, Y. Gouttenoire, K. Petraki and F. Sala, *Homeopathic Dark Matter, or how diluted heavy substances produce high energy cosmic rays*, *JCAP* **02** (2019) 014 [1811.03608].

[203] K. Griest and M. Kamionkowski, *Unitarity Limits on the Mass and Radius of Dark Matter Particles*, *Phys. Rev. Lett.* **64** (1990) 615.

[204] E. W. Kolb and M. S. Turner, *The Early Universe*, vol. 69. 1990, 10.1201/9780429492860.

[205] T. Burch, *Heavy hadrons on $N_f = 2$ and $2 + 1$ improved clover-Wilson lattices*, 1502.00675.

[206] K. Abe et al., *Letter of Intent: The Hyper-Kamiokande Experiment — Detector Design and Physics Potential —*, 1109.3262.

[207] G. F. Giudice, A. Riotto and I. Tkachev, *Thermal and nonthermal production of gravitinos in the early universe*, *JHEP* **11** (1999) 036 [hep-ph/9911302].

[208] D. J. H. Chung, E. W. Kolb and A. Riotto, *Nonthermal supermassive dark matter*, *Phys. Rev. Lett.* **81** (1998) 4048 [hep-ph/9805473].

[209] E. W. Kolb, D. J. H. Chung and A. Riotto, *WIMPzillas!*, *AIP Conf. Proc.* **484** (1999) 91 [hep-ph/9810361].

[210] D. J. H. Chung, E. W. Kolb and A. Riotto, *Production of massive particles during reheating*, *Phys. Rev. D* **60** (1999) 063504 [hep-ph/9809453].

[211] N. Arkani-Hamed and J. Maldacena, *Cosmological Collider Physics*, 1503.08043.

[212] N. Arkani-Hamed, D. Baumann, H. Lee and G. L. Pimentel, *The Cosmological Bootstrap: Inflationary Correlators from Symmetries and Singularities*, *JHEP* **04** (2020) 105 [1811.00024].

[213] S. Kumar and R. Sundrum, *Seeing Higher-Dimensional Grand Unification In Primordial Non-Gaussianities*, *JHEP* **04** (2019) 120 [1811.11200].

[214] D. Baumann and D. Green, *Signatures of Supersymmetry from the Early Universe*, *Phys. Rev. D* **85** (2012) 103520 [1109.0292].

[215] B. Batell, W. Huang and K. J. Kelly, *Keeping it simple: simplified frameworks for long-lived particles at neutrino facilities*, *JHEP* **08** (2023) 092 [2304.11189].

[216] L. Randall and C. Csaki, *The Doublet - triplet splitting problem and Higgses as pseudoGoldstone bosons*, in *International Workshop on Supersymmetry and Unification of Fundamental Interactions (SUSY 95)*, pp. 99–109, 3, 1995, hep-ph/9508208.

[217] L. J. Hall and Y. Nomura, *Grand unification in higher dimensions*, *Annals Phys.* **306** (2003) 132 [hep-ph/0212134].

[218] Y. Kawamura, *Gauge symmetry breaking from extra space S**1 / Z(2)*, *Prog. Theor. Phys.* **103** (2000) 613 [hep-ph/9902423].

[219] Y. Kawamura, *Triplet doublet splitting, proton stability and extra dimension*, *Prog. Theor. Phys.* **105** (2001) 999 [hep-ph/0012125].

[220] P. Masjuan, E. R. Arriola and W. Broniowski, *Meson dominance of hadron form factors and large-N_c phenomenology*, *Phys. Rev. D* **87** (2013) 014005.

[221] A. Ritz and S. Foroughi-Abari, *private communication*, .

[222] D. Gorbunov, A. Makarov and I. Timiryasov, *Decaying light particles in the SHiP experiment: Signal rate estimates for hidden photons*, *Phys. Rev. D* **91** (2015) 035027 [1411.4007].

[223] P. Ball and R. Zwicky, *New results on $B \to \pi, K, \eta$ decay formfactors from light-cone sum rules*, *Phys. Rev. D* **71** (2005) 014015 [hep-ph/0406232].

[224] N. Carrasco, P. Lami, V. Lubicz, L. Riggio, S. Simula and C. Tarantino, $K \to \pi$ *semileptonic form factors with* $N_f = 2 + 1 + 1$ *twisted mass fermions*, *Phys. Rev. D* **93** (2016) 114512 [1602.04113].

[225] P. Ball and R. Zwicky, $B_{d,s} \to \rho, \omega, K^*, \phi$ *decay form-factors from light-cone sum rules revisited*, *Phys. Rev. D* **71** (2005) 014029 [hep-ph/0412079].

[226] T. Hahn, *CUBA: A Library for multidimensional numerical integration*, *Comput. Phys. Commun.* **168** (2005) 78 [hep-ph/0404043].

[227] D. Egana-Ugrinovic, S. Homiller and P. Meade, *Light Scalars and the Koto Anomaly*, *Phys. Rev. Lett.* **124** (2020) 191801 [1911.10203].

[228] T. Hubsch and S. Pallua, *SYMMETRY BREAKING MECHANISM IN AN ALTERNATIVE SU(5) MODEL*, *Phys. Lett. B* **138** (1984) 279.

[229] E. Eichten, K. Gottfried, T. Kinoshita, J. B. Kogut, K. D. Lane and T.-M. Yan, *The Spectrum of Charmonium*, *Phys. Rev. Lett.* **34** (1975) 369.

[230] G. S. Bali and A. Pineda, *QCD phenomenology of static sources and gluonic excitations at short distances*, *Phys. Rev. D* **69** (2004) 094001 [hep-ph/0310130].

Appendix A

Time-like form factors

In the extended Vector Meson Dominance (eVMD) formalism, form factors are modelled as sum over meson states $\mathfrak{m}$ sharing the same quantum numbers of the SM operator X involved in the matrix element. Typically the formalism is applied in the space-like region, and the form factors are essentially the sum of the propagators of the virtual mesons. However given that the exchanged momentum $p_{\rm DS}$ in our case is time-like, the form factors are modelled as Breit-Wigners, to allow the virtual exchanged meson to go on-shell and resonantly mix with the DS system:

$$F_{\mathfrak{m}}(p^2_{\rm DS}) = \sum_i f_{\mathfrak{m}_i} \frac{m^2_{\mathfrak{m}_i}}{p^2_{\rm DS} - m^2_{\mathfrak{m}_i} + i m_{\mathfrak{m}_i}\Gamma_{\mathfrak{m}_i}} \,, \tag{A.1}$$

where $m_{\mathfrak{m}}, \Gamma_{\mathfrak{m}}, f_{\mathfrak{m}}$ are the mass, the decay width and the "couplings" for the meson $\mathfrak{m}$ respectively. The number of resonances in the meson tower sharing the $\mathfrak{m}$ quantum numbers is such that it allows to enforce the correct asymptotic behaviour in q^2 of the form factor coming from sum rules. The couplings $f_{\mathfrak{m}_i}$ are fitted from data and by the overall coupling normalization. In order to get the total form factor F_X, we need to also take into account the cut-off for too high virtuality of eq. (3.27):

$$F_X = F_D(Q^2) F_{\mathfrak{m}}(p^2_{\rm DS}) \,. \tag{A.2}$$

We next discuss the Higgs and the Z portal case separately.

A.1 Higgs portal

The Higgs coupling to the protons is of the form

$$g_{hNN} F_H(q^2)\, h\, \bar{u}_p\, u_p \,, \tag{A.3}$$

where u_p is the proton spinor. The form factor F_H also includes the virtuality cut-off of eq. (3.26):

$$F_H = F_D F_S \tag{A.4}$$

The form factor $F_S(p^2_{\rm DS})$ is estimated using eq. (A.1), and we include the first three CP-even, scalar resonances. The values used for masses, width and f used in the FF are given in table A.1.

	f_0 (Scalar)			ω (Z, vector iso-singlet)			ρ (Z, vector iso-triplet)			a_1 (Z, axial iso-triplet)	
$m_{\mathfrak{m}}$ (GeV)	0.5	0.980	1.37	0.782	1.42	1.67	0.775	1.45	1.72	1.23	1.647
$\Gamma_{\mathfrak{m}}$ (GeV)	0.275	0.5	0.35	8×10^{-3}	0.2	0.3	0.149	0.4	0.25	0.4	0.254
$f_{\mathfrak{m}}$	0.28	1.8	-0.99	1.011	-0.881	0.369	0.616	0.223	-0.339	2.26	-1.26

Table A.1: Masses $m_{\mathfrak{m}}$, width $\Gamma_{\mathfrak{m}}$ and coupling $f_{\mathfrak{m}}$ of the mesons $\mathfrak{m}$ for the scalar, vector iso-singlet, vector iso-triplet, and axial iso-triplet proton Form Factors used in the eVMD approach.

A.2 Z portal

The effective Z vertex for the proton is modelled as:

$$\frac{g_{\rm EW}}{\cos\theta_W}\bar{u}_p\gamma^\mu\left(F^\rho(q^2)\left(\frac{1}{2}-\sin^2\theta_W\right)-\sin^2\theta_W F^\omega(q^2)\right)u_p + \frac{g_{\rm EW}}{4\cos\theta_W}g_A F_A(q^2)\bar{u}_p\gamma^\mu\gamma^5 u_p\,, \tag{A.5}$$

where q is the exchanged momentum between the virtual and real proton ($p_{\rm DS}$ in our case) and u_p is the proton spinor. The prefactors in front of the iso-singlet and iso-triplet vector form factors (F^ω and F^ρ respectively) come from the decomposition of the vector piece of the quark Z-current in the singlet and triplet component in isospin space, using the approximate isospin symmetry of proton and neutron. The axial-vector form factor has a slightly different normalization than the vector one. In particular, there is an extra $g_A \simeq 1.2$ multiplying the overall form factor in eq. (A.1), as shown in eq. (A.5). We can see that the vector part is subleading with respect to the axial current due to the absence of $\sin^2\theta_W$ suppressing factor and a $\mathcal{O}(1)$ coupling g_A. Notice that in principle, along with the Dirac-like form factors appearing in eq. (A.5), there should be the non-renormalizable Pauli-like terms [220]:

$$G_V(q^2)i\frac{[\gamma^\mu,\gamma^\nu]}{m_p}q_\nu + G_A(q^2)\gamma^5\frac{1}{m_p}q^\mu\,, \tag{A.6}$$

where the second piece (the axial one) is mediated by pion exchange. It turns out that this contribution vanishes when contracted with the JJ correlator, due to current conservation. The vector piece, corresponding to the anomalous magnetic proton contribution, does not vanish. Given that it's numerically subleading, and that there are large uncertainties to extrapolate such form factor in the time-like region [221, 222], we will neglect this contribution.

The form factors appearing in eq. (A.5) are again computed in the eVMD formalism, as a sum of Breit-Wigners of ρ, ω, a_1 meson for F^ρ, F^ω, F_A respectively. The coefficients used in the form factors are found in table A.1.

The final form factors appearing in eq. (3.31),(3.32) are defined respectively as:

$$F_Z^{\rm V} = F_D\left(-\sin^2\theta_W F^\omega + F^\rho\left(\frac{1}{2}-\sin^2\theta_W\right)\right)\,,$$
$$F_Z^{\rm A} = F_D\frac{g_A}{4}F_A\,. \tag{A.7}$$

We can generalize the formalism for any combination of iso-singlet and iso-triplet axial and axial-vector currents, meaning that we can get the form factor for all the possible flavor-conserving quark coupling structures of generic JJ portals.

Notice that in table A.1 there are no axial-vector iso-singlets form factors, but they can be obtained from lattice computations.

Appendix B

Meson decay matrix elements

Here we summarise the QCD matrix elements and form factor parametrizations we use for computing decays of mesons. For the case of annihilation decays, the meson decays to DS states entirely, while for radiative decays, a heavier meson decays to lighter mesons, along with DS. The matrix element for the process can be factorized into a short distance contribution (and only involves DS matrix elements) and a long distance (QCD) contribution. For the process $\mathbf{M} \to \mathrm{DS}$, where $\mathbf{M}$ is the decaying meson, the full amplitude $\langle \mathrm{DS}|\mathcal{O}_{\mathrm{SM}}\,\mathcal{O}_{\mathrm{DS}}|\mathbf{M}\rangle$ factors into $\langle 0|\mathcal{O}_{\mathrm{SM}}|\mathrm{M}\rangle \times \langle \mathrm{DS}|\mathcal{O}_{\mathrm{DS}}|0\rangle$ while for the process $\mathbf{H} \to \mathbf{L} + \mathrm{DS}$, where $\mathbf{H}$ ($\mathbf{L}$) are the heavy (light) SM mesons, the amplitude $\langle \mathbf{L}, \mathrm{DS}|\mathcal{O}_{\mathrm{SM}}\,\mathcal{O}_{\mathrm{DS}}|\mathbf{H}\rangle$ factors as $\langle \mathbf{L}|\mathcal{O}_{\mathrm{SM}}|\mathbf{H}\rangle \times \langle \mathrm{DS}|\mathcal{O}_{\mathrm{DS}}|0\rangle$. For the annihilation case, we only consider vector mesons, denoted by V[1]. The SM matrix element for annihilation decay is simple, and is generically given as

$$\langle 0|\bar{u}\gamma_\mu u|V(p)\rangle = i f_V m_V \epsilon_\mu(p)\,, \tag{B.1}$$

where u are the quark spinors, $\epsilon_\mu(p)$ is the polarization vector of the vector meson V, f_V is the decay constant, and m_V is the mass of the meson.

For the radiative decay case, the SM contribution to the amplitude is the same as SM semileptonic meson decays, and is less straightforward than the annihilation case. We now give details of the matrix elements and form factors used to compute width of decays of $\mathrm{H} \to \mathrm{L} + \mathrm{DS}$ where H can be B, K and L can either be a light pseudoscalar P (e.g. K, π) or vector V (e.g., K^*, ρ, ϕ).

B.1 Decay to Pseudoscalars

For the decay of mesons to pseudoscalars P (e.g., K, π) we use the usual matrix element definitions (see [223] for example):

$$\langle P(p_P)|\,V^\mu\,|H(p_H)\rangle = f_+(q^2)p^\mu + \big(f_0(q^2) - f_+(q^2)\big)\;D\,q^\mu\,, \tag{B.2}$$

where $V^\mu = \bar{u}_L\gamma^\mu u_H$, $p^\mu = p_H^\mu + p_P^\mu$, $D = (M_H^2 - M_P^2)/p_{\mathrm{DS}}^2$, and $q^\mu \equiv p_{\mathrm{DS}}^\mu = p_H^\mu - p_P^\mu$. Here, u_L (u_H) denotes a light (heavy) quark field, $p_H(p_P)$ is the 4-momentum of the decaying heavy (light) meson with mass $m_H(m_P)$, and $f_0(q^2), f_+(q^2)$ are dimensionless form factors which encode the strong interaction effects. For the case of $\mathcal{O}_{\mathrm{DS}} = J_\mu^{\mathrm{DS}}$, a conserved current, terms proportional to $q^\mu\,J_\mu^{\mathrm{DS}}(q)$ vanish, so that we only need to specify the $f_+(q^2)$ form factors.

[1]For pseudoscalar mesons, the matrix element is proportional to p_μ and vanishes when contracted with the DS current, by current conservation.

For $K^+ \to \pi^+ + \text{DS}$ decay we use the explicit form factor data points defined at each q^2 in table IV of ref. [224]. For $B \to \pi, K$ decays, we use the form factor definitions and values from ref. [223]:

$$f_+^{B\to\pi}(q^2) = \frac{A}{\left(1 - q^2/D^2\right)\left(1 - q^2/E^2\right)} ,$$
$$f_+^{B\to K}(q^2) = \frac{B}{1 - q^2/F^2} + \frac{C}{\left(1 - q^2/F^2\right)^2} , \tag{B.3}$$

where $A = 0.258, B = 0.173, C = 0.162$ and $D = 5.32$ GeV, $E = 6.38$ GeV, and $F = 5.41$ GeV.

B.2 Decay to Vector Mesons

For the case of B meson decaying to light vector mesons V (e.g., K^*, ρ, ϕ), the QCD matrix element is defined as (see ref. [225]):

$$\begin{aligned}\langle V(p_V)|\, J_\mu \,|B(p_B)\rangle &= -i\epsilon_{\mu *}(p_V)(m_B + m_V)\, A_1(q^2) \\ &+ ip_\mu(\epsilon^*(p_V)\cdot q)\,\frac{A_2(q^2)}{m_B + m_V} \\ &+ i\, q_\mu(\epsilon^*(p_V)\cdot q)\,\frac{2m_V}{q^2}(A_3(q^2) - A_0(q^2)) \\ &+ \epsilon_{\mu\nu\rho\sigma}\epsilon^{\nu *}(p_V)p_B^\rho p_V^\sigma\,\frac{2V(q^2)}{m_B + m_V} ,\end{aligned} \tag{B.4}$$

where $J^\mu = \bar{q}_L\gamma^\mu(1-\gamma_5)q_H$, $p^\mu = (p_B + p_V)^\mu$, and $q^\mu \equiv p^\mu_{\text{DS}} = p^\mu_B - p^\mu_V$. Here p_B (p_V) are the 4-momentum of the B (vector) meson, m_B (m_V) is the mass of the B (V) meson, ϵ^μ is the polarization vector of V, and $A_i(q^2), V(q^2)$ are the dimensionless form factors encoding strong interaction effects. Note that, unlike the pseudoscalar case, in the case of vector meson, the $\gamma_5\gamma^\mu$ part of the current does not vanish. Further, the third term in the above does not contribute since it is zero by current conservation, as in the pseudoscalar case.

For the form factors, we use the parametrizations as given in ref. [225]:

$$V(q^2) = \frac{r_1}{1 - q^2/m_R^2} + \frac{r_2}{1 - q^2/m_{fit}^2} , \tag{B.5}$$
$$A_1(q^2) = \frac{r_2}{1 - q^2/m_{fit}^2} , \tag{B.6}$$
$$A_2(q^2) = \frac{r_1}{1 - q^2/m_{fit}^2} + \frac{r_2}{(1 - q^2/m_{fit}^2)^2} . \tag{B.7}$$

We give the values of the various fit parameters for the different decays in table B.1. To evaluate further the squared matrix element, we make the calculations in the rest frame of B meson, where only the longitudinal polarization of $\epsilon^*_\mu(p_V)$ contributes. Thus, using $\epsilon^*_\mu(p_V) = \left(\frac{|\vec{p}_V|}{m_V}, \frac{\vec{p}_V}{|\vec{p}_V|}\frac{E_V}{m_V}\right)$ and $p_{\text{DS}} = p_B - p_V$, we can find the production width of DS from radiative $B \to V$ decays.

B.3 Sensitivity to non-conformal contributions in K, B meson decays

For the case of DS production from irrelevant portals, we expect the production cross-section to grow with p^2_{DS} which is necessary to make the contribution away from the IR threshold more important,

	r_1	r_2	m_R^2 [GeV^2]	m_{fit}^2 [GeV^2]
$V^{B\to K^*}$	0.923	-0.511	28.30	49.4
$A_1^{B\to K^*}$	-	0.290	-	40.38
$A_2^{B\to K^*}$	-0.084	0.342	-	52.00
$V^{B\to \rho}$	1.045	-0.721	28.30	38.34
$A_1^{B\to \rho}$	-	0.240	-	37.51
$A_2^{B\to \rho}$	0.009	0.212	-	40.82
$V^{B_s\to \phi}$	1.484	-1.049	29.38	39.52
$A_1^{B_s\to \phi}$	-	0.308	-	36.54
$A_2^{B_s\to \phi}$	-0.054	0.288	-	48.94

Table B.1: Fit parameters for the form factors defined in eq. (B.5), (B.6), (B.7) for various $B \to V$ transitions where $V = K^*, \rho, \phi$ (taken from [225]).

and is needed for usefulness of our model agnostic approach. For radiative meson decays however, the DS production cross-section does not grow as $p_{\rm DS}^2$, but is rather flat, upto the kinematic threshold. For annihilation decays, $p_{\rm DS}^2$ is fixed and equals the parent meson mass-squared. To justify our model agnostic approach we need to ensure we are away from the thresholds, which must be imposed as a self-consistent criteria.

The overall signal is obtained by an integral over the range of allowed $p_{\rm DS}$. The kinematic condition $p_{\rm DS}/(n_{\rm LDSP}\,\Lambda_{\rm IR}) \geq 1$ is always stronger than the condition to be in the conformal regime $p_{\rm DS}/\Lambda_{\rm IR} \gtrsim 1$. We also need to make sure that the relevant $\Lambda_{\rm IR}$ probed in the experiment under consideration (which depends on the portal and the lifetime) is away from the kinematic threshold $M - m$. For $\Lambda_{\rm IR}$ close to $M - m$, a small change in the lower limit of $p_{\rm DS}$ integration would have a bigger impact, but this does not happen in the cases we consider. For $B \to K+$DS, $(m_B - m_K) \sim 5$ GeV is larger than typical $\Lambda_{\rm IR}$ probed which is $0.001-1$ GeV, while for $K \to \pi+$DS, $(m_K - m_\pi) \sim 0.4$ GeV, while the typical $\Lambda_{\rm IR}$ probed is $0.001 - 0.1$ GeV.

Appendix C

Probability of Decay

To compute the number of signal events, we need to calculate the number of LDSPs that decay inside the detector. To correctly compute this quantity, the differential cross section (in both energy and angle) of LDSP production must be convoluted with the probability P for at least an LDSP to decay inside the detector. The probability P_1 for a particle to decay inside the detector can be roughly estimated as the probability $P_{1,\mathrm{dec}}$ to decay within the radial distance at which the detector is, multiplied with ϵ_{geo}, the geometric acceptance accounting for the particles flying in the detector direction:

$$P_1 \approx \epsilon_{\mathrm{geo}} P_{1,\mathrm{dec}} \ , \tag{C.1}$$

In a simplified setup (see fig. 3.6), $P_{1,\mathrm{dec}}$ can be estimated to be

$$P_{1,\mathrm{dec}} = \exp\left(-\frac{l}{c\tau(\gamma\,\beta)_{\mathrm{LDSP}}}\right) - \exp\left(-\frac{l+d}{c\tau(\gamma\,\beta)_{\mathrm{LDSP}}}\right) \ , \tag{C.2}$$

where l and d are the distance of the detector from the target location and the length of the detector respectively [1], γ_{LDSP} is the (energy dependent) Lorentz factor of the decaying particle, β_{LDSP} is its velocity and τ is its proper lifetime. In general, for more than 1 LDSP, a slightly more refined procedure accounting for the presence of multiple particles that can go inside the detector is needed. We now discuss our procedure for multiple particle events. We consider both the weakly coupled case, where $n_{\mathrm{LDSP}} = 2$, and a generic strongly coupled case in which $n_{\mathrm{LDSP}} \sim \mathcal{O}(10)$ are produced.

For the weakly coupled case, the directions of the two LDSPs are fully correlated, at fixed p_{DS}, by momentum conservation. If the direction of the DS sytem (*i.e.* $\vec{p}_{\mathrm{DS}}$) does not intersect the detector, at most one of the two LDSPs can have the correct direction to hit the detector. Indeed, the two particles have opposite azimuthal angle ϕ (computed with respect to the DS momentum in the lab frame), so that only one particle at most can travel to the correct side. Therefore the probability to have at least one particle decaying inside the detector is (in the notation of eq. (3.8)):

$$\epsilon_{\mathrm{geo}}\, P_{\mathrm{decay}} = 2\epsilon_{\mathrm{geo}} P_{1,\mathrm{dec}} \ ,$$

where the 2 reflects the fact that ϵ_{geo} has been computed for a single particle only, and there are

[1] Notice that the distance should be a function of the direction of the LDSP for generic geometry of the detector. We will work under the assumption of spherical detectors, where the distances appearing in P are independent of the line of flight. This is a good approximation for neutrino experiments, since they consist of small boxes (of size $\mathcal{O}(10)$ m) positioned far ($\mathcal{O}(10^3)$ m) from the target. The error due to the geometrical approximation is therefore of order 1% (the ratio of the typical distances).

two possible particles that can decay in the detector (or in other words, we only considered one of the particles to be aimed toward the detector, but the opposite direction is also a valid choice given the presence of the other LDSP).

If instead the DS direction intersects the detector there is the possibility for both LDSPs to fall inside the detector. This can happen only if the LDSP velocity in the DS frame is slower than the velocity of the DS system in the lab frame, so that the LDSP traveling in the direction $\theta > \pi/2$ (the backward direction) in the DS frame is boosted in the forward direction. The events in which the backward LDSP gets boosted forward in the lab frame are only significant if the DS system velocity is much larger than the velocity of the LDSP in the DS frame. Given that typically $n_{\text{LDSP}}\Lambda_{\text{IR}} \ll \sqrt{p_{\text{DS}}^2}$, and that the bulk of the cross section is dominated by high p_{DS}^2 events, the events will have fast LDSPs in the DS frame. Therefore events with two particles boosted forward are negligible, and the formula to have a particle decaying inside the detector holds unchanged.

In the strongly coupled case, where n_{LDSP} is large, we can neglect the fact that the momenta are correlated by momentum conservation. Therefore we will assume that the n_{LDSP} particles share democratically the energy in the rest frame, and that the directions are independent samples from an isotropic distribution in such a frame. In this scenario, multiple particles can in principle have the correct direction to get inside the detector in the lab frame. Using the probability for a single particle to decay inside the detector from eq. (C.2), and recalling that this probability is very small (both $P_{1,\text{dec}}$ and typical ϵ_{geo} are small), it follows that events in which multiple particles simultaneously decay inside the detector are very rare. Therefore we can approximate the probability for a single event to contain at least one particle decaying inside the detector as

$$\epsilon_{\text{geo}}\, P_{\text{decay}} = n_{\text{LDSP}}\, \epsilon_{\text{geo}}\, P_{1,\text{dec}}\,.$$

Notice that in the end (although for slightly different reason) this formula matches the one in the weakly coupled case for $n_{\text{LDSP}} = 2$.

C.1 ϵ_{geo} estimates

In order to compute the signal events, we have to compute the fraction of events that contain at least one LDSP with the direction intersecting the detector. Given the assumptions outlined in Section C, we define ϵ_{geo} as the probability for a single particle to have such a direction. We work under the assumption that LDSPs are produced isotropically in the DS rest frame, the frame in which only the time component of p_{DS} is non-zero. We will also assume that in this frame, all the LDSPs produced share the same energy $p_{\text{DS}}^0/n_{\text{LDSP}}$. We take the beam direction to be aligned to the z-axis ($\theta = 0$ in polar coordinates), and ϕ as the azimuthal angle (measured in the plane orthogonal to the beam line).

In order to get an estimate for the angular coverage of the neutrino detector, we work under the simplifying assumption that the detector surface lies on a 2D plane orthogonal to the beam (for the off-axis case, the angle is very small) and all points on the detector are at the same distance from the interaction point. This is a good approximation for neutrino detectors since corrections are of order $(d/l)^2 \ll 1$, where l is the distance at which the detector is placed, and d is the typical size of the detector. There are two relevant cases where this approximation fails.

For a closer experiment like SHiP, l and d are of same order, and the proposed shape is a rectangle of dimensions $(a, 2a)$, $a = 5$ m. We will compute the angular acceptance by taking the largest side of the rectangle and requiring the trajectory to intersect the first layer, which gives $\theta_{\text{acc}} = \text{ArcTan}\,(2a/2l)$. Being more specific about the shape of the detector does not change the

estimate significantly since the DS is produced very boosted, with a small opening angle, and is fully covered by the extent of the detector. The geometric acceptances are close to unity, see table 3.1.

For MicroBooNE, the produced Kaons are at rest in the lab frame, and not collimated, so that the DS is produced isotropic in the lab frame. In this case, the above approximation again does not hold. We calculate ϵ_{geo} without this approximation for MicroBooNE.

To calculate ϵ_{geo}, we need to find the overlap of the LDSPs with the detector, which is easier to do in the $*$ frame. By the assumption of isotropic decay, the LDSP directions are distributed uniformly in the $(\cos\theta^*, \phi^*)$ plane. In this plane ϵ_{geo} is the area (normalized by $1/4\pi$) that corresponds to lab frame configurations in which the LDSP falls inside the detector. This in general depends on p_{DS} and n_{LDSP} through the boost factor.

To be precise, we need to introduce some notation. There are two frames to consider, the lab frame, and the DS frame (the one where p_{DS} only has a time component). We refer to the DS frame as the * frame, in what follows. The angles and the boost factors with a * superscript are defined in the DS frame, and without a * superscript are in the lab frame.

The detector direction, the DS direction, and the LDSP direction are all defined by a θ, and the last two depend in general on kinematical quantities such as p_{DS} and other process-dependent quantities *e.g.* z in bremsstrahlung. We take the detector to be positioned at $\theta = \theta_{\text{det}}$. The accepted directions form a cone around it with an angle θ_{acc} around it. The DS system may be along the beam line or at an angle from it. We define the DS system to be at $\theta = \theta_{\text{DS}}$. Finally, the LDSP is at an angle θ_{LDSP} w.r.t. the DS system, so that the DS direction has a cone of angle θ_{LDSP} around it. It is useful to also define the DS direction w.r.t. the detector, which is denoted by $\theta^{\text{eff}}_{\text{det}} \approx \left(\theta^2_{\text{DS}} + \theta^2_{\text{det}} - 2\theta_{\text{det}}\theta_{\text{DS}}\cos\phi_{\text{DS}}\right)^{1/2}$. All these quantities are shown in fig C.1 (drawn not to scale), and are defined in the lab frame.

We additionally denote the LDSP in the * frame to be at (θ^*, ϕ^*). For a given p_{DS} and θ^*, θ_{LDSP} is given as

$$\tan\theta_{\text{LDSP}} = \frac{\sin\theta^*}{\gamma_{\text{DS}}\left(\beta_{\text{DS}}/\beta^*_{\text{LDSP}} + \cos\theta^*\right)}\,, \tag{C.3}$$

where $\beta_{\text{DS}}, \gamma_{\text{DS}}$ are the boost factors to go from $*$ to the lab frame and β^*_{LDSP} is the velocity of the LDSP with respect to the $*$ frame. Note that the boosts along the DS direction do not change ϕ. Given the width θ_{LDSP} of the lab cone there is only a range of $\phi_* = \phi_{\text{lab}}$ for which the LDSP direction intersects the detector. ϵ_{geo} is then the area (computed in the $*$ frame) of the overlap between the circular detector and all the possible LDSP cones in the lab frame, in general a function of z and of p_{DS}. To compute such area, we will make a *linearization approximation*: we will consider that in the $*$ frame the shape of allowed $\cos\theta^* - \phi^*$ is bound by straight lines and not curved ones. This approximation is expected to hold at the 10% level for the relevant boosts.

We now discuss the details specific to the three production modes considered in this work.

C.1.1 ϵ_{geo} for meson decay production

In order to find ϵ_{geo} for LDSPs in the meson case, we use the prescription explained in the section before. For this, we must boost the DS kinematic variables twice: once from the meson rest frame to the lab frame, then from the lab frame to the DS rest frame (or $*$ frame). We will denote all quantities in the meson rest frame with a subscript 0.

The energy and 3-momentum of the DS can be easily computed using momentum conservation in the parent meson rest frame as shown in eq. (3.18). Using the parent meson boost γ_M and velocity v_M (obtained from simulation), we can find the DS lab frame variables and express them as

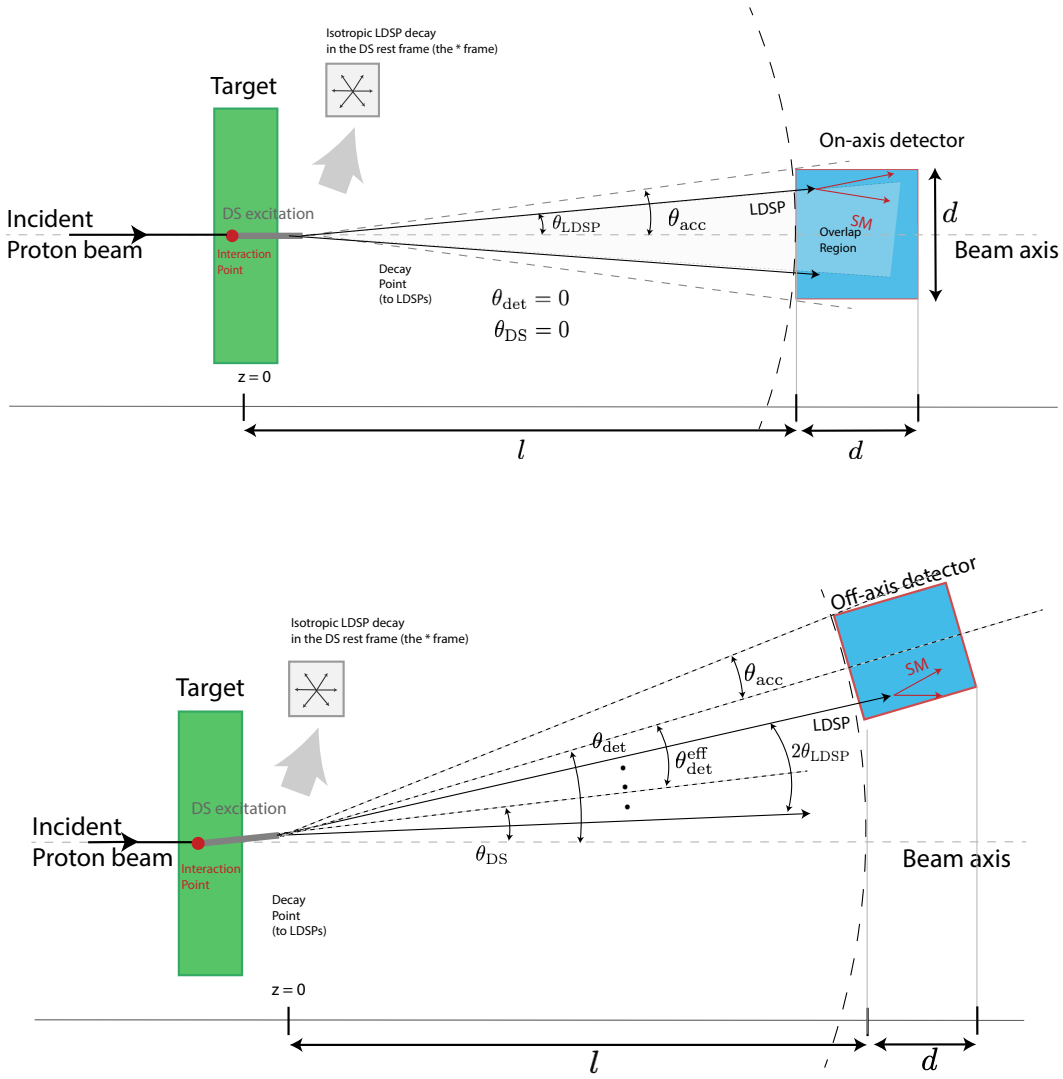

Figure C.1: The geometry relevant for the estimation of ϵ_{geo} in the on- and off-axis case (top and bottom respectively). Various quantities defined in the text, and involved in the estimation of ϵ_{geo} are shown, not to scale. In particular, the DS line (gray thick) is drawn exaggerated for clarity.

a function of $\cos\theta_0$ (angle of DS with meson flight direction in the meson rest frame, DS is isotropic in this) and p^2_{DS} i.e. $E^{\text{lab}}_{\text{DS}}(\cos\theta_0, p^2_{\text{DS}})$, $|\vec{p}^{\,\text{lab}}_{\text{DS}}|(\cos\theta_0, p^2_{\text{DS}})$.

In order to compute ϵ_{geo} we must find the θ^* values corresponding to the angular coverage of the detector. For this, we must boost the lab frame DS variables to the DS rest frame (or $*$ frame) using the DS boost given by $\gamma_{\text{DS}}(\cos\theta_0, p^2_{\text{DS}}) = E^{\text{lab}}_{\text{DS}}/\sqrt{p^2_{\text{DS}}}$ and DS velocity $\beta_{\text{DS}}(\cos\theta_0, p^2_{\text{DS}}) = |\vec{p}^{\,\text{lab}}_{\text{DS}}|/E^{\text{lab}}_{\text{DS}}$ (which will be close to 1). Note that for the annihilation decay mode $M \to \text{DS}$, $E^{\text{lab}}_{\text{DS}}$ gets fixed by momentum conservation to $\sqrt{M^2 + |\vec{p}_{\text{M}}|}$ where M is the parent meson mass, and $|\vec{p}_{\text{M}}|$ is the parent meson momentum in the lab frame. Thus, γ_{DS} is fixed to $\sqrt{M^2 + |\vec{p}_{\text{M}}|}/M$.

We can now solve for the θ^* angle using eq. (C.3), plugging $\beta^*_{\text{LDSP}} = |\vec{p}^{\,*}_{\text{LDSP}}|/E^*_{\text{LDSP}}$, $E^*_{\text{LDSP}} = \sqrt{p^2_{\text{DS}}}/n_{\text{LDSP}}$ and using $\Lambda_{\text{IR}} = \sqrt{(E^*_{\text{LDSP}})^2 - |\vec{p}^{\,*}_{\text{LDSP}}|^2}$ to get $|\vec{p}^{\,*}_{\text{LDSP}}|$.

We also need θ_{DS} for estimating ϵ_{geo}. Note that in the annihilation decay case, θ_{DS} is 0 due to momentum conservation, Whereas for the radiative decay case, θ_{DS} can be expressed in terms of

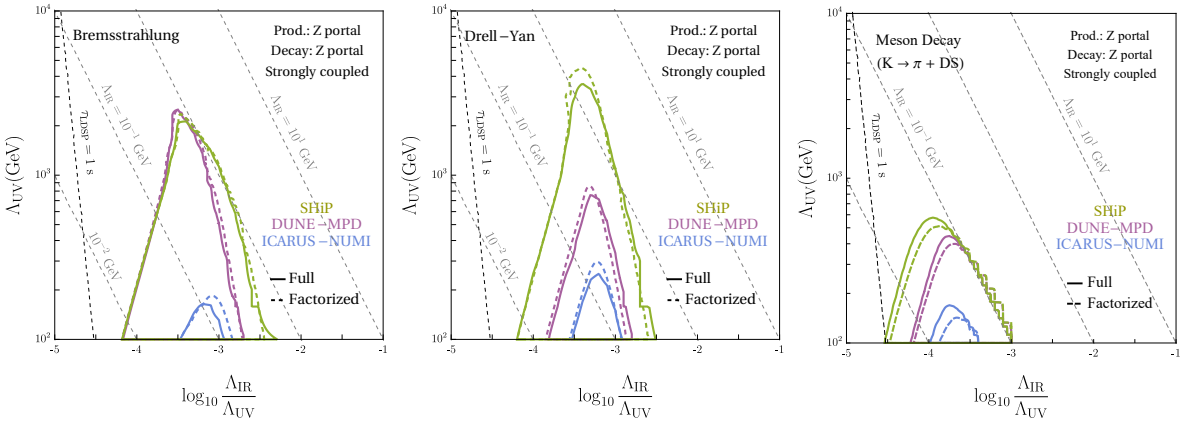

Figure C.2: Comparison of the factorized (dashed) vs full (solid) approach for production and decay through Z portal of a strongly interacting DS, for various production modes: DB (left), DY (mid) and MD (right). The experiments considered are ICARUS-NuMI (blue), DUNE-MPD (purple) and SHiP (green).

meson rest frame variables as $\tan\theta_{\rm DS} = \sin\theta_0\,|\vec{p}|_{\rm DS,0} \,/\, \Big(\gamma_M\,(|\vec{p}|_{\rm DS,0}\cos\theta_0 + v_M E_{\rm DS,0})\Big)$.

Finally, we calculate $\langle\epsilon_{\rm geo}\rangle$ by a weighted average over the differential decay width $d\Gamma/dp_{\rm DS}^2\,d\lambda_i$, which is a function of $\Lambda_{\rm IR}$ only (the $\Lambda_{\rm UV}$ dependence factors out):

$$\langle\epsilon_{\rm geo}\rangle = \frac{\int {\rm d}p_{\rm DS}^2\,{\rm d}\lambda_i\,\epsilon_{\rm geo}(\lambda_i, p_{\rm DS}^2)\,\frac{d\Gamma}{dp_{\rm DS}^2 d\lambda_i}}{\int {\rm d}p_{\rm DS}^2\,{\rm d}\lambda_i\,\frac{d\Gamma}{dp_{\rm DS}^2 d\lambda_i}}\,, \tag{C.4}$$

where λ_i are the angular variables θ_0, ϕ_0 integrated over the full range and $p_{\rm DS}^2$ is integrated in the allowed kinematic range. Note that for the annihilation decay case, $p_{\rm DS}^2 = M^2$ and $\theta_{\rm DS} = 0$ by momentum conservation, which simplifies the equation above.

C.1.2 $\epsilon_{\rm geo}$ for DY

In DY mode the DS system is by construction directed along the original beam line (the z direction). The boost of the DS system is $\gamma_{\rm DS} = E_{\rm DS}/\sqrt{p_{\rm DS}^2}$, where $E_{\rm DS}$ is the energy of the DS system in the lab frame. While $p_{\rm DS}$ is already one of the variables used in DY production, $E_{\rm DS}$ is computed by first getting the DS energy in the DY CM frame, $E_{\rm DS,CM} = \sqrt{s}(x + p_{\rm DS}^2/(sx))/2$ using the DY variables introduced in 3.2.2, and then boosting it to the lab frame with Lorentz parameter $\gamma_{\rm CM} = E_{\rm beam}/\sqrt{s}$. This gives $E_{\rm DS} = xE_{\rm beam}$. Putting everything together, the boost factor to go from the lab frame to the DS system is $\gamma_{\rm DS} = xE_{\rm beam}/\sqrt{p_{\rm DS}^2}$. To get the average value of $\epsilon_{\rm geo}$, we compute the integral as in eq. (C.4) with the appropriate distribution where now we average over the kinematic variables x and $p_{\rm DS}^2$.

C.1.3 $\epsilon_{\rm geo}$ for DB

DB mode is different from the DY mode because in general the DS system will be produced at an angle with the beam-line. We will call $\theta_{\rm DS}, \phi_{\rm DS}$ the pair of angles indicating the direction of the radiated DS system relative to the beam line. Using the kinematic variables introduced in 3.2.3, we have $\theta_{\rm DS} = \tan^{-1}(p_T/zE_{\rm beam})$. The boost factor to go from the lab to the DS frame is $\gamma_{\rm DS} \approx zE_{\rm beam}/\sqrt{p_{\rm DS}^2}$. As before, to get the average value of $\epsilon_{\rm geo}$, we average over the kinematic quantities z, p_T^2, and $p_{\rm DS}^2$. we have checked that these values are in good agreement with the $\epsilon_{\rm geo}$ for the average DS angle, as expected for very collimated DS excitations.

C.2 Factorization approximation

In this appendix, we compare the approximate method we delineated in the main text with the correct procedure of doing the integral of the product of the differential quantities ($\epsilon_{\rm geo}$, cross-section, decay probability) without factorizing them.

In order to get the correct number of signal events, the differential cross section $\mathrm{d}\sigma/\mathrm{d}\lambda_i$ must be folded with $n_{\rm LDSP}\,\epsilon_{\rm geo}\,P_{1,\rm dec}$, all of which are a function of kinematic variables λ_i:

$$N_S(\Lambda_{\rm IR},\Lambda_{\rm UV}) = \frac{N_{\rm POT}}{\sigma_{pN}} \int \mathrm{d}\lambda_i \,\frac{\mathrm{d}\sigma}{\mathrm{d}\lambda_i}\, n_{\rm LDSP}\,\epsilon_{\rm geo}\,P_{1,\rm dec}\,. \tag{C.5}$$

We call this procedure the *full* approach. We compute the integrals numerically, using the CUBA integration tools [226]. The method used in the main text is done instead by replacing the full integral with the average $\epsilon_{\rm geo}$ and using average kinematic quantities to estimate the decay probability and the average $n_{\rm LDSP}$[2]:

$$N_S \approx N_{\rm POT}\,\frac{\sigma_S}{\sigma_{pN}}\, n_{\rm LDSP}(\langle\lambda_i\rangle)\,P_{1,\rm dec}(\langle\lambda_i\rangle)\,\langle\epsilon_{\rm geo}\rangle\,. \tag{C.6}$$

where the average is defined by a weighted integral over the differential cross-section/decay-width (e.g. see eq. (C.4)). We call this approach the *factorized* approach. The advantage of this approach is that the production integral must be done only once, and not repeated for each $(\Lambda_{\rm IR},\Lambda_{\rm UV})$ pair: the dependence on them is essentially factorized. In particular, for a fixed production portal, this allows changing the decay portal, without having to redo the production integral from scratch. This is particularly useful when exploring all the various combinations of production and decay portals.

To compare the factorized and the full approach, and to show that the factorized approach is very efficient, in fig. C.2 we show the comparison for DB, DY and radiative meson decay $K \to \pi + \mathrm{DS}$, for the strongly coupled DS, for DUNE, SHiP and ICARUS. The two approaches are in very good agreement. The factorized approach is conservative at most, and can miss rare events appearing in the tails of distributions (see e.g. ref. [227]). However for the purposes of the present work, the factorized approach suffices.

[2]We have checked that this procedure agrees very well (percent level) to a true average of $n_{\rm LDSP}$.

Appendix D

Classification Results: Viable Models

In this section, we tabulate all the viable models that pass the requirements discussed in Section 5.1.

D.1 SU$(N)_{DC}$ Models

Here we tabulate the models for $SU(N)_{\rm DC}$. Each table below gives the viable model passing our model building criteria, the allowed number of dark colours $N_{\rm DC}$, the DM candidate as well and the parent GUT theory needed to embed the low energy model.

Models with T

The perturbativity condition on $U(1)_Y$ hypercharge sets an upper bound on the number of dark colours, $N_{\rm DC} < 5$. Furthermore, for $N_{\rm DC} = 3$, $SU(2)_L$ and $U(1)_Y$ perturbativity forbid the presence of any additional electroweak triplet, hence combinations with V, $\tilde{T}$, and $E \oplus \tilde{E}$ cannot work as low energy models. Moreoever, the following $SU(3)_{\rm DC}$ models:

$$T, \quad T \oplus \tilde{L}, \quad T \oplus E, \quad T \oplus \tilde{E}, \quad T \oplus \tilde{L} \oplus E \tag{D.1}$$

contain no DM candidate and are not further considered. Finally, for $N_{\rm DC} = 4$ only N can be added.

Model	Range for $N_{\rm DC}$	DM candidate	Parent theory
$T \oplus N$	$N_{\rm DC} = 3, 4$	$N^{N_{\rm DC}}$	$15 \oplus 1$(or 24)
$T \oplus L(\oplus N)$	$N_{\rm DC} = 3$	$TLL\,(, NNN)$	$\overline{5} \oplus 15 \oplus 5 \oplus 1$(or 24)
$T \oplus \tilde{L} \oplus N$	$N_{\rm DC} = 3$	NNN	$5 \oplus 15 \oplus 1$(or 24)
$T \oplus E \oplus N$	$N_{\rm DC} = 3$	NNN	$10 \oplus 15 \oplus 1$(or 24)
$T \oplus \tilde{E} \oplus N$	$N_{\rm DC} = 3$	NNN	$\overline{10} \oplus 15 \oplus \overline{5} \oplus 1$(or 24)
$T \oplus L \oplus \tilde{L}(\oplus N)$	$N_{\rm DC} = 3$	$TLL\,(, NNN,\, NL\tilde{L})$	$\overline{5} \oplus 15 \oplus 5(\oplus 1$ or 24)
$T \oplus L \oplus E(\oplus N)$	$N_{\rm DC} = 3$	$TLL,\, LLE(, NNN)$	$\overline{5} \oplus 10 \oplus 15 \oplus 1 \oplus 5$
$T \oplus L \oplus \tilde{E}(\oplus N)$	$N_{\rm DC} = 3$	$TLL(, NNN)$	$\overline{5} \oplus \overline{10} \oplus 15 \oplus 1 \oplus 5$
$T \oplus \tilde{L} \oplus E \oplus N$	$N_{\rm DC} = 3$	NNN	$15 \oplus 5 \oplus 10 \oplus 1($ or 24)
$T \oplus \tilde{L} \oplus \tilde{E}(\oplus N)$	$N_{\rm DC} = 3$	$\tilde{L}\tilde{L}\tilde{E}(, NNN)$	$15 \oplus 5 \oplus \overline{10} \oplus 1 \oplus \overline{5}$

Models with V

$V^{N_{DC}}$ is always a good DM candidate for any $N_{\rm DC}$. In the table below in the third column, we list any additional DM candidates in the theory. The DM candidates are written as gauge singlet components where the indices $n,\ m,\ l,\ h$ can take any integer values from 0 and should sum up to the total number of dark colours $N_{\rm DC}$.

Model	Range for $N_{\rm DC}$	DM candidate	Parent theory
$V(\oplus N)$	$N_{\rm DC} \leq 4$	$V^n N^m$	24
$V \oplus L(\oplus N)$	$N_{\rm DC} = 3$	$V^n N^m$	$24 \oplus \overline{5}$
$V \oplus E(\oplus N)$	$N_{\rm DC} \leq 4$	$V^n N^m$	$24 \oplus 10$
$V \oplus L \oplus \tilde{L}(\oplus N)$	$N_{\rm DC} = 3$	$V^n N^m (\tilde{L}L)^l$	$24 \oplus \overline{5} \oplus 5$
$V \oplus L \oplus E(\oplus N)$	$N_{\rm DC} = 3$	$V^n N^m (LLE)^l$	$24 \oplus \overline{5} \oplus 10$
$V \oplus L \oplus \tilde{E}(\oplus N)$	$N_{\rm DC} = 3$	$V^n N^m$	$24 \oplus \overline{5} \oplus \overline{10}$
$V \oplus E \oplus \tilde{E}(\oplus N)$	$N_{\rm DC} \leq 4$	$V^n N^m (\tilde{E}E)^l$	$24 \oplus \overline{10} \oplus 10$
$V \oplus L \oplus \tilde{L} \oplus E(\oplus N)$	$N_{\rm DC} = 3$	$V^n N^m (\tilde{L}L)^l$	$24 \oplus \overline{5} \oplus 5 \oplus 10$
$V \oplus L \oplus E \oplus \tilde{E}(\oplus N)$	$N_{\rm DC} = 3$	$V^n N^m (\tilde{E}E)^l$	$24 \oplus \overline{5} \oplus \overline{10} \oplus 10$
$V \oplus L \oplus \tilde{L} \oplus E \oplus \tilde{E}(\oplus N)$	$N_{\rm DC} = 3$	$V^n N^m (\tilde{L}L)^n (\tilde{E}E)^h$	$24 \oplus \overline{5} \oplus 5 \oplus \overline{10} \oplus 10$

Models with E

The models with dark fermionic content given by E and $E \oplus \tilde{L}$ have no DM candidate, hence they are not good models. The DM candidates are written as gauge singlet components where the indices $n,\ m,\ l,\ h$ can take any integer values from 0 and should sum up to the total number of dark colours $N_{\rm DC}$.

Model	Range for $N_{\rm DC}$	DM candidate	Parent theory
$E \oplus N$	$N_{\rm DC} \leq 13$	$N^{N_{\rm DC}}$	$10 \oplus 1$(or 24)
$E \oplus L(\oplus N)$	$N_{\rm DC} \leq 9$	$(LLE)^n N^m$	$\overline{5} \oplus 10(\oplus 1$ or 24)
$E \oplus \tilde{L} \oplus N$	$N_{\rm DC} \leq 9$	$N^{N_{\rm DC}}$	$10 \oplus \overline{5} \oplus 1$(or 24)
$E \oplus \tilde{E}(\oplus N)$	$N_{\rm DC} \leq 6$	$(E\tilde{E})^n N^m$	$10 \oplus \overline{10}(\oplus 1$ or 24)
$E \oplus L \oplus \tilde{L}(\oplus N)$	$N_{\rm DC} \leq 6$	$(E\tilde{E})^n (LLE)^m N^l$	$10 \oplus 5 \oplus \overline{5}(\oplus 1$ or 24)
$E \oplus L \oplus \tilde{E}(\oplus N)$	$N_{\rm DC} \leq 5$	$(L\tilde{L})^n (LLE)^m N^l$	$10 \oplus \overline{5} \oplus \overline{10}(\oplus 1$ or 24)
$E \oplus L \oplus \tilde{E} \oplus \tilde{L}(\oplus N)$	$N_{\rm DC} \leq 4$	$(E\tilde{E})^n (L\tilde{L})^m (LLE)^l N^h$	$10 \oplus \overline{5} \oplus \overline{10} \oplus 5(\oplus 1$ or 24)

Models with L

The model L has no DM candidate. The integer indices will sum as $n + m = N_{\rm DC}$ where $N_{\rm DC}$ is the allowed number of dark colours.

Model	Range for $N_{\rm DC}$	DM candidate	Parent theory
$L \oplus N$	$N_{\rm DC} \leq 18$	$N^{N_{\rm DC}}$	$\overline{5} \oplus 1$(or 24)
$L \oplus \tilde{L}(\oplus N)$	$N_{\rm DC} \leq 9$	$(L\tilde{L})^n N^m$	$\overline{5} \oplus 5 \oplus 1$(or 24)

Coloured dark fermion models

Good DM models can be built only out of combinations of $Q,\ \tilde{U},\ \tilde{D}$. No DM candidate can exist for $\tilde{U} \oplus Q$, since the hypercharges of the two are of the same sign. We are thus left with the following possibilities:

Model	Range for $N_{\rm DC}$	DM candidate	Parent theory
$Q \oplus \tilde{D}$	$N_{\rm DC} = 3$	$QQ\tilde{D}$	$5 \oplus 10$
$Q \oplus \tilde{D} \oplus \tilde{U}$	$N_{\rm DC} = 3$	$QQ\tilde{D},\ \tilde{D}\tilde{D}\tilde{U}$	$5 \oplus 10 \oplus \overline{10}$
$\tilde{D} \oplus \tilde{U}$	$N_{\rm DC} = 3,\ 6$	$\tilde{D}\tilde{D}\tilde{U},\ \tilde{D}\tilde{D}\tilde{U}\tilde{D}\tilde{D}\tilde{U}$	$5 \oplus 10 \oplus \overline{10}$

Note that for the $\tilde{D} \oplus \tilde{U}$ model, dark colour confinement and perturbativity can allow for a larger number of dark colours upto $N_{\rm DC} \leq 8$. However, the requirement for a gauge singlet DM candidate selects only two allowed values of $N_{\rm DC}$ given by $3, 6$. A similar conclusion applies to the $Q \oplus \tilde{D}$ and $Q \oplus \tilde{D} \oplus \tilde{U}$ models.

D.2 $\mathbf{SO}(N)_{DC}$ Models

Models with T

Dark color asymptotic freedom requires $N_{DC} > 3$, however the condition on SMS hypercharge perturbativity forces $N_{DC} < 5$. Hence, only $N_{\rm DC} = 4$ is allowed. Note that for $SO(N)_{DC}$ we do not impose the stronger constraint on $N_{\rm DF}$ coming from confinement. The model with T alone is not allowed because there is no operator up to dimension-6 breaking the leftover $U(1)$ species symmetry responsible for TT states stability.

Model	Range for $N_{\rm DC}$	DM candidate	Higher dimensional operators	Parent theory
$T \oplus N$	$N_{\rm DC} = 4$	$(T\overline{T})^2,\ T\overline{T}NN$	$\overline{T}^i N H^{c\dagger} \sigma^i H$	$\overline{15} \oplus 15 \oplus 1/24$

Models with V

$V^{N_{DC}}$ is always a good DM candidate. Below we shall list the additional DM candidates as well as the higher dimensional operators required to break species symmetries and the limits on N_{DC}.

Model	Range for $N_{\rm DC}$	DM candidate	Higher dim operators	Parent theory
V	$N_{\rm DC} \leq 4$	$V^{N_{\rm DC}}$	/	24
$V \oplus L$	$4 \leq N_{\rm DC} \leq 6$	$(\overline{L}L)^n V^m$	/	$24 \oplus \overline{5} \oplus 5$
$V \oplus E$	$N_{\rm DC} \leq 9$	$(\overline{E}E)^n V^m$	$\overline{E} V^i H^{c\dagger} \sigma^i H$	$24 \oplus \overline{10} \oplus 10$
$V \oplus E \oplus L$	$4 \leq N_{\rm DC} \leq 6$	$(\overline{L}L)^n (\overline{E}E)^m V^l$	as $V \oplus E$	$24 \oplus \overline{5} \oplus 5 \oplus \overline{10} \oplus 10$
$V \oplus N$	$N_{\rm DC} \leq 9$	$V^n N^m$	/	24
$V \oplus L \oplus N$	$4 \leq N_{\rm DC} \leq 6$	$(\overline{L}L)^n V^m N^l$	/	$24 \oplus 5 \oplus \overline{5}$
$V \oplus E \oplus N$	$4 \leq N_{\rm DC} \leq 9$	$(\overline{E}E)^n V^m N^l$	as $V \oplus E$	$24 \oplus \overline{10} \oplus 10 \oplus \overline{5} \oplus 5$
$V \oplus E \oplus L \oplus N$	$4 \leq N_{\rm DC} \leq 6$	$(\overline{L}L)^n (\overline{E}E)^m V^l N^h$	as $V \oplus E \oplus L$	$24 \oplus 10 \oplus \overline{10} \oplus 5 \oplus \overline{5}$

Models with E

The model with $\Psi = E$ is not a good DM model, since there once again there operator that can break the $U(1)$ species symmetry under which EE is stable. Since dark fermions transform as real representations under $O(N)_{DC}$ dark colour, $\bar{E}$ can be substituted with E, which renders the meson EE stable (which is an allowed dark colour singlet state in $SO(N)_{DC}$ theories).

Models with $(LLE)^l$ combining the DM candidates have odd $N_{\rm DC}$, due to the flavor neutrality assumption on the DM candidate in the case of even $N_{\rm DC}$.

Model	Range for $N_{\rm DC}$	DM candidate	Higher dim operators	Parent theory
$E \oplus L$	$4 \leq N_{\rm DC} \leq 9$	$(\overline{E}E)^n(\overline{L}L)^m(LLE)^l$	$E\overline{L}HHH$	$\overline{5} \oplus 5 \oplus \overline{10} \oplus 10$
$E \oplus N$	$3 \leq N_{\rm DC} \leq 13$	$(\overline{E}E)^n N^m$	$\overline{E}\gamma^\mu N H^{c\dagger} D_\mu H$	$24 \oplus 10 \oplus \overline{10} \oplus 5 \oplus \overline{5}$
$E \oplus L \oplus N$	$4 \leq N_{\rm DC} \leq 9$	$(\overline{E}E)^n(\overline{L}L)^m N^l$	$E\overline{L}HHH$	$24 \oplus \overline{10} \oplus 10 \oplus 5 \oplus \overline{5}$

Models with L

For model $\Psi = L$, the DM candidate exists for n even.

Model	Range for $N_{\rm DC}$	DM candidate	Higher dimensional operators	Parent theory
L	$3 \leq N_{\rm DC} \leq 18$	$(\overline{L}L)^n$	$LLHH$	$\overline{5} \oplus 5$
$L \oplus N$	$3 \leq N_{\rm DC} \leq 18$	$(\overline{L}L)^n N^m$	/	$24 \oplus \overline{5} \oplus 5$

Colored dark fermion models

From the list of allowed operators, we can see that in no model with $\Psi = U$, D, Q all the species symmetries can be broken. Similarly to $\Psi = S$, dark color and $SU(3)_c$ perturbativity are not compatible. Hence, the only representation allowed is $\Psi = G$ which leads to the following model:

Model	Range for $N_{\rm DC}$	DM candidate	Higher dimensional operators	Parent theory
$G(\oplus N)$	$N_{\rm DC} = 4, 5$	$G^n N^m$	/	24

Appendix E

Unification Checks

We summarise the gauge coupling unification analysis that we performed for each viable DM model under our criteria given by:

(i) $\tilde{M}_{GUT} \geq M_{GUT}^{SM}$,

(ii) $\mathcal{A}_{\Delta} \leq \mathcal{A}_{SM}$,

(iii) $\alpha_{GUT} < 4\pi$.

In the Table below, the first column gives the light dark fermionic content of the model and the second column reports whether the model passes or fails the unification check. In case the model passes the check, we have given the allowed values of M_H. In case the model fails the check, we have reported the unification condition that is not satisfied along with the values of M_H. We consider all the heavy GUT partners are degenerate in mass denoted by M_H. For example, the first row depicts the $L \oplus E$ model, and the entry in the second column conveys that the model does not work for unification due to $M_{GUT} < M_{GUT}^{SM}$ for $M_H > 10^5$ GeV.

E.1 $\mathbf{SU}(N)_{\mathbf{DC}}$ Models

Model	Unification Check
LLE	
$L \oplus E$	(i) $M_H > 10^5$ GeV
$L \oplus E \oplus \tilde{E}$	(i) $M_H > 10^5$ GeV, (ii) $M_H > 10^5$ GeV, (iii) $M_H \leq 10^6$ GeV.
$L \oplus E \oplus \tilde{L}$	(i) $M_H > 10^5$ GeV, (ii) $M_H \geq 10^{14}$ GeV
$L \oplus E \oplus V$	(i) $M_H > 10^5$ GeV, (ii) $M_H \geq 10^8$ GeV, (iii) $M_H \leq 10^9$ GeV.
$L \oplus E \oplus N$	Same as $L \oplus E$
$L \oplus E \oplus \tilde{E} \oplus \tilde{L}$	(i) $M_H > 10^5$ GeV, (iii) $M_H < 10^7$ GeV.
$L \oplus E \oplus \tilde{E} \oplus V$	(i) $M_H > 10^5$ GeV, (ii) $M_H \geq 10^8$ GeV, (iii) $M_H \leq 10^9$ GeV.
$L \oplus E \oplus \tilde{E} \oplus N$	Same as $L \oplus E \oplus \tilde{E}$
$L \oplus E \oplus \tilde{L} \oplus V$	(i) $M_H > 10^5$ GeV, (ii) $M_H \geq 10^7$ GeV, (iii) $M_H \leq 10^8$ GeV.
$L \oplus E \oplus \tilde{L} \oplus N$	Same as $L \oplus E \oplus \tilde{L}$
$L \oplus E \oplus \tilde{E} \oplus \tilde{L} \oplus V$	(i) $M_H > 10^5$ GeV, (ii) $M_H \geq 10^8$ GeV, (iii) $M_H \leq 10^8$ GeV.

$L \oplus E \oplus \tilde{E} \oplus \tilde{L} \oplus N$	Same as $L \oplus E \oplus \tilde{E} \oplus \tilde{L}$
$L \oplus E \oplus T$	(i) $M_H > 10^5$ GeV, (ii) $M_H \geq 10^9$ GeV, (iii) $M_H < 10^8$ GeV.
$L \oplus E \oplus N \oplus T$	(i) $M_H > 10^5$ GeV, (ii) $M_H \geq 10^9$ GeV, (iii) $M_H < 10^8$ GeV.
LLT	
$L \oplus T$	(i) $M_H > 10^5$ GeV, (ii) $M_H \geq 10^8$ GeV, (iii) $M_H < 10^8$ GeV.
$L \oplus T \oplus \tilde{L}$	(i) $M_H > 10^5$ GeV, (ii) $M_H \geq 10^8$ GeV, (iii) $M_H < 10^8$ GeV.
$L \oplus T \oplus \tilde{E}$	(i) $M_H > 10^5$ GeV, (ii) $M_H \geq 10^8$ GeV, (iii) $M_H < 10^8$ GeV.
$L \oplus T \oplus N$	(i) $M_H > 10^5$ GeV, (ii) $M_H \geq 10^8$ GeV, (iii) $M_H < 10^7$ GeV.
$L \oplus T \oplus \tilde{L} \oplus N$	(i) $M_H > 10^5$ GeV, (ii) $M_H \geq 10^8$ GeV, (iii) $M_H < 10^8$ GeV.
$L \oplus T \oplus N \oplus \tilde{E}$	Same as $L \oplus T \oplus \tilde{E}$
$N \oplus L \oplus \tilde{L}$	(i) $M_H > 10^5$ GeV, (ii) $M_H \geq 10^{12}$ GeV
$NL\tilde{L}$ or $NE\tilde{E}$	
$N \oplus E \oplus \tilde{E}$	(i) $M_H > 10^5$ GeV, (ii) $M_H > 10^5$ GeV, (iii) $M_H \leq 10^6$ GeV.
VVV, VVN, VNN	
V	(i) $M_H > 10^5$ GeV, (ii) $M_H \geq 10^8$ GeV, (iii) $M_H < 10^9$ GeV. (iii) fails for $M_H < 3.5 \times 10^8$ GeV,
$V \oplus N$	Same as V
$V \oplus L$	(i) $M_H > 10^5$ GeV, (ii) $M_H \geq 10^8$ GeV, (iii) $M_H \leq 10^8$ GeV.
$V \oplus \tilde{E}$	(i) $M_H > 10^5$ GeV, (ii) $M_H \geq 10^8$ GeV, (iii) $M_H \leq 10^9$ GeV.
$V \oplus \tilde{E} \oplus L$	(i) $M_H > 10^5$ GeV, (ii) $M_H \geq 10^8$ GeV, (iii) $M_H \leq 10^9$ GeV.
NNN	
N ($N \in 24$)	$\tilde{M}_{GUT} = \tilde{M}^{SM}_{GUT}$, $A_\Delta = A_{SM}$, $\alpha_{GUT} < 4\pi$ for $M_H \geq 10^9$ GeV.
$N \oplus L$	(i) $M_H > 10^5$ GeV, (iii) $M_H \leq 10^9$ GeV.
$N \oplus \tilde{E}$	(i) $M_H > 10^5$ GeV, (ii) $M_H > 10^5$ GeV, (iii) $M_H \leq 10^9$ GeV.
NNN	
$N \oplus T$	(i) $M_H > 10^5$ GeV, (ii) $M_H \geq 10^9$ GeV, (iii) $M_H \leq 10^8$ GeV.
$N \oplus L \oplus \tilde{E}$	(i) $M_H > 10^5$ GeV, (ii) $M_H \leq 10^9$ GeV.
$N \oplus L \oplus \tilde{T}$	(i) $M_H > 10^5$ GeV, (ii) $M_H \geq 10^8$ GeV, (iii) $M_H \leq 10^8$ GeV.
$N \oplus \tilde{E} \oplus T$	(i) $M_H > 10^5$ GeV, (ii) $M_H \geq 10^{10}$ GeV, (iii) $M_H \leq 10^8$ GeV.
$N \oplus \tilde{E} \oplus \tilde{T}$	(i) $M_H > 10^5$ GeV, (ii) $M_H \geq 10^{10}$ GeV, (iii) $M_H \leq 10^8$ GeV
$N \oplus T \oplus E \oplus \tilde{L}$	(i) $M_H > 10^5$ GeV, (iii) always fails
$QQ\tilde{D}$	
$Q \oplus \tilde{D}$, ($Q \in 10$)	$5 \times 10^{14} > M_H > 6.5 \times 10^6$ for $M_P > \tilde{M}_{GUT} > 3 \times 10^{15}$ GeV
$Q \oplus \tilde{D}$, ($Q \in 15$)	$M_H \geq 3.9 \times 10^{11}$ GeV for $\alpha_{GUT} < 4\pi$ 5×10^{14} GeV $> M_H > 6.5 \times 10^6$ GeV for $M_P > \tilde{M}_{GUT} > 3 \times 10^{15}$ GeV
$Q \oplus \tilde{D} \oplus \tilde{U}$	(ii) $M_H > 10^5$ GeV, (iii) $M_H \leq 10^9$ GeV
DDU	
$D \oplus U$	(ii) $M_H > 10^5$ GeV (iii) $M_H < 10^7$ GeV
$\tilde{L}L\tilde{L}L$	
$\tilde{L} \oplus L$	(i) $M_H > 10^5$ GeV, (ii) $M_H \geq 10^{10}$ GeV

$\tilde{L} \oplus L \oplus N (N \in 24)$	(i) $M_H > 10^5$ GeV, (ii) $M_H \geq 10^{10}$ GeV, (iii) $M_H \leq \times 10^9$ GeV
$\tilde{E}E\tilde{E}E$	
$\tilde{E} \oplus E$	All conditions always fail

Table E.1: Viable SU(N) models checked for unification along with the respective failing unification condition for models not good for unification under our criteria.

E.2 $\mathbf{SO}(N)_{\mathbf{DC}}$ Models

Model	Unification Check
Models with T	
$N \oplus T$	(i) $M_H > 10^5$ GeV, (ii) $M_H \geq 10^8$ GeV, (iii) $M_H < 10^9$ GeV.
Models with V	(M_H constraints for min N_{DC} allowed)
V	(i) $M_H > 10^5$ GeV, (ii) $M_H \geq 10^{10}$ GeV.
$V \oplus N$	Same as V
$V \oplus L$	(i) $M_H > 10^5$ GeV, (ii) $M_H \geq 10^8$ GeV, (iii) $M_H \leq 10^7$ GeV
$V \oplus E$	(i) $M_H > 10^5$ GeV, (ii) $M_H \geq 10^{10}$ GeV, (iii) $M_H \leq 10^8$ GeV
$V \oplus E \oplus L$	(i) $M_H > 10^5$ GeV, (ii) $M_H \geq 10^9$ GeV, (iii) $M_H \leq 10^8$ GeV
$V \oplus E \oplus N$	(i) $M_H > 10^5$ GeV, (ii) $M_H \geq 10^{10}$ GeV, (iii) $M_H \leq 10^8$ GeV
$V \oplus L \oplus N$	Same as $V \oplus L$
$V \oplus L \oplus E \oplus N$	Same as $V \oplus L \oplus E$
Models with E	(M_H constraints for min N_{DC} allowed)
$E \oplus N$	(i) $M_H > 10^5$ GeV, (ii) $M_H \geq 10^6$ GeV, (iii) $M_H < 10^8$ GeV
$E \oplus L$	(i) $M_H > 10^5$ GeV
$E \oplus L \oplus N$	(i) $M_H > 10^5$ GeV, (iii) $M_H \leq 10^8$ GeV
Models with L	(M_H constraints for min N_{DC} allowed)
L	(i) $M_H > 10^5$ GeV
$L \oplus N$	(i) $M_H > 10^5$ GeV.
Models with G	(M_H constraints for min N_{DC} allowed)
G	(i) $M_H > 10^5$ GeV, (ii) $M_H \geq 10^5$ GeV, (iii) $M_H \leq 10^{10}$ GeV

Table E.2: Viable SO(N) models checked for unification along with the respective failing unification condition for models not good for unification under our criteria.

Appendix F

Mass Splitting

Here, we consider our benchmark model $Q \oplus \tilde{D}$ and aim at the production of a natural hierarchy of scales in the theory of $m_Q, m_{\tilde{D}} \ll M_H = m_{\tilde{L}}, m_U, m_E$. For this, we compute the mass spectrum at tree level and including dimension-5 contributions coming from scalars in our SU(5) level theory. We find that this is not possible and a natural mass hierarchy between the light dark fermions and their GUT partners cannot be obtained. For the mass spectrum in this appendix, we choose the parent GUT theory given by $5 \oplus 10$.

Using Yukawa couplings

We first consider the possibility of using contributions coming from the Yukawa couplings with the SU(5) scalars available to us. In addition, we also include contributions from dimension-5 operators with two scalars. These can give substantial contribution to the mass spectrum if the tree level mass parameters $m_{5,10}$ and $y_{5,10}$ are small and if $v_{\rm GUT} \sim \Lambda$ where $v_{\rm GUT}$ is the vev of the GUT breaking scalar and Λ is the scale suppressing the dimension-5 operator in the GUT Lagrangian. We consider various combinations of SU(5)-breaking scalars in SU(5) representations containing an SM singlet.

In general, the role of the higgs-like scalar required for SU(5) breaking can be played by a scalar in any other higher dimensional SU(5) representation, in addition to the minimal case with scalar in 24_H. However, requiring that the addition of this scalar does not give a Landau pole for the GUT coupling $\alpha_{\rm GUT}$ below $M_{\rm P}$ puts a constraint on the Dynkin index of this GUT-breaking scalar's representation:

$$T_s(R_s) = 6\left(\frac{85}{6} - \frac{4}{3}N_{DC}\sum_f T_f(R_f) + 2\pi\frac{\alpha_{\rm GUT}}{\log\left(\frac{M_{\rm Pl}}{M_{\rm GUT}}\right)}\right) \tag{F.1}$$

where $T_f(R_f)$ denotes the dynkin index of the (Dirac) fermion representation R_f (for Weyl or Majorana fermions $\frac{4}{3}$ must be replaced with $\frac{2}{3}$). Note that $\alpha_{\rm GUT}$ would depend on the mass of the GUT fermions M_H.

For the $Q \oplus \tilde{D}$ model, the highest allowed value of $T_s(R_s)$ is 500. The lowest SU(5) representation containing an SM singlet and fulfilling Eq. (F.1) is 200 ($T_s(R_s) = 100$). In addition, we also have the possibility of considering combinations of scalars upto $200 + 75 + 24$. We will now consider each case separately, starting with the minimal case of the GUT breaking scalar in the adjoint 24 of $SU(5)$:

- $\mathbf{\Phi_{24}}$:

The $SU(5)$ breaking scalar present in the minimal $SU(5)$ GUT theory is the one in the adjoint. The SM preserving vev $\langle\Phi\rangle$ for this 24-dimensional scalar is given by:

$$\langle\Phi\rangle^i_j = \frac{1}{\sqrt{30}} v_{\rm GUT}\ \mathrm{diag}(2,2,2,-3,-3) \tag{F.2}$$

From hereon, we denote the dark fermions as entire GUT multiplets using $q^i \in 5$ and $A^{ij} \in 10$ and write the $SU(5)$ invariant mass terms along with Yukawa interactions including also nonrenormalizable operators at the dimension-5 level:

$$\begin{aligned}\mathcal{L} = {} & m_5 \bar{q}_i q^j \delta^i_j + y_5 \bar{q}_i q^j \Phi^i_j + y_{10} \bar{A}_{ij} A^{jk} \Phi^i_k + m_{10} \bar{A}_{ij} A^{jk} \delta^i_k + \frac{c_1}{\Lambda} \bar{q}_i q^i \Phi^m_n \Phi^n_m \\ & + \frac{c_2}{\Lambda} \bar{A}_{ij} A^{ij} \Phi^m_n \Phi^n_m + \frac{d_1}{\Lambda} \bar{q}_i q^j \Phi^i_n \Phi^n_j + \frac{d_2}{\Lambda} \bar{A}_{im} A^{jm} \Phi^i_n \Phi^n_j + \frac{d_3}{\Lambda} \bar{A}_{ij} A^{mn} \Phi^i_m \Phi^j_n\end{aligned} \tag{F.3}$$

After SSB of $SU(5)$ down to SM, the 24-dimensional scalar takes its vev value given in Eq. F.2 and we get the following mass spectrum:

$$\begin{aligned} m_{\tilde{D}} &= m_5 + \frac{2}{\sqrt{30}} y_5 v_{\rm GUT} + \frac{1}{30} \frac{v^2_{\rm GUT}}{\Lambda} (30c_1 + 4d_1) \\ m_{\tilde{L}} &= m_5 - \frac{3}{\sqrt{30}} y_5 v_{\rm GUT} + \frac{1}{30} \frac{v^2_{\rm GUT}}{\Lambda} (30c_1 + 9d_1) \\ m_U &= m_{10} + \frac{2}{\sqrt{30}} y_{10} v_{\rm GUT} + \frac{1}{30} \frac{v^2_{\rm GUT}}{\Lambda} (30c_2 + 4d_1 + 4d_3) \\ m_E &= m_{10} - \frac{3}{\sqrt{30}} y_{10} v_{\rm GUT} + \frac{1}{30} \frac{v^2_{\rm GUT}}{\Lambda} (30c_2 + 9d_2 + 9d_3) \\ m_Q &= m_{10} - y_{10} \frac{v_{\rm GUT}}{\sqrt{30}} + \frac{1}{30} \frac{v^2_{\rm GUT}}{\Lambda} (30c_2 + \frac{13}{2} d_2 - 6d_3) \end{aligned} \tag{F.4}$$

Here $\Lambda = M_{\rm P}$ is the scale by which the dimension-5 operators are suppressed. From the mass spectrum in Eq. (F.4) we can see that the Yukawa couplings with the 24-dimensional scalar give a comparable contribution to both the light fermions Q and $\tilde{D}$ as well as the GUT partners U, E, and $\tilde{L}$.

- $\mathbf{\Phi_{75}}$:

  The role of the 24-dimensional scalar can be replaced by a scalar in the $SU(5)$-representation 75 (See Ref. [228] and references within). The 75-dimensional GUT scalar is described by a rank-4 tensor (twice covariant and twice contracovariant) traceless in pairs of upper and lower indices and anti-symmetric in both upper and lower pairs of indices separately. We can thus, write:

$$\Phi^{ij}_{mn} = -\Phi^{ji}_{mn} = -\Phi^{ij}_{nm}, \quad \Phi^{ij}_{in} = 0 \quad \text{where} \quad (i,j,... = 1,...5) \tag{F.5}$$

  The decomposition of 75-dimensional tensor wrt the SM gauge group $SU(3) \times SU(2) \times U(1)$ subgroup is:

$$75 = (1,1,0) + (8,1,0) + (8,3,0) + (3,2,-5/6) + (\bar{6},2,-5/6) + (\bar{3},1,-5/3) \tag{F.6}$$

  The SM-preserving sub-tensor $(1,1,0)$ for the 75-dimensional tensor is given by [228]:

$$\langle\Phi\rangle^{ij}_{mn} = s_{\rm GUT}[(\delta^\alpha_\gamma \delta^\beta_\delta - \delta^\alpha_\delta \delta^\beta_\gamma) + 3(\delta^a_c \delta^b_d - \delta^a_d \delta^b_c) - (\delta^\alpha_\gamma \delta^b_d - \delta^\alpha_\gamma \delta^b_c + \delta^\beta_\delta \delta^a_c - \delta^\beta_\gamma \delta^a_d)] \tag{F.7}$$

where we have used the conventional index splitting given by:

$$i, j, m, n \to (\alpha, a), (\beta, b), (\gamma, c), (\delta, d) \tag{F.8}$$

$$\alpha, \beta, \gamma, \delta = 1, 2, 3 \qquad a, b, c, d = 4, 5 \tag{F.9}$$

Here, $s_{\rm GUT}$ is the vev of the 75-dimensional GUT breaking scalar. In the index splitting notation $\alpha, \beta, \gamma, \delta$ are $SU(3)$ indices $1, 2, 3$, and a, b, c, d are $SU(2)$ indices $4, 5$. Thus, in our notation, the sub-tensor in Eq. F.7 has three blocks: the first where i, j, m, n can run over only $SU(3)$ indices, the second block where i, j, m, n can run over only $SU(2)$ indices and the last block where the indices can be mixed.

For this case, we have only one SU(5) invariant Yukawa term given by contractions of $\bar{10}_{\rm F} 10_{\rm F} \langle 75_{\rm H} \rangle$. Including the dimension-5 contributions, we get:

$$\begin{aligned}\mathcal{L} = {} & m_5 \bar{q}_i q^j \delta^i_j + m_{10} \bar{A}_{ij} A^{ij} + y' \bar{A}_{mn} A^{ij} \Phi^{mn}_{ij} + \frac{f_1}{\Lambda} \bar{q}_i q^i \Phi^{mn}_{rs} \Phi^{rs}_{mn} + \frac{f_2}{\Lambda} \bar{A}_{ij} A^{ij} \Phi^{mn}_{rs} \Phi^{rs}_{mn} \\ & + \frac{t_1}{\Lambda} \bar{q}_i q^j \Phi^{mi}_{rs} \Phi^{rs}_{mj} + \frac{t_2}{\Lambda} \bar{A}_{im} A^{jm} \Phi^{ni}_{rs} \Phi^{rs}_{nj} + \frac{t_3}{\Lambda} \bar{A}_{ij} A^{mn} \Phi^{ij}_{rs} \Phi^{rs}_{mn}.\end{aligned} \tag{F.10}$$

This yields the mass spectrum in the case of the 75-dimensional scalar as:

$$\begin{aligned} m_{\tilde{D}} &= m_5 + \frac{s^2_{\rm GUT}}{\Lambda}(72 f_1 + 8 t_1) \\ m_{\tilde{L}} &= m_5 + \frac{s^2_{\rm GUT}}{\Lambda}(72 f_1 + 8 t_1) \\ m_U &= m_{10} + 2 y' s_{\rm GUT} + \frac{s^2_{\rm GUT}}{\Lambda}(72 f_2 + 8 t_2 + 4 t_3) \\ m_E &= m_{10} + 6 y' s_{\rm GUT} + \frac{s^2_{\rm GUT}}{\Lambda}(72 f_2 + 8 t_2 + 4 t_3) \\ m_Q &= m_{10} - 2 y' s_{\rm GUT} + \frac{s^2_{\rm GUT}}{\Lambda}(72 f_2 + 8 t_2 + 36 d_3) \end{aligned} \tag{F.11}$$

We can also consider the case in which both a scalar in 24 and in 75 are included, however, it would not lead to a successful mass splitting as can be seen by summing the Eq. (F.4) and (F.11). In addition to these, there will be contributions coming from the mixed scalar dimension-5 operators:

$$\mathcal{L}^{24-75}_{\rm mass} = \frac{h_1}{\Lambda} \bar{q}_i q^j \Phi^{ir}_{js} \Phi^s_r + \frac{h_2}{\Lambda} \bar{A}_{im} A^{jm} \Phi^{ir}_{js} \Phi^s_r + \frac{h_3}{\Lambda} \bar{A}_{ij} A^{mn} \Phi^{ir}_{mn} \Phi^j_r \tag{F.12}$$

These additional contributions in no way suffice to naturally split the mass of the light dark fermions from their GUT partner.

The additional contributions from these terms can be written as:

$$\begin{aligned}
\Delta m_{\tilde{D}} &= \frac{s_{\rm GUT} v_{\rm GUT}}{\sqrt{30}\Lambda} 10 h_1 \\
\Delta m_{\tilde{L}} &= -\frac{s_{\rm GUT} v_{\rm GUT}}{\sqrt{30}\Lambda} 15 h_2 \\
\Delta m_{U} &= \frac{s_{\rm GUT} v_{\rm GUT}}{\sqrt{30}\Lambda} (10 h_2 + 4 h_3) \\
\Delta m_{E} &= \frac{s_{\rm GUT} v_{\rm GUT}}{\sqrt{30}\Lambda} (-15 h_2 - 18 h_3) \\
\Delta m_{Q} &= \frac{s_{\rm GUT} v_{\rm GUT}}{\sqrt{30}\Lambda} \Big(-\frac{5}{2} h_2 + h_3 \Big)
\end{aligned} \tag{F.13}$$

- $\mathbf{\Phi_{200}}$:

  The SM preserving vev for this scalar is given by:

$$\langle \tilde{\Phi}^{ij}_{mn} \rangle = \sigma_{\rm GUT} [(\delta^\alpha_\gamma \delta^\beta_\delta + \delta^\alpha_\delta \delta^\beta_\gamma) + 2(\delta^a_c \delta^b_d + \delta^a_d \delta^b_c) - 2(\delta^\alpha_\gamma \delta^b_d + \delta^\alpha_\gamma \delta^b_c + \delta^\beta_\delta \delta^a_c + \delta^\beta_\gamma \delta^a_d)] \tag{F.14}$$

  where we have followed the splitting index notation introduced earlier for the case of the 75-dimensional scalar. We can only write dimension 5 operators in this case:

$$\begin{aligned}
\mathcal{L}^{200}_{\text{dim-5}} = &\frac{r_1}{\Lambda} \bar{q}_i q^i \tilde{\Phi}^{mn}_{jk} \tilde{\Phi}^{jk}_{mn} + \frac{r_2}{\Lambda} \bar{A}_{ij} A^{ij} \tilde{\Phi}^{mn}_{hk} \tilde{\Phi}^{hk}_{mn} + \frac{r_3}{\Lambda} \bar{q}_i q^j \tilde{\Phi}^{mn}_{jk} \tilde{\Phi}^{ik}_{mn} \\
&+ \frac{r_4}{\Lambda} \bar{A}_{ij} A^{hj} \tilde{\Phi}^{il}_{mn} \tilde{\Phi}^{mn}_{hl} + \frac{r_5}{\Lambda} \bar{A}_{ij} A^{hl} \tilde{\Phi}^{im}_{hn} \tilde{\Phi}^{jn}_{lm}
\end{aligned} \tag{F.15}$$

  which leads to the spectrum:

$$\begin{aligned}
\Delta m_{\tilde{D}} &= \frac{\sigma^2_{\rm GUT}}{\Lambda} (168 r_1 + 24 r_3) \\
\Delta m_{\tilde{L}} &= \frac{\sigma^2_{\rm GUT}}{\Lambda} (168 r_1 + 48 r_3) \\
\Delta m_{U} &= \frac{\sigma^2_{\rm GUT}}{\Lambda} (168 r_2 + 24 r_4 - 12 r_5) \\
\Delta m_{E} &= \frac{\sigma^2_{\rm GUT}}{\Lambda} (168 r_2 + 48 r_4 + 24 r_5) \\
\Delta m_{Q} &= \frac{\sigma^2_{\rm GUT}}{\Lambda} (168 r_2 + 36 r_4 - 24 r_5)
\end{aligned} \tag{F.16}$$

  However, in addition, we can also have mixed cases where 200-dimensional scalar occurs with Φ_{24} leading to the following dimension 5 contributions:

$$\mathcal{L}^{200-24}_{\text{dim-5}} = \frac{s_1}{\Lambda} \bar{q}_i q^j \Phi^h_k \tilde{\Phi}^{ik}_{jh} + \frac{s_2}{\Lambda} \bar{A}_{il} A^{jl} \Phi^h_k \tilde{\Phi}^{ik}_{jh} \tag{F.17}$$

$$\begin{aligned}
\Delta m_{\tilde{D}} &= \frac{s_{\mathrm{GUT}} v_{\mathrm{GUT}}}{\sqrt{30}\Lambda} 20 s_1 \\
\Delta m_{\tilde{L}} &= -\frac{s_{\mathrm{GUT}} v_{\mathrm{GUT}}}{\Lambda} \sqrt{30} s_1 \\
\Delta m_U &= \frac{s_{\mathrm{GUT}} v_{\mathrm{GUT}}}{\sqrt{30}\Lambda} 20 s_2 \\
\Delta m_E &= -\frac{s_{\mathrm{GUT}} v_{\mathrm{GUT}}}{\Lambda} \sqrt{30} s_2 \\
\Delta m_Q &= -\frac{s_{\mathrm{GUT}} v_{\mathrm{GUT}}}{\sqrt{30}\Lambda} 5 s_2
\end{aligned} \tag{F.18}$$

For the case of Φ_{200} and Φ_{75}, we have instead:

$$\mathcal{L}^{200-75}_{\text{dim-5}} = \frac{w}{\Lambda} \bar{A}_{ij} A^{kh} \Phi^{im}_{kn} \tilde{\Phi}^{jn}_{hm} \tag{F.19}$$

leading to the additional contributions to the masses of the fermions as:

$$\begin{aligned}
\Delta m_U &= \frac{s_{\mathrm{GUT}} \sigma_{\mathrm{GUT}}}{\Lambda} 8 w \\
\Delta m_E &= -\frac{s_{\mathrm{GUT}} \sigma_{\mathrm{GUT}}}{\Lambda} 8 w \\
\Delta m_Q &= \frac{s_{\mathrm{GUT}} \sigma_{\mathrm{GUT}}}{\Lambda} 24 w
\end{aligned} \tag{F.20}$$

We see that in neither of these cases differential contributions can help make the GUT partners way heavier than the light fermions in a natural way.

Appendix G

Matter Dominated Era

The Boltzmann equations governing Matter Dominated (MD) era can be written (See [83, 201] for example) in terms of the energy densities of the non-relativistic component ρ_M, contained in the heavy H dark fermions, and a relativistic one ρ_R, contained in the SM relativistic particles. The evolution of ρ_M and ρ_R is given by:

$$\dot{\rho_M} + 3H\rho_M = -\Gamma_M \rho_M \tag{G.1}$$

$$\dot{\rho_R} + 4H\rho_R = \Gamma_M \rho_M \tag{G.2}$$

where H is the Hubble parameter given by

$$H^2 = \frac{8\pi G}{3}(\rho_M + \rho_R) \tag{G.3}$$

and $\Gamma_M = \frac{2}{3}\Gamma_H$ where Γ_H was defined in Eq. 5.3. The fraction 2/3 accounts for the fraction of H contributing to SM d.o.f.s.

The solution to Eq. G.2 can be obtained analytically as (valid for time $\bar{t} \leq t \ll \frac{1}{\Gamma_M}$)

$$\rho_M = \bar{\rho}_M \left(\frac{\bar{a}}{a}\right)^3 \tag{G.4}$$

$$\rho_R = \bar{\rho}_R \left(\frac{\bar{a}}{a}\right)^4 + \frac{2}{5}\left(\frac{3}{8\pi}\right)^{1/2} \Gamma_M M_{Pl} \bar{\rho}_M^{1/2} \left(\left(\frac{\bar{a}}{a}\right)^{3/2} - \left(\frac{\bar{a}}{a}\right)^4\right) \tag{G.5}$$

$$\tag{G.6}$$

where $\bar{\rho}_M$ and $\bar{\rho}_M$ are the densities at some initial $\bar{a}$ (or $\bar{T}$) at time $\bar{t}$. Let us now define T_i as the temperature at which the non-standard scaling of the scale factor $a \propto T^{-8/3}$ begins. Hence at $T > T_i$, we will have the standard $a \propto T^{-1}$ scaling. This transition occurs, as is clear when ρ_R is dominated by the second term in Eq. G.6. Equating the first term and the second one in Eq. G.6 gives T_i as in terms of the initial conditions:

$$T_i = \bar{T}\left(\frac{\Gamma_M M_{Pl}}{2.38\frac{g_*(\bar{T})\bar{T}^4}{\bar{\rho}_M^{1/2}} + \Gamma_M M_{Pl}}\right)^{2/5} \tag{G.7}$$

where $M_{Pl} = 1.2 \times 10^{19}$ GeV. Without any loss of generality, $\bar{T}$ can be picked to be T_{MD} (See also

Ref. [201]). At T_{MD}, the temperature at which MD begins at which the following equality holds:

$$\bar{\rho}_M = \bar{\rho}_R = \frac{\pi^2}{30} g_*(T_{MD}) T_{MD}^4 \tag{G.8}$$

This non-standard scaling of the scale factor with temperature between the temperature intervals T_i and T_f leads to a further dilution in the number density of DM [201]. This dilution factor can be written as:

$$\mathcal{F} = \left(\frac{T_f}{T_i}\right)^5 \tag{G.9}$$

where $T_f = T_D$ is the temperature at which H decays to the SM d.o.f.s given by:

$$T_D = \sqrt{\frac{\Gamma_M M_{Pl}}{g_*(T_D)^{1/2} 1.67}} \tag{G.10}$$

We can finally write the expression for the suppression is

$$\mathcal{F} = \left(\frac{T_f}{T_i}\right)^5 = \frac{0.28}{g_*^{5/4}} \frac{\Gamma_M^{5/2} M_{Pl}^{5/2}}{T_{MD}^5} \left(\frac{4.15 g_*^{1/2} T_{MD}^2 + \Gamma_M M_{Pl}}{\Gamma_M M_{Pl}}\right)^2 \tag{G.11}$$

When the H bound states are long-lived enough, the terms involving Γ_M above can be ignored which gives us Eq. 6.70 in the main text.

Appendix H

Epoch of Recombination

Considering the epoch of recombination involves the formation of different types of bound states, in this appendix, we will show how different recombination reactions interplay to give us the result we discuss in the main text.

H.1 Type I hybrids

At $T = \Lambda_{\rm DC}$, we begin with fraction f of the H abundance in the form of type I mesons and $(1-f)$ as type I baryons At first, the following reactions involving type I hadrons and light hadrons start interchanging type I hadrons as *meson* $\leftrightarrow$ *baryon* in addition to the baryonic annihilations:

$$HLL + \bar{L}L \leftrightarrow LLL + H\bar{L} \tag{H.1}$$

$$HLL + \overline{LLL} \leftrightarrow H\bar{L} + n\bar{L}L \tag{H.2}$$

$$LLL + \overline{LLL} \leftrightarrow n\bar{L}L \tag{H.3}$$

The above reactions proceed with a geometric cross-section given by Eq. 6.54. This geometric cross-section is due to the fact that the size of the hybrids HLL and $H\bar{L}$ is $\mathcal{O}(\Lambda_{\rm DC}^{-1})$. The Boltzmann equations for these reactions governing the abundance of HLL and $H\bar{L}$ states is given by:

$$\begin{aligned}\frac{dY_{H\bar{L}}}{dz} =& +\frac{\langle\sigma_{rec}v\rangle\ s}{Hz}\left(Y_{HLL}Y_{\bar{L}L} - Y_{H\bar{L}}Y_{LLL}\frac{Y^{eq}_{HLL}}{Y^{eq}_{H\bar{L}}}\frac{Y^{eq}_{\bar{L}L}}{Y^{eq}_{LLL}}\right) \\ &+ \frac{\langle\sigma_{rec}v\rangle\ s}{Hz}\left(Y_{HLL}Y_{LLL} - Y^{eq}_{HLL}Y^{eq}_{LLL}\frac{Y_{H\bar{L}}Y^{n}_{\bar{L}L}}{Y^{eq}_{H\bar{L}}(Y^{eq}_{\bar{L}L})^{n}}\right)\end{aligned} \tag{H.4}$$

$$\begin{aligned}\frac{dY_{HLL}}{dz} =& -\frac{\langle\sigma_{rec}v\rangle\ s}{Hz}\left(Y_{HLL}Y_{\bar{L}L} - Y_{H\bar{L}}Y_{LLL}\frac{Y^{eq}_{HLL}}{Y^{eq}_{\bar{L}H}}\frac{Y^{eq}_{\bar{L}L}}{Y^{eq}_{LLL}}\right) \\ &- \frac{\langle\sigma_{rec}v\rangle\ s}{Hz}\left(Y_{HLL}Y_{LLL} - Y^{eq}_{HLL}Y^{eq}_{LLL}\frac{Y_{H\bar{L}}Y^{n}_{\bar{L}L}}{Y^{eq}_{H\bar{L}}(Y^{eq}_{\bar{L}L})^{n}}\right)\end{aligned} \tag{H.5}$$

The above coupled equations should be solved together with the Boltzmann equation for LLL, which can be written as:

$$\frac{dY_{LLL}}{dz} = -\frac{\langle\sigma_{rec}v\rangle s}{Hz}\left(Y_{LLL}^2 - (Y_{LLL}^{eq})^2\frac{(Y_{\bar{L}L})^2}{(Y_{\bar{L}L}^{eq})^2}\right) + \frac{\langle\sigma_{rec}v\rangle s}{Hz}\left(Y_{HLL}Y_{\bar{L}L} - Y_{H\bar{L}}Y_{LLL}\frac{Y_{HLL}^{eq}}{Y_{\bar{L}H}^{eq}}\frac{Y_{\bar{L}L}^{eq}}{Y_{LLL}^{eq}}\right) \tag{H.6}$$
$$- \frac{\langle\sigma_{rec}v\rangle s}{Hz}\left(Y_{HLL}Y_{LLL} - Y_{HLL}^{eq}Y_{LLL}^{eq}\frac{Y_{H\bar{L}}Y_{\bar{L}L}^2}{Y_{H\bar{L}}^{eq}(Y_{\bar{L}L}^{eq})^2}\right)$$

where $z = \Lambda_{\rm DC}/T$ where T is the temperature and $H(z)$ is the Hubble parameter.

H.2 Type II and III hybrids and recombination

Before moving on to describing the formation of type II and III H containing hadrons, let us discuss these bound states.

1. Each hybrid state has a tight "partonic" static core comprising one or more H quarks attached to some light quark "muck" comprising two or two light L quarks to make a gauge singlet. [1]

2. Recombination reaction between these non-perturbative hybrid hadrons occurs with a large geometric cross-section and leads to the formation of a final state with a large angular momentum l. This has been discussed in detail in Refs. [83, 191, 192].

3. The overlap of the partons between these hybrids would result in the formation of an *unbreakable* bound state. The cross-section for this given by σ_{fall} is much smaller than the geometric cross-section.

4. The tower of large l bound states are excited and in general can be either broken by the bath or else can de-excite to the ground state which is unbreakable via the emission of dark radiation.

5. As has been shown already in Ref. [83], these de-excitation rates require many assumptions and are plagued with large uncertainties. We will not attempt to repeat these calculations here.

6. We model each of the partonic core of the ground states as a bound state in a Coulombic potential given by [229]:
$$V(r) = -\frac{\alpha_{eff}}{r} \tag{H.7}$$
where
$$\alpha_{eff} = \left(\frac{2C_N - C_J}{2}\right)\alpha_{\rm DC}(M_H) \tag{H.8}$$
where C_N is the quadratic Casimirs (C_2) for the fundamental representation of dark colour gauge group under which H transform and C_J is C_2 of the core direction picked. (See Table **??**)

[1] A "muck" of two L states does not differ much from a "muck" of only one L. We use the example of Λ_b baryon (containing a single bottom b quark) and B meson from SM.

Bound State	α_{eff}
HHL	0.67 $\alpha_{\rm DC}(M_H)$
$\bar{H}H$	1.33 $\alpha_{\rm DC}(M_H)$
HHH	1.33 $\alpha_{\rm DC}(M_H)$

Table H.1: Table showing the α_{eff} for each unbreakable bound states.

In order to compute the cross-section for forming an unbreakable bound state: HHL, $\bar{H}H$, HHH, we use the analytical formula given in [192]:

$$\sigma_{\rm fall} = \frac{\pi}{\Lambda_{\rm DC}^2} \frac{\alpha_{eff}^{7/4} \Lambda_{\rm DC}^{5/2}}{(2\mu)^{1/2} T^2} \tag{H.9}$$

where α_{eff} for each bound state has been tabulated in Table **??** calculated using the formula above in Eq. H.8. Here, μ is the reduced mass of the partonic core of the unbreakable state formed. For the HHL and $\bar{H}H$ system, modelling the 2-body partonic core is straightforward, indeed, in these cases $\mu = M_H/2$. However, for the HHH system can be modelled as a 2-body system between HH system interacting with a single H. In this case, $\mu = 2M_H/3$. Note that for the formation of the dark colour singlet HHL, the HH partonic core should transform in the anti-fundamental representation under dark colour.

In the main text and in our computation described here, we consider all the $2 \to 2$ recombination reactions which proceed *only* in the forward direction. These reactions can be determined by the energy balance equation. Let us demonstrate this using:

$$HLL + H\bar{L} \to HHL^u + \bar{L}L$$

For the above reaction to proceed in the backward reaction, the following energy balance equation should be satisfied in the centre-of-mass frame:

$$M_{HHL^u} + M_{\bar{L}L} + K_{HHL} + K_{\bar{L}L} \geq M_{HLL} + M_{H\bar{L}} \tag{H.10}$$

where K_i is the kinetic energy of the colliding particles. We can write the masses of the initial bound states in terms of the mass of the constituent heavy quark and the binding energy term as:

$$M_{HLL} = M_H + B_{HLL}, \qquad M_{H\bar{L}} = M_H + B_{H\bar{L}}. \tag{H.11}$$

where we set the binding energy of the heavy-light meson $H\bar{L}$ to the lattice value of the binding energy in a B meson system $B_{H\bar{L}} = 1.85\ \Lambda_{\rm DC}$ [230] while we vary the binding energy of the singly heavy baryon as $B_{HLL} = a\ {B_{H\bar{L}}}^2$. The parameter a was varied between 1 and 2 and the conclusions of this section are found to be robust against this variation.

We can similarly write the mass of the unbreakable state HHL^u as:

$$M_{HHL^u} = 2M_H + B_{HHL} \tag{H.12}$$

where $B_{HHL} \sim -\alpha_{\rm DC}^2(M_H) M_H + \mathcal{O}(\Lambda_{\rm DC})$.

The kinetic energy K_i can be set to $\sim \frac{3}{2}kT$ (with $k = 1$) of the bath, hence $K \lesssim \Lambda_{\rm DC}$ right

[2]This assumption is not far from the mass difference in the Λ_b baryon and B meson system in QCD. For this see Fig. 9 in Ref [205] where the mass difference is close to 1

after confinement. From Eq. H.12 and Eq. H.11, it is clear that Eq. H.10 will be violated, thus this reaction cannot proceed in the backward direction. A similar energy conservation will hold for each of the recombination reactions written in the main text in Eqs. 6.64 and Eq. 6.62 for the formation of unbreakable $\bar{H}H^u$ and HHH^u bound states.

As mentioned in the main text, the formation of the type II and III (unbreakable) states proceeds via the following reactions:

$$HLL + H\bar{L} \to HHL^u + n\bar{L}L, \tag{H.13}$$
$$HLL + HLL \to HHL^u + LLL \tag{H.14}$$
$$HLL + \bar{H}L \to \bar{H}H^u + LLL \tag{H.15}$$
$$H\bar{L} + \bar{H}L \to \bar{H}H^u + n\bar{L}L \tag{H.16}$$
$$HLL + \overline{HLL} \to \bar{H}H^u + n\bar{L}L \tag{H.17}$$
$$HHL + H\bar{L} \to HHH^u + n\bar{L}L \tag{H.18}$$
$$HHL + HLL \to HHH^u + LLL \tag{H.19}$$

Using the equations above, we can write the coupled Boltzmann equations for the formation of type II and type III bound states (where we have dropped the u superscript for the bound states):

$$\frac{dY_{HHL^u}}{dz} = \frac{\langle\sigma^{HHL}_{fall}v\rangle s}{Hz}(Y_{HLL}Y_{H\bar{L}} + Y^2_{HLL}) \tag{H.20}$$
$$\frac{dY_{\bar{H}H^u}}{dz} = \frac{\langle\sigma^{\bar{H}H}_{fall}v\rangle s}{Hz}(Y_{HLL}Y_{H\bar{L}} + Y^2_{HLL} + Y^2_{H\bar{L}}) \tag{H.21}$$
$$\frac{dY_{HHH^u}}{dz} = \frac{\langle\sigma^{HHH}_{fall}v\rangle s}{Hz}(Y_{HHL}Y_{H\bar{L}} + Y_{HHL}Y_{HLL}) \tag{H.22}$$

Note that by definition of σ_{fall}, the backward reaction rate is 0 in the above equations. Since all these type II and III hadrons form from type I hadrons, the Boltzmann equations for the abundances of type I hadrons in Eq H.4 must be modified accordingly. In order to track the abundances of DM and these mixed hybrid states together, we numerically solve these coupled equations. As is clear, this is a rather complicated system however, we find a simplification that allows us to decouple the equations.

In the absence of type II and III recombinations, for small values of $z \sim 1$, the ratio of abundances of type I baryons to mesons follows the equilibrium distribution given by:

$$\frac{Y_{HLL}}{Y_{H\bar{L}}} = \frac{Y^{eq}_{HLL}}{Y^{eq}_{H\bar{L}}} = \frac{g_{HLL}}{g_{H\bar{L}}} e^{-1.85\ (a-1)\ z} \tag{H.23}$$

where $M_H \gg \Lambda_{\rm DC}$. Here $g_{HLL},\ g_{H\bar{L}}$ are the total degrees of freedom for the bound states equal to 1944 and 108 respectively, while the exponential factor originates from $e^{(-M_{HLL}+M_{H\bar{L}})/T}$ and where we have used Eq. H.11. Moreover, we use the following conditions:

$$Y_H(z) = 3Y_{HHH} + 2Y_{HHL} + 2Y_{\bar{H}H} + Y_{\bar{L}H} + Y_{HLL} = constant \tag{H.24}$$

with the initial conditions at $z = 1$ given by:

$$Y_{HHH}(z=1) = 0, \quad Y_{HHL}(z=1) = 0, \quad Y_{\bar{H}H}(z=1) = 0, \quad Y_{\bar{L}H}(z=1) = Y_{HLL}(z=1) \tag{H.25}$$

where in writing $Y_{\bar{L}H} = Y_{HLL}$ at $z = 1$, we have used $f = 0.5$ (see Sec. H.1). We can solve

Eqs. H.20 - Eq. H.22 for the abundances of type II and III hybrids with these conditions in Eq. H.25 and Eq. H.23. Numerically solving these equations, we find that these reactions almost instantly populate and saturate these unbreakable states at $z \sim 1$ as can be seen from Fig. 6.2. As type II and III hybrids begin to saturate, the abundance of type I hadrons almost entirely depletes, setting the type I recombination reaction rates to 0 almost instantly right after confinement.

Now, we comment on the recombination epoch during an MD era. Depending on the value of M_H (see Fig. 6.3, recombination processes can either take place during the RD era (for $T_{MD} \lesssim T_{F.O.}^{DM}$) or else during the MD era ($T_i < T_{F.O.}^{DM} < T_{MD}$). We solved the Boltzmann equations for these two cases where the only difference lies in the Hubble parameter H. For the MD era, Hubble parameter $H(z)$ is dominated by the energy density of H given by ρ_M (see Eq. G.3, which is always valid).

Our numerical solution shows that at the end of recombination, most of the H abundance is confined in the form of heavy mesons $\bar{H}H$. The fractional abundance of H in heavy baryons HHL, HHH is $f_H^{\mathcal{B}} \sim 0.3$. These baryons can contribute to the DM density as described in the main text.

Finally, we discuss the fate of the breakable states formed during recombination alongside the unbreakable states. As discussed in the main text, these can involve any of the type II and III bound states with binding energies $B \sim \mathcal{O}(\Lambda_{\rm DC})$, which are easily broken by the thermal bath. To simplify our discussion, let us consider the reaction for breakable heavy mesons $\bar{H}H^*$ given by:

$$HLL + \bar{H}L \xleftrightarrow{\sigma_{break}} \bar{H}H^* + LLL \tag{H.26}$$

where $\sigma_{break} \sim \sigma_{geo}$ is the cross-section for this reaction. In order to keep track of this breakable bound state, we should add the following Boltzmann equation to our set of equations:

$$\frac{dY_{\bar{H}H^*}}{dz} = \frac{\langle \sigma_{break} s \rangle}{Hz} \left(Y_{HLL} Y_{\bar{H}L} - \frac{Y_{\bar{H}H^b} Y_{LLL}}{Y^{eq}_{\bar{H}H*} Y^{eq}_{LLL}} Y^{eq}_{HLL} Y^{eq}_{\bar{H}L} \right) \tag{H.27}$$

Since the formation of $\bar{H}H^*$ will also deplete the abundance of HLL and $H\bar{L}$, the RHS in Eq. H.27 should be added with a $-$ sign to the boltzmann equations for Y_{HLL} and $Y_{H\bar{L}}$. Our numerical solution can be seen in Fig. H.1, where we show the comoving abundance of the states: $\bar{H}H^u$, $\bar{H}H^*$, $H\bar{L}$, HLL in (solid) yellow, (solid) blue, (dashed) green, (dashed) red respectively. It is evident that the population of breakable $\bar{H}H^*$ is negligible with respect to the other bound states in the dark sector during recombination. We have also checked the inclusion of the remaining equations for other breakable species such as HHL^*, HHH^*, and found that their abundances are negligible as well.

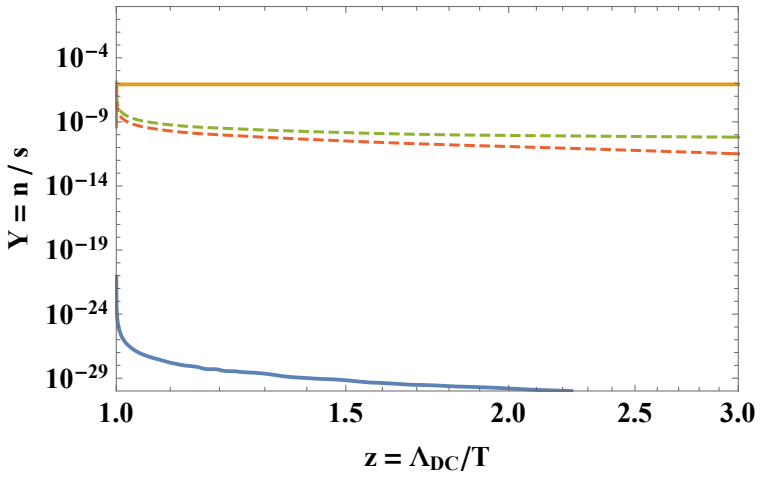

Figure H.1: Plot showing the comoving abundances Y_i various bound states for $M_H = 10^{10}$ GeV after including type II recombination for unbreakable $\bar{H}H$ and breakable $\bar{H}H$ reaction given in Eq. H.27. The solid green blue and solid yellow lines show the abundances Y of unbreakable $\bar{H}H^u$ and breakable $\bar{H}H^*$ respectively. The dashed green and dashed red lines show the depleting abundance of type I meson $H\bar{L}$ and type I baryon HLL. It is evident that the breakable state abundance is negligible with respect to the unbreakable state abundance.